SEISMICALLY INDUCED TILTING POTENTIAL OF SHALLOW MATS ON FINE SOILS

A THESIS SUBMITTED TO
THE GRADUATE SCHOOL OF NATURAL AND APPLIED SCIENCES
OF
MIDDLE EAST TECHNICAL UNIVERSITY

BY

MUSTAFA TOLGA YILMAZ

IN PARTIAL FULFILLMENT OF THE REQUIREMENTS
FOR
THE DEGREE OF DOCTOR OF PHILOSOPHY
IN
CIVIL ENGINEERING

SEPTEMBER 2004

Approval of the Graduate School of Natural and Applied Sciences

Prof. Dr. Canan Özgen
Director

I certify that this thesis satisfies all the requirements as a thesis for the degree of Doctor of Philosophy

Prof. Dr. Erdal Çokca
Head of the Department

This is to certify that we have read this thesis and that in our opinion it is fully adequate, in scope and quality, as a thesis for the degree of Doctor of Philosophy

Assoc.Prof. Dr. B.Sadık Bakır
Supervisor

Examining Committee Members

Prof. Dr. Atilla Ansal	(BOUN, KOERI)	
Assoc. Prof. Dr. B.Sadık Bakır	(METU, CE)	
Prof. Dr. M.Yener Özkan	(METU, CE)	
Prof. Dr. Haluk Sucuoğlu	(METU, CE)	
Assoc. Prof. Dr. M.Zülfü Aşık	(METU, ES)	

I hereby declare that all information in this document has been obtained and presented in accordance with academic rules and ethical conduct. I also declare that, as required by these rules and conduct, I have fully cited and referenced all material and results that are not original to this work.

Name, Last name : Mustafa Tolga Yılmaz

Signature :

ABSTRACT

SEISMICALLY INDUCED TILTING POTENTIAL OF SHALLOW MATS ON FINE SOILS

Yılmaz, Mustafa Tolga
Ph.D., Department of Civil Engineering
Supervisor: Assoc. Prof. Dr. Bahadır Sadık Bakır

September 2004, 259 pages

Occurrence of displacements of shallow mat foundations resting on saturated silt-clay mixtures were reported in Mexico City during 1985 Mexico Earthquake, and in Adapazarı during 1999 Kocaeli (İzmit) Earthquake. Soft surface soils, shallow ground water, limited foundation embedments and deep alluvial deposits were the common features pertaining to such foundation displacements in either case. Experience shows, while uniform foundation settlements, even when excessive, do not limit post earthquake serviceability of building structures, tilting is particularly problematic. In this study, a simplified methodology is developed to estimate the seismically induced irrecoverable tilting potential of shallow mats on fine saturated soils.

The undrained shear and deformation behavior of silt-clay mixtures encountered at the Adapazarı sites with significant foundation displacements are investigated through a series of standard and rapid monotonic, and stress-controlled cyclic triaxial tests conducted over anisotropically consolidated natural soil samples. Test results show that, while the shear strength of these soils do not significantly degrade under means of loading comparable to that of Kocaeli earthquake, their plastic strain accumulation characteristics critically depend on the mode of loading as well as the relative levels of applied load with regard to the monotonic strength.

Based on the results of laboratory tests, the response of nonlinear soil-foundation-structure system is reduced to a single-degree-of-freedom oscillator with elastic-perfectly plastic behavior. The natural period of the system is expressed by simplified soil-structure-interaction equations. Pseudo-static yield acceleration, which is required to initiate the foundation bearing capacity failure when applied to the structural mass, is estimated by the finite-element method. Eventually, the tilting potential of the foundations is estimated utilizing inelastic response of the nonlinear oscillator. Response of the deep alluvium sites, which involves velocity pulses with periods consistent with the fundamental site period, is significant in determination of inelastic response of low bearing capacity systems.

Predictive capability of the methodology developed is tested with actual case data. The methodology is observed to predict irrecoverable tilting potential of foundations consistent with the observations, except for the cases with low seismic bearing capacity. Deviations are explained considering the sensitivity of low-strength systems to asymmetrical behavior and uncertainties involved in seismic demand.

Keywords: Adapazarı, Clay, Foundation displacements, Foundation tilting, Kocaeli Earthquake, Mat foundations, Mexico Earthquake, Seismic performance, Silt, Site response.

ÖZ

İNCE DANELİ ZEMİNLER ÜZERİNDEKİ SIĞ RADYELERİN SİSMİK EĞİLME POTANSİYELİ

Yılmaz, Mustafa Tolga
Doktora, İnşaat Mühendisliği Bölümü
Tez Yöneticisi: Doç. Dr. Bahadır Sadık Bakır

Eylül 2004, 259 sayfa

1985 Meksika depreminde Mexico-City'de ve 1999 Kocaeli Depreminde Adapazarı'nda, doygun silt-kil karışımları üzerinde yer alan sığ radye temeller kalıcı deplasmanlara maruz kalmıştır. Yumuşak yüzey zeminleri, sığ yer altı suyu, kısıtlı temel derinliği, ve derin alüvyon çökelleri her iki durumda temel deplasmanlarına ilişkin olarak görülen ortak özelliklerdir. Deneyime bağlı olarak, düzgün temel oturmalarının, aşırı olmaları durumunda dahi, bina türü yapıların deprem sonrası kullanılabilirliğini etkilememekte, ancak temellerde meydana gelecek kalıcı eğilmelerin özellikle bu bakımdan sorun yarattığı bilinmektedir. Bu çalışmada, ince daneli zeminler üzerinde yer alan sığ radyelerin sismik yükler altındaki kalıcı eğilme potansiyelinin öngörülebilmesi amacıyla basitleştirilmiş bir yöntem geliştirilmiştir.

Adapazarı'nda temel deplasmanlarının belirgin olarak meydana geldiği sahalarda karşılaşılan silt-kil karışımlarının drenajsız kayma ve deformasyon davranışları, anisotropik olarak konsolide edilmiş doğal zemin örnekleri üzerinde bir seri standart ve hızlı monotonik, ve gerilme-kontrollü çevrimsel üç eksenli testler gerçekleştirilerek incelenmiştir. Test sonuçları, bu zeminlerin kayma dayanımının Kocaeli depremi ile kıyaslanabilir yükler altında önemli oranda değişmediğini; ancak plastik birim deformasyon özelliklerinin, yükleme moduna ve yükün monotonik kayma dayanımına göre seviyesine bağlı olduğunu ortaya koymaktadır.

Laboratuvar sonuçlarına bağlı olarak, doğrusal olmayan zemin-temel-yapı sisteminin tepkisi tek-derece-serbestisi olan elastik-mükemmel plastik titreşir

sistem davranışına indirgenmiştir. Bu idealize sistemin doğal peryodu basit zemin-yapı-etkileşimi denklemlerine bağlı olarak ifade edilmiştir. Temelde taşıma kapasitesi yenilmesine sebep olan ve yapısal kütleye uygulanan pseudo-statik akma ivmesi, sonlu elemanlar yöntemi ile tahmin edilmektedir. Neticede, temellerin eğilme potansiyeli sistemin doğrusal olmayan tepkisi kullanılarak tahmin edilmektedir. Saha peryodu ile tutarlı peryoda sahip hız dalgasının meydana gelebildiği derin alüvyon sahaların tepkisi, düşük taşıma kapasitesine sahip sistemlerin elastik olmayan davranışını belirgin şekilde etkiler.

Geliştirilen yöntemin tahmin kapasitesi vaka verileri kullanılarak denenmiştir. Yöntemin, düşük sismik taşıma kapasitesinin söz konusu olduğu durumlar dışında, kalıcı temel eğilmesi potansiyelini tutarlı olarak tahmin edebildiği belirlenmiştir. Sapmalar, düşük mukavemetli sistemlerin asimetrik davranışa olan hassasiyeti ve sismik talepteki belirsizlik ile açıklanmıştır.

Anahtar Kelimeler: Adapazarı, Kil, Kocaeli Depremi, Meksika Depremi, Radye temeller, Sismik performans, Silt, Saha tepkisi, Temel deplasmanları, Temel eğilmesi

To My Wife

ACKNOWLEDGEMENTS

This study was conducted under the supervision of Assoc. Prof. Dr. B. Sadık Bakır. I am grateful for the hours he spent providing guidance, insight, and encouragement during the course of this study. I would like to thank Prof. Dr. Haluk Sucuoğlu, Prof. Dr. M. Yener Özkan, Assoc. Prof. Dr. Zülfü Aşık, and Prof. Dr. Yalçın Mengi for their contributions and encouragements throughout my thesis study. Also I would like to thank Prof. Dr. Atilla Ansal for his constructive criticism and for serving in my graduate committee. Onur Pekcan and Ali Bal are also acknowledged for their contributions regarding laboratory work. I owe thanks to Assist. Prof. Dr. Altuğ Erberik and Dr. Cemalettin Dönmez for their support, whose friendships are invaluable for me. I gratefully acknowledge the financial support provided by the Scientific and Technical Research Council of Turkey (TÜBİTAK) through grants İÇTAG A0208 and İÇTAG I590. I would like to thank to my mother and brother, Sezgül and Gökhan Yılmaz, for their endless support and encouragement throughout my life. I also owe special thanks to Ergün and Filiz Soğlalı for their invaluable support with unlimited forbearance. Finally, I would like to express my deepest gratitude to my wife Dilek for the unlimited tolerance and help. I believe, this study would never be possible in case of absence of her.

TABLE OF CONTENTS

LIST OF TABLES

LIST OF FIGURES

FIGURES

LIST OF ABBREVIATIONS AND SYMBOLS

ABBREVIATIONS AND SYMBOLS

A	Area of the foundation
A_S	Skempton's pore water pressure parameter due to increase in major principal stress
A_{st}	Area of a storey
A_x	Cross-sectional area
a_0	Dimensionless frequency in Gazetas' impedance formulations
a_h, a_v	Horizontal and vertical acceleration acting on inertia of foundation soils
a_y	Pseudo-static yield acceleration
B	Width of the shallow foundation
B´	Effective width of foundation due to eccentric loading
B_S	Skempton's pore pressure coefficient for isotropic stress increase
c	Cohesion of soil
c´	Effective cohesion of soil
c^*	Modified cohesion due to nonassociated flow rule
c_v	Viscous damping of a SDOF oscillator
c_s, $c_{h,}$ c_θ	Viscous damping coefficient for structural distortion, foundation translation and foundation rocking modes in SSI analyses
C_c, C_r	Compression and recompression index for consolidation
CSR	Cyclic stress ratio
CD	Consolidated-drained test
CU	Consolidated-undrained test
D_e	Embedment depth of foundation
d_θ	First moment of inertia for rocking of foundation
e	Load eccentricity
E	Young's modulus

E', E_u	Young's modulus of soil during drained and undrained loading
f_{cyc}	Frequency of the cyclic load
f , g	Functions utilized in rapid loading tests
f_{ci}, $f_{\gamma i}$, f_{qi}	Load inclination factors for bearing capacity, regarding cohesion, unit weight of soil, and surcharge at foundation level
f_{cs}, $f_{\gamma s}$, f_{qs}	Shape factors for bearing capacity, regarding cohesion, unit weight of soil, and surcharge at foundation level
f_s	Resistance force of a nonlinear spring
$\bar{f}_s$	Normalized f_s
f_y	Yield strength of an ideally elastic-perfectly plastic system
FS	Factor of safety against bearing capacity failure by static (gravitational) forces
FS_{net}	Net factor of safety against bearing capacity failure by static (gravitational) forces
FS_{seis}	Factor of safety against seismic bearing capacity failure
G	Shear modulus
g_p	Plastic potential function
g	Gravitational acceleration
h	Height of the lumped mass from the base, defined for the SDOF oscillator in SSI analyses
H	Base shear acting on foundation
$\bar{h}$	Equivalent height of a multi-storey structure
h_i	Height of the i^{th} storey from the base
i	Load inclination
I	Moment of inertia
I_{bx}	Area moment of inertia of foundation about x (longitudional) axis
I_θ	Second moment of inertia for rocking of foundation
k	Stiffness
$\tilde{k}$	Equivalent spring coefficient for reduced nonlinear SSI model
$\breve{k}_h$, $\breve{k}_\theta$,	Gazetas' frequency dependent dynamic stiffness correction factors for horizontal translation and rocking of foundation
K_h, K_θ	Static stiffness coefficients for horizontal translation and tilting of foundation
k_s, k_h, k_θ	Stiffness coefficients for structural distortion, horizontal displacement and tilting of foundation

k'_θ	Incremental stiffness of ideally elastic-perfectly plastic rotational spring
$\bar{k}_\theta$	Rotational spring coefficient for reduced linear SSI system
LL	Liquid limit
m	Lumped mass representing the inertia of the structure
M	Overturning moment acting on foundation
M_{st}	Total mass of structure
M_y	Yield (ultimate) moment for foundation
m_i	Lumped mass of the i^{th} storey
m_{fdn}	Mass of the foundation system
n	Number of stories
n_p	Number of successive pulses
N_c, N_γ, N_q	Bearing capacity factors regarding to cohesion, unit weight of soil, and surcharge at foundation level
N_{cyc}	Number of cycles
L	Length of the shallow foundation in direction perpendicular to the failure direction
p´	Effective mean principal stress (Cambridge definition)
PGA, PGV	Peak ground acceleration and velocity
PI	Plasticity index
q	Deviator Stress
q_A, q_B	Traction A and B applied on foundation during Plaxis analyses
q_{BH}, q_{BV}	Horizontal and vertical components of traction B
q_{fdn}	Component of bearing pressure due to weight of foundation system
q_{max}	Maximum pressure beneath foundation for a linear pressure distribution
q_{net}	Net pressure exerted on soil by the foundation
q_p	Bearing pressure acting on foundation
q_s	Surcharge pressure
q_{str}	Component of bearing pressure due to weight of superstructure
$(q_s)_h$, $(q_s)_v$	Horizontal and vertical components of surcharge load at foundation level
q_u	Ultimate bearing pressure on foundation
$(q_u)_{seis}$	Ultimate undrained load of foundation during seismic loading

RC	Reinforced concrete
R_y	Yield reduction factor
r_θ	Equivalent radius of oscillation for rocking of foundation
s'	Effective mean principal stress (M.I.T. definition)
SA	Spectral acceleration
SDOF	Single degree of freedom
SSI	Soil-structure interaction
S_u	Undrained shear strength
t_d	Degradation parameter for cyclic test
t	Time
t	Maximum shear stress due to principal stress difference
$\bar{t}$	Dimensionless time
$\bar{t}_1$	Dimensionless time parameter utilized in cyclic tests
$\bar{T}$	Equivalent natural period of the total SSI system
T_b	Lower bound period for the constant acceleration region of the spectrum
T_c, T_c'	Periods separating the acceleration and velocity sensitive regions for the elastic and inelastic spectrum respectively
T_g	Predominant ground period
T_h	The natural period of horizontal translation mode of foundation displacements
T_n	Natural period
T_p	Period of the sinusoidal velocity pulse
T_r	The natural period of rocking mode of foundation displacements
T_s	Fixed-base natural period of the structure
$u, \dot{u}, \ddot{u}$	Relative displacement, velocity and acceleration
$u_g, \dot{u}_g, \ddot{u}_g$	Free-field surface displacement, velocity and acceleration
u_h	Displacement of the lumped mass due to horizontal translation of the foundation in SSI analyses
u_{hp}	Cumulative irrecoverable displacement due to horizontal translation of foundation
u_{ir}	Irrecoverable displacement demand on a ideally elastic-perfectly plastic system
URF	Undrained behavior reduction factor
u_{pore}	Pore-water pressure

u_s	Structural distortion
u_t	Total displacement of the lumped mass in SSI analyses
u_y	Yield displacement of an ideally elastic-perfectly plastic system
UU	Unconsolidated-undrained test
u_θ	Displacement of the lumped mass due to tilting of the foundation in SSI analyses
$u_{\theta p}$	Cumulative irrecoverable displacement due to tilting of foundation
v	Paolucci and Pecker's seismic loading reduction factor for bearing capacity
V	Vertical bearing load acting on foundation
v_h, v_e, v_i	Components of v due to load inclination, load eccentricity, and horizontal inertial acceleration acting on soil mass
V_p	Amplitude of the sinusoidal velocity pulse
V_s	Shear wave-velocity of the foundation soil in SSI analyses
V_{s0}	Small-strain shear wave velocity of foundation soils
V_u	Ultimate vertical (gravitational) load on foundation
w_n	Water content
Δq	Undrained component of the change in deviator stress
Δu_{cyc}	Accumulated excessive pore pressure during cyclic loading
Δu_{pore}	Change in pore-pressure during undrained tests
Δu_f	Pore-pressure change up to failure of the specime in monotonic CU type triaxial tests
$\Delta \varepsilon_{cyc}$	Accumulated irrecoverable strain during exceedence of σ_{mon} during a succesive load cycle
$\Delta \sigma_{cyc}$	Amplitude of cyclic deviator stress
Φ	Angle of internal friction of soil
Φ'	Effective angle of internal friction of soil
Φ^*	Modified angle of internal friction due to nonassociated flow rule
Ψ	Dilatancy angle
α, β	Rapid loading parameters
γ	Unit weight of soil
γ_B	Buoyant unit weight of soil
γ_D	Buoyant unit weight of soil above foundation level, for surcharge calculations
γ_{sat}	Saturated unit weight of soil

$\dot{\varepsilon}$	Strain Rate
ε_A	Total irrecoverable axial strain (compression positive)
ε_N	Strain amplitude at the end of N^{th} cycle during a stress-controlled cyclic test
$\dot{\underline{\varepsilon}}_p$	Plastic strain rate matrix
ε_v	Volumetric strain
$\dot{\underline{\varepsilon}}_v^p$	Volumetric plastic strain rate
ε_θ	Error in approximation of θ
θ	Tilting angle of the foundation
$\tilde{\theta}$	Approximation of θ
θ_{ir}	Irrecoverable tilting demand on foundation
θ_y	Yield rotation angle for ideally elastic-perfectly plastic system
μ	Ductility ratio
μ_{max}	Ductility demand
$\mu_{symmetric}$	Ductility demand for a symmetric elastic-ideally plastic system, which is equal to μ_{max}
$\mu_{asymmetric}$	Ductility demand for a asymmetric elastic-ideally plastic system, for which yield strength is different in two directions
ν	Poisson's ratio
ς	Damping ratio
$\bar{\varsigma}$	Effective damping ratio
ς_s, ς_h, ς_θ	Damping ratio for structural distortions, horizontal translation and rocking of foundation in SSI analyses
δ_D	Degradation index for cyclic loading
σ	Normal stress acting on a plane
σ_1	Major principal stress
σ_3	Minor principal stress
σ_1'	Effective major principal stress
σ_3'	Effective minor principal stress
$(\sigma_1)_c$	Major principal stress during consolidation stage of a test
$(\sigma_3)_c$	Minor principal stress during consolidation stage of a test
σ_{ave}	Average stress during cyclic test
σ_{max}	Maximum stress during cyclic test
σ_{mon}	Monotonic strength
σ_n	Normal stress acting on failure plane

σ_r	Cell pressure during triaxial test
σ'_{v0}	Initial confining stress
τ	Shear stress acting on a plane
τ_c	Amplitude of cyclic shear stress
τ_f	Shear strength of soil on a failure plane
τ_N	Stress amplitude at the end of N^{th} cycle during stress-controlled cyclic test
φ	Phase angle of the velocity pulse
ω	Frequency of the cyclic load (rad/s)
$\overline{\omega}$	Equivalent natural frequency of the total SSI system
ω_h	The natural frequency of horizontal translation mode of foundation displacements (rad/s)
ω_n	Natural frequency (rad/s)
ω_s	Fixed-base natural frequency of the structure (rad/s)
ω_r	The natural frequency of rocking mode of foundation displacements (rad/s)

CHAPTER 1

INTRODUCTION

1.1. General

After September 19, 1985 earthquake that hit Mexico City, bearing capacity failures of shallow mat foundations, inducing tilting and settlement of the building foundations, were observed in the city, which is situated over deep alluvial soils. In worst cases, buildings had to be demolished, due to excessive displacements in foundations. Subsoil conditions under the failed foundations are reported to be silty clays, with high compressibility. The peak ground acceleration (PGA) recorded by SCT station, located on the alluvium, is 0.091 g in NS, and 0.16 g in EW directions. Due to the significant site-amplification capability of the Mexico-City basin, the SCT records exhibit relatively high peak ground velocity (PGV), as 39 cm/s in NS and 57 cm/s in SE directions (Zeevaert, 1991). The predominant period of the recorded motion is about 2.0 s, which is compatible with the natural period of the recording site (Seed et al., 1988).

The city of Adapazarı, which is mostly located on a deep alluvial basin in the near field of the ruptured North Anatolian Fault, was among the worst affected urban areas during the 17 August 1999 İzmit (Kocaeli), Turkey earthquake (M_w 7.4). A quite remarkable aspect from the geotechnical engineering point of view was the occurrence of numerous cases of displacements in various forms and levels at the foundations of, by and large, three- to six-story reinforced concrete buildings in the city. Based on the post earthquake observations and subsequent studies, the factors that might have contributed to certain extents in those displacements were listed as the variability of induced seismic excitation throughout the city, building height and foundation aspect ratio as well as the presence of adjacent buildings, and generally soft surface soils with occasional apparent potential for liquefaction (Bakır et al., 2002).

Earlier studies at Adapazarı sites with excessive foundation displacements (Sancio et al., 2002; Karaca, 2001) reveal that the subsoil conditions are dominated by silt-clay mixtures. Although the foundation displacements at the sites consisting silt-sand mixtures can be attributed to the soil liquefaction related phenomena, those on silt-clay mixtures may not be simply explained by the liquefaction mechanism as discussed for sands. Also, the observed tendency of increase in foundation displacements for relatively higher buildings underlines the importance of inertial effects on the seismic response of these foundations. Occurrence of ground failure in the city almost invariably in association with the foundations and lack of solid evidence of liquefaction in free-field point out the seismic bearing capacity failure as a possible mechanism in which soil-structure interaction plays an important role.

As in the case of Mexico-City, Adapazarı is also reported to suffer from strong site-amplification effects, reflected as increasing spectral acceleration levels at longer periods: The fundamental site period at the center of the city is estimated to be in the order of 1.8 s, excluding the sites consisting rather soft or liquefiable surface deposits (Bakır et al., 2002). The EW record obtained during 17 August 1999 event at a stiff (weathered rock) site yields PGA of 0.4g, and PGV of 57 cm/s: The site periods and peak ground velocities are comparable to Mexico City records of 1985 earthquake. Hence, the common properties of Mexico City and Adapazarı cases, such as presence of soft shallow silt-clay mixtures, shallow ground water table, amplification of long-period components of motion by deep alluvial basin, and shallow mat foundations appear to be the significant features that should be considered in investigation of available cases.

Post earthquake observations in Adapazarı revealed additional important consequences regarding engineering practice. Two strongly contrasting modes of damage were observed at deep alluvium sites in the city over relatively new reinforced concrete buildings with similar characteristics: structural system failures due to excessive structural vibrations and foundation displacements of various forms and levels due to bearing capacity failure. These two modes of damage were observed to be remarkably mutually exclusive as well. It is to be pointed out that due to the water table seasonally fluctuating between 50 and 200 cm below the ground surface in the city, there are no basements, and the foundations are commonly rather shallow rigid mats. Hence the buildings were insensitive to

potential detrimental impact of differential settlements on the load bearing system. Although the foundation displacements exceeded tolerable limits in several cases, a great majority of the buildings sustained such mode of damage had uniform settlements within tolerable limits and were safely habitable following the earthquake. The alignments of several others tilted slightly or moderately, were effectively adjusted later (Bakır et al., 2004).

Reduction of seismic demand due to nonlinear soil response displays an obvious potential that can be exploited for innovative future engineering applications. On the other hand, strong mat foundation appears to be a fundamental requirement for any realistic engineering approach aiming at utilization of this potential advantage. Therefore, the need is obvious for a practical methodology, through which the seismically induced ultimate foundation displacements can be estimated reasonably, so that they can be checked to be whether acceptable from the point of post-earthquake serviceability. Thus, the available beneficiary effects can be retained, while any unnecessary counter measures are avoided. Based on the experience gained in Adapazarı and Mexico-City cases, tilting mode of foundation displacements has a greater potential of adverse effect regarding post-earthquake serviceability of building structures. In Adapazarı cases, buildings that experienced excessive tilts during the earthquake are observed to have poor aspect ratios (i.e., relatively greater building height with respect to foundation width). However, the criterion for a limiting aspect ratio, which forms the basis for the potential of excessive foundation tilting, is unclear. In case a simple methodology to estimate the tilting potential for conventional building structures is provided, it can be possible to limit the aspect ratio of the building, so that foundation failure mode will be restricted to horizontal translation and vertical settlement modes. This will make the utilization of foundation soils as a natural base-isolator mechanism possible.

1.2. Literature Review

A brief review of the literature covering the relevant background for the development of a simplified approach aiming at estimation of foundation displacements under seismic loading conditions for the case of surface foundations is presented. Available cases in Adapazarı and Mexico-City are shortly discussed in order to clarify the object of study.

1.2.1. Investigations of Adapazarı cases

Sancio et al. (2002) presented geotechnical data, obtained from site explorations in Adapazarı (Bray et al. 2001a). Generally, two typical types of soil deposits are observed to be responsible of excessive foundation displacements: the dominant type of deposit is the nonplastic silts and sandy silts, generally consistent with the Chinese criteria (Seed and Idriss, 1982); the other type is the silt-clay mixtures with low penetration resistance. In the aforementioned study, geotechnical properties of those deposits are evaluated mainly in the perspective of the Chinese criteria, which state that soils with LL<35, w_n>0.9LL, and having the percentage of very fine particles (i.e., diameter less than 5μm) less than 15% are susceptible to significant strength loss during earthquakes. However, the mechanism leading to the strength loss is unclear, and no relationship with the intensity of shaking is specified. Utilizing the damage survey data, they also concluded that, no relationship existed between the magnitude of settlement and the foundation width, which is in contradiction with sand-liquefaction cases observed in past earthquakes. Also, the reported tendency of increase in settlements as the number of stories increase implies the significance of influence of building mass and height on foundation settlements. In addition, Bray et al. (2001b) provided detailed geotechnical information for two cases in Adapazarı with excessive foundation displacements, with silt clay mixtures dominating the subsoil conditions. Detailed geotechnical site investigation data for 12 similar cases compiled from Adapazarı are presented in the Internet (Bray et al. 2001a) where supplementary information is also given in the study Bray et al. (2004). These constitute a part of the cases utilized in this study, and are referred to as PEER cases.

Yasuda et al. (2001) compiled survey data regarding foundation displacements from Adapazarı and compared it to the liquefaction cases from Niigata and Dagupan city. The database consisted of information on number of stories, building width, foundation settlement, and angle of tilt of foundation. It appears that, the settlements of buildings in Adapazarı were in general, much smaller than those in Niigata and Dagupan city, despite the fact that the story numbers are significantly higher in Adapazarı. An important observation from plots of tilting angle versus settlement for foundations is that, although the tilting angle tends to increase with increasing settlement for Dagupan city and Niigata cases, no

such trend exists in Adapazarı data. Finally, foundation soils in Adapazarı cases consist by and large finer deposits (mainly silt) compared to Dagupan City and Niigata cases (mainly sand). These findings imply that the mechanism behind the foundation displacements in Adapazarı is quite possibly not related to liquefaction phenomena.

Pekcan (2001) performed cyclic triaxial tests on undisturbed samples, consisting of silt-clay mixtures of variable proportions obtained from PEER sites. All samples were isotropically consolidated, and no initial shear stress was applied before cyclic tests. Undrained cyclic loading rate was selected as 1 Hz for compatibility with seismic loading rates. Pekcan reported that Adapazarı silt-clay mixtures can be identified as liquefiable, in case the liquefaction is defined by the same criteria as applied to sands: accumulation of pore-pressure ratio (r_u) of 100%, or development of 5% double amplitude axial strain. It is also reported that the pore-pressure build-up in silty clays and clayey silts is slow when compared to sands and non-plastic silts. Low to medium plasticity silty clays can develop significant pore pressures under relatively high cyclic stress amplitudes and reasonable number of cycles. Also, cyclic resistance of silts and clays is reported to increase with decreasing void ratio and increasing plasticity index (PI).

However, the mechanism leading to the accumulation of cyclic strains is not rigorously investigated in the study by Pekcan (2001): the reported pore pressure ratios are not the residual values when undrained load amplitude is zero, but the maximum values obtained at cyclic load peaks. Hence, for the tests for which the liquefaction was reported to occur based on the r_u=100% criterion, pore pressures are observed to bounce back to considerably low levels during the reversal of cyclic loads. This observation may lead to the conclusion that, the “excessive” pore pressure ratios are mainly due to elastic response of the specimen, and the net effect on effective stresses can be relatively small. Ishihara (1996) reports that the strain accumulation mechanism for fine soils is different from conventional loose sand-liquefaction mechanism: In nearly all of the experiments, double-amplitude maximum strain levels are observed to increase consistently for each successive load cycle, up to the end of experiment, without displaying any significant jump in strain accumulation rate. In comparison, considering liquefaction of loose sands, no significant increase in cyclic strain levels occurs up to the instant of liquefaction, at which the strain accumulation rate suddenly increases due to the plastic flow

initiated. Besides, the isotropic initial load condition, which in fact is not representative of the stress state beneath building foundations, is utilized in the study (Figure 1.1).

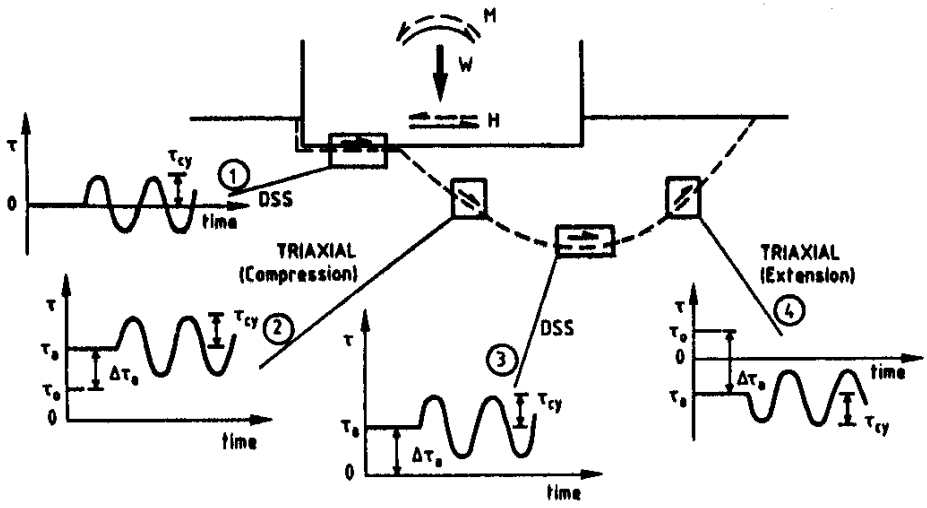

Figure 1.1. Idealized load conditions for selected locations on failure plane, for a foundation under inclined and eccentric load (Andersen and Lauritzsen, 1988).

Besides the cases reported by PEER, Karaca (2001) reported additional cases with excessive foundation displacements, which is utilized in this study, and is referred to as METU cases. The data consists of measured displacements, CPT and SPT logs, soil index properties, and cyclic triaxial test results for undisturbed samples. The cases were observed to be underlain by subsoil conditions altering between silt-sand mixtures to silt-clay mixtures. Excluding the nonplastic (NP) samples, all samples plot practically along the A-line in plasticity chart, implying a transition zone between silt (ML and MH) and clay (CL and CH). Cyclic test results were similar to Pekcan's. Karaca also states a tendency of increase in foundation settlements for heavier buildings.

1.2.2. Investigation of Mexico-City cases

Mendoza and Auvinet (1988) reported cases of excessive displacements of mat foundations, during the 1985 Mexico Earthquake. In extreme cases, the settlements are reported to exceed 1 m, and tilting in the order of 5º. Low foundation bearing capacity under static conditions, and relatively high load eccentricities of buildings under seismic loads led to the shear failure of foundation

systems during seismic loading. Before the earthquake, most cases were also subjected to various levels of consolidation settlements, implying rather compressible foundation soils. Utilizing two of such cases, Auvinet et al. (1996) proposed a simplified methodology to estimate seismically induced foundation settlements and rotations. The fundamental considerations of the methodology were soil-structure interaction mechanism, pseudo-static analysis of ultimate bearing capacity under seismic loads, and incremental accumulation of deformations due to exceedence of ultimate load capacity. However, uncertainties involved have a significant influence on the calculation results.

Zeevaert (1991) provided the mechanical properties of shallow deposits in Mexico City, on which the aforementioned foundation displacements occurred. These soils are highly compressible and sensitive silty clay deposits, starting at shallow depths, they reach in excess of 30 m. The water content can be as high as about 400%, as measured from natural samples obtained from those sites. Zeevaert reported that, when shear strength of natural samples are measured under stress conditions similar to those of field, significant cohesion is observed. This would imply a preconsolidated soil behavior, yielding relatively high peak shear strength compared to post-peak (i.e., critical state) strength. The specimens, when consolidated to stress levels considerably higher than field conditions, gave results consistent with zero cohesion (i.e., normally consolidated behavior), and effective angle of internal friction in the order of 26°-30°.

1.2.3. Simple methods for estimation of foundation displacements

Pecker (1998) proposes two possible approaches to investigate the dynamic bearing capacity of building foundations.

The first is the rigorous numerical analysis of the total soil-structure system. Such an analysis consists mainly of a realistic dynamic nonlinear analysis of the problem, and the numerical model should efficiently model the behavior of soil, structure, and their interaction. However, such an analysis would be rather costly and hence cannot be practically utilized for analyses of relatively simple structures. Full numerical analyses can only be utilized for the final stage of a design, since analyses for each design alternative will multiply the analysis cost. Hence, simple methodologies in order to provide estimations for different displacement modes of foundations (i.e., settlement, horizontal displacement, and tilting) are needed.

Similar to conventional foundation engineering problems, these methodologies can be restricted to general characteristics of foundations, such as shallow or deep.

The second type of approach consists of the simplified analysis of the system, in which the involved mechanisms can be decoupled for simplification purposes. Also, the mechanisms that are considered to be of secondary importance regarding response can be omitted. In practical geotechnical applications, load calculation procedures (i.e., calculation of load-history at a selected calculation point) can be decoupled from nonlinear behavior, and final plastic deformations can be estimated by utilizing calculated load-history independently. Yield load level for a system can also be analyzed by independent pseudo-static analyses, based on assumptions on distribution of inertial loads on soil-structure system.

Hence the second approach can be practically utilized, especially when uncertainty is significant in material properties. Such simplified approaches are commonly utilized for seismic design of earth dams and retaining walls in engineering practice, and may provide basic ideas regarding behavior in applications of foundation engineering: As an example, such methods utilized in seismic design of earth dams are based on sliding rigid block model proposed by Newmark (1965), as depicted in Figure.1.2. A widely utilized methodology is the Makdisi and Seed (1978) procedure, which combines the impact of dynamic response of a dam with the sliding block behavior in order to estimate final displacements. One of the most important conclusions for such analyses is that, in the case of pseudo-static factor of safety calculations, pseudo-static accelerations can be selected as considerably smaller values than peak accelerations, provided that small residual displacement levels can be accepted from the point of seismic performance (Seed, 1979; Hynes-Griffin and Franklin, 1984). There are also methods (e.g., Seed et al. 1973; Serff et al. 1976) based on the basic idea of Stress-Path method (Lambe, 1967; Lambe and Marr, 1979), such that, strain potentials for different sections of the dams are approximated based on cyclic laboratory tests. Load-histories applied in these tests are kept consistent with those calculated using a simple numerical model of the dam. Hence, these methods basically utilize the degradation behavior of cyclically yielding soil. In case of retaining walls, for which the displacements govern the behavior, Newmark sliding block analysis is applicable since governing sliding mode is in one direction (i.e.,

towards free face) only (Richards and Elms, 1979). Those methods were developed in the light of failure case studies following major several earthquakes; they provide valuable insight for development of simple design procedures, and verification by rigorous numerical analyses (e.g., by transient nonlinear-dynamic analyses) can be achieved at final stage of design.

For the case of shallow mat foundations, several approaches have been proposed by various authors. Sarma and Iossifelis (1990), and Richards et al. (1993), proposed methodologies of calculation to estimate settlements, utilizing a similar approach to Newmark sliding block analysis: The soil block and foundation resting on failure plane are assumed to behave as a single sliding block. Using empirical relationships based on statistics of sliding block analyses via actual earthquake records, it is possible to estimate final settlements without performing excessive analyses utilizing different acceleration-histories. Implicitly, the solution assumes a flow-rule for plastic deformation of foundations, validity of which limits the acceptability of the calculations: test results are needed for verification. Auvinet et al. (1996) also utilized a similar approach in order to estimate foundation settlements as well as foundation tilting. Considering the significance of building response on load-histories acting on foundation, the dynamic force-history acting on foundation level is calculated utilizing linear soil-structure-interaction (SSI) approaches.

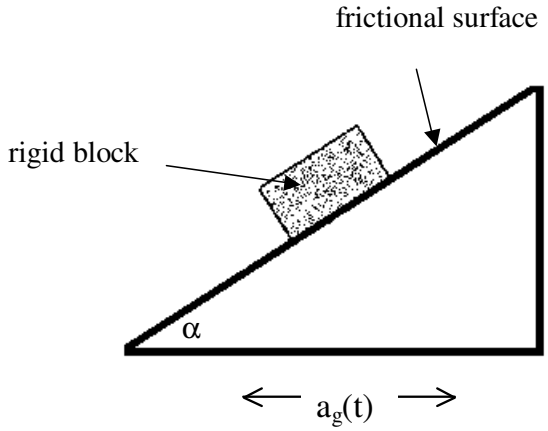

Figure 1.2. Sliding block analogy used for estimation of slope displacements during seismic loading (Newmark, 1965).

Although the aforementioned methodologies are based on either direct utilization of free-field time histories, or output of a linear SSI analysis as foundation input motion, Paolucci (1997) reported that, the force-history acting at foundation level can be significantly different for the case of nonlinear SSI. Discussing the potential weaknesses of approaches based on decoupling of building and foundation response, Paolucci proposed use of a 4-degrees-of-freedom (DOF) system for nonlinear dynamic analyses: 1 DOF for structural distortion, and 3 DOF for horizontal, vertical and rocking impedances of foundation (Figure 1.3). Only the foundation behavior is modeled to be nonlinear. Mass of the structure and mass of foundation are modeled by two lumped masses in the model. Soil (foundation) behavior is modeled as elastic-perfectly plastic, and both, the radiation damping and material damping are considered in linear-phase and yielding-phase of foundation motion. In calculation of foundation level plastic deformations, the yield function and plastic potential function proposed by Nova and Montrasio (1991), which considers impact of load eccentricity and inclination only (i.e., inertial load on soil body is ignored), is utilized. Comparing the approach by 2D FEM analyses, the foundation displacements were observed to agree with FEM results, except for the rocking mode. Based on parametric analyses, it is concluded that, when nonlinear foundation behavior is considered, the base-shear history transmitted by superstructure to foundation level can be quite different from the case of linear soil-structure interaction. The load eccentricity appears to be the main factor affecting the nonlinear response of shallow foundations under seismic loading. Spectral acceleration, when compared to PGA and Arias Intensity (I_A), is the best parameter in correlation with plastic foundation displacements.

Regarding the relevant experimental studies, Zeng and Steedman (1998) performed centrifuge tests in order to visualize the seismic bearing capacity failure mechanisms for the case of surface foundations resting on nonliquefiable soil. Buildings are modeled with tall (heavy) or short (light) blocks resting on dry or saturated soil. They experimentally demonstrated that, foundation rotation plays a significant role in seismic bearing capacity failure mechanism, and for the case of strain-softening soils, seismic bearing capacity calculations that are based on angle of friction dictated by the peak shear strength can be very unconservative. Soils can mobilize critical angle of friction when strain levels corresponding to peak strength is exceeded. Hence, irrecoverable foundation displacements can be

underestimated if calculations are based on peak-shear strength, rather than critical-state strength.

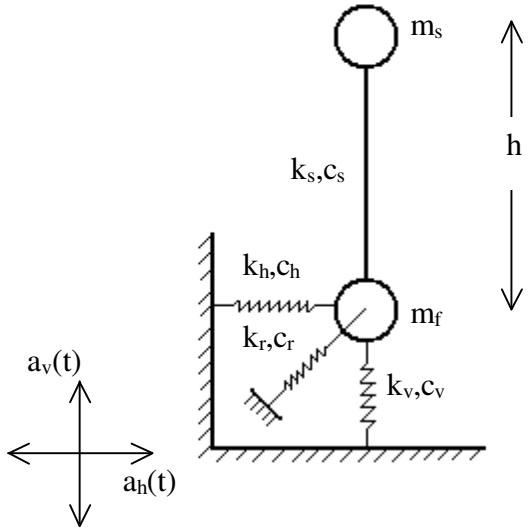

Figure 1.3. Simplified SSI model utilized by Paoulicci (1997): m_f and m_s are the lumped masses representing inertia of the building and foundation; k and c are the spring and dashpot coefficients; a_v and a_h are vertical and horizontal input acceleration-histories.

Prevost et al. (1981a, 1981b) investigated the deformation behavior of surface foundations under inclined and eccentric cyclic loading conditions by performing centrifuge tests and numerical analyses. However, the load-histories are of typical one-way loading, which are not consistent with realistic earthquake loading. Results of their studies reveal that, numerical models involving realistic constitutive models for soil behavior can be utilized to simulate the load-deformation behavior of foundations with sufficient accuracy.

For the case of fine-grained (nonliquefiable) soils, Yasuhara et al. (2001) proposed to utilize reduced stiffness modulus and shear strength in order to calculate immediate settlement of the foundations during seismic loading, by introducing these reduced parameters into static settlement formulations. The difference between settlement calculations performed utilizing reduced and non-reduced parameters gives the expected settlement during seismic loading. Consolidation settlements can be calculated by estimating pore-pressure increase

during seismic loading, and utilizing a seismic recompression index. A similar approach is also proposed by Andersen et al. (1988) for the case of offshore gravity structures exposed to storm (wave) loads.

1.3. The Objective and Scope of the Study

Based on the findings reported in literature and considering the limitations of previous studies, this study aims at development of a simple methodology to estimate tilting performance of structures having shallow mat foundations, resting on nonliquefiable soft soils. The methodology is based on utilization of elastic design spectrum pertaining to the site, and static bearing capacity of the foundation, both of which are quite easily determined through conventional procedures. The methodology can be utilized to detect the potential for excessive foundation tilting considering foundation aspect ratio for specified seismic demand and geotechnical conditions. The scope of the study is restricted by the followings:

1. Foundation soils are nonliquefiable, soft, fine soils. That is, foundations are safe against bearing capacity failure under static (vertical) loads, but can be driven to successive plastic flow under seismic (horizontal) loads.

2. Foundation subsoil can be practically assumed to be homogeneous and isotropic. Since the procedure is dependent on this assumption, reliability of the calculation procedure is limited with the significance of variation of the foundation subsoil from homogeneity.

3. Structures are multistory, freestanding buildings with no nearby building that may significantly affect the stability and seismic load demand on them.

4. Foundations are shallow mats with negligible depths of embedment.

5. Slope at building sites is practically zero.

The primary objectives of the study can be stated as follows:

1. Understanding of the behavior of normally consolidated silt-clay mixtures obtained from Adapazarı cases with excessive foundation displacements by performing undrained cyclic and monotonic triaxial tests on undisturbed specimens.

2. Formulation of a simple elasto-plastic SDOF system, adequately representative of the nonlinear soil-structure interaction.

3. Derivation of equations for utilization of elastic spectrum in order to estimate irrecoverable tilting demand on foundation.

4. Evaluation of the developed methodology utilizing available cases in Adapazarı and Mexico City.

Development and evaluation of the methodology is presented in the proceeding several chapters, where in the beginning of each, a brief literature survey relevant to the specific chapter context is presented.

The first chapter, which is the present, consists of the objective and scope of the subject, and the literature review that reveals the statement of the engineering problem and the fundamental mechanisms involved.

In the second chapter, results of cyclic and monotonic triaxial tests performed on undisturbed soil specimens obtained from Adapazarı are presented along with the engineering properties, sampling locations and depths. Additional data is also presented in the Appendix. The mechanisms that result in accumulation of relatively high strain levels for silt-clay mixtures under seismic loading conditions are discussed. The validity of elasto-plastic behavior assumption is evaluated accordingly.

In Chapter 3, simple linear SSI equations that couple the foundation and structural response are presented. By formulating the equation of motion in terms of total horizontal displacements, and introducing the nonlinear behavior for the foundation displacements, basic equations relating to the motion of nonlinear (elasto-plastic) single-degree-of-freedom oscillator model are derived, and simplified determination of natural period of this basic system is presented consequently.

In Chapter 4, the load capacity (i.e., maximum overturning moment) of a shallow strip foundation is formulated. Utilizing Plaxis, which is a finite-element analysis package for geotechnical applications, simple equations for the case of cohesive and cohesionless homogeneous soil conditions are determined, and compared with the available solutions in literature. Since the case studies consist of building structures resting naturally on consolidated soils, which behave in an undrained manner under seismic loading conditions, neither cohesive nor cohesionless soil assumptions are directly applicable. Hence, based on elasto-

plastic soil assumption, load-capacity equations for foundations resting on saturated, and consolidated under static foundation loads, are presented.

Outline of the methodology is given in Chapter 5. Since the proposed methodology is based on a number of assumptions, verification with available cases is important. Hence, utilizing the available cases from Adapazarı and Mexico-City, performance of the calculation methodology is investigated in Chapter 5. The significance of site response is also introduced.

Chapter 6 presents the conclusions of the study. The limitations of the methodology in practice, and possible future extensions of the study is also discussed.

CHAPTER 2

EXPERIMENTAL STUDIES

2.1. General

A through understanding of the behavior of silt-clay mixtures when bearing the foundation loads during severe seismic loading is necessary for development of a simplified calculation procedure, as stated in Chapter 1. Accordingly, undisturbed soil samples obtained from the sites that were extensively investigated by Karaca (2001) are utilized for laboratory studies. The investigated sites predominantly consisted of fine-grained surface soils of low plastic nature (silt-clay mixtures), defined as silty clays (CL) or clayey silts (ML), according to the Unified Classification System. The information already documented by Karaca includes SPT and CPT data for boreholes opened at these sites. The soil profiles, SPT test results, and depths of extracted samples pertaining to the study by Karaca are presented in Appendix A, together with the plan-views of the sites with some modifications.

To investigate the undrained shear and deformation behavior of Adapazarı silt-clay mixtures, a series of monotonic and stress-controlled cyclic triaxial tests are performed in parallel on the natural soil specimens. The specimens were anisotropically consolidated to simulate the stress paths of soil elements at shallow depths beneath foundations, and tests were carried out for various combinations of initial static and subsequent cyclic shear stresses. Applied cyclic stress amplitudes and loading frequencies were selected as to be representative of the ranges relevant to the Adapazarı case during 17 August earthquake. Following cyclic loading phase, the samples were sheared to failure under rapid monotonic loading, to investigate the strength and deformability response under strong pulse loading during seismic shaking. Test results were evaluated utilizing a methodology developed as part of this study to estimate the irreversible strain accumulation due

to cyclic loads that exceed monotonic strength. Consequently, based on the implications of the results obtained, the possible mechanisms that might have led to the observed foundation displacements on silt-clay mixtures in Adapazarı are discussed.

2.2. Literature Review

Predictability of seismic response of foundations on silt-clay mixtures requires understanding of behavior of such materials under repeated loading. The samples tested in this study have PI values ranging between 7-25, and are tested by the triaxial apparatus. A brief literature review on cyclic loading behavior of low to medium plasticity silt and clay mixtures is presented in the following.

Cyclic behavior of silt-clay mixtures is relatively less studied compared to those of sandy soils. Pore pressure buildup and deformation characteristics of such soils under cyclic loading can be remarkably different from those of sands. Accordingly, the criteria used to define the liquefaction of sand may no longer be applicable for silt-clay mixtures (Perlea 2000, Guo and Prakash, 1999). The other important issue pertaining to fine soils that display cohesion is the strong dependency of strength and stiffness responses on the speed of loading. While the resistance of fine soils to deformation increases due to the inherent viscous behavior, which becomes more profound with the increasing speed of loading, they tend to become softer and weaker with the increasing number of cycles as well. Hence, the overall response of fine-grained soils under dynamic loading is a combination of two distinct mechanisms, and their undrained strength under dynamic loading can be significantly higher or lower than the static strength depending on the characteristics of loading as well as material properties (Ishihara, 1996; Lefebre and LeBoueuf, 1987; Matešić and Vucetic, 2003; Procter and Khaffaf, 1984; Lefebvre G, Pfendler P., 1996). Based on the correlations of foundation displacements with the subsoil conditions in Adapazarı, it has been reported that the levels of foundation displacements were largely reduced with the increasing clay fraction in foundation soils (Sancio et al, 2002; Karaca, 2001).

Building foundations resting on fine deposits can displace due to two distinct mechanisms with regard to seismic loading: one, shear strain accumulation during loading phase due to successive bearing capacity failures; the other, development of volumetric strains induced by the dissipation of excess pore pressure (Andersen

et al. 1988a, Yasuhara et al., 2001). Degradation of soil stiffness and strength can be substantially influential over the seismic behavior of foundations. In the case of saturated soils, degradation of mechanical properties is dependent on the pore pressure increase induced by the cyclic loading. However, the seismic performance of saturated soil beneath a foundation can be significantly different from that of at free-field due to the sustained initial stress (Andersen et al., 1988b).

During cyclic loading, an important phenomenon that results in strength reduction for soils is the increase in excess pore-pressure. In the case of sands, the pore-pressure increase can occur relatively fast, leading to liquefaction for the case of loose sands. The cyclic stress ratio (CSR), defined as the ratio of amplitude of cyclic shear stress (τ_{cyc}) to (effective) initial confining stress (σ'_{v0}), is utilized as the principal parameter in laboratory tests for investigation of this phenomenon (Seed and Idriss, 1982). Whereas, for the case of clays, undrained shear strength of the specimen (S_u) can be the normalizing parameter in investigations of cyclic strain and pore-pressure accumulation, instead of σ'_{v0} for the case of sands (Ansal and Erken, 1989; Ishihara, 1996; Andersen et al., 1988a; Lefebre and Pfendler, 1996; Zhou and Gong, 2001). In addition, Procter and Khaffaf (1984) proposed use of monotonic shear strength obtained in rapid loading tests, with strain rates similar to seismic loading conditions. On the other hand, σ'_{v0} can still be the normalizing parameter utilized as in the case of sands (Andersen et al., 1988a; Hyde and Ward, 1985).

Average pore-pressure increase, which is defined as the residual pore pressure at the end of each full load cycle (i.e., at initial stress condition) is utilized in monitoring of pore-pressure accumulation during cyclic triaxial loading tests by Yasuhara et al. (1992), and Andersen et al. (1988a). This is compatible with calculation of post-cyclic loading consolidation, and determination of undrained strength reduction, since pore-pressure increase due to octahedral stress increase is recovered instantaneously at the end of cyclic loading. Similar to the case of sands (Tokimatsu and Seed, 1987; De Alba et al., 1975), formulations for pore-pressure increase due to cyclic loading are provided for clays (Ansal and Erken, 1989; Ohara and Matsuda, 1988; Matsiu et al. 1980; Hyde and Ward, 1985; Hyodo et al., 1994), which can be utilized when pore-pressure accumulation is of interest.

However, parameters should be determined by conducting cyclic tests on natural samples. In measurements of pore-pressure in cyclic triaxial test, Konrad

and Wagg (1993) reported that, pore-pressure distribution is not uniform in the specimen unless the loading rate is sufficiently low. For clayey silt specimens, a strain rate as low as 0.001%/s is required to obtain uniform pore-pressure distribution in sample. In case relatively high strain rates, the pore-pressures measured in the bottom or top end of the triaxial specimen is not representative of the pore-pressure value at the mid-sections of the specimen. Hence, in this case, the effective-stress plots of the test will provide a significant effective cohesion (i.e., c´) for the test specimen, but the effective angle of internal friction (i.e., Φ´) is not significantly affected from the rate of loading. On the other hand, Ansal and Erken (1989) discussed that, such low strain rates is not representative of earthquake loads, and viscous response of fine soils is significant under those loads. Hence, relatively high load frequencies (e.g., in the order of 1.0 Hz) during cyclic loading tests should be preferred, when simulating seismic loading conditions in laboratory tests.

Considering the average levels of developed pore pressure during stress-controlled cyclic tests performed over anisotropically consolidated cohesive soil specimens, the pore pressure ratio at failure is observed to decrease with the increasing amplitude of cyclic shear stress (Hyodo et al., 1994; Konrad and Wagg, 1993). This is due to the fact that, depending on the intensity of applied initial stress, the specimen can fail before the average pore pressure develops to a level to effect the soil stiffness and strength significantly. Accordingly, the cyclic strength and hence the excess pore pressure generation beneath a foundation during seismic shaking would be further limited with the increasing initial stress induced by the structure while residual settlements due to successive bearing capacity failures accumulate. For comparison, in the free-field case, where instantaneous settlements would not normally occur at level ground during seismic shaking, post-earthquake settlements can be of significance since larger excess pore pressures are generated than in the case beneath a foundation (Yasuhara, 2001).

Post liquefaction consolidation behavior of silty clays is similar to the reloading behavior of over-consolidated clays: due to increase in pore-pressures, effective stresses decrease, leading the soil to a preconsolidated state. Hence, similar to conventional consolidation calculations, post-cyclic loading consolidation can be estimated utilizing recompression (C_r) index for cyclic loading. However, due to severe seismic loading, the recompression index can be somewhat higher

(e.g., in the order of 50%) than the recompression index determined through one-dimensional compression tests (Yasuhara et al., 1992, Ohara and Matsuda, 1988; Hyodo, 1994; Yasuhara, 1994). Hence, considering the magnitude of compression index (C_c) with respect to that of recompression index (C_r), consolidation settlements due to seismic loading appear to be of minor importance. This statement is consistent with the results of centrifuge and shaking-table tests that model buildings resting on liquefiable saturated sand deposits, such that the excess pore-pressure ratios beneath the building foundations are much less compared to those at free-field, and while a great majority of the settlements occurs during the shaking, only a negligible portion occurs afterwards (Yoshimi and Tokimatsu, 1977; Whitman and Lambe, 1982; Liu and Dobry, 1997; Hausler and Sitar, 2001).

When accumulation of cyclic strains under isotropic stress conditions, and stress levels below monotonic shear strength are considered, the stiffness degradation (i.e., secant stiffness during loading) of clayey soil can be expressed by the degradation index δ_D, such-that, for a strain-controlled test,

$$\delta_D = \frac{\tau_N}{\tau_1} \tag{2.1.a}$$

or, stress-controlled test,

$$\delta_D = \frac{\varepsilon_1}{\varepsilon_N} \tag{2.1.b}$$

where, for a strain-controlled test τ_N is the stress amplitude at the end of N^{th} cycle and τ_1 is the stress amplitude at the end of 1^{st} cycle. Similarly, for a stress-controlled test ε_N is the strain amplitude at N^{th} cycle and ε_1 is the strain amplitude at the end of 1^{st} cycle. The relationship between number of cycles and degradation index is proposed as,

$$\delta_D = N^{-t_d} \tag{2.2}$$

where, t_d is the degradation parameter, which is dependent on OCR and PI: High plasticity and overconsolidated clays degrade at a much slower rate than low plasticity and normally consolidated clays (more linear behavior). Also, t_d is

observed to be dependent on shear strain amplitude (γ_c) in cyclic simple shear test with zero initial shear (Vucetic and Dobry, 1988; Ishihara, 1996; Idriss et al. 1978). Hence, for stress levels below monotonic shear strength, degradation in secant modulus during each successive load cycle is proportional to the logarithm of number of load cycles (N). This will result in monotonically decreasing rate of stiffness degradation with the increasing number of load cycles. A representative plot is provided in Figure 2.1 for the case of strain-controlled test, as proposed by Ishihara (1996).

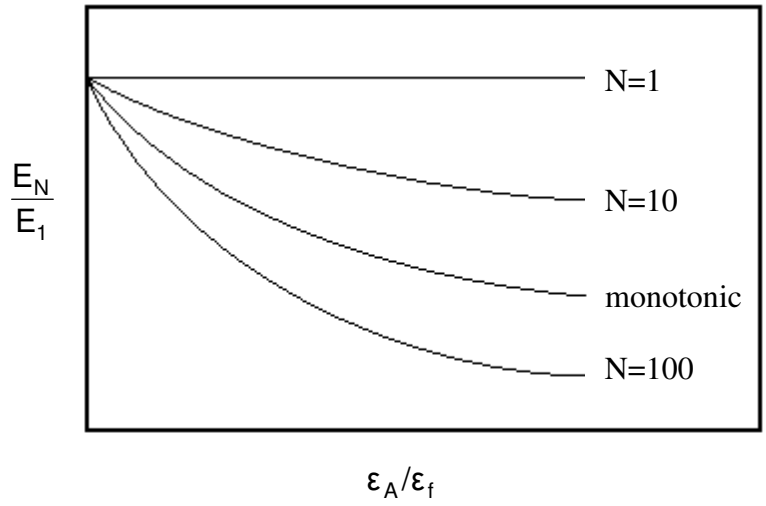

Figure 2.1. Typical degradation curves by Ishihara (1996): ε_f and ε_A are the strain amplitude at failure (due to monotonic loading test) and in cyclic loading respectively, and E_N and E_1 are the deformation modulus at N^{th} and 1^{st} cycles respectively.

As shown in Figure 2.1, the difference in the modulus of deformation between rapid (N=1) and static (monotonic) loading depends on the magnitude of shear strain, and this difference of the modulus becomes more pronounced as the level of strain increases. Ansal et al. (2001) reported similar findings for the case of stress-controlled cyclic tests, which are consistent with the relationship in equation 2.1.a, by utilizing cyclic simple shear test on normally-consolidated, organic, fat marine clays.

The behavior is investigated by Hyde and Brown (1976): stress-strain behavior of silty clays under cyclic loading is very similar to that under creep loading. Thus, using creep test results, strain accumulation under dynamic loading can be estimated by numerical integration of accumulated creep strains under given load amplitudes with time, provided that correlation between strain rate, time and load amplitude is determined using creep tests; this relation is observed to be logarithmically linear, explaining the logarithmic degradation behavior as proposed by equation 2.2.

Above definition of degradation index can be practically used for regular cyclic loading conditions. On the other hand, earthquake load-histories are very irregular in nature. Thus, a manipulation is necessary to estimate degradation under irregular loading condition. A detailed study, which is based on extensions over Masing Rules, is presented by Vucetic (1990), and can be utilized for estimation of degradation effect due to repeated loading. However, verification of such degradation models are provided for simple-shear stress conditions (i.e., unidirectional loading), which can be practically utilized for one-dimensional problems. Considerations due to changes in orieantation of plane of maximum shear are unclear.

Influence of soil properties such as plasticity index, void ratio and clay content as well as the fabric and aging on the cyclic behavior of silt-clay mixtures is not very clear at the present stage (Guo and Prakash, 1999; Matešić and Vucetic, 2003). Taking into account the multitude of factors affecting the cyclic response, testing appears to be inevitable for proper understanding of the seismic performance of such deposits in specific cases. On the other hand, due to the major difficulties in accurately replicating the fabric of field conditions through reconstituted laboratory specimens, use of undisturbed samples is a necessity. Pre-existence of shear stresses on the planes of maximum applied stress should be given consideration, as shear stress reversal is an important factor in liquefaction triggering and evolution of strength degradation with accumulated displacement (Perlea, 2000; Lefebvre and Pfendler, 1996).

There exist two different test patterns for stress-controlled cyclic triaxial tests, as defined by Ishihara (1996). The first is the two-way loading, during which the specimen is subjected to successive compression and extension type of loading, so that the deviator stress can have both negative and positive values. This type of

loading results in full stress-reversals on failure plane, which may have a significant effect on strength or stiffness degradation of the material. The second pattern is the one-way loading, in which the application of load cycles results in only compression or extension type of loading, without reversals of stress on failure plane. The deviator stress has negative or positive values throughout a cycle. In both of the tests, initial shear can be applied through an undrained or drained stress-path, depending on the relevant stress history.

Normally-consolidated clay specimens under two-way and one-way loading behave quite differently. A clay specimen under two-way cyclic loading exhibits the so called cyclic mobility: the specimen undergoes plastic-flow during the cyclic test, except when stress conditions are returned to initial (average), whereas a specimen under one-way does not. Specimens under two-way loading are observed to proceed to critical state line (CSL) faster than specimens under one-way compression loading, implying a faster rate of degradation. In two-way tests with zero average deviator stress (i.e., residual), although stress amplitudes in positive and negative directions are symmetrical during two-way loading, considerable average (residual) shear strain can still accumulate, since the undrained shear strength of the specimen in extension is lower than the compression strength. Hence, in extension period of the cyclic load, the stress levels will be relatively closer to failure state, when compared to compression period (Yasuhara et al., 1992; Konrad and Wagg, 1993; Andersen et al, 1988). Thus, double amplitude shear strain criterion can not be commonly used for either of the two types of cyclic loading, since during two-way loading the cyclic strain is predominant where the average shear strain is relatively small, and, during one-way loading average shear strain is decisive contrary to the cyclic shear strain. Furthermore, the decrease in cyclic strength occurs more appreciably in the two way loading then in the one way-loading conditions (Yasuhara et al., 1992, 2001; Andersen et al., 1998). Similar observations were also reported from tests on clays with simple shear apparatus, where stress reversal causes higher rate of strength degradation; in tests with initial shear stress, stress reversal effects are minimized, resulting in a lesser degree of strength degradation (Lefebre and Pfendler, 1996).

Based on the review of literature and the discussions in Chapter 1, one-way loading cyclic triaxial tests are accepted essentially as the basis for tests of this study. Stress-paths beneath a building with poor aspect ratio are assumed to be

similar to triaxial compression test, as illustrated in Figure 1.1. Initial shear stress is applied through a drained stress-path, assuming that the soils beneath building foundations were fully consolidated, before being subjected to seismic loading. Hence, specimens are anisotropically consolidated during consolidation stage of consolidated-undrained (CU) triaxial tests. Cyclic loading is applied consecutively in an undrained manner, to simulate seismic loading conditions. In order to visualize its effect on cyclic degradation, two-way loading tests are also performed. The monotonic shear strength is of major importance in understanding the behavior of fine soils, and is a fundamental parameter utilized in foundation design practice. Hence, simultaneous monotonic shear strength tests are performed in parallel, keeping consolidation stresses the same for corresponding cyclic and monotonic tests. Volumetric strains that might occur following dynamic loading is out of scope of the testing program, since such strains are considered to be relatively insignificant due to stress conditions beneath a building foundation. Hence, the results of laboratory tests are considered to be representative of the cases involving foundation displacements.

2.3. Testing Methodology

Shear and deformation characteristics of Adapazarı silt-clay mixtures are studied through a series of undrained monotonic and stress controlled cyclic triaxial tests. The tests were carried out on the undisturbed specimens, representative of foundation soils, sampled from depths of 2-4.5 m. The specimens are obtained from the sites of cases of Karaca (2002), details of which are presented in Appendix A.

The cyclic triaxial tests are performed by utilizing the Geonor cyclic triaxial test apparatus, with the contribution of Onur Pekcan. Details of the apparatus, including the loading and data acquisition systems, are presented by Pekcan (2002). The sample preparation, consolidation, and saturation stages are as explained in the study. Only the differences from the Pekcan's study are presented here.

The first difference is the anisotropic consolidation applied following the initial isotropic consolidation stage. At the end of isotropic consolidation, the cell pressure valve is closed, and the axial pressure (q) is increased. Then the drainage valve is opened in order to initiate the anisotropic consolidation. At the cyclic loading stage,

these loads are removed, and pneumatic actuator is set to the target initial deviator stress level. The actuator cycled around this stress level depending on the amplitude of the cyclic deviator stress. The second difference is due to the interest to simulate a representative state of the post-seismic shaking stability of these soil specimens with relevance to the effects of shaking on soil strength. To this purpose, at the end of each cyclic test, samples were brought back to the anisotropic stress-state of pre-cyclic loading and kept for about five minutes under undrained conditions to observe whether an imminent state of failure exists or any deformations occur due to possible substantial loss of strength during cyclic loading. This phase is presumed to simulate the post-cyclic stability of the buildings. With a few exceptions, the applied initial stress is considerably large, when compared to the monotonic shear strength of the specimens.

The third difference is that, no volumetric strains are measured following the cyclic test stage, which simulates the consolidation settlement of the buildings after the seismic loading. Instead, as the final stage for those samples tested cyclically, they are sheared under rapid monotonic loading (in about 2 seconds) with a range of stress rates between 10–160 kPa/s. The objective is to observe the effect of more pronounced viscous response on the apparent strength increase under strong pulse loading on soils subjected to seismic shaking. This stage, in essence, simulates the effect of a strong pulse acting on soil, after the action of a strong seismic-loading history.

Depending on the sampling tube diameter, two or three soil samples with initial dimensions of 36 mm diameter and 71 mm height were extruded side by side from the same level in a tube. In view of the highly heterogeneous nature of surface soils of the Adapazarı basin, such that the engineering properties can vary to a large extent even in a single tube, samples thus obtained are presumed to consist of identical material and considered to form a set. Samples in each set are consolidated under similar initial isotropic and subsequent anisotropic stress conditions, so as to follow comparable stress paths to the long-term pre-earthquake condition of the soil elements beneath foundations. Following consolidation phase, one of the samples in each set is subjected to triaxial monotonic compression test, while the remaining sample(s) are tested cyclically. Utilizing the pore pressure parameter B_S (i.e., B in the original study) defined by

Skempton (1954), the relationship between the pore-pressure increase under isotropic undrained stress increase and parameter B_S can be expressed as,

$$B_S = \frac{\Delta u_{pore}}{\Delta \sigma_r} \tag{2.3}$$

where Δu_{pore} is the change in pore-pressure, and $\Delta \sigma_r$ is the change in isotropic pressure (i.e., change in cell pressure). B_S values of about 0.95 were provided before proceeding with the tests, for verification of the validity of the full saturation assumption.

During monotonic tests samples were sheared to failure with a strain rate of 1%/min, consistent with the standard testing procedures specified by ASTM for undrained testing. Stresses applied corresponding to the nine monotonic triaxial tests performed, each representing a set, are presented in Table 2.1 along with the plasticity indexes of the samples. The corresponding borehole and sampling depth information is also provided in Table 2.1, compatible with the information in Appendix A.

Table 2.1. Summary data for monotonic strength tests.

Monotonic test number	$(\sigma_3)_c$ (kPa)	$(\sigma_1)_c$ (kPa)	$(\sigma_1-\sigma_3)_f$ (kPa)	Δu_f (kPa)	PI	Borehole ID	Sampling Depth (m)
1	60	90	171	12	14	GE-1	2.2
2	70	100	118	18	25	GE-1	2.2
3	80	120	189	18	13	GE-1	6.3
4	80	120	123	1	8	GE-2	2.3
5	60	140	165	6	22	GE-2	2.3
6	40	140	123	2	19	GD-2	2.0
7	80	200	193	8	19	GD-2	2.0
8	100	205	217	7	7	GA-2	4.0
9	50	170	170	0	10	GA-2	4.0

$(\sigma_1)_c$ = major principle stress during consolidation;
$(\sigma_3)_c$ = minor principle stress during consolidation;
$(\sigma_1-\sigma_3)_f$ = deviator stress at failure;
Δu_f = pore pressure increase at failure.

Utilizing the results of monotonic loading tests, Figure 2.2 summarizes the deviator stress ratio q/p´ at failure against plasticity index (PI), where p´ is the effective mean principal stress,

$$p' = \frac{\sigma_1' + 2\sigma_3'}{3} \qquad (2.4.a)$$

and, q is the deviator stress,

$$q = \sigma_1 - \sigma_3 \qquad (2.4.b)$$

where, σ_1 and σ_1' are the total and effective major principal stress, σ_3 and σ_3' are the total and effective minor principal stress acting on the specimen. Details on the monotonic tests are presented in Appendix B. Considering the strain levels at yielding during monotonic loading, and the bulging type of behavior during yielding, the membrane effect on the measured deviator stresses are approximated to be in the order of 10 kPa. Hence, ignoring apparent cohesion increase due to membrane effect, and the possible apparent cohesion due to rate of loading in monotonic tests, the friction angle at failure (Φ') can be calculated by the formula (Azizi, 2000),

$$q = \frac{6\sin\phi'}{3 - \sin\phi'} p' \qquad (2.5)$$

Hence, by reducing the q values by 10 kPa due to membrane effect, the q and p' values at failure are compared with failure lines corresponding to Φ'=26°, 30° and 34° in Figure 2.3. Considering also possible apparent cohesion due to strain rate effect, the values of Φ′ are estimated to be around the value of 30°. However, the trend of Φ′ for lower PI values reduces to values considerably lower than 30°, implying that, for the case of nonplastic fine soils, the monotonic shear strength can be considerably low. Since, it was not possible to obtain undisturbed soil specimens for this range, the monotonic shear strength values for these soils are somewhat unclear. Recovery of undisturbed samples from low-strength nonplastic fine soil deposits requires special sampling techniques. Therefore, similar monotonic shear-strength tests for this range are left as a future study for Adapazarı cases. However, the impact of possible lower Φ' values will also be discussed in this study, when investigating the specific Adapazarı cases.

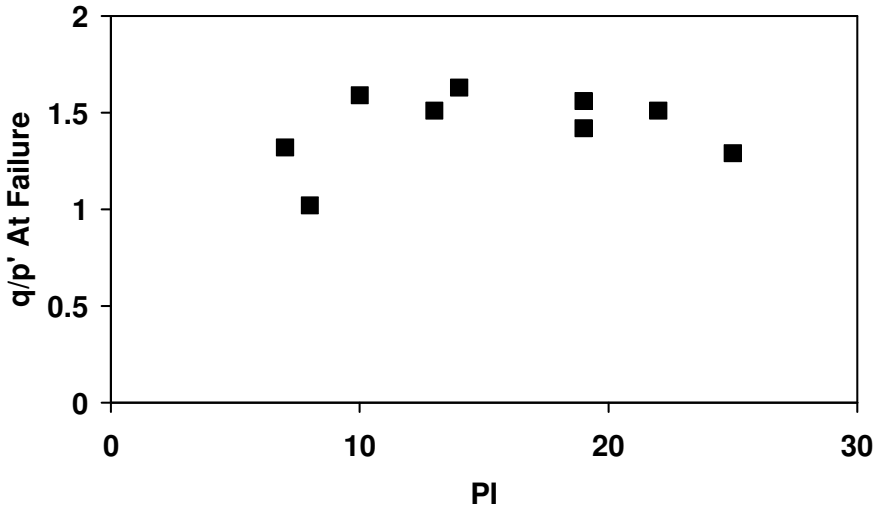

Figure 2.2. Ratios of effective mean principal stress to deviator stress at failure in monotonic triaxial tests versus plasticity index.

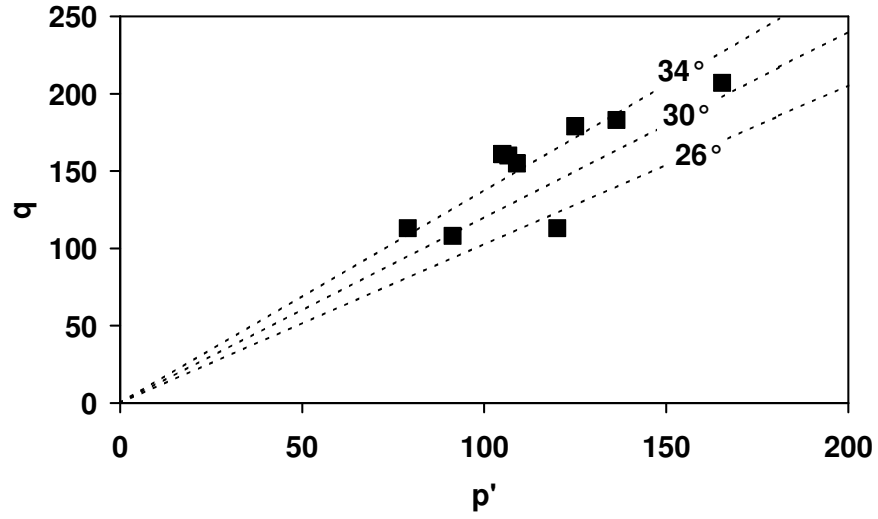

Figure 2.3. Measured p' and q at failure in monotonic triaxial tests are compared with different Φ' values via equation 2.5: q values at failure are reduced by 10 kPa due to membrane effect.

The data regarding the Atterberg limits of the tested samples is plotted in Figure 2.4. All samples are observed to be transition material between ML and CL on the plasticity chart. Accordingly, the tested soils, which are not definitely either clay or silt, are referred in this study as “silt-clay mixtures”.

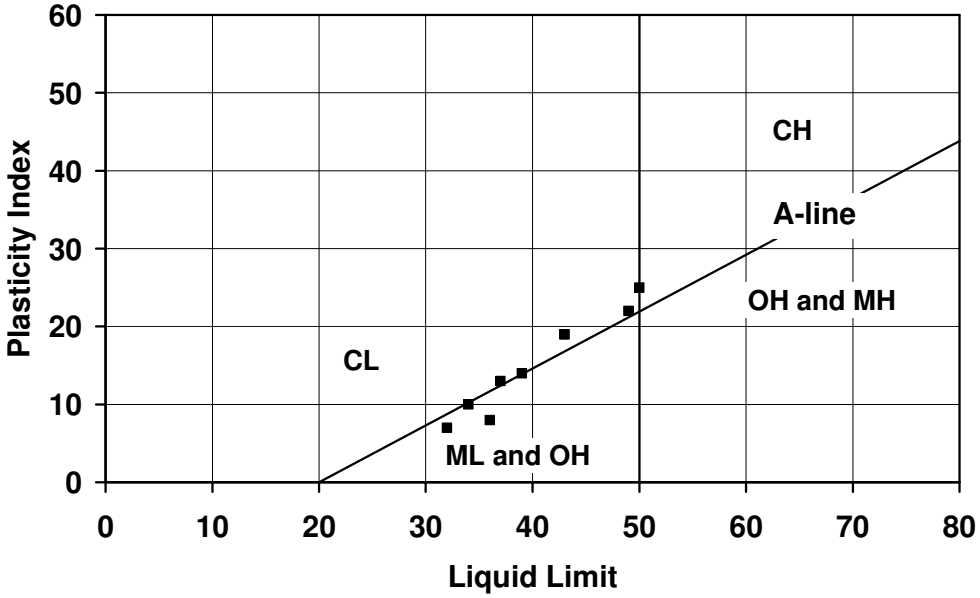

Figure 2.4. The Atterberg limits of the tested specimens.

In cyclic tests, majority of the samples were subjected to one-way (compression only) cyclic loading with peak stresses exceeding or remaining below the monotonic strength, since this load form is presumed to have dominated the soil-foundation system response during shaking. On the other hand, to be able to discuss the effects of extension type of loading and the impact of successive stress reversal on soil behavior as well, a number of tests with two-way cyclic loading (i.e., deviator stress cycled between negative and positive values) were also performed. Considering the expected frequency content characteristics of surface motion during 17 August earthquake on the alluvial basin in Adapazarı, sinusoidal cyclic axial loads were applied with frequencies of mostly 1.0 Hz and alternatively 0.5 Hz, so that the viscous behavior of soil is properly reflected in response. Cyclic triaxial test conditions are summarized in Table 2.2: The first two letters in test name specify the USCS soil type for the specimen. The monotonic test number is the corresponding ID number for the monotonic test. Plots pertaining to both cyclic and monotonic loading tests are presented in Appendix B. In Table 2.2, $\Delta\sigma_{cyc}$ is the amplitude of the cyclic deviator stress applied on the specimen, σ_{max} is the maximum deviator stress level applied on the specimen during the cyclic test, σ_{mon} is the monotonic strength of the specimens, which is utilized as the normalizing parameter for σ_{max} in this study, N_{cyc} is the number of load cycles, f_{cyc} is the

frequency of cyclic load, ε_a is defined as the total irrecoverable axial strain accumulated during cyclic loading stage (compression direction is positive). CSR is the cyclic stress ratio, conventionally utilized for soil liquefaction and formulated as,

$$CSR = \frac{\Delta\sigma_{cyc}}{(\sigma_1)_c + (\sigma_3)_c} \tag{2.5}$$

where, $(\sigma_1)_c$ and $(\sigma_3)_c$ are respectively the major and minor principal stresses applied during the anisotropic consolidation stage. For the case of isotropic consolidation (i.e.,$(\sigma_1)_c = (\sigma_3)_c$), equation 2.5 will reduce to the classical form of CSR definition for cyclic triaxial tests (Ishihara, 1993)

Table 2.2. Summary of the cyclic triaxial test conditions (the first two letters in test name specify the USCS soil type for the specimen).

Test	Monotonic test number	$\Delta\sigma_{cyc}$ (kPa)	$\frac{\sigma_{max}}{\sigma_{mon}}$	N_{cyc}	CSR	f_{cyc} (Hz)	ε_a (%)	Δu_{cyc} (kPa)
CL0106	1	80	0.64	13	0.53	0.90	2.8	32
CL0218	2	64	0.80	16	0.38	0.76	-2.5	18
CL0321	3	62	0.54	7	0.31	0.94	-7.3	10
CL0324	3	30	0.37	18	0.15	0.91	1.4	21
ML0409	4	63	0.84	9	0.63	1.06	-2.4	45
ML0410	4	86	1.02	7	0.43	1.07	-8.3	75
CL0516	5	94	1.05	15	0.47	1.04	5.6	25
CL0518	5	82	0.98	25	0.41	1.03	2.4	10
CL0608	6	73	1.41	15	0.41	1.04	3.6	6
CL0717	7	62	0.93	41	0.22	1.03	1.2	7
CL0705	7	85	1.06	12	0.30	0.94	0.4	5
CL0709	7	53	0.90	26	0.19	0.93	0.6	20
ML0811	8	82	0.86	43	0.27	0.88	1.4	47
ML0812	*	82	1.54	17	0.38	0.93	8.9	40
ML0813	*	84	1.55	27	0.38	0.53	17.3	72
ML0924	9	84	1.20	32	0.38	0.94	3.3	50
ML0929	9	87	1.22	32	0.40	0.43	7.2	0

* Samples (PI=7) are preferred to be tested cyclically to observe the frequency effect, and monotonic strength is estimated as 125 kPa from Figure 2.4.

2.4. Test Results and Initial Observations

Distinct trends are observed in the cyclic behavior of samples regarding axial strain accumulation, depending on whether the applied loading is one-way or two-way. The other essentially influential factor over deformation behavior was the respective levels of maximum and minimum deviator stresses applied during cyclic testing. Test results, representative of the general trends are presented in Figures 2.5.a-d, where monotonic compression, cyclic and consequent rapid loading responses are superposed for each relevant set of samples for easier visual perception. Remaining test results are presented in Appendix B.

In the case of one-way loading with the applied peak stress exceeding monotonic strength, consistent with the observations of Konrad and Wagg (1993), plastic strains are observed to accumulate with almost a constant rate for each cycle after few initial cycles. Accordingly, plots similar to Figure 2.5.a are obtained from such tests. Whereas in the case of peak cyclic stress remaining below monotonic strength, plastic strains still occur in each cycle; however, the incremental strain amplitudes per cycle are much smaller and tend to decrease rapidly with increasing number of cycles, consistent with those trends cited in literature (Hyodo et al. 1994, Hyde and Brown, 1976; Mitchell and King, 1977; Andersen et al. 1980), except that the tests are terminated before reaching the number of load cycles for which the instability (i.e., rapid increase in strains) is triggered. Hence, after a few cycles the plastic strain increment per cycle reduces practically to none; and when compared, for a specific number of cycles, to the tests in which the maximum cyclic deviator stress exceeds the monotonic strength, the accumulated plastic strain remains negligibly small. Figure 2.5.b illustrates the typical result from such tests. No significant cyclic degradation (i.e., ultimate load capacity) was observed in stiffness and strength of the samples tested under one-way loading conditions, even in cases in which the monotonic strength is exceeded.

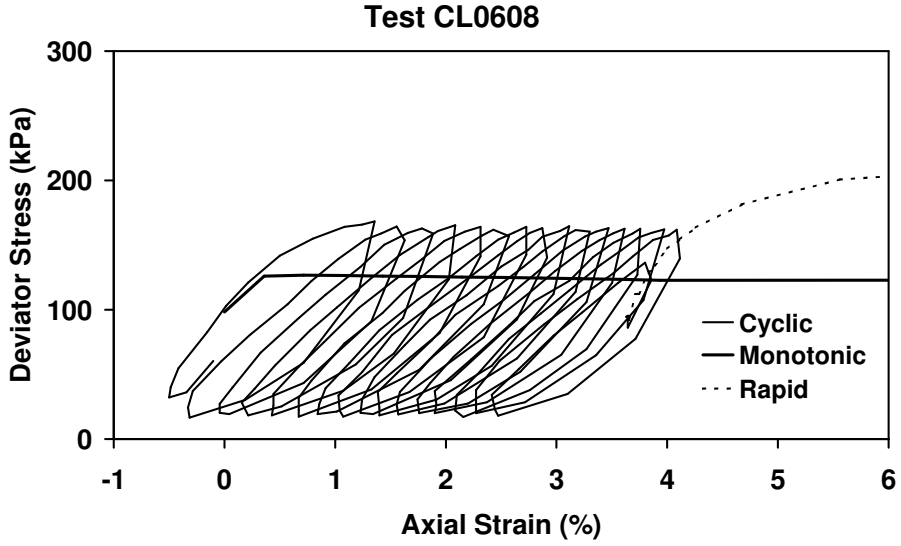

(a)

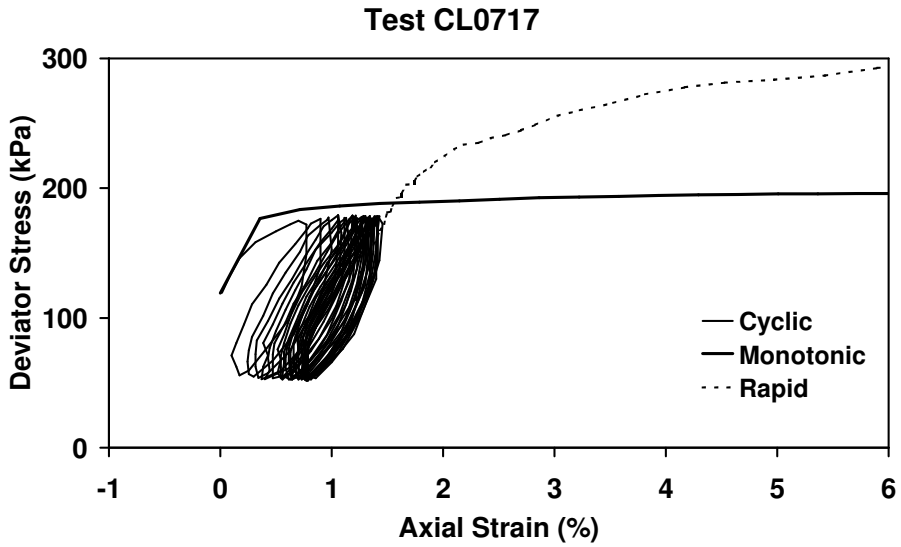

(b)

Figure 2.5. Stress-strain responses representative of distinct trends observed in cyclic triaxial tests with corresponding monotonic and rapid compression triaxial test results: (a) one-way compressive loading with peak axial stress exceeding monotonic strength, (b) one-way compressive loading with peak axial stress remaining below monotonic strength, (c) two-way loading with specimen cyclically failing in compression, (d) two-way loading with specimen cyclically failing in extension.

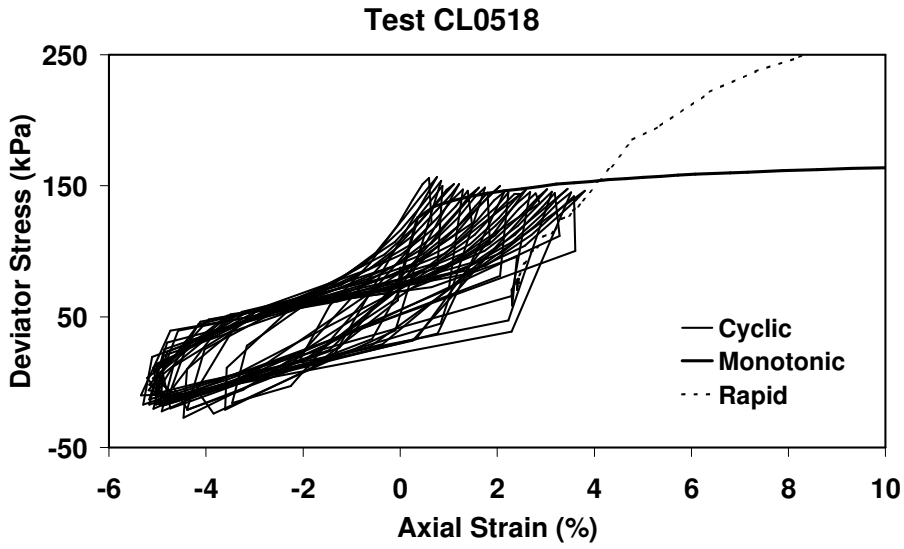

(c)

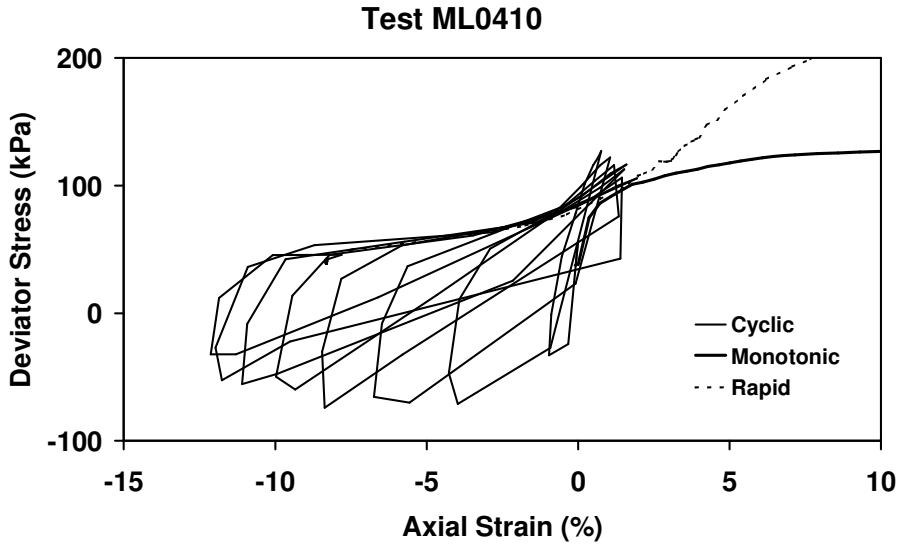

(d)

Figure 2.5 (continued).

In the case of two-way loading, the specimens are observed to display a "strain memory:" That is, during loading and unloading stages, the strain history targeted the values of maximum past strains in compression and extension, respectively, and the incremental irreversible strains occurring in each additional

cycle are added to those of previous. Accordingly, based on the maximum and minimum levels of deviator stress applied during a test, the specimen can develop incremental cyclic strains in compression and/or extension, corresponding representative plots of which are presented in Figures 2.5.c and d. Specimen stiffness is observed to vary through a transition zone between compressive and extensional behavior segments in this group of tests. These results underline the dependency of undrained stress-strain response of cohesive soils on loading history, a systematic analysis of which under irregular shear loading is presented by Vucetic (1990).

Despite demanding cyclic load combinations applied in several of the tests, none of the samples in the series, subjected to either one-way or two-way loading, displayed a state of failure or even any limited deformations upon imposition of initial anisotropic state of stress following cyclic loading. This observation indicates that the soils, for which the tested samples are representative, were not likely to have been subjected to loss of strength due to seismic shaking, at levels such that the building foundations would experience post-shaking instability. The other noteworthy observation from Figures 2.5.a-d is that the apparent strength increase with reference to monotonic strength is significant in each case under rapid loading, applied as the final stage following the rest period after cyclic loading. Such behavior, which is peculiar to cohesive soils, can be explained considering the pronounced viscous response induced by the increased speed of loading.

An overall evaluation of the observed trends from the series of tests conducted over representative soil samples indicates that the relatively large permanent displacements of foundations situated over comparable soils are not possible, unless the capacity defined by monotonic strength is significantly exceeded during seismic disturbance. Whereas test results also indicate that the viscous behavior dominates the strength and plastic deformation accumulation response of these soils under loads with increased rates of application. Hence, any reasonable estimate of the degree of foundation displacements due to strong seismic shaking would necessarily depend on the information regarding soil performance beyond monotonic strength as well as the characteristics of the seismic load.

Figure 2.6 presents plots of peak axial strain development during one-way compressive cyclic tests in the series for which the monotonic strength is exceeded

by peak deviator stress. These plots display quite a wide range of strain accumulation characteristics, as they are representative of tests involving different soil samples, stress amplitudes and loading frequencies. Further investigation of the dependency of strain accumulation on such distinct factors is attempted in the following section through use of a methodology developed based on strain-rate and load history relationship.

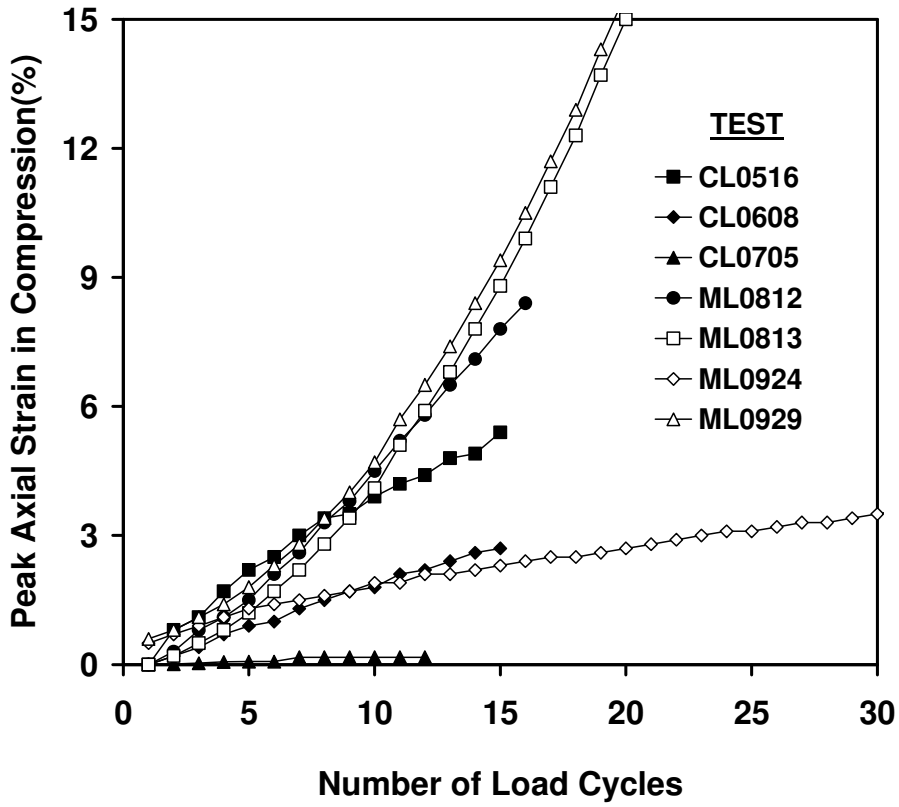

Figure 2.6. Peak axial strain development during one-way compression tests in which the monotonic strength are exceeded.

2.5. Plastic Strain Accumulation Due to Cyclic Loading

Hyde and Brown (1976) studied the sub-failure stress-strain-time relationships of reconstituted silty clays utilizing the similarity in the behavior of clay under repeated loading compared with that under creep loading. They concluded that the relationship between logarithm of strain-rate ($\ln(\dot{\varepsilon})$), applied stress (σ) and logarithm of time (ln(t)) can be simply expressed in the form:

$$\ln(\dot{\varepsilon}) = A + B\sigma + C\ln(t) \tag{2.6}$$

Thus, determining parameters A, B and C, accumulated strains can be estimated through numerical integration for a given load history of repeated loading for which the stress levels remain below monotonic strength. Test results provided by Vaid and Campanella (1977) made clear that clay behavior could also be represented by equation 2.6 for creep stresses exceeding monotonic strength, until eventual rupture.

In this study, the relationship expressed in equation 2.6 is presumed to be valid under load-histories ($\sigma(t)$) that exert stresses beyond shear strength, in the following modified form, in which the strain-rate does not explicitly depend on time:

$$\ln(\dot{\varepsilon}) = \alpha + \beta \cdot \sigma(t) \tag{2.7.a}$$

or,

$$\dot{\varepsilon}(t) = e^{\alpha+\beta\sigma(t)} \tag{2.7.b}$$

The modification is due to the fact that, when specimens are loaded below shear strength, the parameter C in equation 2.6 has negative values, implying that the strain-rate will tend to decrease in time; hence, accumulated strains will converge to finite values. Whereas in case the shear strength is exceeded, deformations would continue without a bound till failure (a predefined strain level of interest) of the specimen is reached. Clearly, the parameters α and β are dependent on the specimen mechanical properties associated with deformation response, as well as the characteristics of the imposed load. Accordingly, integrating equation 2.7, plastic strain due to loads exceeding monotonic strength can be estimated (or the role of various parameters on strain accumulation characteristics can be investigated) for specific cases, provided that the utilized soil specimens and testing procedures are comparable.

Parameters α and β can be determined based on rapid load test data through least squares fitting of equation 2.7 to part of the load history exceeding monotonic strength, for each test. The stress-strain variations and strain time histories, predicted using parameters thus determined are compared to those measured. Exemplary results are presented for two of the tests in Figure 2.7. Plots for

remaining test results can be found in Appendix B. Based on the results, it is concluded that, under imposed rapid loading, the deformation behavior of a sample beyond monotonic strength can be represented appropriately by the two parameters. Corresponding values of α and β calculated for the set of rapid load test data are plotted in Figure 2.8 to observe any interdependency between the two parameters. Despite scatter, which can largely be attributed to variations in sample properties and loading speed in the data set, the two parameters are clearly observed to be dependent.

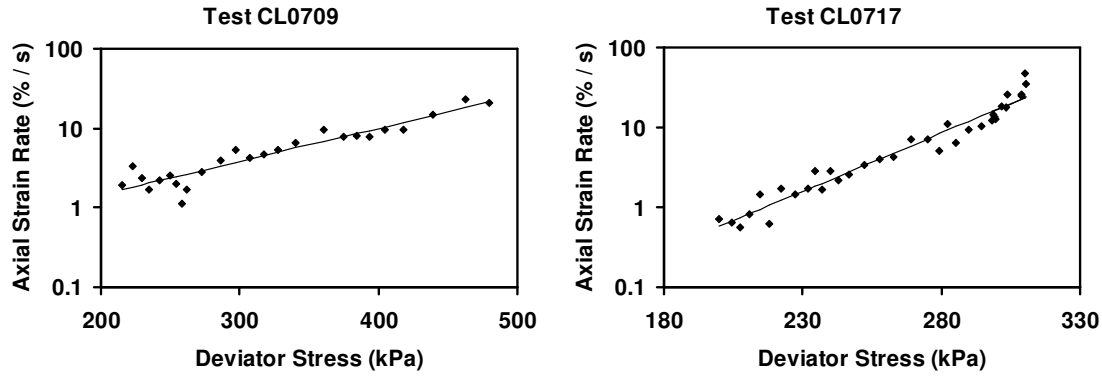

(a)

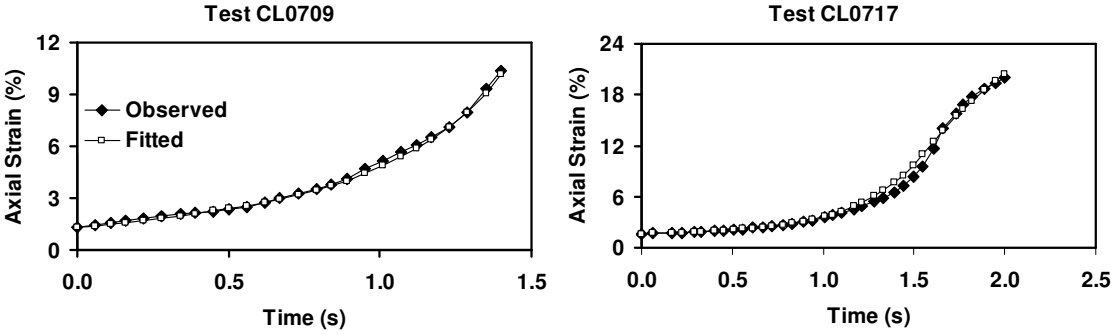

(b)

Figure 2.7. Examples of rapid load test simulation: (a) least squares fit of Equation 2, (b) comparison of fitted and observed strain-time histories, (b) comparison of fitted and observed stress-strain variation.

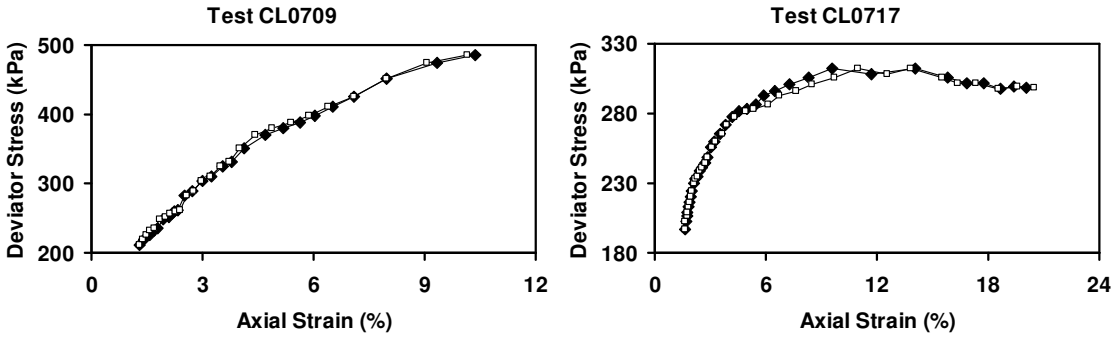

(c)

Figure 2.7 (continued).

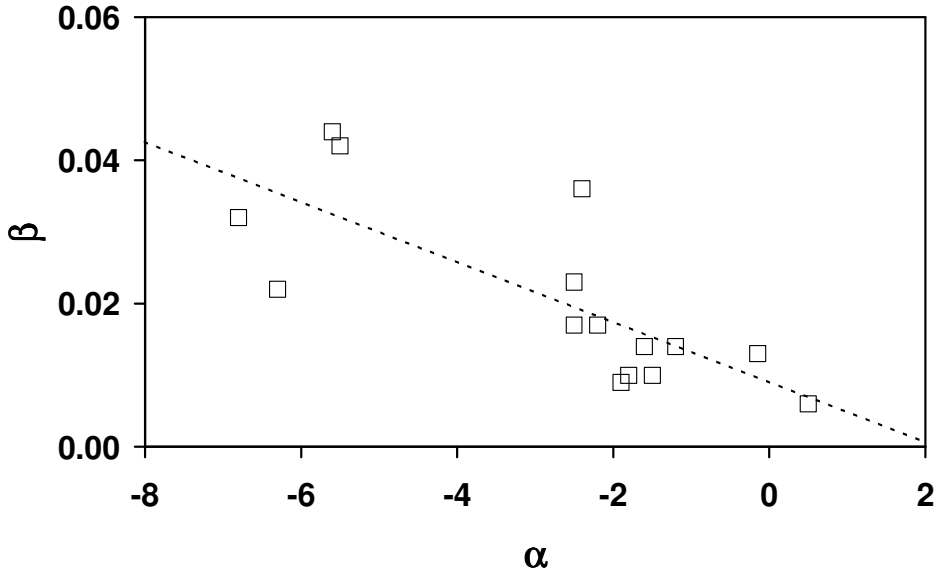

Figure 2.8. Relationship between α and β parameters calculated from rapid load test data.

Effects of soil properties on the strain rate can be investigated utilizing shear strength as the normalizing parameter so as to remove any dependency of the α and β parameters on the stress range. Accordingly, the two parameters were obtained from a regression analysis of the data representative of 1.5 times the monotonic strength, an arbitrarily selected factor. Corresponding strain rates calculated using equation 2.7 are plotted against plasticity index and water content in Figure 2.9.a and 2.9.b, respectively. With significant scatter existing in either case, trends, though not very distinct, are visible. The tendency of increase in

strain rate with increasing plasticity index, observed in Figure 2.9.a, is contradictory to the expectation that the soils with higher plasticity index will behave more viscous, displaying higher apparent strength increase under rapid loading. On the other hand, in Figure 2.9.b, the axial strain rate increases with increasing water content, which is proportionally related to void ratio in the case of saturated samples. This trend is in conformance with that would be expected: As the void ratio increases, soils become less viscous, and thus deform relatively faster under rapid loading. However, it is to be emphasized that the observed trends cannot be generalized, as the samples tested within the scope of this study are all low plastic and that they plot along A-line on the plasticity chart (Figure 2.4). The rather wide range of strain rates in Figure 2.9 shows that, depending on loading and material characteristics, specimens may develop insignificant amounts of irreversible strains, or may rapidly accumulate large amounts when stressed above monotonic strength for relatively short durations.

Plastic strain accumulation due to a cyclic load can be estimated integrating equation 2.7, if the contribution from part of the load remaining below monotonic strength is regarded as negligible:

$$\varepsilon(t_2) - \varepsilon(t_1) = \int_{t_1}^{t_2} e^{\alpha+\beta\sigma(t)} dt \qquad (2.8)$$

where t_1 and t_2 are the instants between which the monotonic strength is exceeded by the imposed deviator stress in a load cycle. A cyclic load history having a nonzero average value (σ_{ave}) can be defined as

$$\sigma(t) = \sigma_{ave} + \sigma_{cyc} \cdot \sin(\omega t) \qquad (2.9)$$

Then, plastic strain accumulation per cycle is given by

$$\varepsilon(t_2) - \varepsilon(t_1) = \int_{t_1}^{t_2} e^{\alpha+\beta(\sigma_{ave} + \sigma_{cyc}\cdot\sin(\omega t))} dt$$

or,

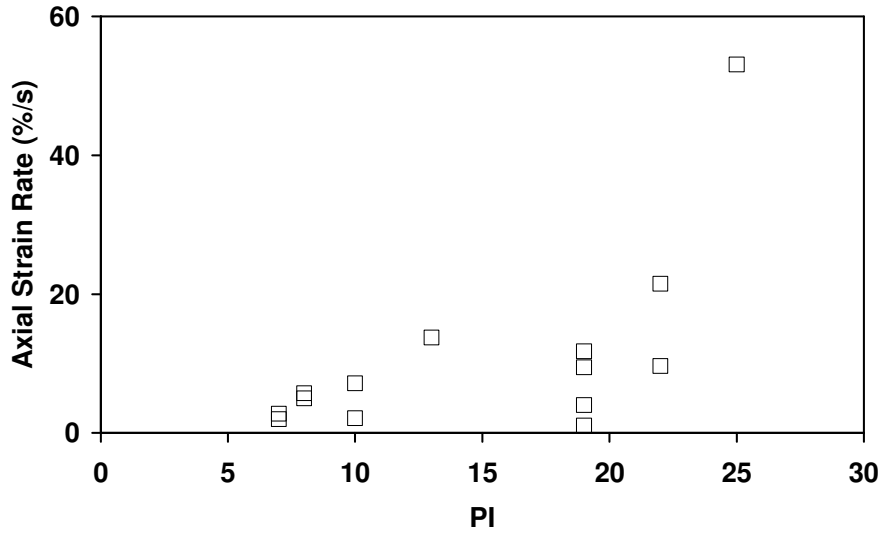

(a)

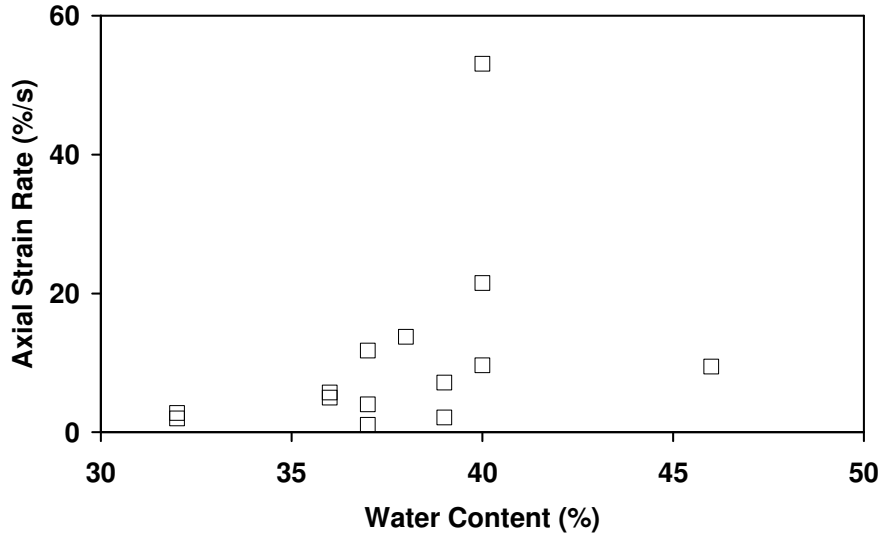

(b)

Figure 2.9. Relationship between axial strain rate calculated at deviator stress level of 1.5 times the monotonic strength and (a) plasticity index, and (b) water content.

$$\varepsilon(t_2) - \varepsilon(t_1) = e^{\alpha+\beta\sigma_{ave}} \int_{t_1}^{t_2} \left(e^{\beta\sigma_{cyc}} \right)^{\sin(\omega t)} dt \qquad (2.10)$$

Referring monotonic strength as σ_{mon}, t_1 and t_2 can be expressed as follows:

$$t_1 = \frac{1}{\omega}\arcsin\left(\frac{\sigma_{mon} - \sigma_{ave}}{\sigma_{cyc}}\right) \qquad (2.11.a)$$

and,

$$t_2 = \frac{\pi}{\omega} - t_1 \qquad (2.11.b)$$

Thus, since the integrated function is symmetric around π/2ω, equation 2.10 takes the form

$$\Delta\varepsilon_{cyc} = 2 \cdot e^{\alpha+\beta\sigma_{ave}} \int_{t_1}^{\pi/2\omega} \left(e^{\beta\sigma_{cyc}}\right)^{\sin(\omega t)} dt \qquad (2.12)$$

Equation 2.10 can be evaluated through numerical integration, and then, the parameters α and β can be determined by back calculation using equation 2.12 and cyclic test data. Owing to the time independency assumption regarding α and β, reliability of these parameters depends on the similarity between the characteristics of the presumed load form and those of the cyclic tests. Also, due to the logarithmic nature of equation 2.7, strain rate can be very sensitive to small variations in α. Accordingly, the formulated approach can be utilized as an engineering tool serving to distinguish major behavioral differences between different soils under dynamic loads exceeding monotonic strength and to evaluate the impact of viscous behavior on the foundation performance.

It is of interest to investigate the significance of stress range on plastic strain accumulation. To this purpose, by means of the transformation $\bar{t} = t \cdot \omega$, equation 2.12 is modified into the following form:

$$\Delta\varepsilon_{cyc} = \frac{2}{\omega} \cdot e^{\alpha+\beta\sigma_{max}} \int_{\bar{t}_1}^{\pi/2} \left(e^{\beta\sigma_{cyc}}\right)^{(\sin(\bar{t})-1)} d\bar{t} \qquad (2.13.a)$$

or,

$$\Delta\varepsilon_{cyc} = \frac{2}{\omega} \cdot f(\alpha, \beta, \sigma_{max}) \cdot g(\sigma_{cyc}, \beta, \bar{t}_1) \qquad (2.13.b)$$

where, σ_{max} is the maximum stress applied during cyclic testing (i.e., $\sigma_{max}=\sigma_{ave}+\sigma_{cyc}$), and,

$$f(\alpha,\beta,\sigma_{max}) = e^{\alpha+\sigma_{max}\beta} \tag{2.14}$$

$$g(\sigma_{cyc},\beta,\bar{t}_1) = \int_{\bar{t}_1}^{\pi/2} \left(e^{\beta\sigma_{cyc}}\right)^{(\sin(\bar{t})-1)} d\bar{t} \tag{2.15}$$

$$\bar{t}_1 = \arcsin\left(\frac{\sigma_{mon}-\sigma_{ave}}{\sigma_{cyc}}\right) = \arcsin\left(\frac{\sigma_{mon}-\sigma_{ave}}{\sigma_{max}-\sigma_{ave}}\right) \tag{2.16}$$

Plots of function *g* containing the data range of the performed rapid load tests are presented in Figure 2.10 as a function of dimensionless parameter $\bar{t}_1$. It is observed that the function is relatively insensitive to variations in $\bar{t}_1$, except for near $\bar{t}_1 = 0$ and $\bar{t}_1 = \pi/2$ (i.e. where σ_{ave} is very close to monotonic strength, and σ_{max} marginally exceeds the monotonic strength). Hence, within the range where it is relatively insensitive, function *g* can be reasonably approximated with coarse estimates, and plastic strain accumulation will be more critically dependent on the function *f* defined by equation 2.14.

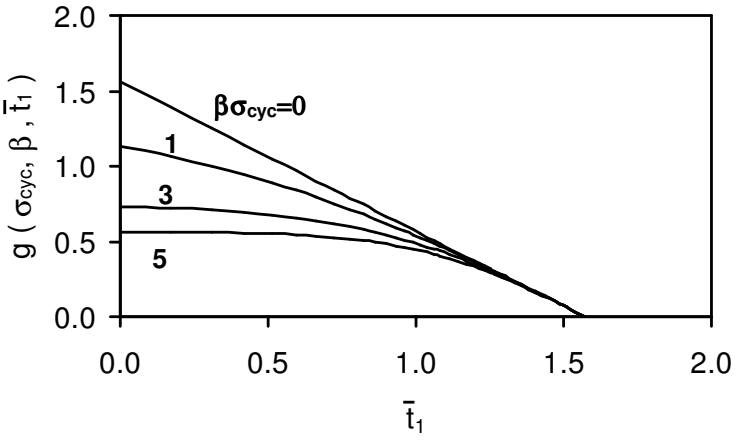

Figure 2.10. Variation of function *g*.

Outlined procedure appears to require at least two cyclic tests that simulate stress levels and loading rates of the presumed shaking to obtain a set of α and β parameters. However, depending on the equivalence of the parameters obtained from cyclic and rapid loading tests, a parameter set can alternatively be determined through consequent cyclic and rapid load tests performed over a single specimen. Such an approach can be convenient regarding sample availability and heterogeneity in the case of natural soils, as well as providing economy and speed in testing. Due to the limitations of the test data, parameter equivalence can be investigated here, through comparison of α values obtained from series of cyclic tests in which the monotonic strength is exceed, and consecutive rapid load tests. Figure 2.11 presents the comparison based on back-calculated values of α tabulated in Table 2.3. Although the loading patterns as well as existing load histories before initiation of each type of test are radically different, values are seen to be consistent with only minor deviations. This result also implies the dependency of seismic soil performance on the viscous response.

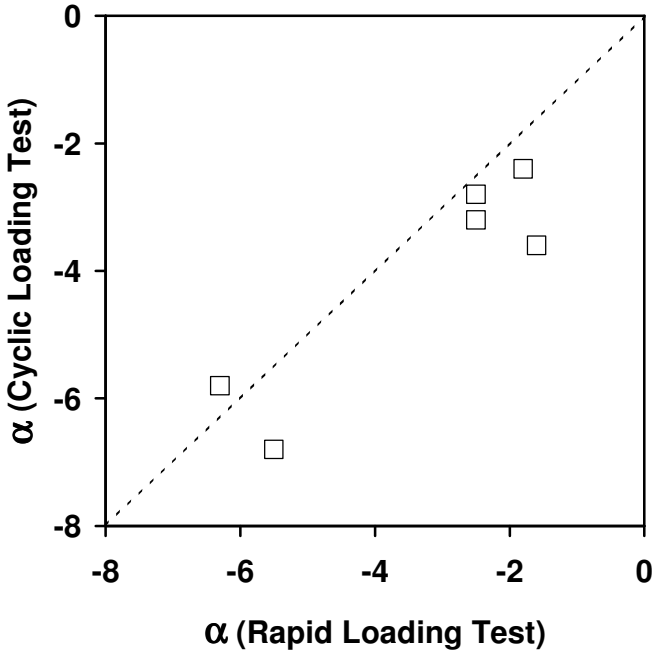

Figure 2.11. Correlation of α parameters calculated from cyclic and rapid load test data.

Table 2.3. Back calculation of α parameters from results of cyclic tests in which the monotonic strength is exceeded.

Test	average $\Delta\varepsilon_{cyc}(\%)$	ω (rad/s)	T_1	$\beta\cdot\Delta\sigma_{cyc}$	g	f	α	β
CL0608	0.24	6.5	0.45	3.1	0.69	1.1	-6.8	0.042
CL0705	0.033	5.9	1.2	1.9	0.39	0.25	-5.8	0.022
ML0812	0.52	5.9	0.12	1.4	1.0	1.5	-2.8	0.017
ML0813	0.64	3.3	0.22	1.4*	0.96	1.1	-3.2	0.017
ML0924	0.10	5.9	1.0	2.3	0.54	0.54	-2.4	0.010
ML0929	0.22	2.7	0.79	1.2	0.69	0.43	-3.6	0.014

* Parameter β of test ML0812 is utilized due to non-availability of rapid loading test.

As an application of the proposed methodology, plastic strain accumulation per cycle due to a hypothetical test is calculated for the six cases in which the samples were stressed beyond monotonic strength during cyclic tests. Relevant α and β parameters are those provided in Table 2.3. For the hypothetical test, average and peak deviator stresses are set to 0.5 and 1.5 times the monotonic strength, correspondingly, and period of load cycles is set to 2 s. Calculated plastic strains per cycle are presented in Figure 2.12. Despite differences in load histories and test conditions, plastic strain accumulations are seen to be comparable, indicating comparable deformation characteristics for these samples. This is not unexpected, however, considering that all the samples are representative of sites of observed foundation displacements, and that they plot on the low plastic side in a very narrow range around A-line on the plasticity chart (Figure 2.3).

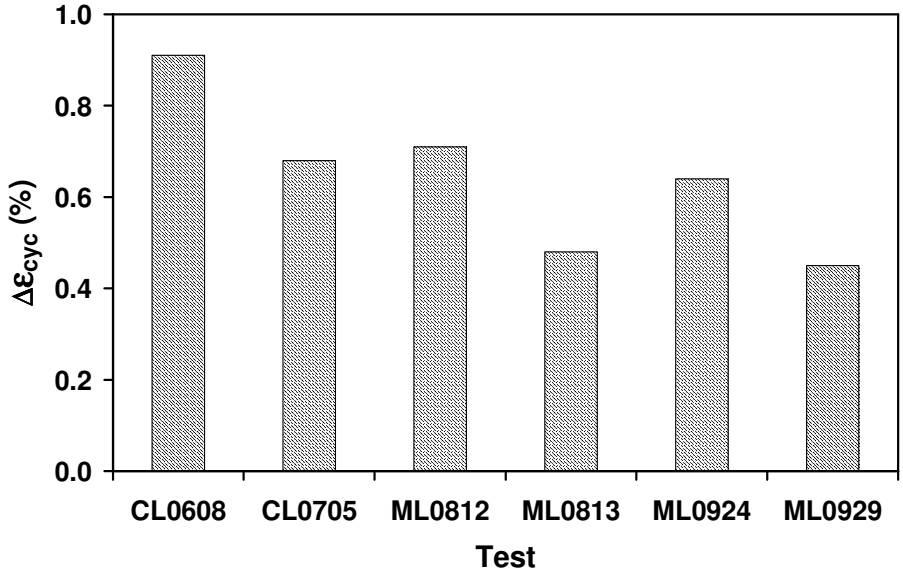

Figure 2.12. Estimated plastic strains per load cycle for a hypothetical test for which $\sigma_{ave} = 0.5\sigma_{mono}$, $\sigma_{max} = 1.5\sigma_{mono}$ and $\omega = \pi$ rad/s.

2.6. Observed Dilatancy During Plastic Flow

The dilatancy angle is important in calculations of ultimate foundation bearing capacity, as will be discussed in Chapter 4. For non-associative flow rule, the plastic strain rate for perfectly plastic material can be expressed as (Davis and Selvadurai, 2002):

$$\dot{\underline{\varepsilon}}_p = \lambda \frac{\partial g_p}{\partial \underline{\sigma}} \tag{2.17}$$

where, $\dot{\underline{\varepsilon}}_p$ is the plastic strain rate matrix, g_p is the plastic potential function defined as a function of the components of the stress matrix $\underline{\sigma}$, and λ is a positive multiplier. For the plane strain condition and Coulomb yield criterion, the plastic potential function can be defined as:

$$g_p = \sigma_{yy} - J\sigma_{xx} \tag{2.18}$$

where,

$$J = \frac{1+\sin\psi}{1-\sin\psi} \tag{2.19}$$

Here, Ψ is the angle of dilatancy. In case Ψ=Φ′, the flow rule will be associated. For values of Ψ different from Φ′ the flow rule will be non-associated. Hence, for the plain-strain case, the volumetric strain rate during plastic flow is,

$$\dot{\varepsilon}_v^p = \lambda(1 - J) \tag{2.20}$$

The volumetric strain rates can be determined from consolidated-drained tests, by measuring the quantity of water sucked into the specimen. However, the volumetric strain rate can not be directly measured during undrained tests. On the other hand, the pore-pressure measurements during undrained tests can be utilized to observe the signifcance of dilatancy during yielding.

In case of consolidated-undrained (CU) tests, if the specimen dilates (i.e., the volume of the specimen tends to increase), then the pore pressures will tend to decrease during plastic flow (Ortigao, 1995). For investigation of change in pore-water pressure during yielding, the pore-pressure readings (u_{pore}) during monotonic shear strength tests are normalized with the deviator stress increase (Δq) during undrained phase, and plotted in Figure 2.13. It is observed that, no significant tendency for volume decrease exists, implying that $\dot{\varepsilon}_v^p \cong 0$, or Ψ≅0 can be presumed for further practical discussions. On the other hand, in estimations of bearing capacity based on perfect plasticity, the assumption of Ψ=0 provides conservative ultimate load capacity for the foundations, and this issue is discussed in Chapter 4 in detail.

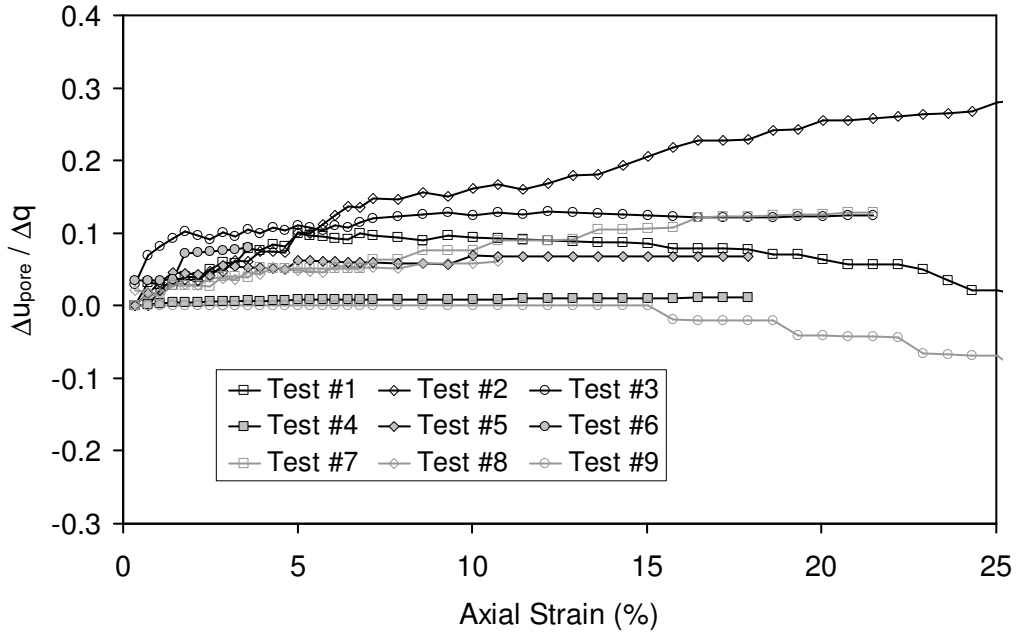

Figure 2.13. Change in pore-pressure (Δu_{pore}), normalized by deviator stress increase (Δq) during undrained phase in monotonic loading tests.

2.7. Conclusions

Among other factors, the highly variable characteristics of alluvial sediments underlying the city of Adapazarı evidently played a major role in the occurrence of peculiar building foundation displacements associated with the 17 August earthquake. Results of the series of tests performed over low plastic silt-clay mixtures which dominate the studied sites of foundation displacements show that, under means of dynamic loading comparable to that of 17 August earthquake, and considering stress paths beneath buildings, these soils do not display any trends that can be interpreted as "liquefaction," regarding stiffness and strength response. Their cyclic strain accumulation characteristics, however, critically depend on the relative level of peak cyclic stress with regard to the monotonic shear strength: While plastic strains can rapidly accumulate at practically constant rates per cycle in case the monotonic strength is exceeded, they tend to remain insignificantly small, otherwise. Substantial increases of apparent strength observed during rapid loading tests reflect the pronounced viscous nature of these soils under loads with increased rates.

With reference to the seismic foundation response on soils of comparable characteristics, these results imply that substantial permanent displacements are not likely to occur, unless the foundation capacity defined by monotonic strength is exceeded during seismic shaking; whereas the residual strain accumulation response beyond the capacity would depend upon viscous soil response. These implications also explain the observed dependency of occurrence and severity of foundation displacements on the clay content of foundation soils, that relate to viscous soil response, as well as on factors (such as story number and foundation aspect ratio) that relate to seismically induced foundation loads and seismic vulnerability of structure-foundation systems.

The viscous response of the soils for stress levels exceeding the monotonic strength level is considered as reserve strength for design purposes. This is due to the fact that, viscous response parameters calculated may not be directly utilized, since they can be dependent on the test procedures (i.e., triaxial testing). Further studies are required in order to relate the viscous parameters to actual foundation behavior. Thus, the soils are assumed to obey Mohr-Coulomb failure rule, with no further reserve load capacity due to viscous response. Still, the deformation behavior depends on the parameters such as angle of dilatation (Ψ), which is observed to be nearly 0º during monotonic shear strength tests performed in this study. As it will be discussed in Chapter 4, bearing capacity calculation procedures involve significant uncertainty, even under static load conditions. The pore pressure measurements during cyclic loading tests are not reliable, since the rate of loading does not permit pore-pressures in the specimen to be distributed uniformly. Still, in all tests, no sudden increase in strain accumulation rate is observed during the cyclic loading phase, which implies that liquefaction of the specimens due to pore-pressure increase does not occur. The effective friction angle at critical state is measured to be about 30°, somewhat compatible with the shallow silty clay deposits of Mexico City, as reported by Zeevaert (1991). However, more specimens are required to estimate shear-strength of nonplastic fine-deposits, which can have effective angle of friction values lower than 26°. This is left as a future study.

To conclude with, dependency of cyclic plastic strain accumulation response of Adapazarı silt-clay mixtures on soil properties is investigated utilizing the methodology developed as part of this study. No particularly distinct trends were

observed regarding strain accumulation properties for the tested samples, all of which are low plastic and cluster around A-line on the plasticity chart. Recognizing that these samples are representative of foundation displacement sites, the variability of viscous soil behavior under dynamic loading, and its consequences on seismic foundation performance cannot be thoroughly identified without similar testing of soils representative of sites where no such displacements were observed in the city. This is also left as a future study.

CHAPTER 3

SOIL-STRUCTURE-INTERACTION CONSIDERATIONS

3.1. General

As discussed in Chapter 1, the rigorous analysis of nonlinear soil-structure-interaction (SSI) is too complicated and costly to utilize in simple design. Hence, a methodology that is based on simplified SSI approaches is to be developed. In this study, simple multistory buildings resting on shallow mat foundations are considered (Figure 3.1). The buildings are assumed to be excited by vertically incident SH waves, which results in free-field surface motion history $u_g(t)$. Linear SSI equations can be presumed to be applicable for the cases of low intensity ground motion in which the building, soil and the foundation-soil interface behave practically linearly. However, under strong earthquake excitation and for soft soil conditions, three components of the SSI system can behave significantly nonlinear, resulting in accumulation of irrecoverable displacements during the earthquake.

Consideration of the nonlinear behavior of both, the structure and the foundation results in a complicated problem for practical applications. On the other hand, considering the degree of uncertainty involved in the problem, it is appropriate to assume either the building or the foundation-soil system behaves linearly. Excluding the case of nonlinearly behaving building, estimation of magnitudes of irrecoverable foundation displacements are targeted in this study assuming that the foundation-soil system is the only component that behaves nonlinearly.

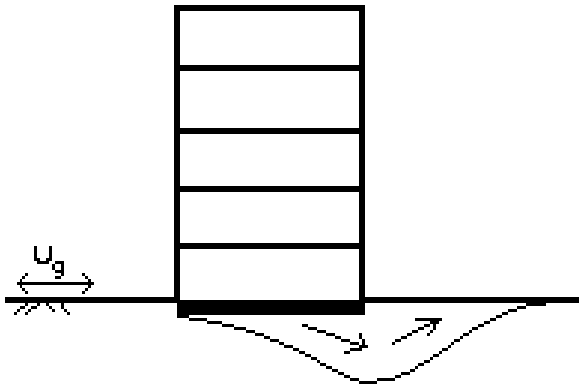

Figure 3.1. The simple sketch for the problem statement: multistory building resting on shallow mat foundation.

In Chapter 4, it is discussed that, for a given vertical static load level on a shallow mat foundation, there is a corresponding level of horizontal pseudo-static acceleration acting on building mass, which will initiate plastic flow of foundation-soil system. This ultimate acceleration value depends not only on the geotechnical considerations for the soil-foundation system, but also on the dynamic characteristics of the whole oscillating system. As discussed in Chapter 1, rigorous analysis of nonlinear soil-structure interaction requires sophisticated numerical models. Such models would involve details on constitutive behavior of soil, foundation-soil interface and structure, and the results are dependent on the uncertainty involved in material properties, especially due to variation of the soil profile beneath the foundation and utilized input motions.

Hence, in this chapter, governing equations for a simple methodology that can be utilized to estimate the irrecoverable rotation demands on shallow mat foundations are derived. The methodology depends on basic linear SSI principles to estimate the fundamental period and damping of the linear system. Basic equations will be extended to nonlinear range for the foundation response, such that the total behavior of the system will be reduced to simple elasto-plastic behavior. This final simplification will provide a link to the practical design approach, based on design spectrum for a given site, as it will be shown in Chapter 5.

3.2. Literature Review

Dynamic response of the system depicted in Figure 3.1 requires soil-structure-interaction (SSI) considerations. In the literature review of this Chapter, references pertaining to the SSI concepts are discussed.

Most rigorous study on SSI analysis is presented by Wolf, and published in three books (Wolf, 1985, 1988, 1994). The first book (Wolf, 1985) involves the fundamental principles in rigorous SSI approaches for applications in machine foundation problems and seismic interaction. The methodologies for linear numerical modeling of the structure and the soil medium are presented in frequency domain. Impact of nonlinearity can be analyzed through incremental equations of motion in time domain, which is the subject of the second book (Wolf, 1988). Since the methodologies presented in the first two books are rather complicated for practical use, simple approaches for practical applications are utilized in the third book (Wolf, 1994), based on approximations of the SSI analysis via truncated cones and lumped-parameter models.

Accordingly, the investigation of effect of the structure-foundation stiffness on seismic forces is referred to as the “kinematic-interaction analysis”, while the analysis integrating the effect of mass is referred to as the “inertial-interaction analysis”. For a linear SSI analysis, both effects can be formulated separately and can be superposed (Wolf, 1985). However, for a nonlinear analysis, superposition is not possible, necessitating a direct numerical solution in time-domain. Wolf also states that, for a surface structure excited by vertically incident waves, only the inertial interaction part of the analysis really has to be analyzed. Hence, in this study, since buildings without significant embedment are considered, only inertial interaction is considered in the analyses.

The impact of SSI on response of structures can be investigated by the simple model described in Figure 3.2: The only lumped mass, representing the inertia of the structure, is located at height h. Utilizing this model, Wolf (1985) presents the derivations of a simplified inertial-interaction analysis for response calculations for the structural distortions (u_s) for this simplified model in the frequency-domain.

As a further study, Stewart et al. (1999a; 1999b) compared the measured SSI effect on period lengthening and damping with the simple predictive equations,

based on the simple model in Figure 3.2. For the purpose, actual records that are obtained on the roof, the base and the free-field locations at various buildings, and the system-identification techniques are utilized. Analyses verified the statement that, the kinematic-interaction can be practically ignored for buildings with shallow foundations, and the SSI formulations can be practically based on inertial interaction alone. Both, the period lengthening and the effective foundation damping ratio are strongly dependent on the dimensionless parameter 1/r, which is formulated as:

$$\frac{1}{r} = \frac{h}{V_s T_s} \tag{3.1}$$

where, h is the effective structure height (i.e., accepted as 70% of total height of the building), V_s is the shear wave velocity of the foundation soil, and T_s is the fixed-base period for the structure. The soil-structure interaction is observed to be more significant for small r values. Hence, SSI impact on dynamic response is more significant for relatively stiff structures resting on relatively soft deposits. The aspect ratio (i.e., ratio of h to foundation width) is also observed to affect the results, such that, buildings with higher aspect ratios provide higher period lengthening and lower foundation damping ratios.

Frequency independent lumped parameter models, composed of spring-dashpot-mass models are presented by Wolf (1994). However, Wolf discusses that, if a lumped mass for the dynamic response of the foundation-soil system is included in the simplified analysis (i.e., a lumped mass is added to the originally-massless foundation node in Figure 3.2), then effective input motion (u_g) applied at the far-end of the SSI model must be calculated: u_g is no more equal to the free-field displacement-history. This may result in a further complication for practical applications. In case the foundation impedances are modeled by only spring and dashpots (without any use of lumped mass), then effective input motion is simply the free-field motion, as it is introduced in Section 3.3. However, in this case, the spring and dashpot coefficients become strongly frequency-dependent.

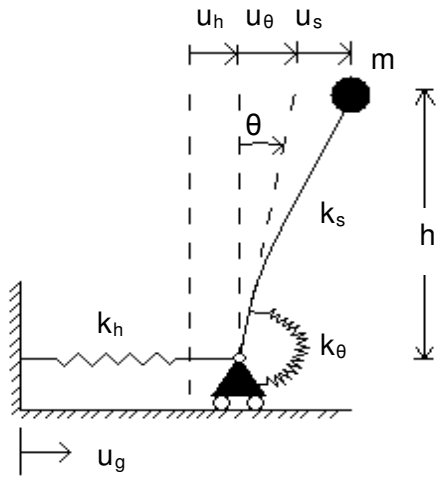

Figure 3.2. Simplified model for SSI analysis: u_h, u_θ, and u_s are horizontal translation, foundation tilting and structural distortion components of the relative displacement of lumped mass with respect to the ground; u_g is the ground displacement; k_h, and k_θ are the horizontal and rocking impedances of foundation; k_s is the structural stiffness, m is the lumped mass representing the inertia of the structure.

Dobry and Gazetas (1986) provide the frequency-dependent foundation impedances without use of lumped masses at foundation nodes in simple SSI models. The equations are applicable to arbitrarily shaped rigid surface foundations placed on presumably homogeneous and deep soil deposits. For the case of machine foundations, frequency dependent spring and dashpot coefficients can be easily obtained by utilizing the operational frequency of the equipment. However, for seismic excitations, selection of a unique representative frequency does not seem to be realistic. On the other hand, considering the degree of uncertainty involved in practical applications, significance of frequency-dependency in SSI calculations is investigated in Section 3.6. Validity of these equations are also examined by model tests by Dobry et al. (1986). A significant outcome of these series of tests is the observation that, in the swaying-rocking mode, damping ratios are over-predicted, due to reflections on model-boundaries: The elastic half-space assumption for the soil tends to over-predict the actual damping values in swaying-rocking mode. For practical use, the formulations are further simplified and presented by Gazetas (1991), which will be utilized in derivations for the study.

Wolf (1994) also rigorously investigated the case of shallow soil layer resting on rigid rock, and stated that, energy radiation can only occur in horizontal direction in this case. Hence, any harmonic excitation applied on the shallow foundation reflects back and forth between the ground surface and rock layer. Also, there is a cut-off frequency, below which practically zero damping occurs due to the radiation of the wave energy. These findings practically lead to the conclusion that, soil stratification in the horizontal and vertical directions can have a very significant impact on damping ratio. This creates a difficulty in practical approaches, enforcing the engineer to investigate the mechanical properties of the foundation soils more rigorously, and to evaluate the actual damping. In case of simple buildings, such an analysis will be difficult and costly. In fact, the importance of the effect can also be observed in the study by Paoulicci (1997), which aims at to compare the simplified (inertial) nonlinear interaction model with a two-dimensional nonlinear finite-elements approach, as discussed in Chapter 1 of this study: The simplified analyses underestimate the rocking-mode displacements when compared to the rigorous finite-elements approach. An abrupt increase is observed in these displacements in the rigorous model, at time the simplified model ceases them. Considering the discussions of Wolf (1994), this may be due the reflections of the waves from the (rigid) base of the model towards ground surface, since the observed (back) arrival time for the severe excitation in rigorous model is consistent with the shear-wave velocity of the soil in the model. Such reflections are not considered in the simplified model, since it is based on the half-space assumption. Hence, the results presented by Paoulicci can be regarded as an example of detrimental impact of utilization of equations that are based on the half-space assumption.

3.3. Simplified SSI Formulation for Linear System

In case the response of the building structure in Figure 3.1 can be approximated by the behavior of a single-degree-of-freedom oscillator, it can be possible to calculate the response of the system by integrating the equation of motion in time-domain. The behavior of the foundation-soil system is idealized to be nonlinear in this study: when a threshold seismic force level is exceeded, plastic-flow behavior is initiated at the foundation. Considering the complicated behavior of soils, as presented in Chapter 2, the foundation response is assumed

to be elastic-ideally plastic. The impact of more complex response of foundation soil is excluded here, and left as a future study.

In engineering applications, generally only the peak values of the response of dynamic systems are investigated. In case the system behavior can be reduced to the response of a SDOF oscillator, calculation of peak response can be achieved utilizing the response spectrum for input motion. Only the period of the SDOF oscillator is required for entry to a response spectrum plot, for a given damping ratio, due to the normalized equation of motion (Chopra, 1995),

$$\ddot{u} + 2\varsigma\omega_n\dot{u} + \omega_n^2 u = -\ddot{u}_g \tag{3.2}$$

where, u is the relative displacement with respect to ground, u_g is the ground displacement, ς is the damping ratio and ω_n is the natural frequency ($T_n=2\pi/\omega_n$ is the natural period) of the linear system. If k, m, and c_v are the stiffness, mass, and viscous damping values for a SDOF oscillator, then the following relations hold for equation 3.3:

$$\omega_n = \sqrt{\frac{k}{m}} \tag{3.3.a}$$

$$\varsigma = \frac{c_v}{2\sqrt{km}} \tag{3.3.b}$$

In case of nonlinear behavior, due to variation of value k (system stiffness), additional parameters describing nonlinear constitutive behavior are required. If system stiffness is dependent on the state of displacement and velocity only, the equation of motion is,

$$m\ddot{u} + c_v\dot{u} + f_s(u,\dot{u}) = -m\ddot{u}_g \tag{3.4}$$

where, $f_s(u,\dot{u})$ is the resistance due to nonlinear spring. The simplest nonlinear behavior involving yield is the elastic-perfectly plastic behavior, which also has a potential to develop practical design approaches. If the yield force level for the elastic-perfectly plastic system is f_y, then equation 3.4 can be reduced as,

$$\ddot{u} + 2\varsigma\omega_n\dot{u} + \omega_n^2 u_y \bar{f}_s(u,\dot{u}) = -\ddot{u}_g \tag{3.5}$$

where, normalized force-displacement relation for nonlinear spring is formulated as,

$$\bar{f}_s(u,\dot{u}) = \frac{f_s(u,\dot{u})}{f_y} \tag{3.6.a}$$

and,

$$u_y = \frac{f_y}{k} \tag{3.6.b}$$

here, k is the stiffness of spring for force levels below f_y, ω_n and ς are calculated utilizing equations 3.3, considering linear system parameters k, c_v and m. Therefore, besides natural period T_n and damping ratio ς, value of function $\bar{f}_y$ (equation 3.6.a) and u_y (equation 3.6.b) are required for response calculations. Further reduction is possible, if equation 3.5 is normalized with u_y: The ductility ratio is defined as,

$$\mu = \frac{u}{u_y} \tag{3.7}$$

and, the pseudo-static yield acceleration, which is the acceleration of the mass necessary to produce yield force f_y is defined as,

$$a_y = \frac{f_y}{m} = \omega_n^2 u_y \tag{3.8}$$

which is referred to as the absolute yield acceleration in this study. Equation 3.5 can be further reduced as,

$$\ddot{\mu} + 2\varsigma\,\omega_n\dot{\mu} + \omega_n^2 \bar{f}_s(\mu,\dot{\mu}) = -\omega_n^2 \frac{\ddot{u}_g}{a_y} \tag{3.9}$$

Therefore, for a given input motion history, $u_g(t)$ and yield acceleration level a_y, it is possible to calculate μ-history, for a given natural period and damping ratio. Actual response-history can be calculated via equation 3.9.

Equation 3.9 is also useful in utilizing elastic design spectrum in estimation of peak response of inelastic system. A practical approach is to utilize relationships between ductility ratio (μ) and yield reduction factor (R_y). The yield reduction factor is defined as,

$$R_y = \frac{f_0}{f_y} \tag{3.10}$$

where, for a given excitation, f_0 is the maximum force on spring for a linear system, and f_y is the yield force for elastic-perfectly plastic behavior. Dividing both the numerator and denominator by m (mass),

$$R_y = \frac{SA(T_n, \varsigma)}{a_y} \tag{3.11}$$

where, SA is the spectral acceleration for a linear SDOF oscillator with natural period T_n, provided by elastic response spectrum for a constant damping ratio ς.

Utilizing a relationship between R_y and μ_{max} (maximum ductility ratio, or ductility demand), it is possible to estimate a μ_{max} value consistent with the design spectrum and R_y factor. Then maximum displacement demand on system can be calculated via equation 3.7, or, by the equation,

$$u_{max} = \mu_{max} \cdot \frac{a_y T_n^2}{4\pi^2} \tag{3.12}$$

and, maximum irrecoverable displacement demand on a elastic-ideally plastic system by,

$$u_{ir} = \begin{cases} (\mu_{max} - 1) \cdot \dfrac{a_y T_n^2}{4\pi^2} & \text{if } \mu > 1.0 \\ 0 & \text{if } \mu \le 1.0 \end{cases} \tag{3.13}$$

Hence, if the behavior of a nonlinear system can be reduced to equation 3.4, then irrecoverable deformations can be estimated via 3.13, utilizing the elastic design spectrum and available R_y-μ_{max} relationships. Such a calculation procedure will provide a basis for an economical design, such that, irrecoverable deformations at foundation will remain below an acceptable limit, where foundation capacity is allowed to be exceeded successively by seismic demand. Hence, the foundation can be accepted to have a capacity lower than that is required for no-yield behavior. Effectiveness of any mitigation procedures can be evaluated based on similar approaches, such that, effect of increase in load capacity, or alteration of system period can be of significance.

In this study, tilting of foundations is accepted to be a more critical permanent displacement mode based on observations in past earthquakes. Buildings with poor aspect ratios (i.e., high building height with respect to foundation width) are more specifically observed to sustain excessive tilting, and a calculation procedure is required in order to estimate tilting performance of buildings with shallow mat foundations, which will help detection of buildings with poor aspect ratio for a given seismic demand. Following assumptions are considered for further discussion:

1. Superstructure (i.e., load bearing system of building) behaves elastically, and foundation's yield strength (load capacity) is lower than the superstructure's yield strength. That is, plastic behavior of foundation is initiated well before that of the superstructure, since the excessive base shear, required to initiate yielding of building, is not transmitted to the superstructure.

2. Foundation response during seismic loading is idealized by elastic-perfectly plastic behavior. The linear behavior parameters are estimated by linear soil-structure interaction equations, with the simplified procedures discussed in Section 3.2. Yield force level (load capacity) is estimated by the procedures presented in Chapter 4.

3. Only inertial soil-structure interaction is considered, based on the assumption that, earthquake waves are vertically incident SH waves, and foundations are rigid plates resting on surface of an elastic-halfspace.

Based on above assumptions, equation of motion for the nonlinear soil-structure interaction (SSI) system is derived in the following sections, in order to utilize methodologies based on equation 3.4 in practice.

3.3.1. Simplified interaction without damping

For a simplified SSI analysis, it is practical to utilize the simple model given in Figure 3.2 (Wolf,1994): The structure is modeled by a mass (m) attached to the top node of a flexible beam with stiffness k_s, and height h. This system is representative for shallow foundations, where only inertial interaction is to be considered. The fixed-base period of the structure is given by

$$T_s = \frac{2\pi}{\omega_s} = 2\pi\sqrt{\frac{m}{k_s}} \tag{3.14}$$

The lumped mass and the beam element simulate the basic structural response. The springs attached to the foundation node simulate the response of a shallow mat foundation resting on the surface of a homogeneous elastic halfspace. Hence, the response of foundation to tilting and horizontal displacements can be adjusted via springs having stiffness coefficients k_θ and k_h, as shown in Figure 3.2. These springs are referred to as foundation impedances for rocking and horizontal translation motions, respectively. Two important period values are defined to represent the deformability of soil: the period of rocking mode of foundation displacements, T_r, and the period of horizontal translation mode of foundation displacements, T_h. These periods are formulated as,

$$T_r = \frac{2\pi}{\omega_r} = 2\pi\sqrt{\frac{mh^2}{k_\theta}} \tag{3.15}$$

$$T_h = \frac{2\pi}{\omega_h} = 2\pi\sqrt{\frac{m}{k_h}} \tag{3.16}$$

Equations 3.14, 3.15 and 3.16 can be derived simply by formulating the equation of motion considering only the flexibility of related spring (Wolf, 1985). Total relative displacement of lumped mass with respect to free-field displacements (u_g) is defined by,

$$u_t = u_h + u_\theta + u_s \tag{3.17}$$

where, u_h is the relative displacement of the rigid foundation with respect to free-field, u_s is the structural distortion component and u_θ (=hθ) is the foundation rotation component of the relative displacement of the lumped mass with respect to the foundation (Figure 3.2). Hence, the equation of motion in terms of u_t can be derived as follows: force equilibrium at lumped mass level requires,

$$m\ddot{u}_t + k_s u_s = -m\ddot{u}_g \tag{3.18}$$

where, second derivative of the variable with respect to time is represented by double dot on the representing symbol. Force equilibrium at foundation level results in,

$$k_h u_h = k_s u_s \tag{3.19}$$

Substitution of equation 3.19 into 3.18 gives,

$$m\ddot{u}_t + k_h u_h = -m\ddot{u}_g \tag{3.20}$$

Hence, moment equilibrium at foundation level results in (note that u_θ=hθ),

$$hm\ddot{u}_t + k_\theta \theta = -hm\ddot{u}_g \tag{3.21}$$

Substituting equations 3.14, 3.15, and 3.16 into equations 3.18, 3.20 and 3.21, following equations are obtained:

$$u_s = -\frac{1}{\omega_s^2}\left(\ddot{u}_t + \ddot{u}_g\right) \tag{3.22.a}$$

$$u_h = -\frac{1}{\omega_h^2}\left(\ddot{u}_t + \ddot{u}_g\right) \tag{3.22.b}$$

$$u_\theta = h \cdot \theta = -\frac{1}{\omega_r^2}\left(\ddot{u}_t + \ddot{u}_g\right) \tag{3.22.c}$$

or, summation of equations 3.22.a-c gives

$$u_s + u_h + u_\theta = -\left(\frac{1}{\omega_s^2} + \frac{1}{\omega_h^2} + \frac{1}{\omega_r^2}\right)\left(\ddot{u}_t + \ddot{u}_g\right) \tag{3.23}$$

Hence equivalent natural vibration frequency of the linear system is defined as,

$$\frac{1}{\overline{\omega}^2} = \left(\frac{1}{\omega_s^2} + \frac{1}{\omega_h^2} + \frac{1}{\omega_r^2}\right) \tag{3.24.a}$$

Accordingly, the equivalent natural period for the total SSI system can be calculated by,

$$\overline{T}^2 = T_s^2 + T_h^2 + T_r^2 \tag{3.24.b}$$

Finally, introducing equations 3.17 and 3.24.a into 3.23, equation of motion for total relative displacement of the lumped mass with respect to the free-field motion can be obtained as,

$$\ddot{u}_t + \overline{\omega}^2 u_t = -\ddot{u}_g \tag{3.25}$$

Hence, for a given free-field acceleration-history ($\ddot{u}_g$), relative displacement history of the lumped mass (u_t) with respect to free field can be calculated utilizing equation the 3.25, disregarding damping. Participations of u_s, u_h and u_θ in u_t are formulated by dividing equations 3.22.a-c by the total relative displacement of lumped mass:

$$\frac{u_s}{u_t} = \frac{\overline{\omega}^2}{\omega_s^2} = \frac{T_s^2}{\overline{T}^2} \tag{3.26.a}$$

$$\frac{u_h}{u_t} = \frac{\overline{\omega}^2}{\omega_h^2} = \frac{T_h^2}{\overline{T}^2} \tag{3.26.b}$$

$$\frac{u_\theta}{u_t} = \frac{\overline{\omega}^2}{\omega_\theta^2} = \frac{T_\theta^2}{\overline{T}^2} \tag{3.26.c}$$

Utilizing equation 3.25, an equivalent conceptual model as shown in Figure 3.3 is proposed, which is useful for further practical discussions. In this model, lumped mass m and height h are the same as the model in Figure 3.2. The natural frequency of the reduced model is set equal to $\bar{\omega}$ in equation 3.24.a by calculating a consistent rotational spring coefficient $\bar{k}_\theta$, utilizing equation 3.15.

$$\bar{k}_\theta = mh^2\bar{\omega}^2 \tag{3.27}$$

or,

$$\bar{k}_\theta = \frac{k_h k_s k_\theta}{k_h k_s + k_h k_\theta / h^2 + k_s k_\theta / h^2} \tag{3.28}$$

Reduced model in Figure 3.3 forms the conceptual idealization, which will be utilized in this study. However, the viscous damping and impact of yielding of foundation complicates this simple behavior. Hence, equations for damping and yielding of the foundation will be considered in the following sections.

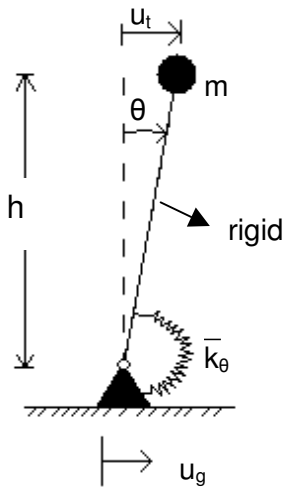

Figure 3.3. Reduced system consistent with the equation 3.25.

3.3.2. Simplified inertial interaction with viscous damping

As the next step, damping is considered in inertial interaction analyses. Viscous dashpots, with coefficients c_s, c_h, and c_θ, are considered to be working in parallel with springs, which have stiffness coefficients k_s, k_h, and k_θ, respectively. Hence, adding damping terms to equations 3.22,

$$\frac{c_s}{k_s}\dot{u}_s + u_s = -\frac{1}{\omega_s^2}\left(\ddot{u}_t + \ddot{u}_g\right) \tag{3.29.a}$$

$$\frac{c_h}{k_h}\dot{u}_h + u_h = -\frac{1}{\omega_h^2}\left(\ddot{u}_t + \ddot{u}_g\right) \tag{3.29.b}$$

$$\frac{c_\theta}{k_\theta}\dot{u}_\theta + u_\theta = -\frac{1}{\omega_r^2}\left(\ddot{u}_t + \ddot{u}_g\right) \tag{3.29.c}$$

or, utilizing the damping ratio definition in equation 3.3.b,

$$\frac{2\varsigma_s}{\omega_s}\dot{u}_s + u_s = -\frac{1}{\omega_s^2}\left(\ddot{u}_t + \ddot{u}_g\right) \tag{3.30.a}$$

$$\frac{2\varsigma_h}{\omega_h}\dot{u}_h + u_h = -\frac{1}{\omega_h^2}\left(\ddot{u}_t + \ddot{u}_g\right) \tag{3.30.b}$$

$$\frac{2\varsigma_\theta}{\omega_r}\dot{u}_\theta + u_\theta = -\frac{1}{\omega_r^2}\left(\ddot{u}_t + \ddot{u}_g\right) \tag{3.30.c}$$

Damped equation of motion for total displacements can be formulated by the summation of equations 3.30.a-c, and by the substitution of equation 3.24.a,

$$2\left(\frac{\varsigma_s}{\omega_s}\frac{\dot{u}_s}{\dot{u}_t} + \frac{\varsigma_h}{\omega_h}\frac{\dot{u}_h}{\dot{u}_t} + \frac{\varsigma_\theta}{\omega_r}\frac{\dot{u}_\theta}{\dot{u}_t}\right)\dot{u}_t + u_t = -\frac{1}{\overline{\omega}^2}\left(\ddot{u}_t + \ddot{u}_g\right)$$

or,

$$2\left(\varsigma_s\frac{\dot{u}_s}{\dot{u}_t}\frac{\overline{\omega}}{\omega_s} + \varsigma_h\frac{\dot{u}_h}{\dot{u}_t}\frac{\overline{\omega}}{\omega_h} + \varsigma_\theta\frac{\dot{u}_\theta}{\dot{u}_t}\frac{\overline{\omega}}{\omega_r}\right)\frac{1}{\overline{\omega}}\dot{u}_t + u_t = -\frac{1}{\overline{\omega}^2}\left(\ddot{u}_t + \ddot{u}_g\right) \tag{3.31}$$

or,

$$2\frac{\bar{\varsigma}}{\bar{\omega}}\dot{u}_t + u_t = -\frac{1}{\bar{\omega}^2}\left(\ddot{u}_t + \ddot{u}_g\right) \tag{3.32}$$

where, effective damping is defined as,

$$\bar{\varsigma} = \varsigma_s \frac{\dot{u}_s}{\dot{u}_t}\frac{\bar{\omega}}{\omega_s} + \varsigma_h \frac{\dot{u}_h}{\dot{u}_t}\frac{\bar{\omega}}{\omega_h} + \varsigma_\theta \frac{\dot{u}_\theta}{\dot{u}_t}\frac{\bar{\omega}}{\omega_r} \tag{3.33}$$

Hence, effective damping for u_t depends on the participations of velocities $\dot{u}_s, \dot{u}_h,$ and $\dot{u}_\theta$ to total velocity of the mass $\dot{u}_t$, at time t. Indeed, frequency - dependent equivalent damping and stiffness for the damped system can be formulated by transferring the equations of motion to frequency space, utilizing Fourier Transform. This can provide further insight for the linear problem, and can provide a selection of an equivalent damping ratio, which is frequency dependent. On the other hand, the yielding of the foundation, which is the major consideration in this study, results in the nonlinear behavior of the foundation-soil system. Hence, utilization of frequency-domain solutions is out of the scope of this study.

In case the damping coefficients are assumed to remain constant (i.e., damping ratios are independent of the nonlinear behavior and frequency content of the excitation), equations 3.30 are solved simultaneously in order to calculate these contributions to total velocity. However, by the following assumptions, effective damping can be further investigated approximately: in case damping components in equations 3.30 are negligible when compared to displacement components (i.e., in case of small damping or low-frequency excitation), then relationships in equations 3.26 will be approximately valid. In this case,

$$\frac{\dot{u}_s}{\dot{u}_t} = \frac{u_s}{u_t} \qquad \frac{\dot{u}_h}{\dot{u}_t} = \frac{u_h}{u_t} \qquad \frac{\dot{u}_\theta}{\dot{u}_t} = \frac{u_\theta}{u_t} \tag{3.34}$$

and substituting equations 3.34 and 3.26 into 3.33, the effective damping can be estimated as,

$$\bar{\varsigma} = \varsigma_s \frac{\bar{\omega}^3}{\omega_s^3} + \varsigma_h \frac{\bar{\omega}^3}{\omega_h^3} + \varsigma_\theta \frac{\bar{\omega}^3}{\omega_\theta^3} \tag{3.35}$$

In the case damping dominates the left hand side in equations 3.30 (e.g., in case of high damping ratios, or high-frequency excitation), displacement terms in equations 3.30 can be ignored, resulting in approximation,

$$\frac{1}{\bar{\varsigma}} = \frac{1}{\varsigma_s}\frac{\bar{\omega}}{\omega_s} + \frac{1}{\varsigma_h}\frac{\bar{\omega}}{\omega_h} + \frac{1}{\varsigma_\theta}\frac{\bar{\omega}}{\omega_\theta} \tag{3.36}$$

which states a different averaging formula for the damping components.

Equations 3.35 and 3.36 imply the frequency - dependence of the equivalent damping ratio formulation. When also the frequency dependency of dashpot coefficients c_θ and c_h (Gazetas, 1991), and sensitivity of damping parameters to soil stratifications (Wolf,1994) are considered, it may be practically difficult to decide on accurate equivalent damping coefficient, especially in case of limited availability of geotechnical site investigation data. Most importantly, provided equations are due to elastic behavior only, and damping coefficients simulating energy dissipation during yielding of foundation soils may not be easily determined. Therefore, considering the irregular nature of earthquake excitation, it is difficult to predict an equivalent constant damping ratio for the simplified SSI system.

The damping discussion becomes problematic in linear system calculations, where peak response is sensitive to the damping value. In case significant nonlinear (i.e., elastic-perfectly plastic) behavior is considered, energy dissipation is governed by the hysteretic behavior. In this case, peak response is respectively less significant to damping value (Chopra,1995). Since the performance of foundations for which the seismic load demand is considerably higher than the load capacity is under investigation here, a constant damping ratio (e.g., 5%) consistent with available design procedures is utilized for further discussions. Actual damping ratio may be higher for soft alluvium cases, and hence low damping ratio assumption may result in somewhat conservative estimates: Majority of the input energy will be dissipated by hysteretic (elastic-perfectly plastic) behavior of the foundation. Hence, the reduced differential equation, based on Figure 3.3 and equation 3.32, is simply

$$\ddot{u}_t + 2\bar{\varsigma}\bar{\omega}\dot{u}_t + \bar{\omega}^2 u_t = -\ddot{u}_g \tag{3.37}$$

which is the damped equation of motion for the reduced system.

3.4. Equations for the Equivalent System for Multistorey Buildings

In order to utilize practical formulations based on the simplified model depicted in Figure 3.2 for calculations of foundation performance of multi-storey buildings, a formulation is required to estimate an equivalent height (h) for the lumped mass from foundation level. For the case of fixed-base structures, the effective height can be calculated from the structural (spectral) analysis, using the formula,

$$h = \frac{M_b}{V_b} \tag{3.38}$$

where M_b and V_b are the maximum overturning moment and base shear, respectively, acting on the base of the structure. Practically, h can be simply estimated if the distribution of inertial forces can be approximated as shown in Figure 3.4:

$$h = \begin{cases} 0.50 \cdot h_n & \text{for constant inertial force distribution} \\ 0.67 \cdot h_n & \text{for linearly changing inertial force distribution} \end{cases} \tag{3.39}$$

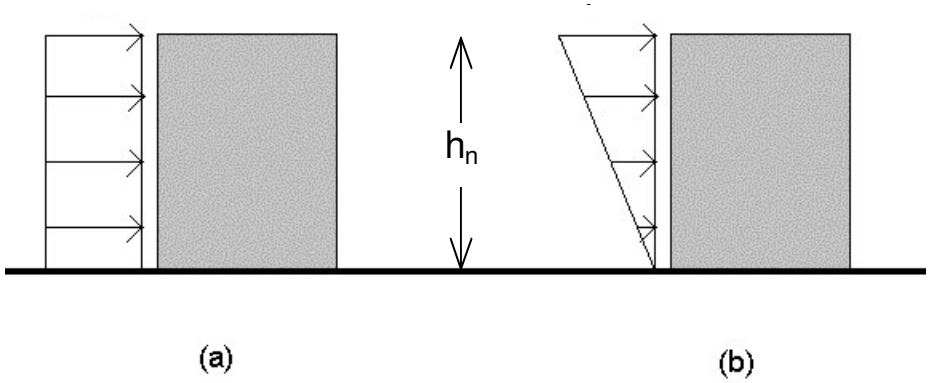

Figure 3.4. Idealized inertial force distributions on a building: (a) constant, (b) linearly changing.

In case of buildings with poor aspect ratio, and of foundations resting on soft deposits, the inertial force distribution is dominated by the rocking-mode of foundation impedance, especially when foundation yielding in the rocking mode plays a significant role in the overall response. Hence, it is reasonable to assume

that the building behaves relatively rigid compared to the foundation behavior, and the rocking mode of foundation governs the SSI.

For practical purposes, the simplified model presented in Figure 3.5, which is a multi-story version of Figure 3.3, is utilized: storey masses (m_1,…,m_n) are lumped at corresponding storey heights (h_1,…,h_n). As the first step, only the equivalent height due to rocking motion of foundation is formulated, by the assumption that both the superstructure and the horizontal displacement spring are rigid. The consequent reduced system with only degree of freedom of foundation rotation θ is shown in Figure 3.5. Hence, total acceleration acting on i^{th} storey mass is,

$$\ddot{u}_i = \ddot{u}_g + h_i \cdot \ddot{\theta} \tag{3.40}$$

where, h_i is the height of the storey mass from foundation level, θ is the tilting angle of foundation (in radians), and $\ddot{u}_i$ is the total acceleration of mass m_i. Hence, equilibrium of overturning moments at foundation node results in the equation:

$$\theta k_\theta + \sum_n \left[\left(\ddot{u}_g + h_i \ddot{\theta} \right) m_i h_i \right] = 0$$

or,

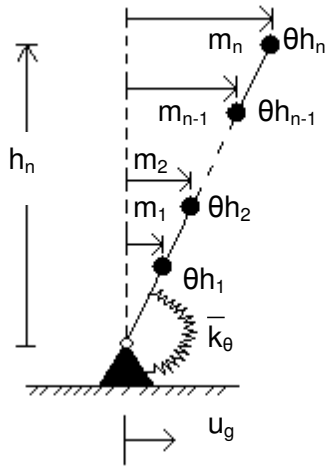

Figure 3.5. Reduced model for multi-storey buildings.

$$\left(\sum_n m_i h_i^2\right)\ddot{\theta} + k_\theta \theta = -\left(\sum_n m_i h_i\right)\ddot{u}_g$$

or,

$$I_\theta \ddot{\theta} + k_\theta \theta = -d_\theta \ddot{u}_g \tag{3.41}$$

where,

$$I_\theta = \sum_n m_i h_i^2 \tag{3.42.a}$$

$$d_\theta = \sum_n m_i h_i \tag{3.42.b}$$

Defining the equivalent radius of oscillation (r_θ) as,

$$r_\theta = \frac{I_\theta}{d_\theta} \tag{3.43}$$

and, natural period of vibration as,

$$T_r = \frac{2\pi}{\omega_r} = 2\pi\sqrt{\frac{I_\theta}{k_\theta}} \tag{3.44}$$

equation 3.41 can be reduced as,

$$\left(r_\theta \ddot{\theta}\right) + \omega_\theta^2 (r_\theta \theta) = -\ddot{u}_g \tag{3.45}$$

Equation 3.45 is equivalent to equation 3.25, and gives the equation of motion for the model in Figure 3.3, such that,

$$h = r_\theta \tag{3.46.a}$$

$$m = d_\theta^2 / I_\theta \tag{3.46.b}$$

On the other hand, updating quantity of lumped mass due to equation 3.46.b creates difficulty for further discussions. Hence, the model is altered by the assumption that, total mass $(\sum m_i)$ of all stories are lumped at a height $\bar{h}$, given by:

$$\bar{h} = \sqrt{\frac{I_\theta}{\sum m_i}} \tag{3.47}$$

Therefore, the same natural period for rocking mode will be calculated. In this case, the equation of motion will be formulated as,

$$\left(\bar{h}\ddot{\tilde{\theta}}\right) + \omega_\theta^2\left(\bar{h}\tilde{\theta}\right) = -\ddot{u}_g \tag{3.48}$$

where, $\tilde{\theta}$ is an approximation to θ. The error can be formulated by,

$$\varepsilon_\theta = \frac{\tilde{\theta} - \theta}{\theta} \tag{3.49}$$

or , since $u = \bar{h}\tilde{\theta} = r_\theta\theta$,

$$\varepsilon_\theta = \frac{r_\theta}{\bar{h}} - 1$$

introducing definitions for r_θ and $\bar{h}$,

$$\varepsilon_\theta = \sqrt{\frac{I_\theta \sum m_i}{d_\theta^2}} - 1 \tag{3.50}$$

In case of simple multistory buildings with constant storey height h_{st}, it is reasonable to model the building with equal lumped masses m_{st} at each storey. This approximation provides further simplification, so that equation 3.50 can be numerically investigated. Hence, equation 3.50 is reduced as,

$$\varepsilon_\theta(n) = \sqrt{\frac{n \cdot \sum_{j=1}^{n} j^2}{\left(\sum_{j=1}^{n} j\right)^2}} - 1 \qquad (3.51)$$

where, n is the number of stories, as shown in Figure 3.5. Plot of equation versus number of stories is given in Figure 3.6: calculated error in estimating θ is observed to be in the order of 10% for most multistory buildings. Therefore, lumping total mass of the stories at height $\bar{h}$ based on equation 3.47 is acceptable.

Figure 3.6. Plot of equation 3.51 for different number of stories (n).

The next consideration is the estimation of ranges of $\bar{h}/h_n$, where h_n is the total height of the building. Based on constant storey mass and height approximation for simple multistory buildings, plot of $\bar{h}/h_n$ vs. number of stories (n) is provided in Figure 3.7. For most multistory buildings, equivalent height is about two-thirds of total height. This is somewhat consistent with the location of resultant horizontal force for a fixed-base simple structure: In case the distribution of inertial forces for a fixed-base model is approximated to be in triangular-form, the height of the resultant seismic force from the foundation level will be about two-thirds of the total height of the building. Therefore, use of equation 3.47 for calculation of equivalent height is appropriate also for fixed base response of buildings, and two-thirds of total height of building can be practically utilized for apartment buildings with number of stories between 2 and 10:

$$h \cong \bar{h} \cong 0.67 h_n \tag{3.52}$$

where, h_n is the total height of the building from the foundation level. All the storey masses, excluding the mass of the foundation, can be practically lumped at height h. This approximation is consistent with SSI calculations due to horizontal translation mode of foundation, provided that the foundation mass can be practically ignored in period estimations. Still, the natural period of the rocking mode is not dependent on selection of h, and is given simply by equation 3.44. Equivalent height h has its most practical importance in estimation of irrecoverable tilting (rotation angle) demand on foundations, as it is discussed in Section 3.5.

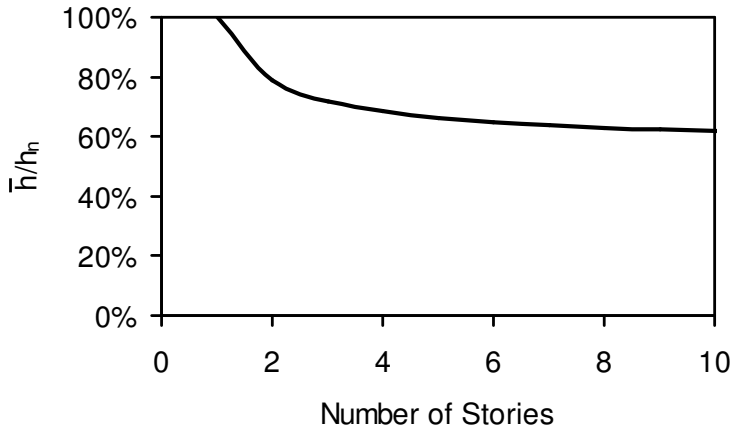

Figure 3.7. Plot of $\bar{h} / h_n$ for different number of stories (n).

By a similar procedure, it can be shown that, the horizontal translation period is simply,

$$T_h = \frac{2\pi}{\omega_h} = 2\pi\sqrt{\frac{M_{st}}{k_h}} \tag{3.53}$$

where, M_{st} is the total mass of the building, formulated by,

$$M_{st} = \sum_n m_i + m_{fdn} \tag{3.54}$$

where, m_{fdn} is the mass of the foundation, which can be omitted for practical applications of multistory apartment buildings.

Calculation of T_s (fundamental period for vibration of structure) is out of the scope this study, and assumed to be directly given by the structural designer or to be calculated by a reasonable approximate equation.

Hence, estimating the periods T_s, T_h and T_r, the natural period $\overline{T}$ for the oscillation of a multistory building resting on a shallow mat foundation can be estimated by equation 3.24.b. As discussed in Section 3.3.2, decision on a single equivalent damping ratio is difficult. Hence, it is reasonable to assign a small damping ratio (i.e., 5%), by the assumption that the majority of the energy is dissipated by the hysteretic behavior in the rocking mode of foundation displacements, which will be further formulated in the next section. These two parameters are adequate to estimate elastic response for the generalized system.

3.5. Simplified Consideration of Nonlinear Foundation Behavior

During severe seismic loading, when an ultimate level of foundation capacity for load eccentricity and inclination is exceeded, foundation-soil system will yield, resulting in irrecoverable displacements for a shallow foundation. This behavior can be simulated by setting k_h and k_θ to zero, which corresponds to ideal elastic-perfectly plastic behavior. In this case, calculated cumulative total irrecoverable plastic displacement, u_{ir} can be formulated as:

$$u_{ir} = u_{hp} + u_{\theta p} \tag{3.55}$$

where, u_{hp} is the plastic deformation component due to plastic flow of the foundation in the horizontal direction, and $u_{\theta p}$ is the plastic deformation component due to plastic tilting response of the foundation.

Although foundation system is assumed to obey elastic-perfectly plastic yield rule, a flow rule is required in order to calculate the contribution of u_{hp} and $u_{\theta p}$ in u_{ir}. Such an analysis is performed by Paoulicci (1997), as discussed in Chapter 1. However, the validity of such a flow rule is not rigorously investigated, and the calculation procedure is rather complicated. On the other hand, the flow rule for the foundation-soil system is not only dependent on the mechanical properties of the foundation soils, but also on the properties of the foundation-soil contact, and the dynamic response of the soil-structure system as well. However, apart from the

difficulties in reliably determination of such a flow rule for idealized cases (i.e., laboratory and numerical models), the actual practical applications will involve significant uncertainties regarding these parameters.

Therefore, for practical purposes, in case of poor aspect-ratio buildings, the nonlinear behavior of foundation due to load inclination and eccentricity are assumed to be uncoupled, and the effect of load inclination is ignored when calculating ultimate load eccentricity capacity. Hence, horizontal irrecoverable displacements (u_{ir}) are ignored when estimating irrecoverable tilting performance of foundations. Due to this assumption, plastic deformations will occur only in rocking mode of foundation displacements. Therefore, when utilizing the simple model in Figure 3.2, it is presumed that k_h and k_s will behave elastic, and k_θ will behave elastic-ideally plastic. In this case, the only nonlinear element in Figure 3.2 is the rocking spring: the irrecoverable displacement of lumped mass in Figure 3.2 (u_{ir}) is directly related to the irrecoverable tilting of foundation. Hence,

$$u_{ir} \cong u_{\theta p} \tag{3.56}$$

or,

$$u_{ir} \cong h \cdot \theta_{ir} \tag{3.57}$$

where, θ_{ir} is the irrecoverable tilting of foundation, in radians.

Since only the rocking spring in Figure 3.2 is considered to behave nonlinear, inelastic displacements will be dependent on the yield (ultimate) moment level (M_y) for elastic-perfectly plastic rocking spring. Hence, rocking spring will initiate plastic flow for the first time, when

$$k_\theta \cdot \left|\theta_y\right| = M_y \tag{3.58}$$

where, θ_y is the yield rotation angle. Substitution of equation 3.58 into 3.21 gives

$$mh\left|\left(\ddot{u}_g + \ddot{u}_t\right)_y\right| = M_y \tag{3.59}$$

For consistency with equation 3.8, absolute yield acceleration is defined due to equation 3.40 as,

$$a_y = \left|\left(\ddot{u}_g + \ddot{u}_t\right)_y\right| = \frac{M_y}{mh} \tag{3.60}$$

since $f_y = M_y/h$. Hence, for the equivalent elastic-perfectly plastic system in Figure 3.3, yielding of equivalent rotational spring will initiate when absolute value of total acceleration acting on mass is equal to a_y (i.e., $|M| = M_y$).

In order to develop incremental equations involving the nonlinear behavior of the rocking-mode spring, linear spring coefficient k_θ in equation 3.21 is replaced by k'_θ, in order to imply nonlinear behavior. The damping is not considered for simplicity. Hence, equations 3.18, 3.20, and 3.21 are expressed in incremental form:

$$m\Delta\ddot{u}_t + k_s\Delta u_s = -m\Delta\ddot{u}_g \tag{3.61.a}$$

$$m\Delta\ddot{u}_t + k_h\Delta u_h = -m\Delta\ddot{u}_g \tag{3.61.b}$$

$$hm\Delta\ddot{u}_t + k'_\theta\Delta\theta = -hm\Delta\ddot{u}_g \tag{3.61.c}$$

where, $\Delta u_t = \Delta u_s + \Delta u_h + \Delta u_\theta$, and $\Delta u_\theta = h\Delta\theta$. Therefore, differential equation of motion for u_t in incremental form is,

$$m\Delta\ddot{u}_t + \tilde{k}\Delta u_t = -m\Delta\ddot{u}_g \tag{3.62}$$

where,

$$\tilde{k} = \frac{k_h k_s k'_\theta / h^2}{k_h k_s + k_h k'_\theta/h^2 + k_s k'_\theta/h^2} \tag{3.63}$$

Introducing idealized elastic-perfectly plastic behavior for rocking spring in Figure 3.2 into equation 3.63, k'_θ is equal to zero when yielding occurs, and equal to k_θ when behaving elastically. Therefore, equation 3.63 can be expressed as,

$$\tilde{k} = \begin{cases} \dfrac{k_h k_s k_\theta / h^2}{k_h k_s + k_h k_\theta / h^2 + k_s k_\theta / h^2} & k'_\theta = k_\theta \\ 0 & k'_\theta = 0 \end{cases} \qquad (3.64)$$

implying elastic-perfectly plastic behavior for equivalent nonlinear spring in the conceptual model (Figure 3.3)

Setting $k'_\theta = 0$ in equations 3.61 for yielding behavior, results in the conclusion that $\Delta u_h = \Delta u_s = 0$. Hence, increments of u_t is directly equal to increments in foundation tilting component (i.e., $\Delta u_t = h \cdot \Delta\theta$), during the yielding phase for an undamped system.

Above discussions results in the utilization of reduced model in Figure 3.3, where equivalent rotational spring is set to behave as an elastic-perfectly plastic spring. Irrecoverable displacement demands can be estimated based on the discussions in Chapter 5. Corresponding irrecoverable foundation tilting demand can be estimated by equation 3.57. Natural period of the SSI system can be calculated by equation 3.24, and yield acceleration can be calculated by equation 3.60. As discussed section 3.3.2, a small damping value (e.g. 5%) can be utilized, for time-history calculations, also for practical utilization of R_y-μ_{max} correlations and relevant design spectrum.

3.6. Formulations for Foundation Impedances

Based on the simplified model in Figure 3.3, in order to estimate the periods T_r and T_h, foundation impedances k_θ and k_h should be reasonably estimated. In the most general case, the foundation impedances depend on mechanical properties of the soil, the problem geometry, and the frequency content of the excitation. In this section, simple formulations to estimate these values are provided, for the case of shallow mat foundations resting on elastic-half space. The formulations are based on the equations presented by Dobry and Gazetas (1986), which are simplified and well-presented by Gazetas (1991) for practical use, as discussed in Section 3.2. Since these equations are frequency-dependent, further simplifications are made for practical utilization.

The dynamic stiffness of foundations for rocking and horizontal translation can be expressed as,

$$k_\theta = \breve{k}_\theta\left(\frac{L}{B}, a_0\right)\cdot K_\theta \tag{3.65.a}$$

$$k_h = \breve{k}_h\left(\frac{L}{B}, a_0\right)\cdot K_h \tag{3.65.b}$$

where, K_θ and K_h are the static stiffness values for rocking and translation respectively, $\breve{k}_\theta$ and $\breve{k}_h$ are the corresponding frequency dependent dynamic stiffness correction factors, L and B are the foundation length and width, and a_0 is the dimensionless frequency, which is expressed as,

$$a_0 = \frac{\omega B}{V_s} \tag{3.66}$$

where, ω is the excitation frequency and V_s is the shear wave velocity for foundation subsoil. Values of $\breve{k}_\theta$ and $\breve{k}_h$ for a given a_0 and L/B ratio depend on the displacement direction with respect to foundation axes. In this study, displacements in weak direction of the foundation of a free - standing building are investigated (Figure 3.8). That is, in case similar seismic load demands exist in both longitudinal and transverse directions, larger foundation displacements (i.e., tilting) are likely to occur in weaker transverse direction (i.e., tilting around longitudinal axis of foundation). In the original study by Dobry and Gazetas (1986), these impedances are referred to as k_{rx} for rocking and k_y for translation, respectively. The expression for $\breve{k}_\theta$ value for rocking around longitudinal axis of surficial foundation is given by,

$$\breve{k}_\theta = 1 - 0.20a_0 \tag{3.67}$$

For further practical discussions, the order of a_0 can be estimated by selecting V_s=100 m/s, which is a reasonable value for soft shallow alluvium formations; B=20 m, which is representative for existing apartment buildings with rectangular section and ω=6 rad/sec, which is the resonance frequency for systems with periods in the order of 1.0 sec. Hence, $a_0 \cong 1.2$ is calculated for practical purposes. Therefore, the assumption of,

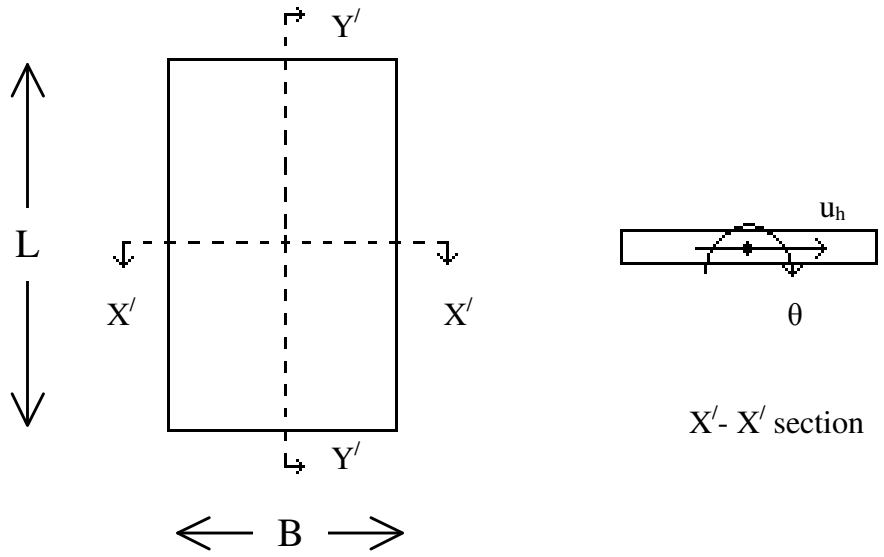

Figure 3.8. Foundation displacements in weak direction of a mat foundation.

$$\breve{k}_{\theta} \cong 1.0 \qquad (3.68)$$

will result in overestimation of the dynamic stiffness in the order of 30%. A further investigation of other possible cases for buildings resting on soft deposits will give the same conclusion with equation 3.63. Error in use of equation 3.63 is not higher than the degree of uncertainty in estimation of K_{θ}, and will have less significance in estimation of the SSI system period ($\overline{T}$).

Dynamic stiffness factor $\breve{k}_h$ for horizontal displacements in transverse direction is dependent on a_0 and L/B ratios is given in Figure 3.9. Similar to $\breve{k}_{\theta}$, for practical ranges of L/B and a_0, it is acceptable that,

$$\breve{k}_h \cong 1.0 \qquad (3.69)$$

As it can be seen from Figure 3.9, the error in underestimation of $\breve{k}_h$ will be less than about 30% for most practical cases. The error in estimation of period of soil-structure system period ($\overline{T}$) due to error in $\breve{k}_h$ will be much less. Hence, for practical applications,

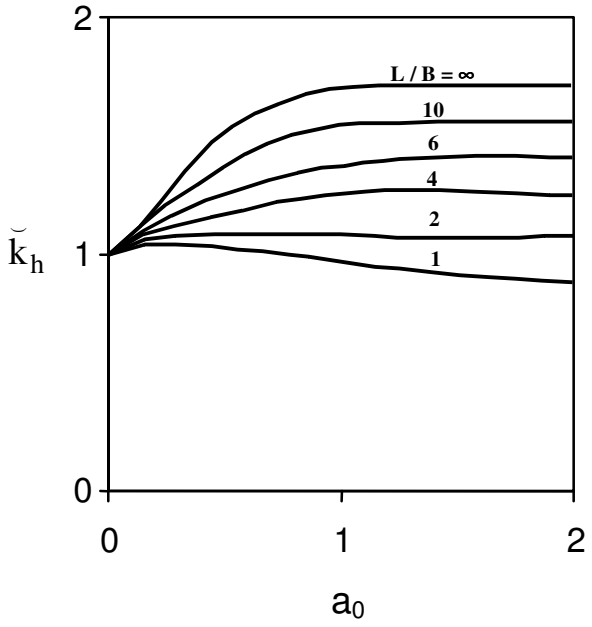

Figure 3.9. Dynamic stiffness correction factor for horizontal displacements in transverse direction (reproduced from Gazetas, 1991).

$$k_\theta \cong K_\theta \tag{3.70.a}$$

$$k_h \cong K_h \tag{3.70.b}$$

Static stiffness of a shallow rigid foundation in rocking around longitudinal direction is given as (Gazetas, 1991),

$$K_\theta = \frac{G}{1-\nu}(I_{bx})^{0.75}\left(\frac{L}{B}\right)^{0.25}\left(2.4+0.5\frac{B}{L}\right) \tag{3.71}$$

where, ν and G are the Poisson's ratio and shear modulus for the subsoil, I_{bx} is the area moment of inertia about x (longitudinal) axis. For a rectangular foundation,

$$I_{bx} = \frac{1}{12}LB^3 \tag{3.72}$$

hence, substituting equation 3.72 into 3.71, for a rectangular foundation,

$$K_\theta = \frac{GB^3}{1-\nu}\left(0.37\frac{B}{L}+0.08\right) \tag{3.73.a}$$

or, since $V_s = \sqrt{G/\rho}$, where ρ is the soil's density,

$$K_\theta = \frac{\rho V_s^2 B^3}{1-\nu}\left(0.37\frac{B}{L}+0.08\right) \tag{3.73.b}$$

Static stiffness for translation of foundation in transverse direction is formulated as,

$$K_h = \frac{GL}{2-\nu}\left(2+2.50\left(\frac{A_b}{L^2}\right)^{0.85}\right) \tag{3.74}$$

where, A_b is the area of the foundation. For a rectangular foundation,

$$A_b = L \cdot B \tag{3.75}$$

hence, substituting equation 3.75 into 3.74, for a rectangular foundation,

$$K_h = \frac{GL}{2-\nu}\left(2+2.50\left(\frac{L}{B}\right)^{-0.85}\right) \tag{3.76.a}$$

or, since $V_s = \sqrt{G/\rho}$,

$$K_h = \frac{\rho V_s^2 L}{2-\nu}\left(2+2.50\left(\frac{L}{B}\right)^{-0.85}\right) \tag{3.76.b}$$

Utilizing static spring coefficients, period for the rocking and horizontal translation mode of linear soil-structure-interaction system can be estimated reasonably, utilizing formulae 3.44, and 3.53: period for the fixed base structure (T_s) should to be provided by the structural designer.

3.7. Ranges of Natural Periods for Nonlinear SSI: Adapazari Case

It is beneficial to investigate practical ranges of periods for actual cases. this is especially beneficial in observing the significance of the above parameters. In

case the period elongation due to SSI on soft deposits is observed to be insignificant, the fixed-base period of a structure (T_s) can be directly utilized instead of $\overline{T}$. Hence, in this section, the practical ranges of period for the simplified SSI system for the case of reinforced-concrete frame buildings with rigid mat foundations resting on soft surface deposits are estimated. The calculations are based on the information obtained from Adapazarı cases. Besides, at the end of the section, cases at Mexico-city are compared with the Adapazari cases.

The detailed case studies presented in the appendices of this study are based on site-investigations conducted in the city of Adapazarı, after 17th August 1999 İzmit (Kocaeli) Earthquake, as discussed in Chapter 1. Most buildings that displayed excessive foundation displacements were 4 to 6 storey reinforced concrete buildings. Fixed-base periods for these structures are estimated by the formula:

$$T_s = 0.1 \cdot n \quad (s) \tag{3.77}$$

where, n is the number of storeys. Lumped mass for each storey of a simple apartment building, and the foundation is approximated by,

$$m_{st} \cong 1^{t/m^2} \cdot A_{st} \tag{3.78}$$

where, A_{st} is the area per storey. Storey heights are assumed to be 3 m for each floor, except for the entrance floor, which is estimated to be about 3.5 m for most buildings included in the investigated cases. These values are representative of the general characteristics, and will be utilized to estimate period ranges.

Calculations for T_h and T_r are dependent on the selection of V_s and ρ, the shear wave velocity and density of the foundation soil. During laboratory studies, the average unit-weight of the saturated silt-clay mixtures dominating the profile at the sites are observed in the range of (see Appendix B),

$$\rho_{sat} = 1800\ kg/m^3 \tag{3.79}$$

The results of shear-wave velocity measurements performed by Bray et al. (2001b) at selected sites with excessive foundation displacements are plotted in Figure 3.10. The SASW method is utilized for in-situ measurements of low strain

velocity, at five different sites. Low strain V_s are observed to vary generally between 100 and 150 m/s approximately, for the first five meters zone below (average) foundation level, which is prone to shear failure during seismic loading.

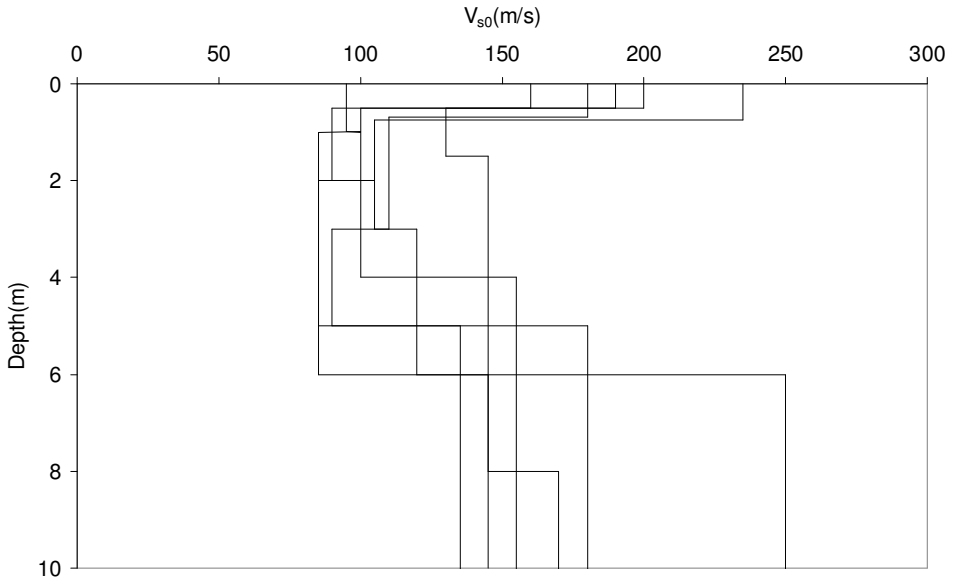

Figure 3.10. Plot of small-strain shear-wave velocity profiles (V_{s0}) for 5 different sites (6 different profiles) with excessive foundation displacement observations in Adapazari (Bray et al., 2001b).

Considering strong nonlinearity of soils, utilization of small strain modulus in calculations is inappropriate. Based on the equivalent linearization concept, the deformation modulus should be reduced considering the strain levels relevant for the problem (Atkinson, 2000). In this case, the solutions provided for linear systems can still be applicable. For SSI analyses, FEMA 368 (Building Seismic Safety Council, 2001) proposes stiffness reduction factors, depending on the severity of the seismic loading. These factors are given in Table 3.1. Hence, small strain velocities should be multiplied by 0.65 in calculations for a severe earthquake, according to FEMA 368 recommendations. Reduced shear velocity profiles are plotted in Figure 3.11.

Table 3.1. Correction factors for shear wave velocity (FEMA 368, Table 5.8.2.1.1)

PGA	0.10 g	0.15 g	0.20 g	≥0.30g
V_s / V_{s0}	0.90	0.80	0.70	0.65

An alternative procedure is to utilize unloading / reloading loop stiffness in large-strain laboratory tests. Based on the observations from cyclic loading tests on silt-clay mixtures encountered (Chapter 2), average shear modulus for reloading tests performed following the monotonic strength tests can be utilized for practical purposes. Accordingly, an unloading / reloading loop is applied at the end of selected monotonic strength tests (see Appendix B). Shear modulus for the large strain behavior is estimated utilizing the variation of deviator stress and axial strain, via Hook's Law. In fact, these tests were performed under anisotropic stress conditions, and a nonzero shear stress exists at initiation of reloading test. The conclusions do not involve the effect of stress reversal in compression and extension, hence the stiffness degradation due to "strain memory" as discussed in Chapter 2 does not exist. Calculated shear modulus for laboratory reloading tests are compared with the reduced V_s values in Figure 3.11: values are comparable, except for the data point at depth 6.3 m. Hence, based on results in Figure 3.11, it is reasonable to assume that,

$$V_S \cong 70 \text{ m/s} \tag{3.80}$$

for practical applications. Since, ground water table level is observed to be near ground surface in Adapazarı, subsoils are assumed to be fully saturated. Hence, Poisson's ratio (ν) is set to 0.5 for utilization of equations 3.73 and 3.76.

Hence, calculated values of T_r and T_h are plotted in Figure 3.12.a and 3.12.b, for buildings with 4, 5 and 6 stories. Foundation length to width ratio (L/B) is arbitrarily selected to be 3. Period calculations are observed not to be sensitive to L/B ratio, since calculations for the ratio of 1 (square) and 5 give similar values. Corresponding period for the total displacement of the soil-structure system, due to equation 3.24.b, is provided in Figure 3.13.

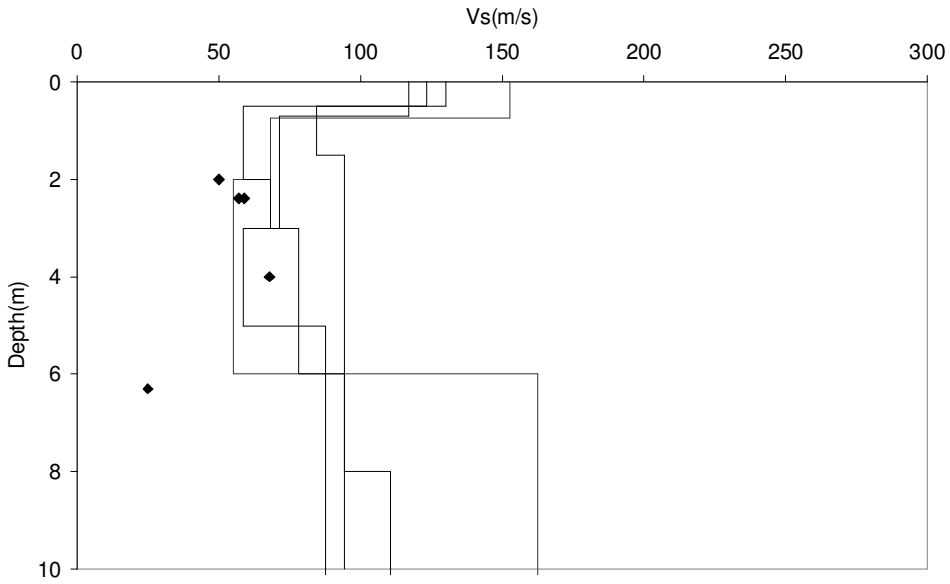

Figure 3.11. Plot of large-strain shear-wave velocity profiles (V_s), and comparisons with the calculated from reloading tests on triaxial test apparatus (diamonds).

Investigation of Figures 3.12 and 3.13 reveals that, for aspect ratios greater than 1.0 (i.e., buildings with narrow foundation width) rocking period is greater than the translational period, consistent with the statement that SSI is governed by the rocking mode for buildings with aspect ratios greater than one. When period elongation due to SSI is investigated (i.e., $\overline{T} / T_s$), rocking mode govern the response of buildings with poor aspect ratios. On the other hand, period for the cases with relatively wide foundation width (i.e., good aspect ratio) will be governed by horizontal translation mode of foundation.

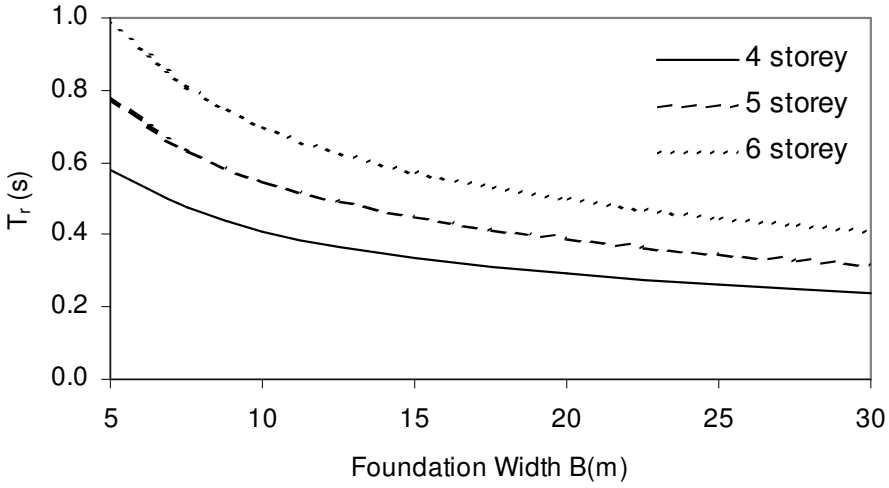

(a)

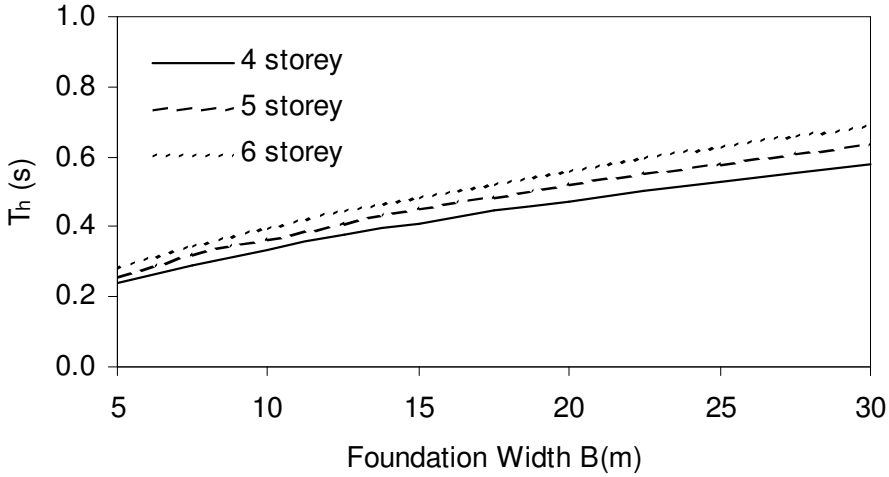

(b)

Figure 3.12. Approximate (a) rocking, and (b) horizontal translation period ranges for buildings resting on shallow mat foundations, with L/B=3. Foundation soil is considered to be undrained (ν=0.5) with a shear wave velocity of 70 m/s.

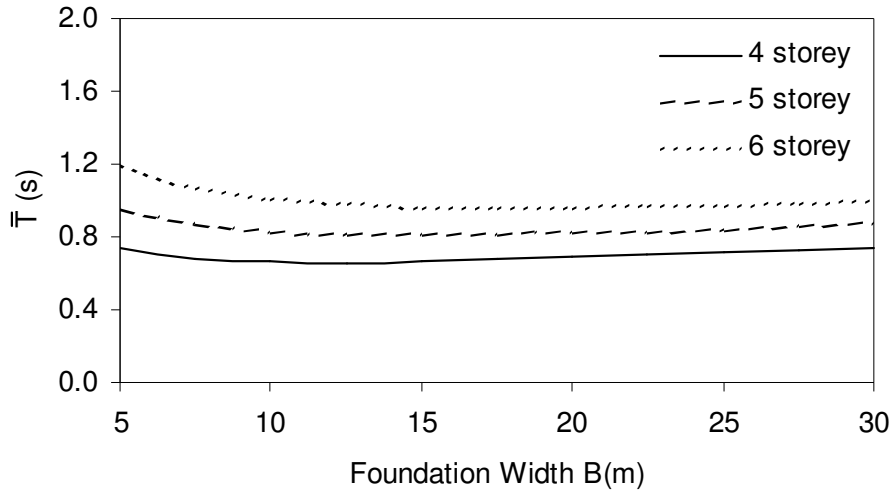

Figure 3.13. Approximate period ranges for coupled soil-structure system, based on equation 3.24.

In comparison, it is discussed in Chapter 4 that, failure mode for poor aspect ratio buildings is governed by the load eccentricity (i.e., overturning moment acting on foundation). On the other hand, when buildings with good aspect ratio are considered, failure mode will involve both load inclination effect and load eccentricity effect. Hence, for a given building height, as foundation width increases, participation of horizontal translation in total displacements (u_t) for a nonlinear soil-structure interaction system increases. Omitting the participation of horizontal displacements in irrecoverable displacements, conservative irrecoverable tilting values are calculated for buildings with good aspect ratios. Still, the calculation procedure is asymptotically correct, that is, zero irrecoverable tilting will result in for very wide foundations (i.e., for very low aspect ratios), since the seismically induced overturning moment will tend to zero as the aspect ratio approaches to zero.

Another practical result that can be inferred from Figure 3.13 is that, flexible-base period range for 4 to 6 storey buildings are approximately in the range of 0.65-1.0 sec. Accordingly, for practical discussions on available cases, it is assumed that,

$$\overline{T} \cong 0.8 \text{ s} \tag{3.82}$$

for all typical 4 to 6 storey buildings, resting on soft sit-clay mixtures. Considering the uncertainties involved, it does not worth to utilize rigorous estimate of linear system period at this step. Hence, reasonable estimates for magnitudes of foundation displacements are sufficient for practical purposes.

As discussed further in Chapter 5, the small-strain shear wave velocity for Mexico-City soft clays are reported to be in the order of 75 m/s (Seed et al., 1988). The reduced shear wave-velocity is in the order of,

$$V_s \cong 60 \text{ m/s} \tag{3.83}$$

which is comparable to Adapazarı cases. However, significant uncertainty exists in estimation of T_s for Mexico City cases, which can have a value in the range of 1.0 to 2.0 s. The contribution of SSI is observed to increase $\overline{T}$ value in the order of 0.3 s, which can be omitted considering the uncertainty in calculations. Hence, the $\overline{T}$ value can be as high as 2.0 s or more, which coincides the predominant site periods in the heavily-damaged sections of the city. This uncertainty is considered in calculations for the Mexico City in Chapter 5.

3.8. Conclusions

Based on simplified inertial soil-structure interaction discussions, it is concluded that the overall behavior of the soil-structure interaction system for buildings resting on surficial mat foundations can be reduced to the simplified model in Figure 3.3. For multistory buildings, total mass of the structure is assumed to be lumped at an equivalent height $\overline{h}$, calculated by equation 3.47. This equivalent height is observed to be about 2/3 of total height of most reinforced concrete multistory buildings. The natural period of the simplified model can be estimated by equation 3.24. For a given vertical load on a shallow mat foundation, ultimate level of overturning moment capacity can be estimated by procedures presented in Chapter 4. Neglecting the damping, yield acceleration for the lumped mass can be estimated by equation 3.60. Hence, overall behavior of the system will be simple elastic-perfectly plastic, and irrecoverable displacements will be due to irrecoverable tilting of the foundation, which can be calculated by the relationship 3.57.

Implementation of effective damping of the system into the calculation procedure is a difficult task. This is not only because the equivalent damping ratio

is frequency dependent, but also because the conventional SSI formulae will become obsolete in case of yielding, as such formulation is based on elastic-halfspace assumptions. Even in the case of linear behavior, damping ratio is dependent on geotechnical details, such as soil stratification beneath the foundation. Still, all the discussions are based on the assumption that the seismic loads are due to vertically incident SH waves. As a practical conservative assumption, it is presumed that all input energy to the system is dissipated by the hysteretic behavior of the elastic-perfectly plastic system. Hence, for time history analyses and for utilization of elastic design spectrum, a small damping (e.g., 5%) can be incorporated in the formulations.

Utilization of a relatively low damping ratio for radiation-damping may not be sufficient to suppress the impact of some unconservative factors involved in the response. One important unconservative assumption is ignoring the effect of seismic loading in the longitudinal direction (i.e., strong direction), which may tend to increase inelastic displacement demand in the transverse direction. Hence, due to geotechnical and geometrical uncertainties, it is reasonable not to involve a significant reduction in irrecoverable displacement demand due to radiation damping. Similarly, as discussed in Chapter 2, visco-plastic response of fine soils may have similar impact as the damping, reducing the displacement demand. Since it is difficult to develop a relationship between the measured laboratory viscous behavior and expected site response, it is practical to consider the impact of viscous response and possible significant radiation damping as reserve strength for the nonlinear behavior of foundations. Yielding of the superstructure may also result in reduced displacement demands in foundation, which is not considered in the simplified approach presented here. Still, the presented methodology is practically useful and economical for seismic foundation design, as it allows the foundation capacity to be exceeded by seismic demand during strong motion, and it provides a calculation procedure to predict irrecoverable tilt angle of the structure.

CHAPTER 4

OVERTURNING MOMENT CAPACITY OF SHALLOW FOUNDATIONS

4.1. General

In Chapter 3, it is stated that, there is a critical level of horizontal acceleration (a_y) acting on building inertia, such that it can create sufficient overturning moment (M_y) on the foundation level to initiate yielding of the foundation-soil system. In this section, practical methodologies to estimate the value of M_y (hence a_y) are developed.

As discussed further in the literature review, the overturning moment capacity of the foundation is dependent on the static factor of safety of the building. In simple buildings with mat foundations, the static bearing capacity problem will involve only the vertical forces acting on the structure and the soil (Figure 4.1). Hence, the static factor of safety against bearing capacity failure is expressed as (Craig, 1983),

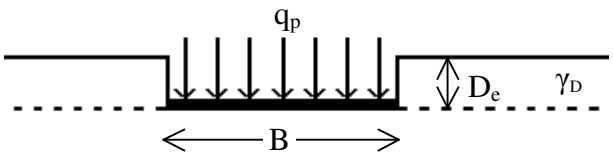

Figure 4.1. Simple sketch for definition of factor of safety against static bearing capacity failure for shallow foundations.

$$FS = \frac{q_u}{q_p} \tag{4.1}$$

where, q_p is the bearing pressure on foundation, and q_u is the ultimate bearing pressure that can be applied on the foundation before the initiation of plastic flow. In case of existence of embedment (i.e., $D_e \neq 0$), the net foundation safety is defined as,

$$FS_{net} = \frac{q_u - \gamma_D D_e}{q_p - \gamma_D D_e} \tag{4.2}$$

where, γ_D is the buoyant unit weight of soil above foundation level, and D_e is the embedment depth. Dividing the foundation pressure q_p into two components,

$$q_p = q_{str} + q_{fdn} \tag{4.3}$$

where, q_{str} is the load component due to weight of superstructure, and q_{fdn} is the component due to weight of the foundation system. For structures without basement, it can practically be assumed that $q_{fdn} \cong \gamma_D \cdot D_e$. Hence, equation 4.2 can be reduced as,

$$FS_{net} = \frac{q_u - \gamma_D D_e}{q_{str}} \tag{4.4}$$

In case of foundations without significant embedment, such as those in Adapazarı, the impact of surcharge can be practically ignored. In this case, $\gamma_D D_e$ term in equation 4.4 can also be practically omitted. Hence, for the mat foundations with small embedment, equation 4.4 eventually reduces to:

$$FS_{net} \cong \frac{q_u}{q_{str}} \tag{4.5}$$

Note that, equation 4.5 is not valid for relatively deeply located mats. Such cases, however, are not dealt within this study. When embedment is of significance and practically cannot be omitted in bearing capacity calculations, the contribution of embedment should be introduced to the analysis procedures discussed in this chapter.

In this study, the net factor of safety (FS_{net}) will be utilized by neglecting the weight of foundation mass and the embedment effect on ultimate load capacity to

simplify the formulations. Also, the subscript in FS_{net} is dropped for practical purposes, and static net factor of safety against bearing capacity failure is simply referred to as factor of safety (FS). Hence, the contribution of embedment is considered as an over-strength factor, which causes the foundation displacements to reduce in practice. Therefore, in case of buildings with no basement, mass of the excavated soil is assumed to be equivalent to the replaced mass of foundation.

Another important matter is that, the foundation system is considered to be a rigid mat, designed as reinforced slab. On the other hand, in many cases, foundation shape may be complicated, and foundations may consist of strong beams, or mats in the shape of a grid. In order to simplify the discussions, effect of foundation type on bearing capacity is ignored. However, for a specific foundation, it is possible to investigate the effect of foundation shape on bearing capacity utilizing the analysis procedures presented in this chapter.

4.2. Literature Review

The seismic bearing capacity of a shallow foundation involves the generalized loads as shown in Figure 4.2: Foundation loads can be summarized by the vertical load V, overturning moment M, and base shear H; the inertial loads acting on the soil is determined by the vertical (including gravitational acceleration g) and horizontal accelerations, a_v and a_h respectively. Multiplication of a_h and a_v with the unit mass of soil (ρ) gives inertial forces acting on the unit volume of soil. These forces can have both the static and dynamic (i.e., time-dependent) contributions. In case of the generalized static problem for a shallow foundation resting on level ground, only the V and $g \cdot \rho$ are the driving static forces. Hence, the success of any methodology aiming at determination of the seismic bearing capacity is inevitably dependent on its success in estimation of the static bearing capacity. Therefore, here, discussions on bearing capacity will preclude the seismic bearing capacity considerations, since any inherent uncertainty in the static problem is directly becomes the controlling factor in the seismic problem. The literature review on combined loading of foundation (i.e., foundation load involving combinations of nonzero M, V and H values), including the uplift behavior, is presented as the second step. Finally, studies related to the seismic bearing capacity problem, which involves the inertial forces acting on soil, are discussed.

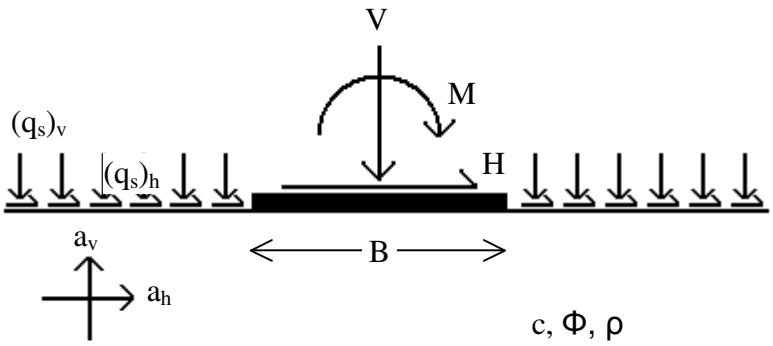

Figure 4.2. The parameters utilized in seismic bearing capacity problem.

4.2.1. Investigation of static bearing capacity

In analytical approaches to the problem of bearing capacity, foundation soil is considered as a rigid - ideally plastic material, obeying the Mohr-Coulomb yield rule. Accordingly, the shear strength (τ_f) on a failure plane is given as:

$$\tau_f = c + \sigma_n \tan\phi \tag{4.6}$$

where, Φ is the angle of internal friction, c is the cohesion intercept, and σ_n is the normal stress acting on the failure plane. The foundation loading is expressed by the vertical load (V), horizontal load H, and overturning moment M. Defining the load eccentricity (e) and the load inclination (i) with respect to the vertical axis of foundation:

$$e = \frac{M}{V} \tag{4.7}$$

and,

$$i = \frac{H}{V} \tag{4.8}$$

The generalized form of the bearing capacity equation (Das, 1999) can be expressed as,

$$q_u = cN_c f_{cs} f_{cd} f_{ci} + q_s N_q f_{qs} f_{qd} f_{qi} + 0.5\gamma B N_\gamma f_{\gamma s} f_{\gamma d} f_{\gamma i} \quad (4.9)$$

where, N_c, N_q and N_γ are the bearing capacity factors; f_{*s} are the foundation shape factors; f_{*d} are the foundation depth (embedment) factors; f_{*i} are the load inclination factors, q_s is the surcharge pressure, B is the foundation width, γ is the unit weight of the soil (i.e., $\gamma = g \cdot \rho$), and q_u is the ultimate bearing pressure. The basic idea beneath equation 4.9 is that, there are three main contributions to ultimate bearing pressure for a foundation: the soil cohesion (c) contribution, the surcharge (q_s) contribution, and soil self-weight contribution (γ), which are dependent on the internal friction angle (Φ). In fact, the equation is the superposition of two different bearing capacity problems: the bearing capacity for a foundation resting on a purely cohesive soil (Φ=0), and for a foundation resting on a purely cohesionless soil (c=0), where surcharge is considered in both cases (Terzaghi, 1943). Both problems can be handled separately by analytical approaches. However, superposition of the two solutions is not mathematically correct, but the approximation is on the safe-site (i.e., predicts lower q_u values than the unknown exact solution).

Load eccentricity (e) is introduced in equation 4.10 by utilizing effective width B′ instead of actual width B of foundation (Meyerhof, 1963), such that,

$$B' = B - 2e \quad (4.10)$$

A summary of analytical formulations for the factors in equation 4.9, which are utilized in different European Union countries, are presented and compared in a study by Sieffert and Bay-Gress (2000). These formulations are mainly based on the proposals of Terzaghi (1943), Meyerhof (1963), Hansen (1970) and Vesic (1973). Sieffert and Bay-Gress observed that, the estimated bearing capacity depends strongly on the selected formulation. The only agreement is on the effect of load eccentricity (stated in equation 4.10): however, this does not imply that it is accurate. Hence, a unique methodology to estimate the bearing capacity does not exist for application, and further studies are still required on this topic.

Analytical approaches depend on significant assumptions, which may not be consistent with the practical engineering applications, in order to reach a closed-form solution. In comparison, numerical approaches are fairly free from such assumptions. In the foregoing, with a few exceptions, soil is considered as purely

cohesive (Φ=0) or purely cohesionless (c=0). Discussions on N_γ factor are presented in detail in this study. There exists no strong agreement on the evaluation of this factor, which plays a significant role in drained factor of safety of existing buildings in case-studies. This is due to the rather low effective cohesion (i.e., practically zero) of normally consolidated silt-clay mixtures.

An important issue in analytical formulation is that, associative flow rule (i.e., Ψ=Φ) is assumed to be valid for the soil behavior, which may introduce significant error in calculations. As discussed in Chapter 2, the dilatation angle is observed to be in the order of zero, implying a strongly nonassociative behavior. Drescher and Detournay (1993) showed that, in plane-strain limit analyses, the effect of non-associativeness can be easily investigated by performing an equivalent associative analysis, with modified Mohr-Coulomb parameters (c* and Φ*):

$$\tan\phi^* = \frac{\cos\psi\cos\phi}{1-\sin\psi\sin\phi}\tan\phi \qquad (4.11.a)$$

$$c^* = \frac{\cos\psi\cos\phi}{1-\sin\psi\sin\phi}c \qquad (4.11.b)$$

Hence, nonassociativeness tends to reduce overall shear strength, and thus the ultimate load capacity, of the soil body.

Utilizing the method of characteristics, Bolton and Lau (1993) investigated bearing capacity factors under vertical loading, for strip and circular foundations resting on Mohr-Coulomb soil. They confirmed that the Terzaghi's approach, consisting of the superposition of bearing capacity terms (i.e, cohesion, soil-weight, and surcharge components) provides safe solutions. Calculated bearing capacity factors N_q and N_γ are observed to be very sensitive to the value of Φ. The interface condition between foundation and soil (i.e., soil - foundation friction) is also observed to strongly influence the bearing capacity: considering the case of Φ=30˚ and strip foundations, calculated values of factor N_γ is 7.74 and 23.6 for smooth and rough foundations, respectively.

Michalowski (1997) investigated N_γ factor using kinematic approach (upper bound) of limit analysis. They investigated the effect of non-associativity of the soil on N_γ factor, by employing the approach proposed by Drescher and Detournay (1993) as stated in equations 4.11. It is observed that, N_γ is sensitive to dilatancy

angle (Ψ), and drops significantly with the decrease in Ψ. Hence, the influence of non-associative flow rule should be considered in engineering design.

Utilizing finite element and finite difference methods for the analysis, Frydman and Burd (1997) investigated N_γ factor for shallow strip foundations. For the case of smooth footings with Φ<35°, dilatation angle is observed to have no practical impact on the value of N_γ. On the other hand, reduction in N_γ by the decrease in ψ is very significant for the case of rough footing. Hence, for the case of Φ=30° and rough footing, calculated values for the N_γ factor are 21.7 and 16.7 corresponding to Ψ=Φ and Ψ=0°, respectively. For the case of smooth footing, calculated values reduce to 8.7 and 7.9 respectively. Frydman and Burd also concluded that, discrete numerical techniques, such as finite-element and finite-difference methods can be utilized for investigations of foundation load capacities, provided that computational difficulties and accuracy problems are handled cautiously. Parallel conclusions regarding N_γ and ψ relationship are also stated by Yin et al. (2001) from a similar study. Considering three-dimensional cases, reduction in bearing capacity for circular foundations due to nonassociativity is demonstrated by the numerical studies of Erickson and Drescher (2002).

Ukritchon et al. (2002) introduced linear programming for the numerical solution of bearing capacity problem, by the discretization of limit analysis problem domain. Calculated Nγ values are compared with reported values in literature: proposed values by Hansen and Christensen (1969), and Meyerhof (1963) are observed to agree with the findings. Similar to the conclusions of Bolton and Lau (1993), roughness of the footing is observed to have significant effect on N_γ values. When compared to the results of Bolton and Lau for Φ=30°, the N_γ factor is calculated as 7.5 and 15.0 for the case of smooth and rough footing interface, respectively.

Apart from all analytical and numerical models, all of which simplify the behavior of soil and soil-foundation interface to provide a simplified solution, an alternative approach is to utilize laboratory models. The laboratory models may not only supply the bearing capacity factors experimentally, but also verify the accuracy of bearing capacity calculation procedures. However, model tests suffer from scale effects when compared with analytical approaches (Perkins and Madson, 2000). Complications due to scale effects involve the nonlinearity of Mohr-Coulomb failure envelope for real soils (i.e., dependency of Φ to normal effective

stress level), and progressive-failure mechanism which will result in different mobilized Φ values in different locations on failure plane, varying between peak-state and critical-state values. Siddiquee et al. (2001) added to the discussion that, inherent anisotropic strength, highly nonlinear stress-hardening or softening behavior, shear banding with a specific band width as a function of the particle size of the test material are also reasons for further complications.

In order to investigate the reliability of theoretical solutions, Ingra and Baecher (1983) studied the uncertainty in bearing capacity calculations for shallow foundations resting on surface of dry sands, by utilizing available experimental data. Due to the statistical analysis of the data, coefficient of variation for the bearing capacity without surcharge (i.e., q_s=0) range from 20% to 30%, even in the case of well-defined soil properties. Theoretical values by different approaches are observed to vary by factors of 2 to 4 for different solutions. These values are also very sensitive to Φ, which is in turn dependent on the intermediate principal stress, anisotropy, strain compatibility, and non-linear nature of the Mohr-Coulomb strength envelope. Even in well-designed laboratory tests, significant difficulties arise due to differences in test apparatus and procedure, identification of failure load, footing material and roughness, soil density, and measurement of friction angle, since the results are observed to be very sensitive to these details. Besides all uncertainties, if the friction angle can not be accurately determined (e.g., having a standard deviation greater than 1˚), the contribution of uncertainty due to Φ dominates the overall uncertainty in bearing capacity estimations. Zadroga (1994) also obtained similar conclusions on the deviation of experimental results from theoretical values, for cohesionless soils. The bearing capacity obtained by model tests are observed to be higher than the theoretical values, possibly due to the effects of soil anisotropy, progressive failure phenomenon, and scale issues. Further research is required to classify the impact of these effects to bearing capacity calculations.

Finalizing the discussions, the N_γ factor has a significant uncertainty in engineering practice. Accordingly, estimation of drained (long-term) static factor of safety for existing buildings suffers significantly from this uncertainty. Results of dynamic numerical analyses are dependent on the reliability of the simulation of static bearing capacity. Hence, within the scope of this study, the results of seismic bearing capacity analyses are normalized with the static bearing capacity, as

proposed by Paolucci and Pecker (1997a). No detailed data is available to decide the exact q_u values for the available cases in Mexico City and Adapazarı. Also, Ψ is observed to be zero as discussed in Chapter 2, which will result in reduction of N_γ factor when compared to the values obtained for associative flow-rule. In any case, a detailed study for understanding static bearing capacity of existing buildings in available cases is required, as a supplementary work. This is left as a future study, and rough estimations of bearing capacity are utilized in the evaluated case studies.

4.2.2. Foundations under combined loading

Apart from the seismic bearing capacity problem, the impact of overturning moment and base shear acting on a shallow foundation is separately discussed in literature in previous decades. The overturning moment (M) and base shear (H) can be normalized by the vertical load (V) as expressed in equations 4.7 and 4.8, yielding load eccentricity (e) and inclination (i). The studies on ultimate bearing capacity of shallow foundations under inclined and eccentric load (i.e., combined loading) are discussed in the following paragraphs.

A simpler problem is the case when foundation uplift is prevented. Numerical approaches and formulations are available for this case, such as the studies of Taiebat and Carter (2000), and Randolph and Puzrin (2003). Although the results are not applicable to foundation failure cases observed in Adapazarı and Mexico City due to restricted uplift behavior in models, still there are foundation applications for which uplift is prevented due to a possible suction at soil-foundation interface, such as spudcam foundations of off-shore platforms (Dyvik et al., 1989). Still, the analysis procedures by Taiebat and Carter provide valuable feedback for finite-element modeling of undrained behavior of soil, which is also extended later to the case of uplifting foundations in a following study by Taiebat and Carter (2002). These studies provide basic finite-elements approaches that are utilized in this study, and basic equations that are utilized for verification purposes.

For the case of circular foundation on cohesive soil, Taiebat and Carter (2000) studied the bearing capacity under combined loading (i.e., involving load eccentricity and inclination), without allowing the separation of the foundation-soil interface (i.e., uplift), and utilizing F.E.M. The soil is modeled as an elastic-ideally plastic material, obeying the Tresca yield criterion with shear strength S_u. The

Young's modulus (E_u) is set to $300S_u$, and Poisson's ratio (ν) is set to 0.49, which will provide sufficient incompressibility of the model soil. Finite-element analysis is based on load-defined approach, in which foundation loads are increased up to the failure (i.e., plastic flow behavior of the foundation). It is proposed that, for the case of zero load inclination, failure loads are best determined by applying a small horizontal load (compared to vertical load and overturning moment) on foundation, and detecting the peak load for load-displacement curve for the closest Gauss point to the center of foundation-soil interface. It is concluded that, shallow foundations on cohesive soils are most vulnerable to load eccentricity and inclination when FS against bearing capacity for the case of zero load inclination and eccentricity is less than 2.

Later, Taiebat and Carter (2002) investigated the problem of bearing capacity of strip and circular shallow foundations resting on undrained clay, subjected to eccentric loads and involving uplift, by utilizing the finite-element approaches discussed by Taiebat and Carter (2000). They utilized a thin layer of 'no-tension' elements beneath the foundation to model uplift of the foundation imposed by the overturning moment. Taiebat and Carter concluded that, when uplifting of the foundation is considered, effective width approach (Meyerhof, 1963) in calculation of ultimate bearing capacity for eccentric load is applicable for both plane-strain and 3D (i.e., circular foundation) problems. Thus, it is reasonable to assume existence of a unique relationship between M_y/VB versus FS, irrespective of foundation shape. For the case of strip foundations with zero load inclination (i.e., H=0), the finite element analysis results are observed to be consistent with the equation proposed by Houlsby and Purzin (1999), and expressed as,

$$\frac{V}{(\pi+2)\cdot B\cdot S_u}=1-2\left(\frac{M_y}{VB}\right) \tag{4.12}$$

where, S_u is the undrained shear strength of the homogeneous soil obeying Tresca failure criterion. Hence, utilizing Prandl's (1920) solution for ultimate vertical load for strip foundations, the factor of safety against bearing capacity failure for a given vertical load can be formulated as:

$$FS=(\pi+2)\cdot S_u\cdot B/V \tag{4.13}$$

Substituting equation (4.13) into (4.12) results in,

$$\frac{1}{FS} = 1 - 2\left(\frac{M_y}{VB}\right) \tag{4.14}$$

for calculation of ultimate M/VB ratio, which is utilized for verification of uplift behavior in this study. An alternative approach for the analytical verification is also provided in Section 4.3.4. For the case of circular foundations, Taiebat and Carter (2002) showed that, the finite element results are consistent with the equation,

$$V = \frac{D^2}{2}\left(1 + 0.2\sqrt{\left(1 - \frac{2M_y}{VD}\right)\Big/\left(1 + \frac{2M_y}{VD}\right)}\left(\arccos\left(\frac{2M_y}{VD}\right) - \frac{2M_y}{VD}\sqrt{1 - \left(\frac{2M_y}{VD}\right)^2}\right)\right) \cdot (\pi + 2)S_u \tag{4.15}$$

where D is the diameter of the circular footing, and S_u is the shear strength of the purely cohesive soil. Defining the static bearing capacity as,

$$FS = \frac{V_u}{V} \tag{4.16}$$

where, V_u is the ultimate vertical load that can be applied on the foundation (i.e., for the case M=H=0), which is equal to,

$$V_u = 5.7\left(\frac{\pi D^2}{4}\right)S_u \tag{4.17}$$

for circular foundations. Hence, substituting equations (4.16) and (4.17) into (4.15), the relationship for determination of ultimate load eccentricity for a given FS is,

$$\frac{1}{FS} = 0.57\left(1 + 0.2\sqrt{\left(1 - \frac{2M_y}{VD}\right)\Big/\left(1 + \frac{2M_y}{VD}\right)}\left(\arccos\left(\frac{2M_y}{VD}\right) - \frac{2M_y}{VD}\sqrt{1 - \left(\frac{2M_y}{VD}\right)^2}\right)\right) \tag{4.18}$$

Hence, utilizing equations 4.14 and 4.18, the relationship between FS and M_y/VB ratio can be compared for the case of strip (i.e., two-dimensional case) and circular (i.e., three-dimensional) foundations. The comparison is given in Figure 4.3, for the case of choosing D=B. In actual applications, if B is the width of foundation, then the minimum length (L) of the foundation will be B, implying a square foundation with dimensions B·B. In this case, the equivalent diameter for a circular foundation with the same foundation area is expressed as D=1.128B. Referring to as "equivalent circular" for this case, the comparison with strip foundation is also given in Figure 4.3. It is observed that, for strip and square foundations, the relationship between M_y/VB ratio and FS is similar. Hence, for practical purposes, the relationships determined for the strip foundations can be applicable to the case of rectangular foundations.

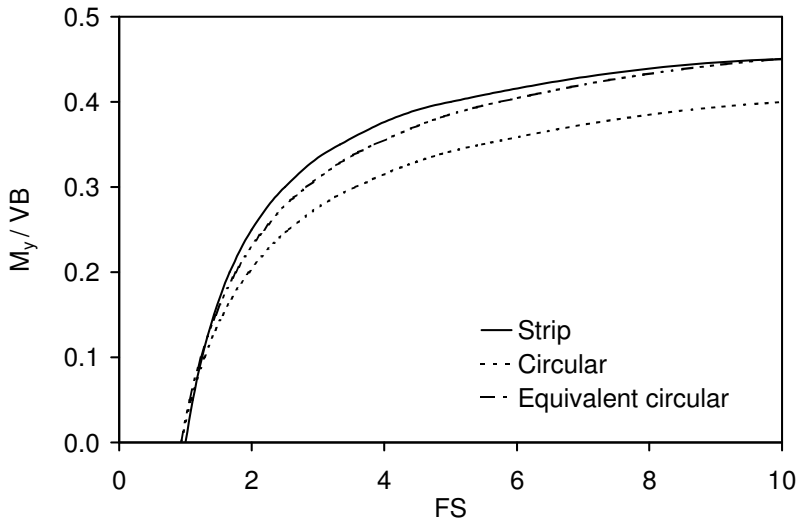

Figure 4.3. Relationship between ultimate M_y/VB and FS for an uplift-permitted foundation, resting on a purely cohesive soil, according to the equations provided by Taiebat and Carter (2002).

Salençon and Pecker (1995) developed lower-bound and upper-bound solutions for shallow strip foundations under inclined and eccentric loads. In their study, soil is assumed to obey Tresca's failure criterion, and the rigid shallow foundation is permitted to uplift. The upper and lower-bound estimates are relatively close to each other for low values of eccentricity, but the difference

increases, as eccentricity gets higher. However, it is concluded that, the effective area concept of Meyerhof (1963) can lead to significant error in bearing capacity estimations.

Bransby (2001) investigated the bearing capacity of rigid strip foundations resting on undrained soil (i.e., obeying Tresca failure criterion) under eccentric loading, both, including and excluding foundation uplift. Bransby introduced Meyerhof's (1963) equivalent area concept for eccentric loading into analytical approaches, and verified the results utilizing finite element method. The methodology is also extended to non-uniform soil strength case, such as increasing linearly by depth. For the case of uniform soil strength and uplifting foundations, Bransby agreed with equation 4.14 for the calculation of ultimate overturning moment.

Similar to discussion on static bearing capacity, laboratory model tests can be utilized in order to develop relationships between M, V, and H. Utilizing the results of model tests on cohesionless soils from different authors, Butterfield and Gottardi (1994) proposed following relationship between vertical load V, horizontal load H, and overturning moment M acting on footing on sand as,

$$\left(\frac{V}{V_u}(V_u - V)\right)^2 = \left(\frac{H}{0.52}\right)^2 + \left(\frac{M_y}{0.35B}\right)^2 - \left(2.4\frac{M_y \cdot H}{B}\right) \tag{4.19}$$

and, introducing the FS (equation 4.16) into equation 4.19,

$$\left(1 - \frac{1}{FS}\right)^2 = \left(1.9\frac{H}{V}\right)^2 + \left(2.9\frac{M_y}{VB}\right)^2 - \left(2.4\frac{M_y}{VB}\frac{H}{V}\right) \tag{4.20}$$

However, Zadroga (1994) discussed that, although the model test results are consistent with the effective width concept due to load eccentricity, the reduction in bearing capacity due to load inclination is observed to be inconsistent with most available equations.

Concluding the discussions on the impact of load eccentricity and inclination on ultimate vertical load capacity of a foundation, for which uplift is permitted, available equations are limited with the constitutive model for the soil, and foundation-soil interface. The test results have significant uncertainties that affect

the reliability of the outcome. In case of practical applications, these uncertainties will be amplified, due the effects of actual soil stratification, limitations in geotechnical data, boundary conditions (e.g., impact of neighbor buildings) and foundation details. However, available equations can be utilized as verification for the analyses of this study. The impact of load eccentricity and inclination play a backbone role in seismic bearing capacity, which is presented in the following section. In any case, if the foundation is not allowed to perform limited foundation displacements, costly foundation improvement techniques are likely required with shallow foundations in severe earthquake hazard regions, especially when these uncertainties are considered.

4.2.3. Seismic bearing capacity

As discussed in the introductory paragraph of Section 4.2, seismic bearing capacity problem involves not only the load eccentricity and inclination for foundation loads, but also the inertial loads acting on the soil mass. The inclination of surcharge (q_s) can also deviate from the vertical axis. The problem can be investigated by pseudo-static approaches, in order to estimate the level of acceleration sufficient to initiate plastic-flow of foundation. In this section, a brief literature survey on the seismic bearing capacity is presented.

The first group of studies involve those that do not separate the effect of inertial loads on soil mass from the effect of load inclination and eccentricity: Richards et al. (1993), Budhu and Al-Karni (1993), Sarma and Iossifelis (1990), investigated the problem of shallow foundation utilizing limit equilibrium method, omitting the load eccentricity on the foundation. A uniform pseudo-static acceleration distribution is considered on the problem model. The practical significance of vertical accelerations is discussed to be very limited when compared to horizontal accelerations. Richards et al. and Sarma and Iossifelis also presented methodologies to estimate the settlements when yield-acceleration (a_y) is exceeded. The settlement calculation methodologies are based on Newmark's (1965) sliding block analogy, such that the foundation and the soil beneath the foundation are considered as a single block sliding over the failure plane. Soubra (1999) introduced the upper-bound method of limit analysis for the solution of the problem. Kumar and Mohan Rao (2002) investigated the same problem utilizing the method of stress characteristics, and obtained lower values of seismic $N\gamma$ factors

when compared to other studies. The difference is higher when Nγ values for the static case are considered; hence, comparatively reduced Nγ factors for the seismic loading case can be explained. Although above mentioned studies consists of uniform pseudo-static acceleration distribution both for the superstructure building and the soil, Fishman et al. (2003) provided seismic to static N_γ and N_q factor ratios (i.e., reduction in N_γ and N_q due to seismic loading), considering different pseudo-static acceleration levels for the superstructure and foundation soils.

The first significant problem for some of the above studies is that, the impact of load eccentricity and inclination on foundation is not separated from the impact of inertial loads acting on the soil mass. Hence, the significance of variation of the seismic bearing capacity problem from the combined loading problem (i.e., as discussed in Section 4.2.2) is somewhat unclear. Hence, considering cohesionless soils, and for the case of zero load eccentricity on foundation, the studies of Sarma and Iossifelis (1990), and Dormieux and Pecker (1995) conclude that, reduction in bearing capacity is mostly due to load inclination on foundation. Therefore, for practical engineering applications, the effect of inertial accelerations acting on soil can be neglected. For the case of cohesive soils, Soubra (2000) concluded that reduction in bearing capacity (i.e., reduction in N_c factor) during seismic loading is mainly due to seismic forces at foundation level, such that inertial forces in soil medium can be ignored. This conclusion is also consistent with results of the study by Paolucci and Pecker (1997b), which investigates the effect of inertial acceleration acting on soil for rectangular shallow foundations resting on cohesive (i.e., obeying Tresca criterion) soils. Accordingly, the effect of soil inertia can be neglected in most practical applications, especially when static factor of safety against bearing capacity is greater than 2.5. For the case of strip foundations, Pecker (1997) concluded that the inertial acceleration has no practical significance if static factor of safety is greater than 2.0. Paolucci and Pecker (1997b) also concluded that, the effect of the soil's inertial acceleration on reduction of N_γ, and N_q is less than 20% for the case a_h (horizontal pseudo-static acceleration) is less than 0.3g, and the reduction of N_c is much smaller.

Pecker (1997b) also stated that, most theoretical seismic bearing capacity studies suffer the following limitations: 1) accelerations acting on both, structure and soil are assumed to be the same, without reasoning, 2) uplift of foundation is

not considered, 3) these solutions are upper bound estimates, and comparisons with lower bound estimates are not provided. Considering these shortcomings, and utilizing upper-bound approach of limit analysis, Paolucci and Pecker (1997a) provided equations to calculate the reduction in static FS under seismic loading. In their study, the associative flow rule is assumed, and the effect of load eccentricity, inclination and inertial accelerations on soil mass are uncoupled. Proposed equations by Paolucci and Pecker are utilized for verification of drained analyses in this study, and investigated in greater detail.

Paolucci and Pecker proposed the reduction factor v, such that;

$$v = v_h \cdot v_e \cdot v_i \tag{4.21}$$

where, v_h, v_e, and v_i are the contributions of load inclination, eccentricity and horizontal inertial acceleration (acting on soil mass), respectively. Hence,

$$v_h = \left(1 - \frac{H}{0.85V}\right)^3 \tag{4.22.a}$$

$$v_e = \left(1 - 2\frac{M}{VB}\right)^{1.8} \tag{4.22.b}$$

$$v_i = \left(1 - \frac{a_h}{\tan\phi}\right)^{0.35} \tag{4.22.c}$$

The reduced factor of safety under seismic loads is calculated by,

$$FS_{seis} = v \cdot FS \tag{4.23}$$

where, FS_{seis} is the factor of safety against seismic bearing capacity failure. Hence, foundation failure is imminent when FS_{seis}=1.0. Therefore, the critical value of static FS for a given acceleration level (a_h) is simply,

$$FS = \frac{1}{v} \tag{4.24}$$

Investigation of equations 4.22 clarifies that the v_i factor can be practically ignored. This will in turn result in a formula that is independent of Φ, which is

practical for design approaches. Also, the impact of load eccentricity on bearing capacity is very strong: when combined effect of load eccentricity and inclination is considered, the safe (nonyielding) design of a shallow foundation may require very high FS values even for relatively low to moderate seismic acceleration levels. However, this is inconsistent with most post-earthquake observations on shallow foundations. This may be explained considering the transient nature of loading, or non-linear characteristics of soil-foundation-structure interaction.

Available detailed laboratory tests for investigation of seismic bearing capacity failure mechanisms are limited in literature. A comprehensive centrifuge test study is presented by Zeng and Steedman (1998). It is observed that, accumulation of rotation and stiffness degradation for foundation soils play a key role in seismic bearing capacity failure mechanism, even in the absence of liquefaction. Comparing the behavior of tall and heavy buildings with the behavior of low and light buildings, it is concluded that, seismic settlements are strongly correlated with foundation rotations. Furthermore, degradation in the bearing capacity during successive cycles is important in seismic bearing capacity failure mechanism. The degradation mechanisms besides that related to pore-pressure accumulation in soils are the reduction in mobilized shear resistance for relatively high shear strain levels, and topics related to P-Δ effects due to accumulated rotation of foundation.

As a conclusion of the discussion on seismic bearing capacity, especially for the case of buildings with higher aspect ratios, the inertial forces acting on soil mass can be practically ignored. Impacts of load eccentricity and inclination acting on the shallow foundation are much more significant, especially when uncertainties in static bearing capacity estimations are considered. Therefore, seismic bearing capacity problem for shallow foundations reduces to the bearing capacity problem under combined loading. One important issue is the consideration of uplifting of foundations, in cases where no special precautions are taken.

4.3. General Layout of the Finite-Element Analyses

In order to provide a finite-element method approach for estimation of ultimate load levels that a shallow foundation can resist, Plaxis v7.2, which is a finite element code particularly for geotechnical analyses, is utilized. A uniform finite element mesh is utilized in all of the analyses. The basic principles followed in

the analyses are based on the approach proposed by Taiebat and Carter (2000 and 2002), with some minor modifications. Details of the mesh and basic analysis procedures, as well as validation of the accuracy of the numerical analyses are presented in this section.

4.3.1. Mesh and element details

A finite element mesh involving 2279 plane-strain elements is developed (Figure 4.4). Soil medium is modeled by 15-node triangular elements, and foundation is modeled by linear beam elements. Standard fixities are chosen as boundary condition: both horizontal and vertical displacements are fixed at the bottom of the mesh, and only horizontal displacement is fixed on right and left sides of the mesh. The model dimensions of the mesh are 100 m x 50 m, and the foundation width is set to 20 m.

All soil elements, which simulate the behavior of a homogeneous half-space, are set to the same soil material parameters. Elasto-plastic material model, with Mohr-Coulomb yield criterion, is selected as the constitutive model for the soil behavior. In those analyses saturated soil behavior is investigated, water table is located at the ground surface (i.e., at foundation level), and initial pore pressures are calculated accordingly (i.e., hydrostatic pressure distribution). In the analyses where undrained saturated soil behavior is investigated, soil element behavior is set to “undrained” in material properties selection window, which results in constant-volume behavior of saturated soil elements. This sets Poisson’s ratio (ν) for the element behavior to 0.495, by modifying bulk modulus of water accordingly. With an error of negligible magnitude (since $\upsilon \neq 0.5$ exactly), all increase in isotropic pressure will result in an equal increase in pore-pressures in elements. The stress-path will follow the elastic stress-path as further discussed in Section 4.4.3. Tension cut-off at zero effective stress is defined for soils, except for the case of constant strength analyses (i.e., $c \neq 0$ and $\Phi = 0$), and further details are given in Section 4.4.1.

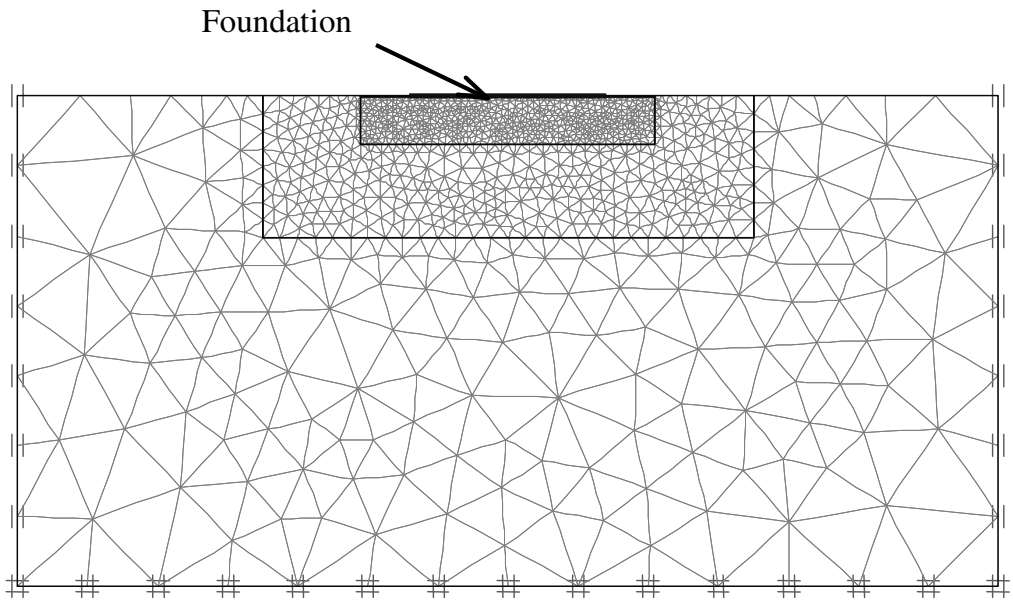

(a)

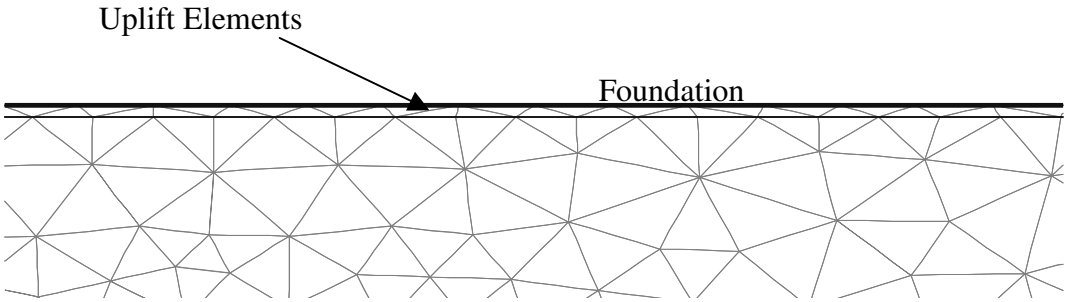

(b)

Figure 4.4. Finite element mesh used in Plaxis analyses: (a) general mesh layout, (b) close view of "uplift elements".

Since foundation uplift is to be considered in realistic investigations of the impact of load eccentricity, a separate region (10 cm thick in the model) that is located immediately beneath the foundation (referred to as uplift elements in Figure 4.4.b) and extending horizontally 5 m away from foundation is permanently set to drained condition with tension cut-off. The permanently drained behavior is due to the fact that, in case the undrained behavior is set for those elements, foundation

uplift will result in negative pore pressures (i.e., suction), which in turn will result in positive effective stresses, and prevent tension cut-off occurrence. The uplift performance of the model is investigated in Section 4.4.1.

Foundation loads are applied as distributed loads on foundation beam, referred to as Traction A and B in Plaxis. The soil shear modulus and saturated unit weight are selected respectively as G= $1.8 \cdot 10^6$ kPa and γ_{sat}=18 kN/m^3, which are compatible for a soil with small strain shear wave velocity (V_s) of 1000 m/s. The reason for selection of such a high shear modulus is to restrict the bearing capacity mechanism to the general bearing failure type, so that the analytical bearing capacity equations will be consistent with the discussions here. As an example, setting a value of V_s=100 m/s results in a highly compressible soil, for which the bearing capacity failure mechanism will not be of the general type, but of the local type (Vesic, 1973). High compressibility of deeper layers will result in punching of foundations into the soil, without forming a Prandl-type shear plane. In that case, the ultimate capacity of foundation will be dependent on the position of relatively stiff layer beneath the foundation. Hence, by increasing the stiffness, failure mechanism is forced to be of general bearing capacity type, and thus consistent with the analytical formulations based on rigid-perfectly plastic soil behavior assumption. Poisson's ratio (ν) of the soil for drained analyses is set to 0.3. The stiffness properties of the foundation are set to EI=10^{10} kN·m^2/m, EA=10^{10} kN/m, and ν=0.3, so that, foundation behaves rigidly when interacting with soil elements. A close inspection of beam deformations revealed that, the left-most and right-most displacements of beams resulted in about 1% error when compared with the rigid behavior.

4.3.2. Basic analysis procedures

Different material parameters and load quantities are utilized for different analyses. Each analysis consists of 3 main steps, for selected sets of parameters and loads:

1. *Calculation of free-field stresses*: this step simulates stress distribution in the free-field (i.e., before foundation placement), depending on unit weight of foundation soil and lateral earth pressure coefficient K_0. For both, consolidated-drained and consolidated-undrained analyses (with c=0 and $\Phi \neq 0$), K_0 is set to 0.5, which is compatible with Φ=30˚ according to Jaky's formula (1944). In case of

cohesive soil analysis (Section 4.4.1), K_0 is set to 1.0 for consistency with Prandl's solution (1920). Effect of K_0 on bearing capacity is also assessed and discussed in Section 4.3.3.

2. *Application of foundation load under drained conditions*: this step simulates the long-term (i.e., drained) stress distribution underneath the foundation. The load on foundation is applied as uniformly distributed vertical pressure acting on foundation beam elements. The magnitude of this pressure is set in accordance with the target factor of safety against bearing capacity failure. This load is referred to as "Traction A" in Plaxis analyses. In all analyses, the material behavior is set to drained behavior, implying that no excess pore-pressure occurs beneath the foundation.

3. *Application of overturning moment and base shear on foundation*: this step simulates the imposition of seismically induced loads. In the case undrained soil behavior is investigated, drainage condition is set to undrained for foundation soils, except for the uplift elements beneath the foundation. Overturning moment and base shear are increased incrementally until the failure is reached. Procedure to detect ultimate values at failure is discussed in the following paragraphs.

Loads on foundations are defined by vertically and horizontally distributed loads on foundation beam by utilizing "traction A" and "traction B" load definitions in Plaxis v7.2. Traction A is utilized to simulate the drained vertical load, and traction B is utilized to introduce load eccentricity and inclination under undrained condition (Figure 4.5). In final calculations, following formulations are utilized in order to calculate the ultimate load and moment values at failure:

$$V = q_A \cdot B \tag{4.25.a}$$

$$H = q_{BH} \cdot B \tag{4.25.b}$$

$$\frac{e}{B} = \frac{M}{VB} = \frac{1}{6}\frac{q_{BV}}{q_A} \tag{4.25.c}$$

$$i = \frac{H}{V} = \frac{q_{BH}}{q_A} \tag{4.25.d}$$

$$\frac{h}{B} = \frac{M}{HB} = \frac{1}{6}\frac{q_{BV}}{q_{BH}} \qquad (4.25.e)$$

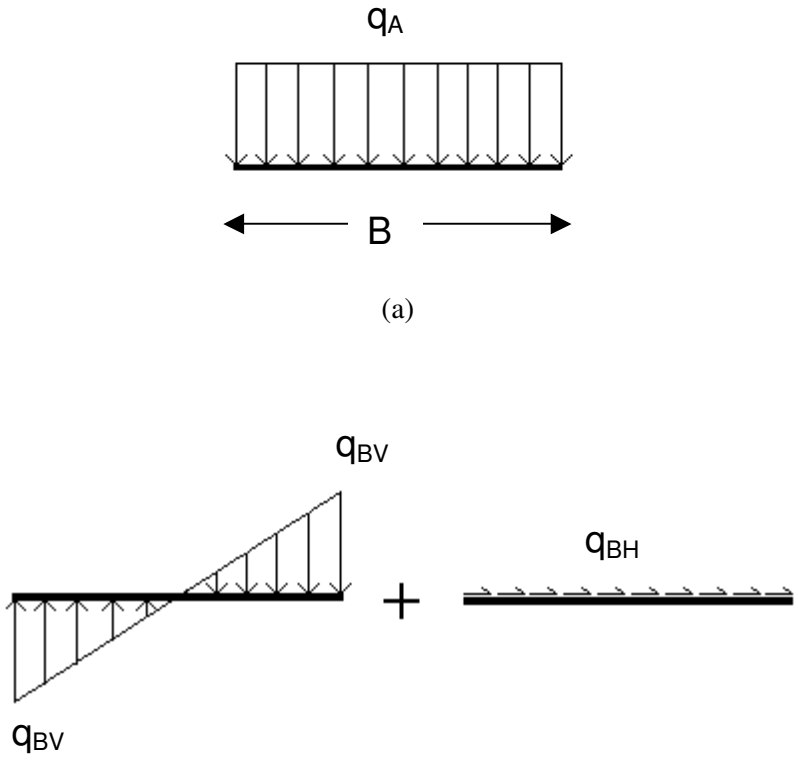

Figure 4.5. Input load schemes in Plaxis: (a) traction A for static case, (b) traction B for seismic loading.

where, q_A, q_{BV}, and q_{BH} are the maximum absolute values of foundation pressure distributions as shown in Figure 4.5, V is the total vertical load, M is the overturning moment, H is the horizontal load acting on strip foundation of width B, e is the load eccentricity, i is the load inclination with respect to the vertical, and h is the moment arm due to effective height of mass center of building (i.e., h=M/H). The ratio h/B is referred to as the aspect ratio of the building.

In tracking of the foundation failure during incremental loading, the center node of the foundation is selected as the control point. This point is utilized for obtaining plots of displacement versus traction A or traction B. A sample plot of horizontal displacement of control point versus traction B is given in Figure 4.6. The ultimate load level for traction B is defined as the value where plot becomes

horizontal. This definition corresponds also to the global stiffness parameter value of ~$1.0 \cdot 10^{-5}$ in Plaxis code. In application, vertical displacement is utilized for the detecting yield, and horizontal displacement plots are also checked to ensure that foundation-soil plastic flow is initiated. Based on the recommendation by Taiebat and Carter (2000), in case there is no horizontal load acting on foundation (i.e., zero load inclination), a small fraction (i.e.,1%) of vertical load (static) under undrained condition is applied horizontally on the foundation in order to obtain plots of load versus horizontal displacement at failure, as shown in Figure 4.6.

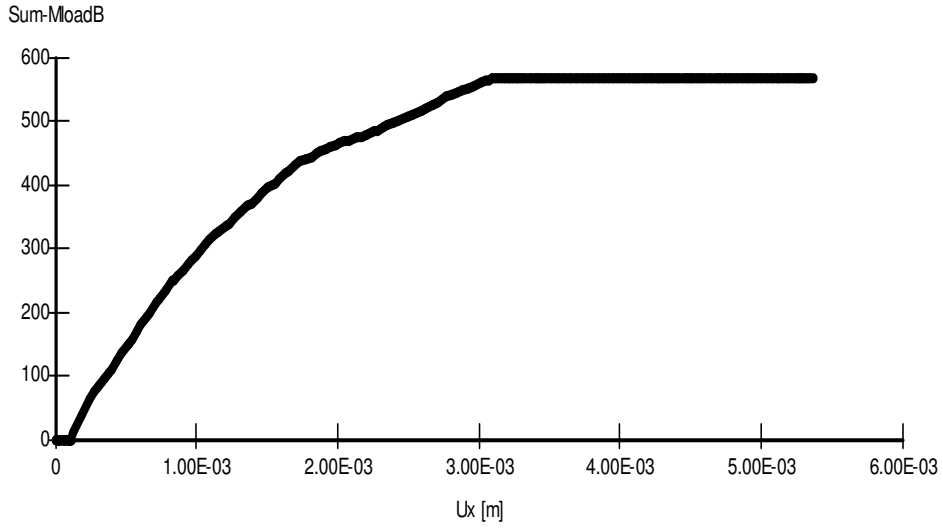

Figure 4.6. Sample for Plaxis analysis output curves: value of traction B (Sum-MloadB) versus horizontal displacement of control point (U_X(m)).

During the iterations, the calculation type is set to “plastic” and to “load advancement ultimate level”. Load multipliers, which are equal to the value of q_a and q_{BV} (q_{BH} is a fraction of q_{BV}), are incrementally increased to the ultimate load level utilizing successive calculation phases. This is due to the limitation that, Plaxis allows at most 100 calculation steps for each phase. Hence, for the refinement of the results, additional calculation steps are generally required (e.g., in the order of 1000 or more in some cases, forcing utilization of about 10 calculation

phases). Each phase starts from the results of the previous, and increases the load multipliers as specified.

At the end of free-field stress calculations stage, the displacements are reset to zero, since these displacements can complicate detection of ultimate state. Hence, the displacements in Figure 4.6 are due to load phases that simulate seismic loading condition alone. Iterative procedure is set manually: The default error tolerance of 0.03 is accepted for most analyses, but reduced to 0.01 in some cases where greater refinement is required, depending on observations in load-displacement plots during iterations. The default value of over-relaxation factor is changed to 1.4, based on the observation that this value provides faster convergence. Maximum iteration number is set to 100, which is the highest value permitted by Plaxis. The desired minimum number of steps is selected as 30 or 50, due to the observed difficulty in convergence for the calculation phase. An important detail is that, arc-length control is set off for all phases, since this technique increases the number of iterations tremendously when ultimate load is reached, without providing any beneficial improvement on results.

4.3.3. Verification with the static bearing capacity equations

Before proceeding with the eccentric and inclined loading of the foundation, performance of the numerical model in calculation of ultimate load levels should be checked utilizing analytical approaches. This is accomplished for the shallow strip foundations through comparing the results obtained from numerical model studies to those provided by the analytical formulations.

For the case of strip foundations, resting horizontally on the surface of homogeneous soil, if the load inclination and eccentricity is zero, equation 4.9 reduces to (Terzaghi, 1943):

$$q_u = cN_c + q_sN_q + 0.5\gamma BN_\gamma \qquad (4.26)$$

For the case $q_s=0$ (i.e., no surcharge exists),

$$q_u = cN_c + 0.5\gamma BN_\gamma \qquad (4.27)$$

Hence, for the purely cohesive soil behavior ($c\neq0$, $\Phi=0$),

$$q_u = cN_c \tag{4.28.a}$$

and, for purely cohesionless soil,

$$q_u = 0.5\gamma B N_\gamma \tag{4.28.b}$$

The factor N_c is equal to $\pi+2$ (Prandl, 1920), which is exact for the rigid-plastic behavior. The unit weight γ should be consistent with the effective stress concept, and should be selected as the buoyant unit weight for soils below ground-water table. The uncertainty in N_γ factor has already been discussed in Section 4.2.1. For comparison, Hansen's (1970) formulations will be utilized in this study. Accordingly,

$$N_q = e^{(\pi \tan\Phi)} \tan^2(45 + \Phi/2) \tag{4.29}$$

and,

$$N_\gamma = 1.50(N_q - 1)\tan\Phi \tag{4.30}$$

Hence, considering clayey silts with typical effective internal angles of friction between 26˚ to 30˚, the range of interest for those parameters are calculated as N_q=11.9-18.4, and N_γ=7.9-15.1.

Utilizing the mesh and calculation procedures as discussed in Sections 4.3.1 and 4.3.2, the capability of the analysis procedure to calculate ultimate bearing capacity for a foundation resting on purely cohesive soil is investigated. The soil parameters are consistent with those utilized in analysis presented in Section 4.4.1: c=100 kPa, υ=0.495, and K_0=1.0, for compatibility with the Prandl's solution. However, the foundation behaves rigidly when compared to flexible foundation assumption inherent in Prandl's solution. Hence, the calculated bearing capacity is,

q_u=512.3 kPa

which results in N_c=5.12, which is slightly lower than $\pi+2$. This may be due to the horizontal force of the magnitude of 1% of the vertical load applied on the foundation. Another analysis performed by setting horizontal force to zero provided

q_u=516.3 kPa, somewhat higher than the theoretical value. Hence, the analysis procedure satisfactorily agrees with the theoretical solution for the case of purely cohesive soil.

The case of cohesionless soil is investigated similarly, by setting the material parameters consistent with the analyses presented in Section 4.4.2. However, since the theoretical approaches consider the case with K_0=1.0 (i.e., no initial shear stress at free-field), and Ψ=Φ (i.e., associative flow rule), the analyses are performed for combinations of two different K_0 (i.e., 0.5 and 1.0), and Ψ (i.e., 0˚ and Φ) values. Values of N_γ are calculated according to the equation 4.28.b, and tabulated in Table 4.1.

Table 4.1. Values of N_γ corresponding to different combinations of Ψ and K_0 (Φ=30˚, γ=18 kN/m^3, and B=20 m)

Ψ	K_0	N_γ
0˚	0.5	10.9
Φ	1.0	15.1
0˚	1.0	10.7
Φ	0.5	15.3

Effect of K_0 is observed to be practically negligible regarding ultimate bearing capacity. For the case of K_0=1.0 and Ψ= Φ, calculated N_γ factor has the same value with that proposed by Hansen. On the other hand, Ψ has a very significant impact on the ultimate bearing capacity, as discussed in Section 4.2. In the case modified Mohr-Coulomb parameters (c* and Φ*) in equations 4.11 are utilized, the Hansen's N_γ factor is calculated as 8.7, which is somewhat lower than 10.7. Further investigation of impact of Ψ on N_γ value is out of the scope of this study. However, since the analysis results are normalized with static ultimate bearing capacity (i.e., due to definition of FS) in the following sections, no further improvement on this issue is deemed necessary. When normalized to FS, foundation load eccentricity capacity is insignificantly influenced by Ψ for the

drained case. Impact of variation in Ψ is relatively more important for calculation of static bearing capacity.

4.3.4. Verification of uplift behavior

The numerical model is assessed for the uplift behavior, utilizing the simplest case for purely cohesive soil behavior. The analysis results are compared with those provided by equation 4.14, which is verified by Houlsby and Purzin (1999), and consistent with the effective width concept of Meyerhof (1963), as it will be shown in the following paragraphs:

As formulated by Prandl's (1920), the ultimate bearing pressure on a flexible strip foundation overlying a purely cohesive soil (i.e., c ≠0 and Φ=0) is,

$$q_u = (\pi + 2) \cdot c \tag{4.31}$$

If the foundation width is B, then the ultimate load (V_u) on foundation is,

$$V_u = (\pi + 2) \cdot c \cdot B \tag{4.32}$$

Considering load eccentricity (M≠0), contact pressure is assumed to be linearly varying beneath foundation. Hence, uplifting of foundation is imminent due to a pressure distribution of triangular form when,

$$M = \frac{VB}{6} \tag{4.33.a}$$

or, substituting equation 4.7,

$$e = \frac{B}{6} \tag{4.33.b}$$

Defining q_{max} as the maximum value of pressure for a triangular foundation pressure distribution beneath strip foundation, total vertical load can be calculated by,

$$V = \frac{q_{max}}{2} B \tag{4.34}$$

In that case, ultimate total vertical load is,

$$V_u = R \cdot c \cdot B \tag{4.35}$$

where, R is an unknown factor, which may not be equal to (π+2). In order to estimate R, equation 4.10 (i.e., equivalent width concept of Meyerhof) can be utilized. Introducing equation 4.10 and 4.33.b into 4.32,

$$V_u = \frac{2}{3} \cdot (\pi + 2) \cdot c \cdot B \tag{4.36}$$

Then, substitution of equation 4.36 into 4.35 gives,

$$R = \frac{2}{3}(\pi + 2) \tag{4.37}$$

For a given load eccentricity, ultimate capacity of a foundation considering uplift can be calculated by replacing B in equation 4.36 by contact width B_c (i.e., zone of uplift is excluded in B):

$$B_c = \frac{3}{2}B - \frac{3 \cdot M}{V} \tag{4.38}$$

Equation 4.38 can be derived combining equations 4.33.a and 4.34. Therefore, by the definition of FS in equation 4.16, the relationship between ultimate overturning moment M_y and FS for both cases with and without uplift is derived as:

$$\frac{M_y}{VB} = \frac{1}{2}\left(1 - \frac{1}{FS}\right)$$

or,

$$\frac{M_y}{VB} = \frac{1}{2}\left(1 - \frac{1}{FS}\right) \tag{4.39.a}$$

or,

$$\frac{1}{FS} = 1 - 2\frac{M_y}{VB} \qquad (4.39.b)$$

which is consistent with equation 4.14. Equation 4.39.b provides the ultimate load eccentricity for a given factor of safety. Without occurrence of bearing capacity failure, uplift under load eccentricity is possible in case FS>1.5, and no uplift of the foundation can occur for lower FS values.

The model parameters and analysis details are given in Section 4.4.1. As discussed in Section 4.3.3, the ultimate bearing pressure under vertical load (q_u) is calculated as 512 kPa. The results of Plaxis analyses are compared with the results of equation 4.39 in Figure 4.7. It is observed that Plaxis analyses can model the uplift behavior with quite good accuracy. The only relatively significant deviation from equation is observed at FS=5. Although an additional analysis is performed with further refinement in calculation parameters, no significant improvement is obtained.

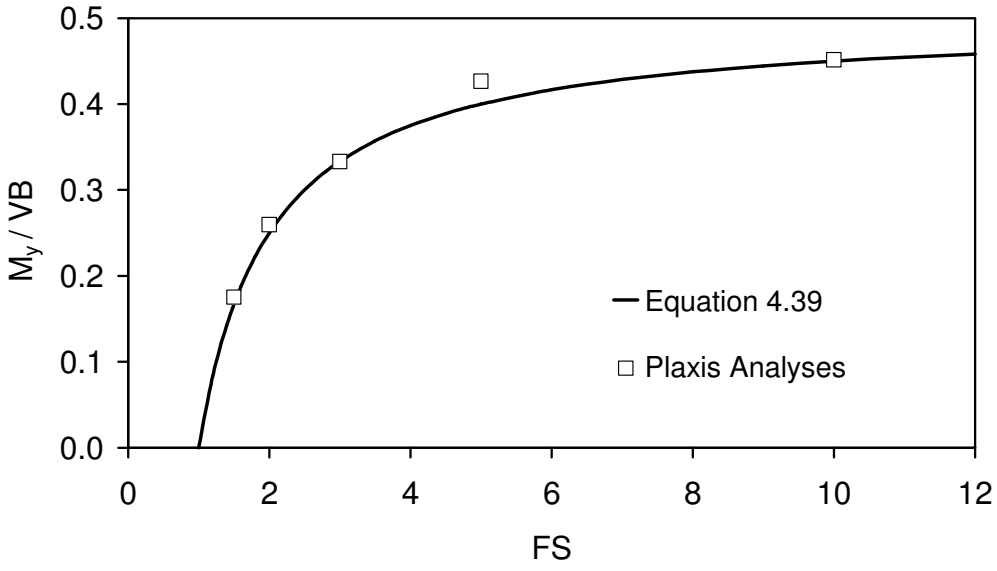

Figure 4.7. Comparison of equation 4.39 with Plaxis analyses results.

4.4. Results of Finite-Element Analyses

Using commercially available packages, the finite element methodology can be practically utilized for estimation of ultimate load capacities of foundations. The main advantage of the numerical approaches is that, realistic constitutive soil and structure behavior, complicated problem geometries, and relatively complex load (or, stress) histories can be introduced. In this section, the results of the Plaxis analyses for the cases of cohesive and cohesionless soil behavior are investigated. The output is compared with the available findings cited in literature to be able to evaluate the proposed analysis method. The assumption of omitting the load inclination for poor aspect ratio buildings is tested and discussed.

The discussion is extended to the case of consolidated-undrained behavior during seismic loading. This case is more realistic for the seismic foundation assessment of buildings resting on normally-consolidated soils for which the consolidation process has already been completed before the earthquake. The results are compared with the cohesive and cohesionless soil models, which practically represent undrained and fully drained cases, respectively, for normally consolidated soils.

4.4.1. The undrained cohesive soil model

The case of purely cohesive soil model (i.e., Mohr-Coulomb parameters with $c \neq 0$ and $\Phi=0$) represents the case for which the shear strength of the saturated soil is practically unaffected by the weight of the structure. This is possible for the case of over-consolidated soils, and for the time-period just after the construction of building during which a greater part of the consolidation process is not yet completed in saturated clayey foundation soils. All of the models consider homogeneous foundation soils, but in practical applications, it is possible to analyze cases with variable soil profiles approximately by the procedures proposed in this study.

In the analyses, following parameters are set as soil parameters:

1) For both the foundation contact soil and the halfspace soil, Mohr-Coulomb parameters are set as c=100 kPa, and $\Psi=\Phi=0^{\circ}$, corresponding to Tresca yield criterion with associative flow rule.

2) Drained behavior with υ=0.495, and K_0=1.0. Hence, although no ground-water exists in the model, soil behavior is set to undrained (i.e., no volume change for soil is allowed) by setting the Poisson's ratio close to 0.5. Since coefficient of lateral earth pressure at-rest is set to 1.0, no initial shear exists at free-field, and model assumptions are compatible with the assumptions inherent in Prandl's solution.

3) Tension cut-off is allowed for the foundation-soil contact elements but not for the halfspace soil. This is due to the fact that, tension cut-off for soil behavior is not considered in theoretical Prandl approach. However, uplift of foundation is permitted by providing tension cut-off for contact elements.

An initial run to calculate q_u resulted in 512 kPa, as discussed in Section 4.3.3. The actual q_A (i.e., traction A) value is calculated according to target FS defined in equation 4.5. The ratio of q_{BV} to q_{BH} is set according to the target load eccentricity and inclination factors, utilizing equations 4.25. Hence, in analyses, h/B (i.e., aspect ratio) values of 0.5, 1.0, and 2.0 are considered. The analyses results are shown in Figure 4.8. For practical purposes, a least-squares fit technique is applied on the data, for an equation of the form:

$$\frac{1}{FS} = \left(1 - 2\frac{M_y}{VB}\right)^n \qquad (4.40)$$

where, n is the coefficient depending on h/B ratio. When load inclination is zero, the n value is 1.0 due to equation 4.39.b. The calculated values of n are 1.0, 1.1 and 1.5 for the aspect ratios of 2.0, 1.0 and 0.5 respectively, where n=1.0 coincides with equation 4.39. The comparisons of fit with the data is given in Figure 4.8. For zero load inclination, equation 4.39.b can be practically utilized in order to obtain rough estimates of M_y/VB ratios, for aspect ratios greater than 0.5. The error is comparatively higher for low FS values (i.e., close to 1.0) and lower for high FS values.

Stress points where plastic state is reached at ultimate capacity is shown in Figure 4.9 for different aspect ratios, and FS=3.0. These points are marked by gray squares. In Figure 4.9.a, the plastic zone is concentrated beneath the foundation-soil contact area. When significant load inclination is considered in Figure 4.9.b. and 4.9.c, the yielding zone is observed to become more concentrated, near the

edge of foundation and under a narrower foundation-soil contact. In three of the analyses, significant uplift behavior of the ultimate state is observable.

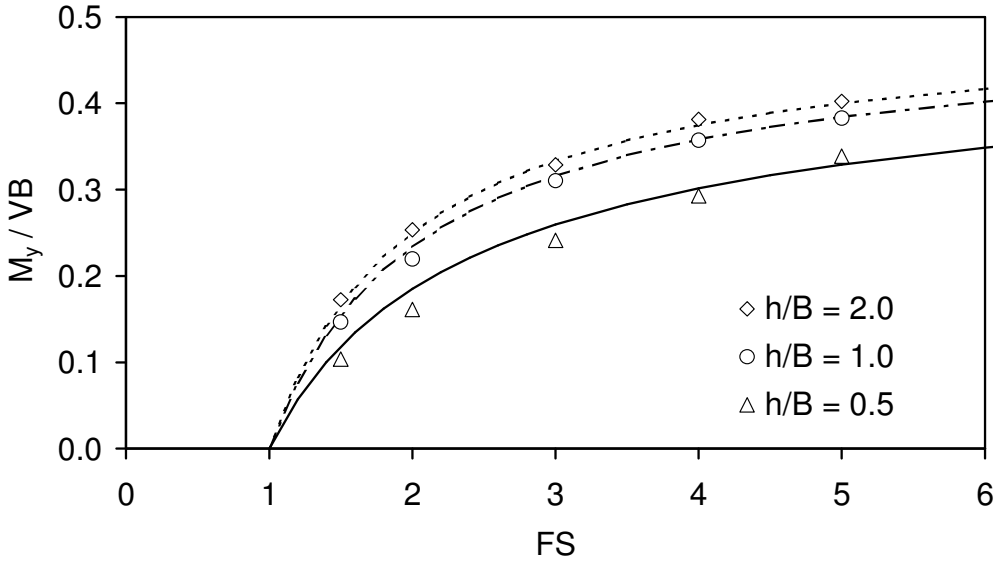

Figure 4.8. Comparison of equation 4.40 with Plaxis analyses results: the h/B=2.0 results coincide with equation 4.39.

Deformations at ultimate states are also presented for the same analyses. For the case of zero load inclination, the foundation soil is observed to flow in both horizontal and vertical directions beneath the contact zone. This is similar to general bearing capacity failure under vertical loads, when the contact zone is considered as the foundation in Prandl's foundation. These observations are consistent with analytical assumptions of Bransby (2001). When significant load inclination is introduced, the foundation soils tend to flow towards the free-field direction. With zero dilatation, the failure surfaces with combinations of linear and circular shapes are comperable with the theoretical discussions on rigid-plasticity (Atkinson, 1993). In Figure 4.10.c., the failure surface spreads back to zones beneath foundation uplift, for the case of h/B=0.5. The foundation displays significant tilting at ultimate capacity. However, significant uplift susceptibility can be expected for h/B>1.0, (Figure 4.10.a and b) but not for h/B<0.5 (Figure 4.10.c). However, the uplift behavior is also dependent on the static factor of safety (FS), such that, for lower values of FS, the foundation failure can occur without significant uplift of the foundation.

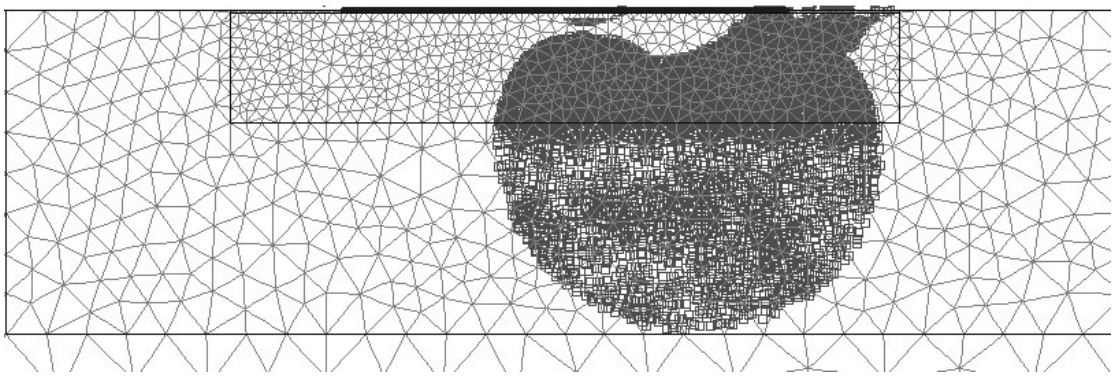

(a)

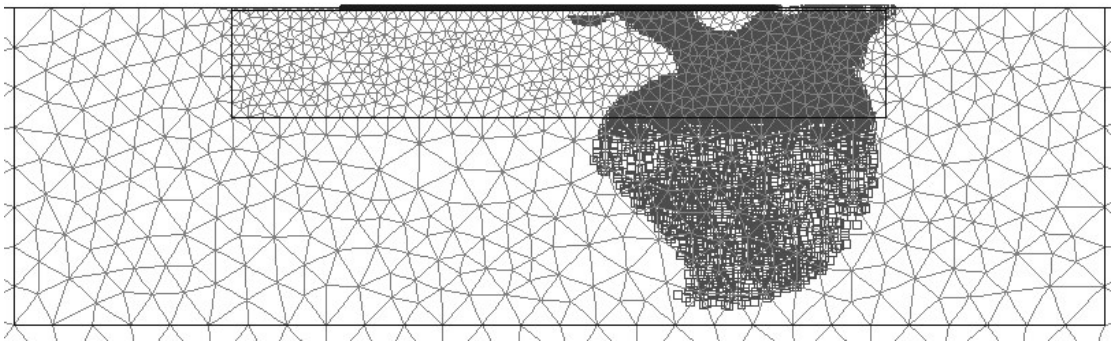

(b)

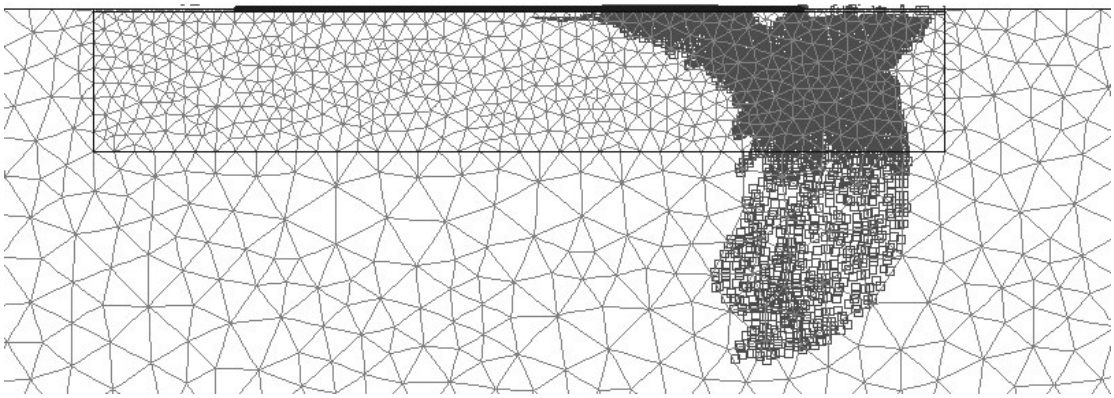

(c)

Figure 4.9. Plastic stress points during ultimate loading, considering undrained cohesive soil model, for analysis with FS=3.0: (a) zero load inclination (h/B is large), (b) h/B=1.0, (c) h/B=0.5.

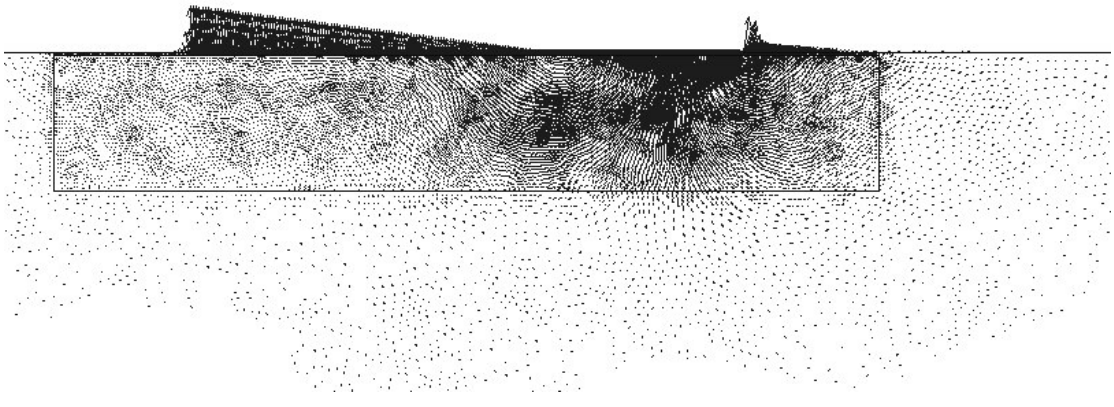

(a)

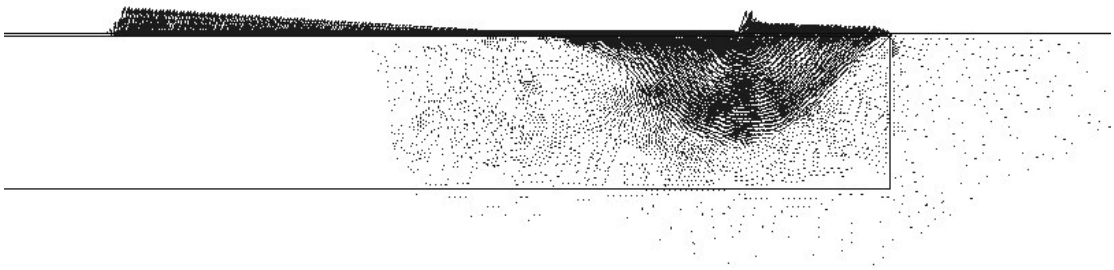

(b)

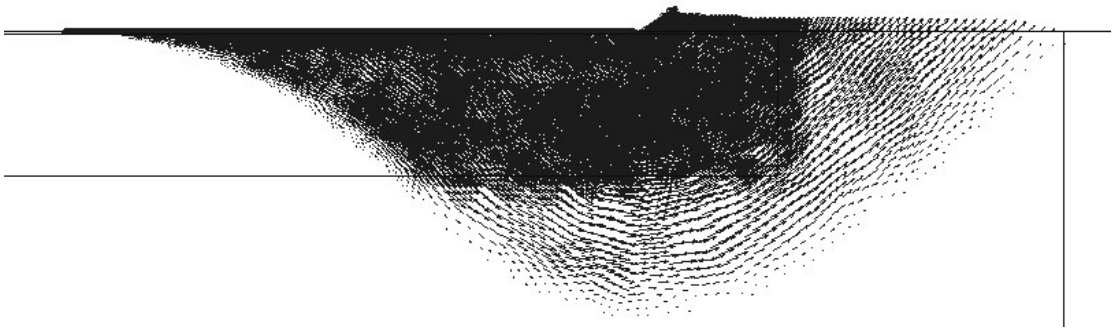

(c)

Figure 4.10. Deformations at ultimate states, considering undrained cohesive soil model, for analysis with FS=3.0: (a) zero load inclination (h/B is large), (b) h/B=1.0, (c) h/B=0.5.

4.4.2. The drained soil model

Drained soil behavior model (i.e., c=0 and Φ≠0) represents the case that no significant cohesion is involved during the shearing of soil. This case corresponds either to the unsaturated normally-consolidated soils, or the condition that loading rate is relatively low compared to the drainage duration, so that no excess pore-pressure exists, and hence may not be applicable for saturated foundation soils under seismic loading. The drained soil model analyses aim to check the consistency of Paolucci and Pecker (1997a) results with the finite element approach, so that the analysis procedures can be utilized in practical where the assumptions inherent in Paolucci and Pecker approach are not valid (e.g., inhomogeneous soil profile, and complex foundation sections). The drained analyses also form the basis for consolidated-undrained analyses, such that the soil drained under static loading will be set to undrained in the analyses of Section 4.4.3. Additionally, comparison of foundation capacity is checked when load inclination is omitted.

In the analyses, following soil parameters and settings are utilized:

1) For both, the soil in contact with the foundation and the halfspace soil: c=0, Ψ=0˚, and Φ=30˚. These parameters imply nonassociative behavior, which provides conservative results. The selection of Ψ and Φ is also consistent with the observations from Adapazarı samples and Mexico City case reports.

2) Drained behavior with ν=0.3, and K_0=0.5, implying that no ground-water exists in the model. Coefficient of lateral earth pressure at-rest is set to 0.5, which is consistent with the Jaky's (1944) formula, so that initial shear exists at free-field.

3) Tension cut-off is allowed for all soil elements.

An initial run to calculate q_u resulted in of 1965 kPa. The actual q_A (i.e., traction A) value is calculated based on the target FS defined in equation 4.1 (or, 4.5). The ratio of q_{BV} to q_{BH} is set according to the target load eccentricity and inclination factors, utilizing equations 4.25. Hence, in analyses, h/B (i.e., aspect ratio) values of 0.5, 1.0, 2.0 and 3.0 are considered. The analysis results are given in Figure 4.11.

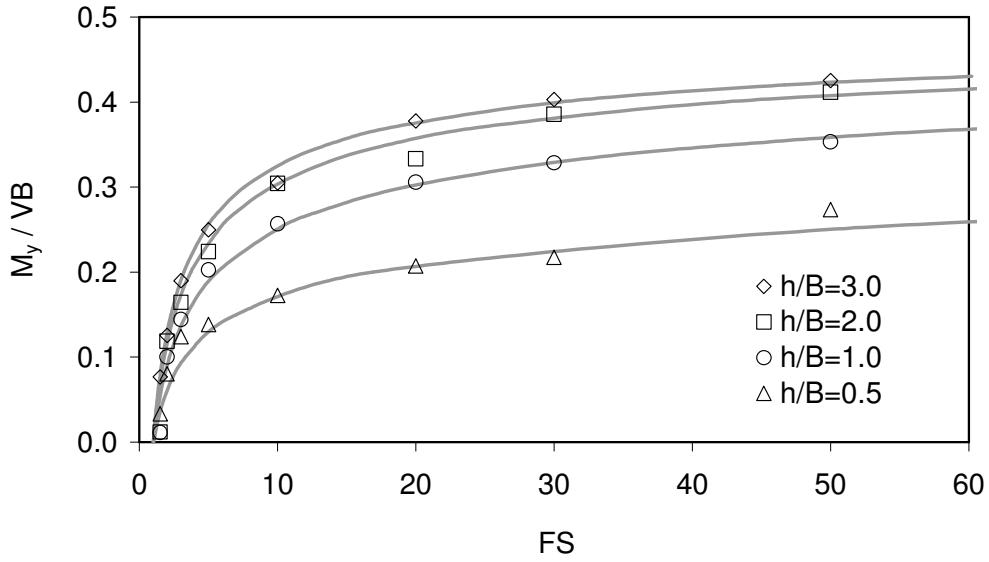

Figure 4.11. Comparisons of numerical results (empty boxes) with equation 4.41 (gray curves).

As discussed by Paolucci and Pecker (1997a), major contributions to the reduction of factor of safety comes from load eccentricity and inclination, especially for horizontal pseudo-static acceleration levels (a_h) below 0.3 g. Hence, omitting equation 4.22.c, the reduction factor for bearing capacity under seismic loading simplifies as,

$$v = \left(1 - \frac{H}{0.85 \cdot V}\right)^3 \left(1 - \frac{2 \cdot M_y}{VB}\right)^{1.8} \tag{4.41}$$

Substitution of equation 4.24 into 4.41 gives,

$$\frac{1}{FS} = \left(1 - \frac{H}{0.85 \cdot V}\right)^3 \left(1 - \frac{2 \cdot M_y}{VB}\right)^{1.8} \tag{4.42}$$

which can be utilized for comparison to Plaxis analysis results directly. For different values of aspect ratio (h/B), computed factors of safety are compared with equation 4.42 in Figure 4.11. Calculated values are found to be compatible with the Paolucci and Pecker's formula, although these formulations are based on associative flow

rule. Therefore, the finite element approaches can provide a useful tool for investigation of rather complicated soil profiles and foundation shapes. In cases with homogeneous soil profile with foundation resting on soil surface, equation 4.42 can be utilized directly.

The next step is the analysis in which the base shear (i.e., inclination) is ignored, and only load eccentricity is considered. Results for the corresponding numerical analyses are provided in Figure 4.12, and compared with equation 4.42 for different aspect ratios. It is observed that, ignorance of the load inclination effect is acceptable for aspect ratio's greater than 1.0. For aspect ratios less than 1.0, the calculation procedure significantly overestimates the capacity for a given FS, and the effect of load inclination can not be ignored in estimation of M_y/VB ratio.

A least-squares analysis utilizing results of the numerical analyses for no-inclination case resulted in:

$$FS = \left(1 - \frac{2 \cdot M_y}{VB}\right)^{-2.3} \tag{4.43}$$

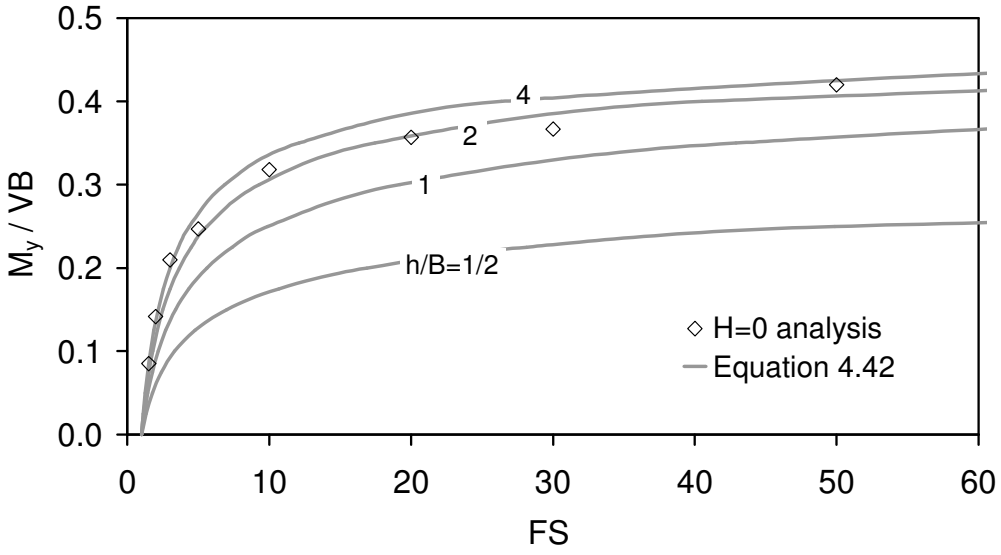

Figure 4.12. Comparisons of numerical results (empty boxes) due to omitted load inclination analyses, with equation 4.42.

For comparison, if the reduction due to load inclination is ignored in equation 4.42, equation 4.22.b can be utilized directly to calculate FS. Hence, plots due to

equation 4.22.b and 4.43 are presented in Figure 4.13. The relationship in equation 4.20, which is based on experimental studies (Butterfield and Gottardi, 1994), is also compared in Figure 4.13.

The effect of Ψ and K_0 on the static bearing capacity is discussed in Section 4.3.3. Since the static bearing capacity is observed to be especially sensitive to the value of Ψ, the sensitivity of M_y/VB versus FS to these parameters is investigated for the drained case. Hence, the analysis results with nonassociative flow rule and K_0=0.5 are compared to those with associative flow rule and K_0=1.0. The analyses are compared for the case of zero load inclination, in which only a vertical resultant force and overturning moment is applied on the foundation. The results of analyses are also presented in Figure 4.13. For the practical analyses of poor aspect ratio buildings resting on drained soil, the associativeness of the flow rule and K_0 value has insignificant importance on the relationship between M/VB ratio and FS. On the other hand, the associative analyses results display a greater compatibility with equation 4.22.b, since soil is modeled in a parallel manner to the study of Paolucci and Pecker. Hence, it is practically sufficient to include the effect of the dilatancy angle and K_0 only when calculating static factor of safety, for practical utilization of derived relationships in this study.

In order to visualize failure mechanisms, stress points with plastic state during ultimate state are presented in Figure 4.14. Well-defined failure surfaces can be observed, especially for h/B=1.0 and 0.5. In case of large h/B (i.e., load inclination is zero), the uplift zone involves nearly half of the foundation width, where, for other cases this zone is more limited. The behavior and flow of the soil during ultimate state can be better observed when incremental displacements are observed (Figure 4.15): The uplift zone clearly decreases as h/B ratio decreases; in any case, tilting behavior of the foundation is observable, but becomes more significant as h/B increases. These sample plots are provided for the case of FS=3.0, and uplift behavior becomes more significant for higher FS values.

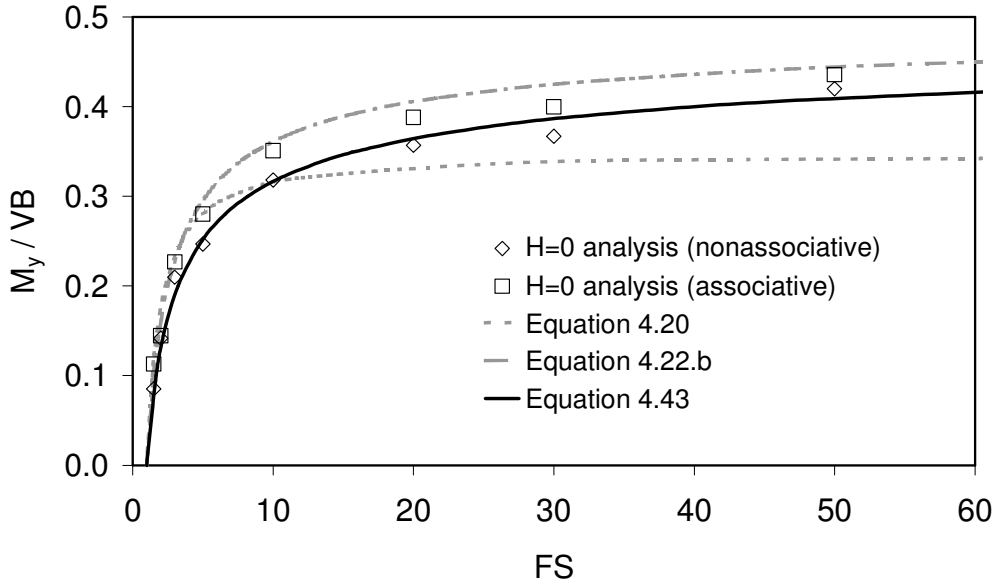

Figure 4.13. Comparisons of numerical results (empty boxes) due to omitted load inclination analyses, with equations 4.20 (Butterfield and Gottardi, 1994), 4.22.b (Paolucci and Pecker, 1997a), and equation 4.43 (least-squares fit for $\Psi=\Phi$ and $K_0=0.5$).

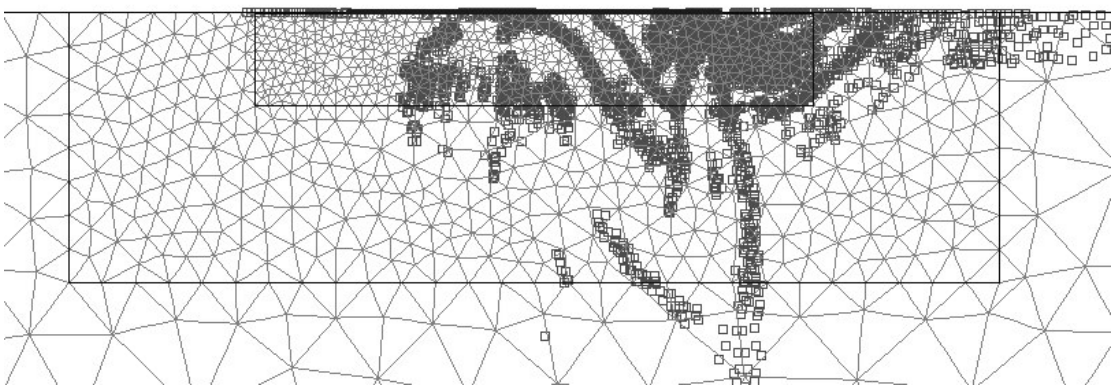

(a)

Figure 4.14. Plastic stress points during ultimate loading, considering drained soil model, for analysis with FS=3.0: (a) zero load inclination (h/B is large), (b) h/B=1.0, (c) h/B=0.5.

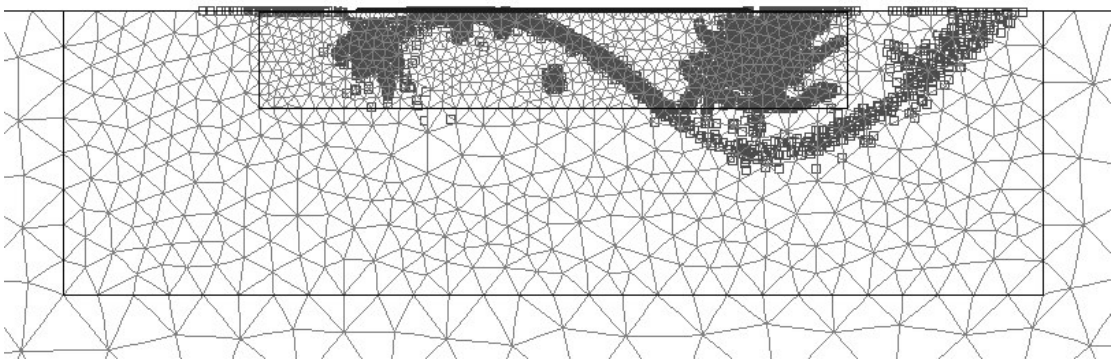

(b)

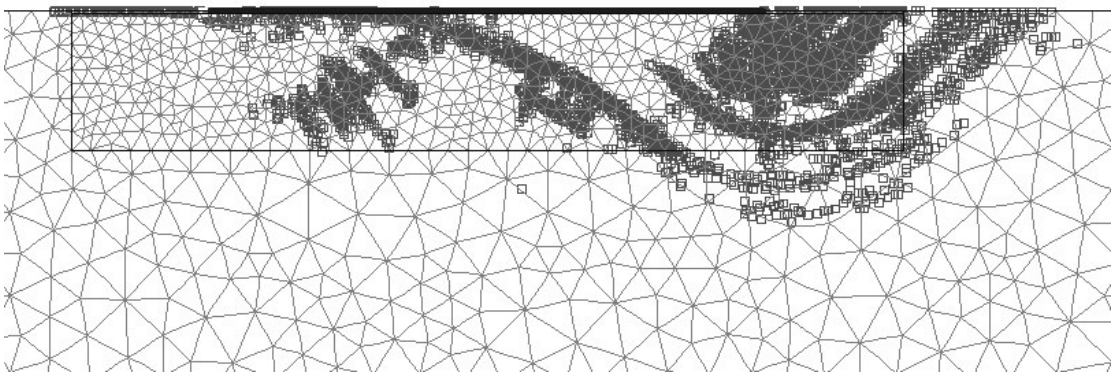

(c)

Figure 4.14 (continued).

Concluding, the analysis procedures outlined in this section can be practically utilized for investigations of more complex drained case problems. However, equation 4.43 is suitable for rapid assessment of drained My/VB values for poor aspect ratio buildings with RC slab-type mat foundations resting on (practically) homogeneous and isotropic soils.

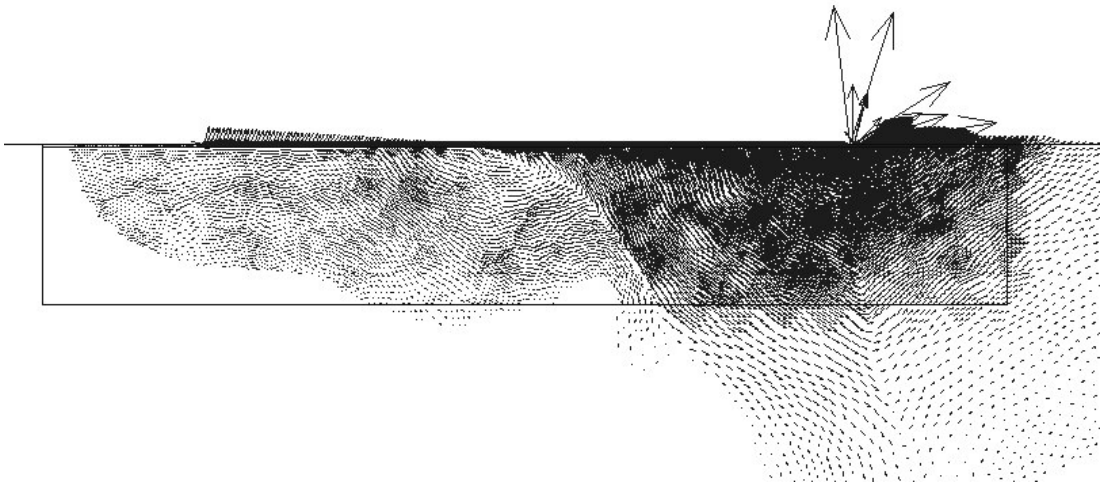

(a)

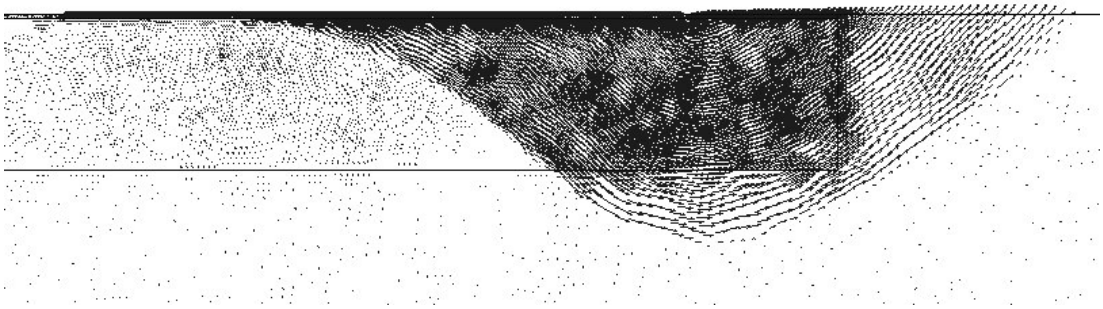

(b)

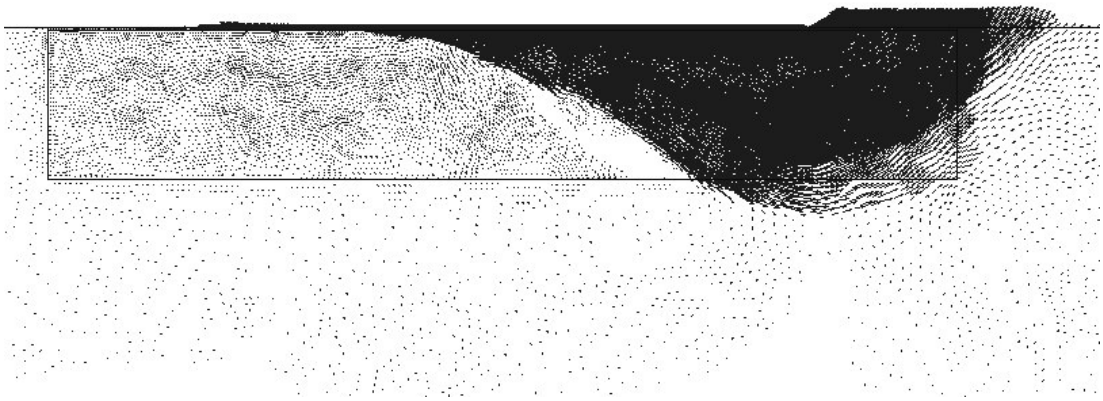

(c)

Figure 4.15. Displacements at ultimate state, considering drained soil model for analysis with FS=3.0: (a) zero load inclination (h/B is large), (b) h/B=1.0, (c) h/B=0.5.

4.4.3. Consolidated-undrained soil behavior

When considering foundations on saturated soils, traditional bearing capacity equations are mainly based on two major assumptions: the fully drained case (depending on unit weight of soil, foundation dimensions, and soil's angle of friction Φ), and the undrained case (depending on cohesion intercept c). In the latter, soil's strength is assumed to be the same as that in the free field. This is valid for over-consolidated soils, for which the shear strength depends on the preconsolidation pressure. For the case of normally consolidated fine soils, the undrained equations are applicable if the drainage duration is relatively very long compared to duration of construction. In the short term, all of the applied load results in an equivalent increase in pore water pressures. Hence, the effective stress and the shear strength practically remain unchanged. As consolidation proceeds, effective stresses increase, resulting in higher strength values, and higher factor of safety for bearing capacity. At the end of the consolidation process, bearing capacity of the foundation is consistent with the drained case formulas.

Use of any of the proposed bearing capacity equations based on above discussions may be inconsistent when investigating foundation performance under seismic loading condition. Very shallow water table will complicate the behavior: during seismic loading, most foundations are expected to rest on soils that have already completed a significant part of their consolidation process. Static bearing capacity can be calculated utilizing conventional bearing capacity equations considering drained shear strength parameters. However, seismic loading results in an undrained situation, especially in the case of fine-grained soils. Therefore, equations provided for fully drained case may not be valid, whereas equations based on stress conditions in free field (i.e., undrained behavior) are already useless, except for the case of over-consolidated soils. This issue is also important for the design and foundation assessment calculations, since too conservative or unconservative ultimate load capacities may be calculated.

Differences between the two behaviors can be explained through comparing effective stress paths for the conventional triaxial consolidated-undrained (CU) and consolidated-drained (CD) tests, applied to isotropically consolidated samples. Defining,

$$s' = \frac{\sigma_1' + \sigma_3'}{2} = \frac{\sigma_1 + \sigma_3}{2} - u_{pore} \quad (4.44.a)$$

$$t = \frac{\sigma_1' - \sigma_3'}{2} = \frac{\sigma_1 - \sigma_3}{2} \quad (4.44.b)$$

where, σ_1 and σ_3 are the major and minor principal stresses respectively, and u_{pore} is the pore water pressure. For a drained test, pore water pressure is always equal to zero. Therefore, in a CD type test, stress path will follow the line 1-2 (making 45˚ with x-axis) in Figure 4.16.a. At point 2, stress path will intersect the failure envelope. On the other hand, during undrained testing pore pressure u will have positive values for normally consolidated soils, and test will follow a stress path along points 1-3, reaching failure at point 3 (Figure 4.16.a). Having lower *s*' values at failure, CU tests will provide lower accompanying *t* values, and hence lower shear strength in compression. Whereas for tests of extension type, undrained shear strength will be higher than the drained strength.

In the case of anisotropic consolidation, both CD and CU tests start at point 2, and follow paths 2-3 and 2-4, respectively, as demonstrated in Figure 4.16.b. Therefore, *t* at failure will be somewhat different and closer to the value at CD type test. At ultimate anisotropic consolidation condition, in which point 2 will coincide with failure envelope, *t* values for CD and CU type tests at failure will coincide. Hence, difference in *t* between CD and CU type will require information about the anisotropy level in consolidation phase, and stress-path followed (i.e., compression or extension).

Slope of the effective stress path during undrained compression test depends on Skempton's (1954) pore pressure parameter A_S (i.e., originally stated as A). For the case of constant cell pressure ($\Delta\sigma_3$=0), increase in pore pressure can be written as,

$$\Delta u_{pore} = A_S \Delta\sigma_1 \quad (4.45)$$

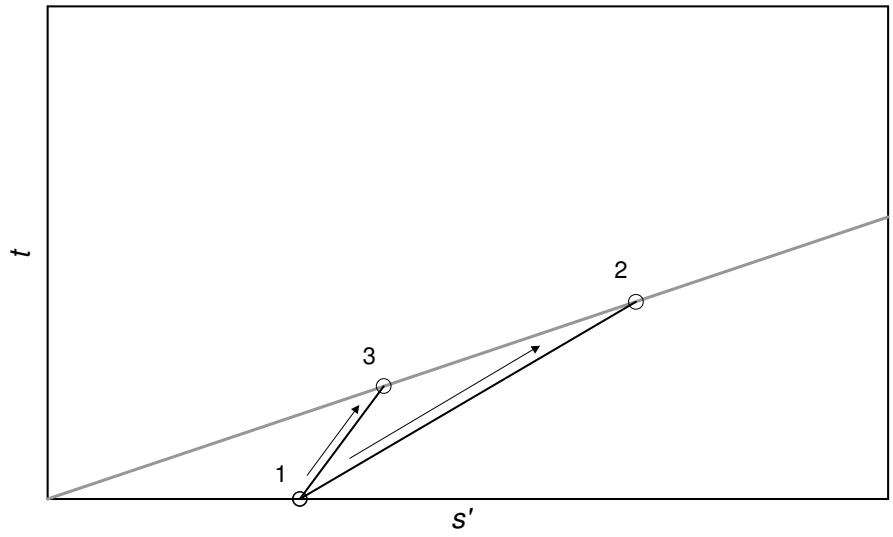

(a)

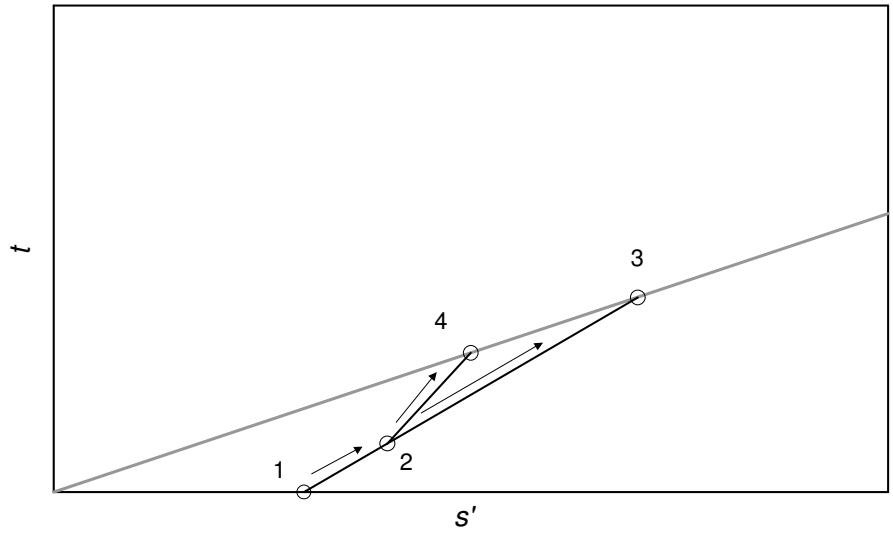

(b)

Figure 4.16. Comparisons of stress paths in CD and CU type triaxial compression tests, for the case of (a) isotropic, and (b) anisotropic consolidation. Gray line is the failure envelope representing Mohr-Coulomb yield criterion with c=0.

where, $\Delta\sigma_1$ is the change in major principal stress, which is equal to the change in deviator stress in a triaxial test. Hence, the relationship between t and s' is,

$$\frac{t}{s'} = \frac{(\sigma_1 + \Delta\sigma_1 - \sigma_3)}{(\sigma_1 + \Delta\sigma_1 + \sigma_3 - 2A_S\Delta\sigma_1)}$$

By taking derivatives with respect to $\Delta\sigma_1$,

$$\frac{dt}{ds'} = \frac{dt}{d\Delta\sigma_1}\frac{d\Delta\sigma_1}{ds'}$$

or,

$$\frac{dt}{ds'} = \frac{1}{1-2A_S} \tag{4.46}$$

For no pore pressure increase (A=0), effective stress path for undrained loading coincides with the drained loading path.

Actual values of A_S should be determined by laboratory tests on natural undisturbed samples. In addition, value of A_S is not constant along the undrained stress path: as stress levels approach to failure envelope, A_S can deviate significantly from its initial values. Parameter A_S is also dependent on the type of test, and on anisotropy inherent in the natural soil. Therefore, rigorous simulations of true undrained loading behavior can only be achieved through numerical analyses utilizing rigorous constitutive soil models.

The assumption of isotropic elastic behavior for non-yielding stress levels is reasonable for practical purposes, especially for the case of normally consolidated soft clays (Parry, 1995). Hence, the effective stress path will be consistent with calculations based on elasticity theory. In that case, the volumetric strain based on small strain assumption is formulated as:

$$\varepsilon_v = \frac{1}{E'}(1-2\nu')(\Delta\sigma_1' + 2\Delta\sigma_3') \tag{4.47}$$

based on effective stress parameters, where E' and ν' are elastic modulus and Poisson's ratio determined by drained loading. Assuming that water is incompressible when compared to soil skeleton, the volume change for an undrained test on a fully saturated soil will be equal to zero $(\varepsilon_V = 0)$. Thus,

$$\left(\Delta\sigma'_1 + 2\cdot\Delta\sigma'_3\right) = 0$$

In this case, slope of the effective stress path in a *t-s'* plot (Figure 4.16) will be equal to 3:1 for a CU type triaxial compression test, and corresponding A_S parameter will be equal to 1/3. Similarly, for the case of plane strain loading, the slope of the effective stress path will be equal to ∞ (i.e., vertical to *s'*-axis), with a corresponding A_S value of 1/2.

The situation beneath a building is rather complicated: at every point in the foundation soil, initial stress condition and the stress-path can be different, and overall reduction in factor of safety against failure will depend on the geometry and dimensions of the foundation, as well as the material properties. Finite element technique can be utilized to provide insight for the problem.

In order to investigate the significance of parameter A_S in seismic bearing capacity, and to obtain preliminary formulations for simple design approaches for normally consolidated fine soils, assumption of isotropic elastic behavior is presumed to be valid. Therefore, elasto-plastic soil model implemented in the Plaxis code can be utilized, assuming undrained behavior for the soil as discussed in section 4.3.1.

Based on elasto-plastic material behavior, since Plaxis code provides plane-strain idealization, pore pressure parameter A_S will be equal to 1/2 in the analyses. Calculated results will be representative of strip foundations with in plane forces, and for rectangular foundations with L>>W under similar loading patterns. The three dimensional cases (e.g., square foundations) are not investigated in this study. As discussed in Section 4.2.2, when only in-plane forces and moments are considered, the foundation shape-effects are likely to be practically ignored for undrained case. The A_S parameter tends to 1/3 in the three dimensional case, and hence provides slightly higher shear strength for the soil under undrained compression. Hence, the practical approach given in this study can also be utilized for these cases. However, when combined effect of in-plane and out-of-plane forces are considered, the approach can overestimate the load capacity of the foundation. Further discussion on impact of out-of-plane forces is left as a future study.

In order to investigate the effect of undrained loading on the foundation capacity, load eccentricity and inclination are applied on the foundation overlying saturated undrained soil. In the analyses, following soil parameters are set:

1) For both the soil in contact with foundation and the halfspace soil: c=0, Ψ=0˚, and Φ=30˚. These parameters imply nonassociative behavior, in order to observe elastic-ideally plastic foundation behavior. A nonzero dilation dilatancy angle results in increasing shear strength at the ultimate condition (i.e., hardening behavior), which would be inconsistent with the results of monotonic consolidated-undrained shear strength tests of Adapazarı specimens (Chapter 2).

2) As the drained soil parameters, Poisson's ratio is set to 0.3, and K_0 is set to 0.5. The ground-water table is located at ground surface. These values are compatible with the drained-case analyses, except the existence of ground water table.

3) Tension cut-off (at zero effective normal stress) is allowed for all soil elements. However, during undrained loading tension cut-off can not occur, since effective stresses do not change, as discussed in Section 4.3.1.

4) Undrained soil behavior is set for the foundation soil, while drained behavior is set for the foundation-soil interface elements, in order to allow uplift behavior.

5) An initial run to calculate q_u resulted in 848 kPa, as the drained ultimate bearing capacity. Calculation procedures of actual values of q_A, q_{BV}, and q_{BH} are the same as the procedures in Section 4.4.1 and 4.4.2. In analyses, h/B values of 0.5, 1.0, and 2.0 are considered.

In Figure 4.17, the analysis results are compared to equation 4.41, in order to visualize reduction in ultimate load eccentricity capacity of foundation due to undrained loading. The results imply a significant reduction due to undrained behavior. This is consistent with the observations of Mexico-City and Adapazarı, such that, significant decrease in ultimate overturning moment capacity of the foundations can occur on saturated soils under seismic loading, when compared to unsaturated soils, due to:

1) The static drained bearing capacity of a foundation is lower for the case of saturated soil than the unsaturated soil, since buoyant unit weight is significantly lower than the unit weight of the unsaturated soil (the ratio of unit weights is approximately 1:2).

2) For a given FS, the consolidated-undrained bearing capacity can be significantly lower than the drained capacity (Figure 4.17), depending on pore-pressure parameter A_S.

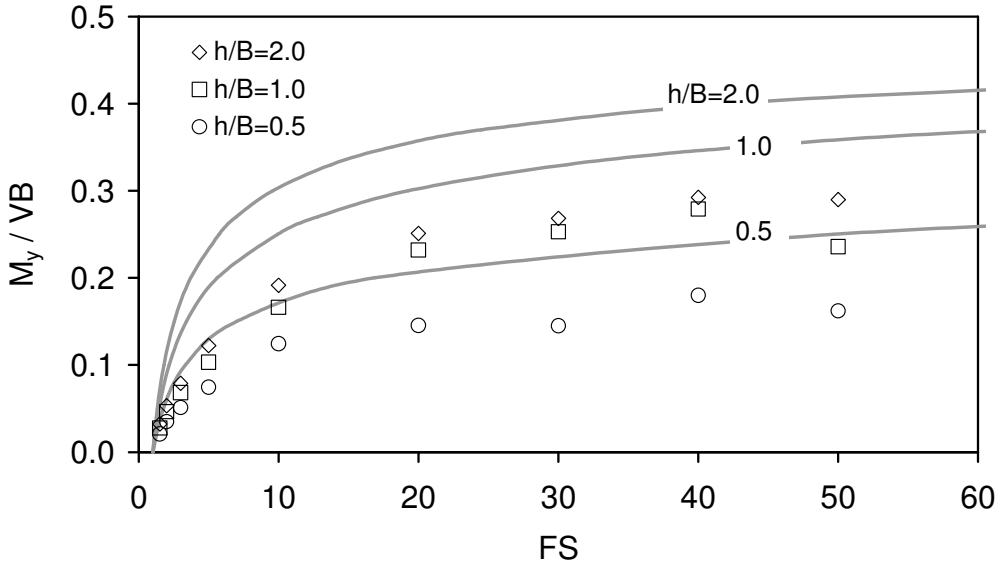

Figure 4.17. Reduction in foundation capacity due to undrained soil behavior: computed data in undrained analyses are plotted against equation 4.41 (drained case).

Performing analyses for the case of zero load inclination (H=0), and fitting a least-squares curve to the results, following equation is obtained for the factor of safety,

$$FS = 266^{\left(2M_y/VB\right)} \qquad (4.47)$$

Results of zero inclination analyses are plotted against curves provided by equations 4.47 (undrained) and 4.43 (drained) in Figure 4.18. Hence, significant reduction in overturning-moment capacity for a given factor of safety is observed for buildings with high aspect ratio and especially for relatively low values of FS.

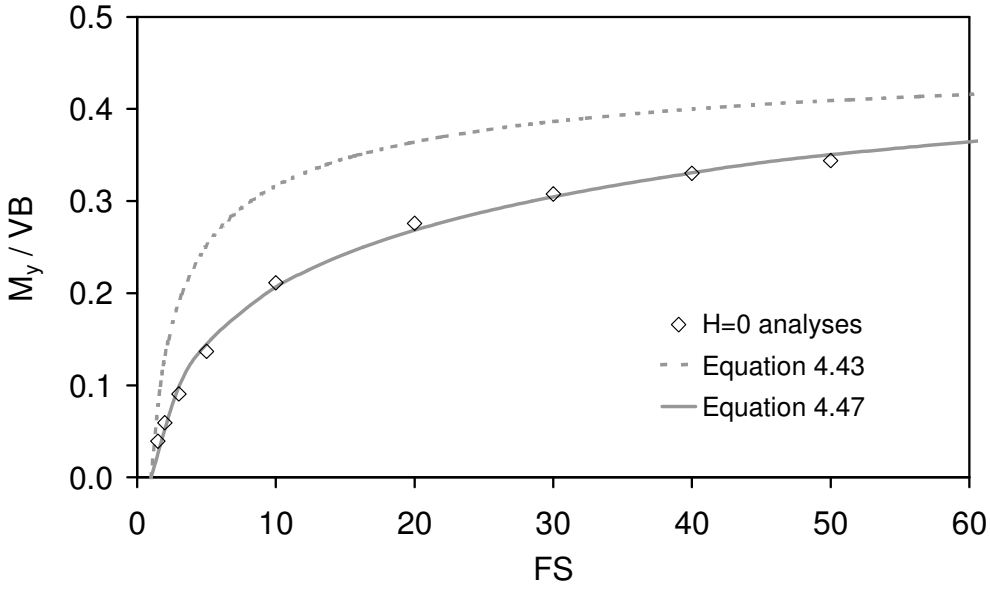

Figure 4.18. Reduction in foundation capacity due to undrained soil behavior, for the case of omitted load inclination.

For further visualization, reduction in ultimate M_y/VB for a given FS is calculated comparing M_y/VB values for drained and undrained analyses. The reduction in ultimate M_y/VB for a given FS is formulated as,

$$URF = \frac{(M_y/VB)_{dr} - (M_y/VB)_{udr}}{(M_y/VB)_{dr}} \tag{4.48}$$

where, URF is undrained behavior reduction factor, and subtitles “dr” and “udr” refer to drained and undrained analyses, respectively. Values of URF for different aspect ratios are plotted in Figure 4.19. The reduction is more significant for lower FS levels: for the range of FS ≅ 10, reduction induced in bearing capacity due to eccentrically applied load is in the range of 30% to 40%. Accordingly, reduction of FS due to consideration of pore pressure parameter A_S is significant.

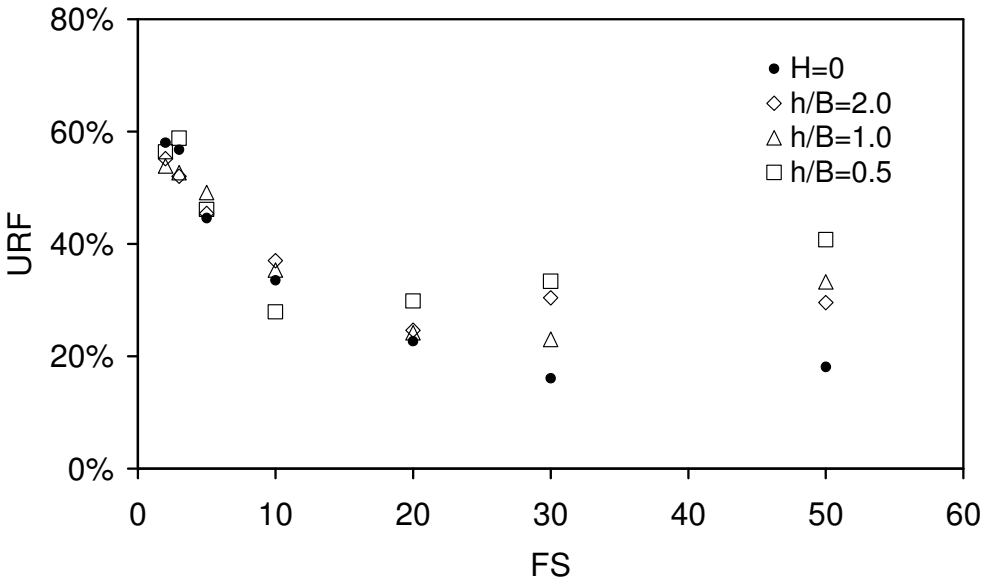

Figure 4.19. Undrained behavior reduction factor (URF) for different aspect ratios, due to equation 4.48.

Therefore, prediction of pore pressure parameter A_S is critical in determination of undrained load capacity. Higher values of A_S can exist for normally consolidated fine soils (Craig, 1983), leading to lower capacities of load eccentricity. On the other hand, development of reduction factors for different A_S factors is out of the scope of this study, and left as a future work. Naturally, more rigorous constitutive models than the simple elastic-ideally plastic model can provide improved results. Within the scope of this study, Equation 4.47 can be utilized for practical approaches.

Indeed, for saturated soils, not only the load eccentricity capacity, but also the static undrained bearing capacity is lower than the drained capacity during seismic loading. Under undrained loading, if any increase in normal stress on a specific plane is compensated by an equivalent increase in pore pressure, then, effective normal stress will remain constant. The shear strength of soil will remain practically unchanged under undrained behavior. Hence, for saturated soils, actual seismic bearing capacity under vertical loading can be significantly different from the drained bearing capacity, similar to CU and CD type triaxial test comparisons. On the other hand, the overall effect of undrained loading on bearing capacity (i.e., difference of seismic bearing capacity from drained bearing capacity) is unclear,

since stress paths for different locations in foundation soils are different: Overall change in capacity will be the sum of gain and loss in shear strength along the failure plane.

Hence, in order to investigate the reduction in bearing capacity under static condition and due to undrained loading, an additional analysis step is included. Following drained loading stage in Plaxis analyses, soil behavior for saturated soils are set to undrained. Then, vertical stress on foundation is increased up to detection of bearing failure. No load inclination and eccentricity exist in this step. Lower q_u values are obtained when compared to drained loading analyses. Accordingly, seismic factor of safety against bearing failure due to vertical loads only is calculated by,

$$FS_{seis} = \frac{(q_u)_{seis}}{q_p} \tag{4.49}$$

where, q_p is the foundation load, and $(q_u)_{seis}$ is the ultimate undrained capacity for the foundation, which has already under foundation load q_p. The relationship between q_u for drained and undrained analyses are presented in Figure 4.20, for selected values of FS, and for a foundation resting on the surface of saturated soil with parameters c=0, Φ=30˚, and Ψ=0˚. As a practical range of interest, the seismic factor of safety, FS_{seis}, is calculated approximately between 1.0 and one tenth of the static factor of safety. Obtained relationship between FS_{seis} and FS values are representative for plane strain conditions, and elastic-stress path compatible A_S value.

Assuming that FS_{seis} is compatible with the factor of safety defined for constant strength (i.e., cohesive: $c \neq 0$, Φ=0˚) undrained soil, ultimate M_y/VB values can be plotted against FS, by utilizing equation 4.39.b. Hence, it is assumed that the FS values in equation 4.39.b are equal to FS_{seis}, and actual drained FS counterparts are determined by the relationship in Figure 4.20. Thus, for no load inclination case, values of M_y/VB for the constant strength approach (Figure 4.7) and consolidated-undrained soil behavior (Figure 4.18), are compared in Figure 4.21. Similarly, considering the case of nonzero load inclination, values of M_y/VB values for different aspect ratios are compared in Figure 4.22.

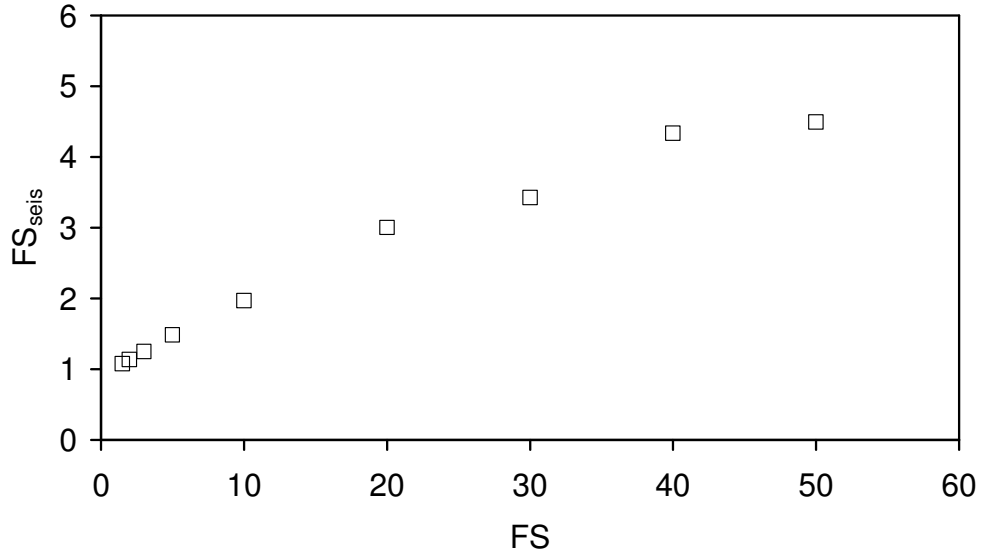

Figure 4.20. Relationship between static factor of safety (FS) and seismic factor of safety (FS_{seis}) equation (4.49) for strip foundation resting on saturated soil with parameters c=0, Φ=30˚, and Ψ=0˚.

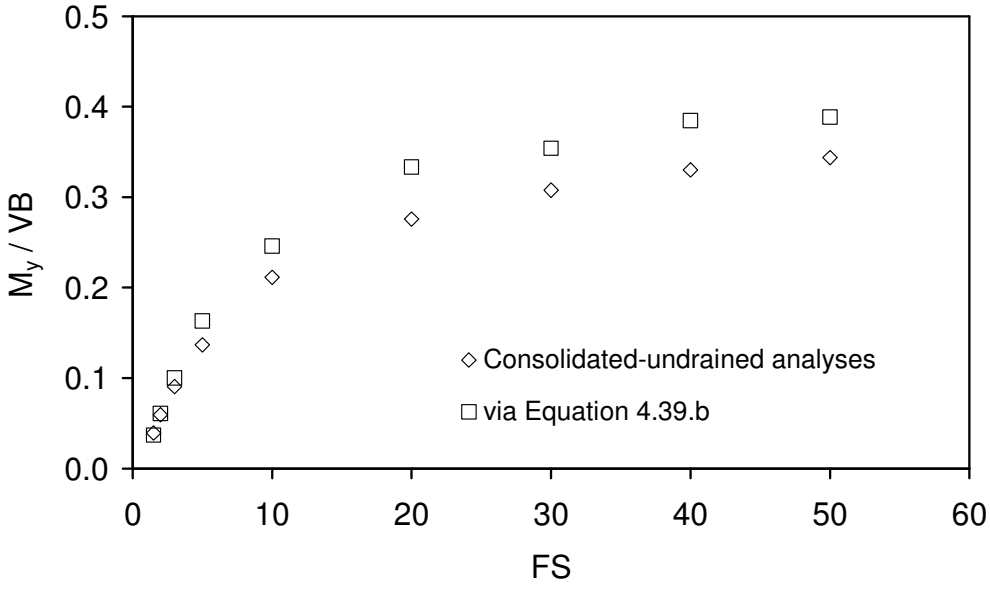

Figure 4.21. Comparison of constant strength and consolidated-undrained loading results via FS_{seis} for the case of no load inclination.

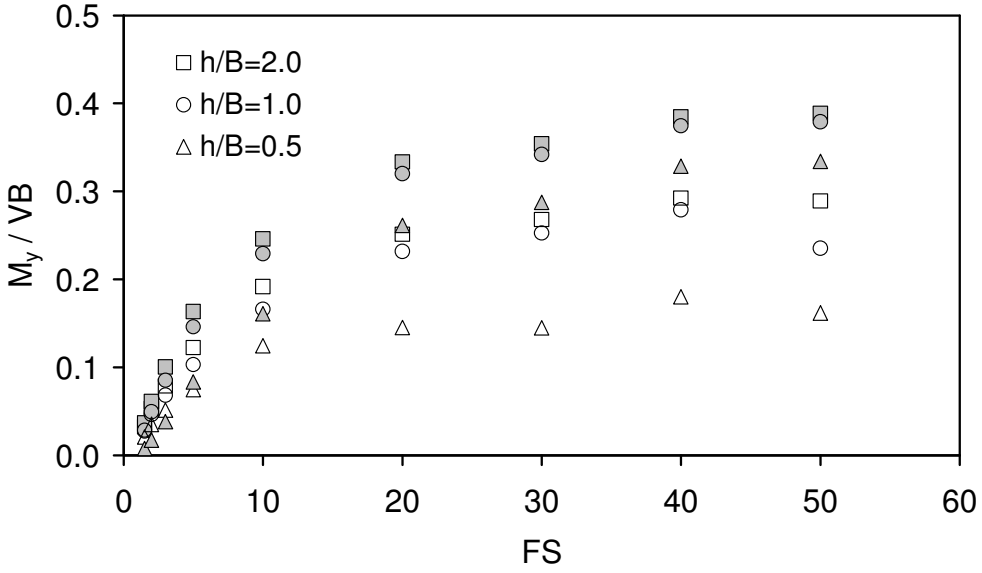

Figure 4.22. Comparison of constant strength approach (filled boxes) and consolidated-undrained loading results (empty boxes) for different aspect ratios for the case including load inclination.

For the case of no inclination, the results are compatible. This can be due to the fact that, for zero load inclination, the foundation failure mechanism is similar to the one under static vertical load. Observed differences can be explained as follows: for the cases of low factor of safety, limited uplift will occur due to load eccentricity before bearing failure is reached, hence, average shear strength for the contact zone will be in the order of the average strength for the case of foundation with full contact. On the other hand, for high values of FS, contact zone of foundation at bearing failure will be narrower: Resultant vertical load due to load eccentricity will move to sides of the foundation, where effective confining stress is lower. Therefore, in this range, it is expected that capacity will be somewhat lower than constant strength approach.

On the other hand, as shown in Figure 4.22, when load inclination is introduced, soil shear strength at shallow depths surrounding the foundation (i.e., towards the free-field) plays a significant role. In constant strength analyses ($c \neq 0$, $\Phi = 0°$), these soil zones have the same shear strength with those remaining below the foundation. Considering the consolidated-undrained loading analyses ($c = 0$, $\Phi \neq 0°$), soils surrounding the foundation will have considerably lower strength

compared to the locations below foundation. This is due to effective stress concept: Soils below foundation will benefit from increased effective stress due to the foundation load. Hence, the error involved in calculations is lower for relatively high h/B values, and higher for relatively low h/B values. The impact of load inclination is more significant for the latter case.

For no load inclination, equations based on cohesive (constant strength) soil are practically applicable, provided that consistent equivalent FS_{seis} is utilized. However, when effect of load inclination is considered, equations provided for constant strength assumption are no longer valid, especially for low aspect ratios, as can be observed in Figure 4.22.

The failure mechanism for consolidated-undrained load path is visualized by plotting stress points reaching plastic state during ultimate state in Figure 4.23, for a static factor of safety of 3. A well-defined failure plane is not observed, as in the case of cohesive soil model in Section 4.4.1.

The deformations at ultimate state are plotted in Figure 4.24. Uplift of the foundation is rather limited when compared to analysis results for cohesive and drained soil models with FS of 3 (Sections 4.4.1 and 4.4.2). As discussed above, the actual undrained factor of safety (i.e., FS_{seis}) is lower than 3 in undrained loading. Hence, failure of the foundation occurs without significant uplift. Failure planes, which are comparable to Prandl mechanisms, are clearly observable in these plots. For any of the h/B ratio, the foundation displacements involve significant tilting during ultimate state.

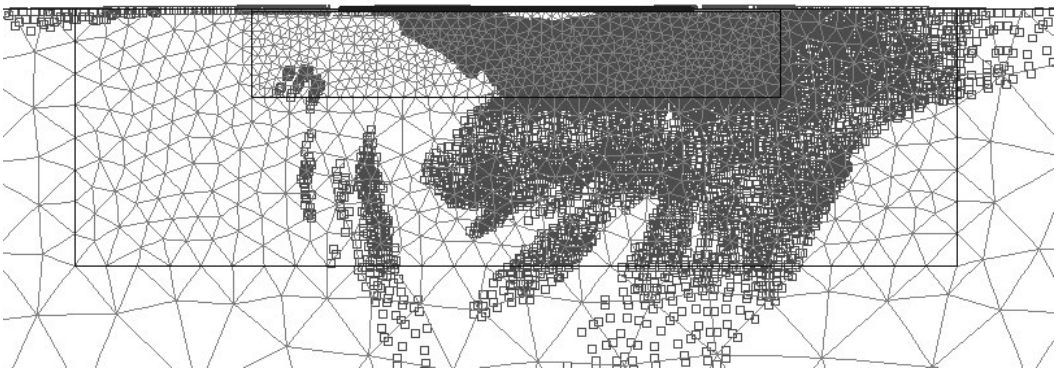

(a)

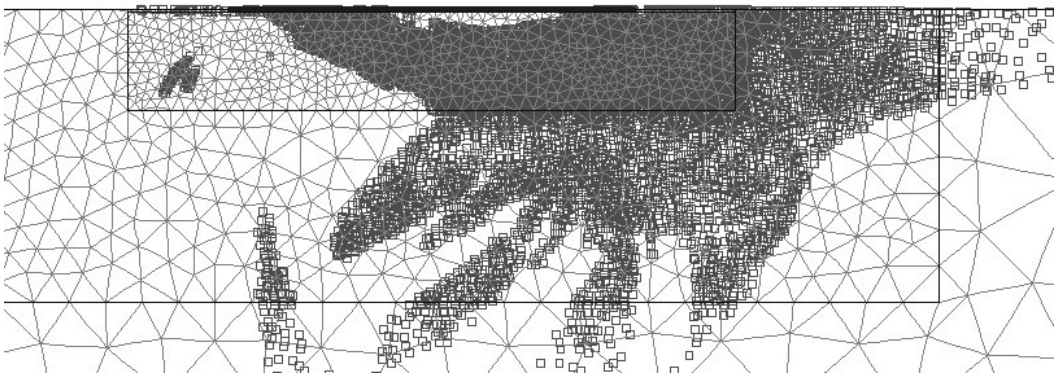

(b)

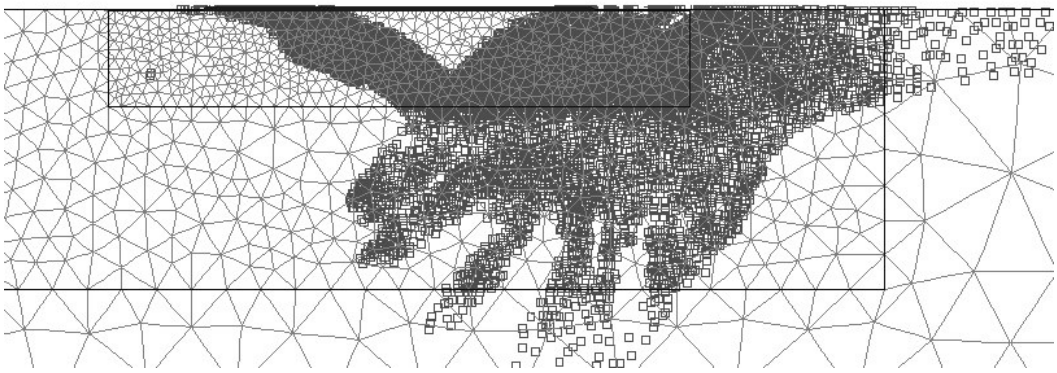

(c)

Figure 4.23. Plastic stress points during ultimate loading for consolidated-undrained analyses with FS=3.0: (a) zero load inclination (h/B is large), (b) h/B=1.0, (c) h/B=0.5.

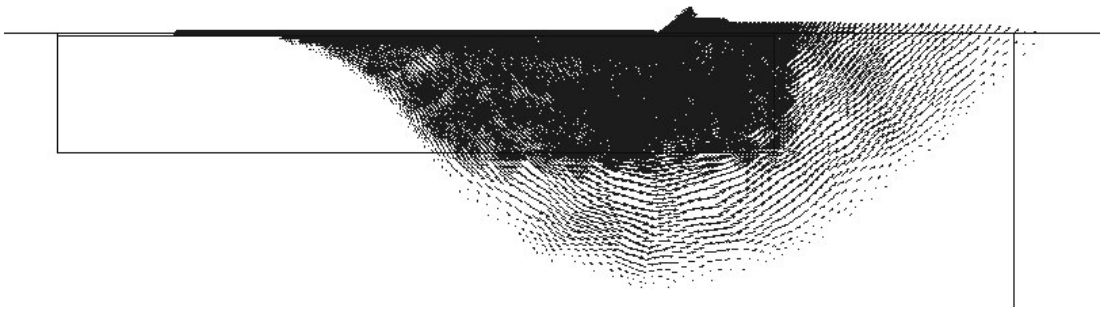

(a)

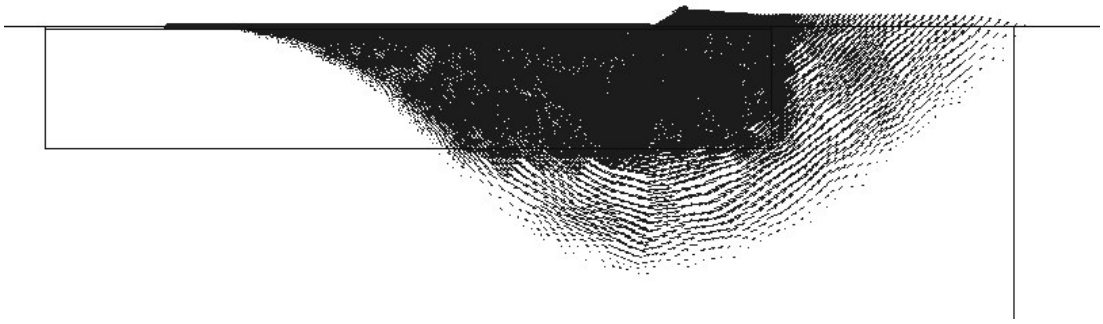

(b)

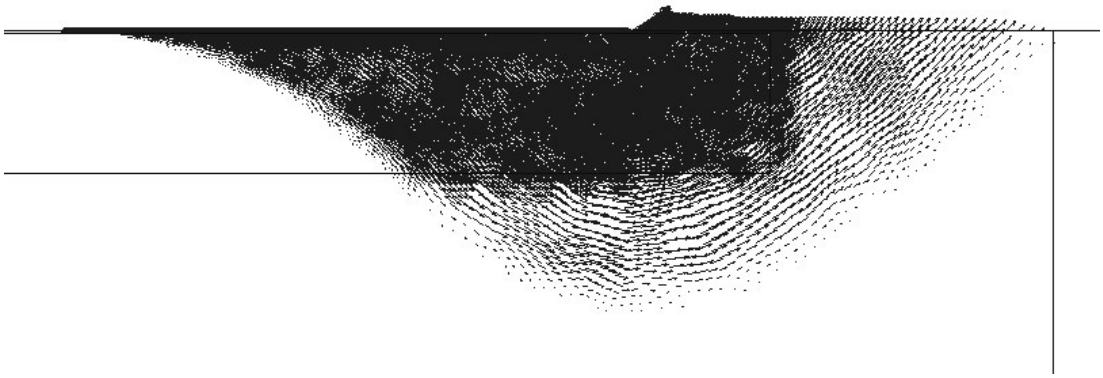

(c)

Figure 4.24. Displacements at ultimate state, for consolidated-undrained analyses with FS=3.0: (a) zero load inclination (h/B is large), (b) h/B=1.0, (c) h/B=0.5.

4.5. Conclusions

The finite element method can be practically utilized to analyze ultimate load capacity of surficial foundations during seismic loading. Procedures to achieve such calculations are implemented and the results are compared to those provided by the analytical approaches. The procedures discussed here can be utilized in cases where use of analytical formulations is limited due to complicated geometry, material behavior or heterogeneity of soil profile.

Results of analyses reveal that, in estimating the overturning moment capacity of shallow foundations, the load inclination effect can be practically omitted when the aspect ratio (i.e., h/B) is about 1.0 or above. However, for lower values of h/B, the overturning moment capacity of the foundation for a given vertical load is over-estimated unless load inclination is included. On the other hand, the tilting component of total roof displacement in this case is likely to reduce, whereas the horizontal translation component tends to increase. Accordingly, use of ultimate M_y/VB ratio without considering load inclination effect will result in higher capacity for the simplified elasto-plastic model, which in turn results in lower irrecoverable tilting. Thus, in case true M_y/VB ratio (i.e., considering actual inclination effect) is utilized, the fraction of tilting mode of irrecoverable displacements should be known, since calculated total irrecoverable displacements are the sum of translation and tilting modes. Hence, it is assumed that, the error due to ignoring partition of horizontal translation in total irrecoverable displacements (i.e., total irrecoverable displacement at the roof level of the structure is due to irrecoverable tilting of foundation) can be compensated by utilization of ultimate M_y/VB ratio calculated omitting the load inclination effect. As the h/B ratio approaches to zero, this simplified approach provides null irrecoverable tilting for foundation, since the overturning moment acting on the foundation becomes much lower than the ultimate moment value.

The consolidated-undrained stress-path beneath building foundations results in significantly reduced ultimate M_y/VB ratios when compared to drained analyses, especially for lower FS values. However, the constant strength (i.e., purely cohesive soil) approach representing the undrained behavior assumes that the soil strength is not effected by the presence of the building, can not be utilized directly for foundations over normally-consolidated soils that have already completed a significant part of the consolidation process.

Hence, for mat foundations resting on normally consolidated soils, the ultimate M_y/VB ratio for buildings with poor aspect ratio can be estimated by equation 4.39 for the undrained case with constant cohesive strength (i.e., saturated over-consolidated soils, or foundations resting on unconsolidated saturated soils for which shear strength can be assumed to be constant), by equation 4.43 for the fully drained case (i.e., foundation resting on unsaturated normally-consolidated soils), and by equation 4.47 for the consolidated-undrained case (i.e., foundation resting on saturated normally-consolidated soil that is fully consolidated). These equation are based on the assumption that $\Psi=0^{\circ}$, hence the results are on the safe-side compared to the analyses with associative flow-rule. In practical cases where a nonzero value of Ψ is known with reasonable accuracy, the analysis procedures discussed in this chapter can be followed to estimate actual ultimate load capacities of foundations. Otherwise, it is practically reasonable to accept the beneficial impact of positive Ψ as an unknown reserve capacity, which helps to decrease inelastic displacements. However, for the case of drained behavior, the impact of Ψ is mostly on FS, rather than the relationship between M_y/VB and FS.

Three equations, namely, equations 4.39, 4.43 and 4.47 are compared in Figure 4.25. The FS definition depends on the problem statement: for fully undrained condition, bearing capacity equations that are based purely on cohesive soil model (i.e., Prandl's solution) should be utilized; where for the other two conditions, equations that are based on effective friction angle should be utilized (i.e., cohesionless soil) for consistency. For hybrid cases involving $c\neq0$ and $\Phi\neq0$, it is proposed that the finite element analysis procedures presented in this chapter should be utilized to estimate M_y/VB ratio. Also, in cases where significant embedment of foundation exists, or soil profile is not uniform, it is recommended to utilize the finite element approach, rather than analytical formulations plotted in Figure 4.25.

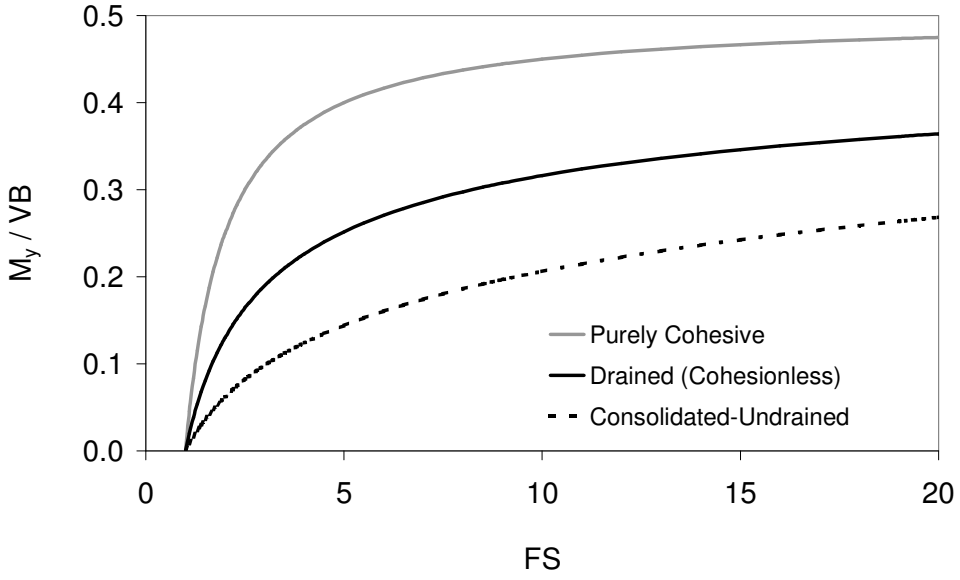

Figure 4.25. Comparison of M_y/VB ratios versus static factor of safety against bearing capacity failure for three simplified soil behaviors.

Figure 4.25 also provides an alternative hypothesis for explanation of why excessive foundation displacements in Mexico City and Adapazarı occurred at sites of shallow ground-water table for surficial mats resting on saturated normally-consolidated soils, with insignificant embedments: The undrained ultimate seismic load capacity can be significantly lower than the drained capacity, due to reductions in both FS and M_y/VB ratio. However, the reduction in M_y/VB ratio is strongly dependent on the deviation of effective stress-path from the total stress-path, based on representative pore-water pressure parameters. Further rigorous investigations, however, require detailed future laboratory tests (e.g., CU and CD type triaxial tests) on natural samples, and introduction of the obtained results into numerical procedures.

Estimation of M_y/VB ratio requires calculation of FS with reasonable accuracy. However, as discussed in Section 4.2, significant uncertainty may be involved in calculation of static bearing capacity. As it can be seen in Figure 4.25, ultimate M_y/VB ratios are sensitive to the variation of FS, in case FS is less than 5. Hence, values of FS below 5 should be calculated as accurately as possible. On the other hand, for FS values greater than 5, relatively rough estimations of FS can be sufficient. Considering the uncertainty in geotechnical parameters, for

foundations resting on normally-consolidated silt-clay mixtures, static bearing capacity for case studies is estimated assuming N_γ=10, which is reasonably consistent with the range of Φ between 26˚ to 34˚ and ψ=0˚. Considerations of the factors that foundation-soil interface may not be perfectly rough, the impact of cyclic loading on shear strength, effect of embedment, and foundation system (which may deviate from RC slab-type) further complicate the problem. Hence, in investigations of foundation displacements of available case studies, it is reasonable to utilize rough estimates of bearing capacity. Rigorous assessments of actual bearing capacity for each case are out of the scope of this study, which require detailed geotechnical investigation of foundation soils.

CHAPTER 5

VERIFICATION OF THE METHODOLOGY WITH CASE STUDIES

5.1. General

In order to validate the applicability of the proposed methodology and discuss the limitations, available case-studies from Mexico City and Adapazarı are utilized. Common properties of these cases are discussed in Chapter 1. In Chapter 2 the cyclic behavior of silt-clay mixtures extracted from the Adapazarı sites of observed building foundation displacements are discussed. In Chapter 3, the governing equations for tilting displacement of mat foundations under horizontal seismic loading are derived. These equations provide a link to elastic design spectrum through relating inelastic displacement demand and the elastic response spectrum. The overturning moment capacity of shallow mats during seismic loading is investigated in Chapter 4. In this chapter, all these preceding discussions are combined to provide a practical calculation procedure, as well as to provide an evaluation of it through available case studies.

Response of a dynamic system is not only a function of the system properties only, but of the input excitation as well. Considering the uncertainties involved in characterization of input motion, design forces are generally defined by utilization of design spectrum, which provides information for the expected peak response of elastic single-degree-of-freedom (SDOF) oscillator with natural period T. Generally, the design spectrum for a specific location is based on a regional seismic hazard study, involving details of local seismological and geological features, and also the target performance for engineered structures.

Hence, for practical assessment of foundation tilting performance for design of simple structures, it is useful to relate the calculation procedure to elastic design spectrum. Two requirements exist for utilization of the spectrum in displacement demand estimation for an oscillating nonlinear system:

1. System behavior should be reduced to, or linked to the response of a single-degree-of-freedom (SDOF) oscillator.

2. Reliable relationships should exist between inelastic displacement demand on nonlinear SDOF oscillator, and response of the linear oscillator.

Regarding the first requirement, formulations and assumptions to reduce the behavior of simple buildings with shallow mat foundations that of simple elasto-plastic SDOF oscillator is presented in Chapters 3 and 4. For the second requirement, some of the available simplified procedures for estimation of irrecoverable displacement demands are presented in Section 5.2.

The simplified calculation procedure proposed here to estimate tilting potential of a structure on a shallow rectangular mat foundation, which is sufficiently away from neighboring structures so that structure to structure interaction does not effect the foundation performance, can be summarized as follows:

1. Determine total building height h_n, foundation width B and length L. Estimate effective height $\overline{h}$ of the building by equation 3.47: for simple multistory residential buildings with uniform storey-heights, $\overline{h}$ can practically be assumed as two-thirds of h_n. Estimate I_θ and M_{st} for the building using equations 3.42 and 3.54. Calculate the aspect ratio of the building by $(\overline{h}/B)$.

2. Estimate the natural (i.e., first) period of the fixed-base building via simple approaches, or rigorous structural analysis.

3. Estimate representative dynamic soil properties: small-strain shear wave velocity (V_{s0}) and density (ρ) of soil based on empirical correlations or geophysical test results. Reduce V_{s0} due to nonlinear soil behavior, utilizing factors provided in Table 3.1, so as to calculate the representative shear-wave velocity (V_s) for the foundation soils during seismic excitation.

4. Estimate modes of rocking (T_r) and horizontal translation periods (T_h) considering soil-structure interaction, using the equations 3.44 and 3.53. The k_θ and k_h values are to be estimated by utilizing V_s and ρ, utilizing equations 3.73.b and 3.76.b.

5. Estimate total soil-structure-interaction system period $\overline{T}$ by equation 3.24.b. This is the natural period for the elastic behavior of the system. The damping ratio

can be selected as a small value (i.e., 5%) consistent with code-based design spectrum: in this study it is assumed that the majority of the energy is dissipated by the hysteretic behavior of the soil.

6. Estimate representative geotechnical soil strength parameters, such as Φ' for the drained behavior of normally consolidated soils, or S_u for the undrained behavior of over-consolidated soils. The cohesion is assumed to be negligible for the case of normally consolidated soils.

7. Estimate the overturning moment capacity (M_y) of the shallow mat foundation by utilizing numerical approaches as discussed in Chapter 4, by omitting the load inclination, and considering the effect due to the eccentric vertical load on the structure. However, in case of negligible foundation embedment and uniform foundation soil, it is practical to utilize figure 4.25 in order to estimate the ultimate M/VB ratio during seismic loading, provided that the consolidation process is completed. The factor of safety is the net static factor of safety, which is defined by equation 4.5. For consistency, q_u value should be calculated via equation 4.28, which is valid for the plane-strain condition. M_y is calculated by introducing V and B, where V is the weight of the superstructure which is simply $q_{str} \cdot B$ in the case net foundation safety is utilized.

8. Calculate pseudo-static yield acceleration a_y by the equation 3.60, or,

$$\frac{a_y}{g} = \left(\frac{M_y}{VB}\right) \Big/ \left(\frac{\overline{h}}{B}\right) \tag{5.1}$$

9. Read spectral acceleration for the linear system, $SA(\overline{T})$, from the elastic spectrum. Estimate R_y value by the equation 3.11. Estimate the ductility demand for the elastic-ideally plastic system through available correlations or simplified approaches, utilizing the R_y value.

10. Calculate the irrecoverable displacement demand (u_{ir}) on the system by equation 3.13. This value is assumed to be equal to $u_{\theta p}$ as a fundamental assumption in this study (see equation 3.56)

11. Estimate the irrecoverable tilting demand on foundation by,

$$\theta_{ir} \cong \tilde{\theta}_{ir} = \frac{u_{ir}}{\bar{h}} \qquad (5.2)$$

For the outlined methodology, verifications will be achieved by utilizing available case studies. Considering the uncertainties inherent in the cases, some simplifications exist for some of the items above, for practical comparisons of the measured and calculated quantities. These are further discussed in Section 5.3.

5.2. Literature Review

In order to estimate inelastic displacement demands by utilizing the elastic spectrum, approximate relationships are required. These approximate methods through which, inelastic displacement demands can be calculated, utilizing response of a linear system, can be divided into two-groups:

1. Methods based on equivalent linearization
2. Methods based on a displacement modification factor

A detailed discussion of the available methodologies is provided by Miranda and Ruiz-Garcia (2002a). The methods based on displacement modification factors are utilized in this study, to ascertain seismic demand in available case studies.

The required information for calculations involves elastic spectrum for a given small damping ratio (i.e., 5%), the period of the elastic system, and yield force for the corresponding elasto-plastic system. Hence, R_y factor is estimated by equation 3.11, and only remaining unknown is the corresponding maximum ductility ratio μ_{max} (equation 3.7), where maximum inelastic displacement of the system can be calculated by equation 3.13. Therefore, correlations between R_y and μ_{max} are needed for practical use. Certainly, irrecoverable deformations can also be estimated by utilizing maximum displacement of inelastic system directly, for a given acceleration-history.

One simple methodology is to utilize the relationships provided by Newmark and Hall (1982), where,

$$R_y = \begin{cases} \sqrt{(2\mu_{max} - 1)} & T_b < T < T_c, \qquad (5.3.a) \\ \mu_{max} & T_c < T \qquad (5.3.b) \end{cases}$$

where, T_c and $T_{c'}$ are the periods marking the acceleration and velocity sensitive regions for the elastic and inelastic spectrum respectively, and T_b is the lower bound period for the constant acceleration region, which generally has a limited practical importance in civil engineering applications.

Riddel et al. (2002), utilizing ensembles of records from Circumpacific Belt and California, developed correlations between R_y and μ_{max}. The proposed relationship for elasto-plastic SDOF oscillator with 5% damping ratio is,

$$R_y = \begin{cases} (1.9 \cdot \mu_{max} - 0.9)^{0.7} & T_b < T < T_{c'} \quad (5.4.a) \\ (4.2 \cdot \mu_{max} - 3.2)^{1/3} & T_c < T \quad (5.4.b) \end{cases}$$

Site dependency of R_y - μ_{max} relationship is investigated by Miranda (1993). It is proposed that, for soft soil sites,

$$R_y = \frac{\mu_{max} - 1}{1 + \frac{T_g}{3T_n} - \frac{3T_g}{4T_n} \exp\left[-3 \left(\ln \frac{T_n}{T_g} - \frac{1}{4} \right)^2 \right]} + 1 \quad \geq 1 \qquad (5.5)$$

where, T_n is the natural period of the system, T_g is the predominant period of the ground motion. The predominant period of the ground motion is defined as the period at which the maximum input energy of 5% damped elastic system is maximum, and can be practically determined by calculating the period for which the spectral relative velocity is the maximum. Equation 5.5 is determined utilizing bilinear behavior for which the post yield stiffness is 3% of the initial. Hence, the equation can also be practically utilized for an elastic- ideally plastic system.

A final detail in determination of maximum inelastic displacement demand is the effect of stiffness-degradation observed in cyclic tests of silt-clay mixtures: Utilizing stiffness-degrading models for structures, and utilizing nonlinear SDOF oscillator, Miranda and Ruiz-Garcia (2002b) observed that, lateral strength demands for degrading structures increase when compared to nondegrading systems, for structures with natural period shorter than T_g. Opposite trends are observed for natural periods higher than T_g. Hence, for a given R_y value, and considering the elastic period of SSI system as discussed in Section 3, the inelastic

displacement demands for foundations are expected to be estimated unconservatively when elasto-plastic model is utilized. In this study, it is assumed that, ignoring the actual damping, and viscous response of soils in simplified SSI models will compensate somewhat the increase in demand due to stiffness-degradation.

Hence, equations 5.3-5 will be utilized for further investigation of cases, especially when discussing the uncertainties in seismic demands. Therefore, these equations can be applied for foundation tilting potential assessments, utilizing 5% damped elastic design spectrum for the site.

5.3. Case Study: Mexico City

The case studies for the foundation settlements from the Mexico City are presented by Mendoza and Auvinet (1989). Four cases with shallow foundations are presented with available geotechnical information and foundation performance data, two of which involve shallow mats and two other cases with compensated foundations. Additional geotechnical information for Mexico-City soils is provided by Zeevaert (1991), and Seed et al. (1988). Attempts to calculate foundation displacements for two of the cases are presented by Auvinet et al. (1996), who also provides supplementary information for these cases.

The seismic demand at heavily damaged zones of Mexico City is investigated by Seed et al. (1988). Results of one-dimensional site-response analyses, however, were found to be extremely sensitive to small variations in shear-wave velocity and layer thickness of the shallow soft clay deposits. Hence, the seismic demand at Mexico City is somewhat chaotic, and estimations of seismic demand at available case locations require detailed geotechnical and geophysical investigations of the site. However, such detailed information is not available. Seed et al. discussed that the SCT record among others during the Mexico City Earthquake best represents the seismic demand at heavily damaged regions of the city. However, this station is located on the southern border of the heavily damaged area, and significant deviations in seismic demand due to SCT record therefore exist.

Gómez et al. (1989) presented dynamic characteristics of the selected damaged buildings in Mexico City, which can be accepted as representatives of the regular mid-rise concrete buildings. The fundamental periods of the 13 buildings

are calculated by modal analysis procedure, and plotted in Figure 5.1. The fundamental periods for these mid-rise buildings are observed to be in the range of 1-2 seconds, with very significant scatter.

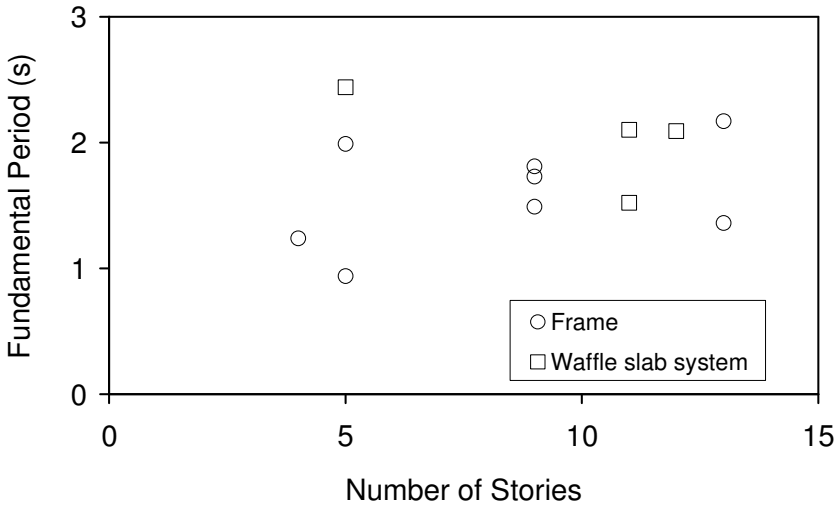

Figure 5.1. Fundamental periods of representative concrete buildings in Mexico-City, for damage assessments for September 19th 1985 earthquake (Gómez et al., 1989).

The soil-structure-interaction effects are estimated to elongate the total natural period of these systems in the order of 0.2 to 0.3 s, based on the V_{s0} data provided by Seed et al. (1988), which can be ignored considering the uncertainty in fundamental periods of these buildings, and actual seismic demand.

5.3.1. Seismic demand

Considering the discussion by Seed et al. (1988), the SCT record during 1985 Mexico City is utilized in seismic demand calculations for Mexico City cases within the scope of this study. However, significant uncertainty exists for actual seismic demands at these sites, due to variations in soil profiles.

The index parameters of SCT records are given in Table 5.1. The acceleration-histories are plotted in Figure 5.2, and the 5% damped elastic response spectra are given in Figure 5.3. The records are somewhat exceptional, consisting of approximately the sinusoidal form having the period consistent with the natural site-period (Seed et al. 1988).

Table 5.1. Index properties of the SCT record.

Component	PGA(g)	PGV(cm/s)	Predominant Ground Period (s) *
EW	0.17	61	2.1
NS	0.10	38	2.1

* Determined by the period for the peak PSV value for 5% damped linear system.

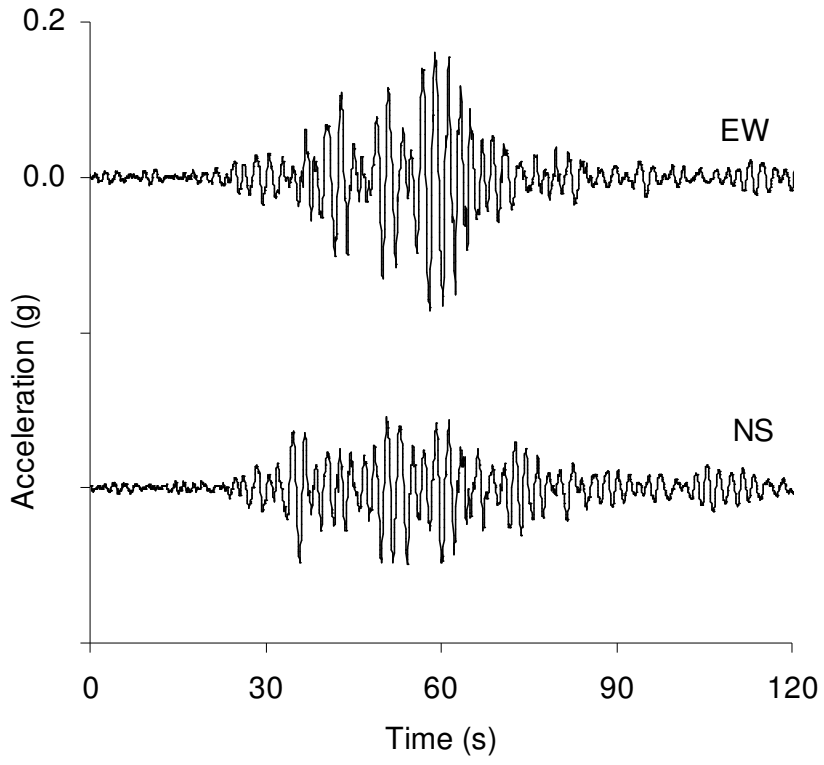

Figure 5.2. Acceleration-history of SCT records.

Considering different pseudo-static yield acceleration levels (equation 3.8), the ductility demands (μ_{max}) are computed for a 5% damped elastic-ideally plastic system. The computations are achieved utilizing Modified Newton-Raphson iteration, which is outlined by Chopra (1995) for numerical evaluation of dynamic response of nonlinear systems. The computed maximum μ values are compared with equations provided by Newmark and Hall (1982), Riddell et al. (2002), and Miranda (1993), which are discussed in Section 5.2, in Figures 5.4-6.

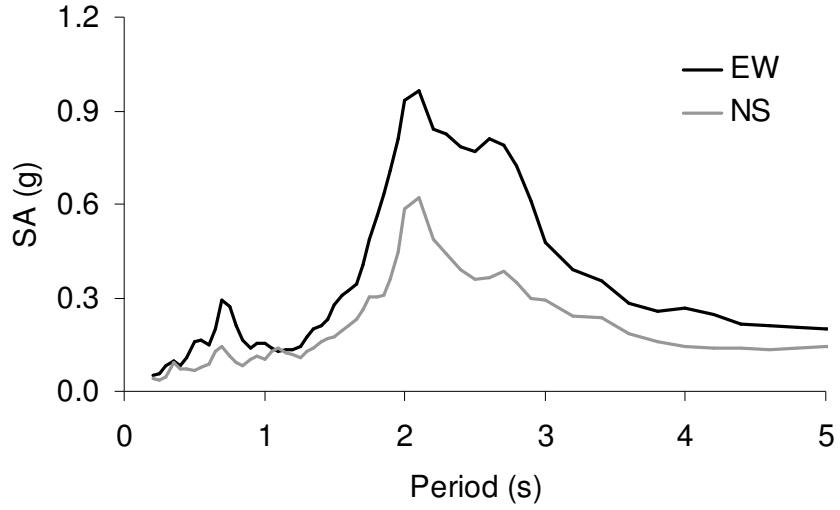

Figure 5.3. Spectral acceleration plots of SCT records for 5% damping.

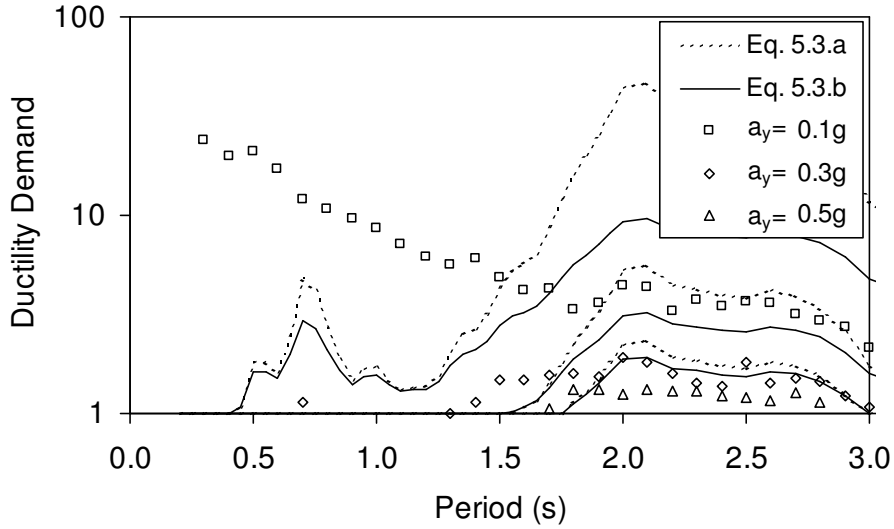

(a)

Figure 5.4. Comparison of calculated μ_{max} with Newmark and Hall (1982) relationship: (a) east-west (b) north-south components.

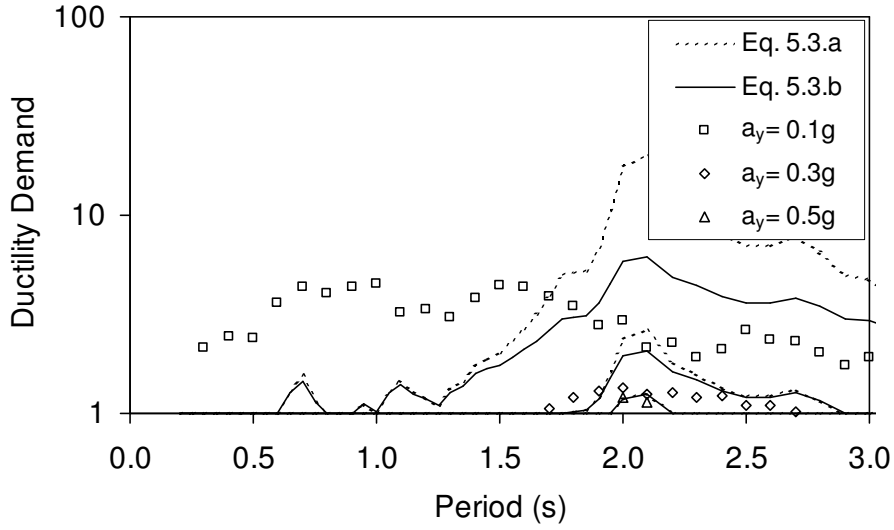

(b)

Figure 5.4 (continued).

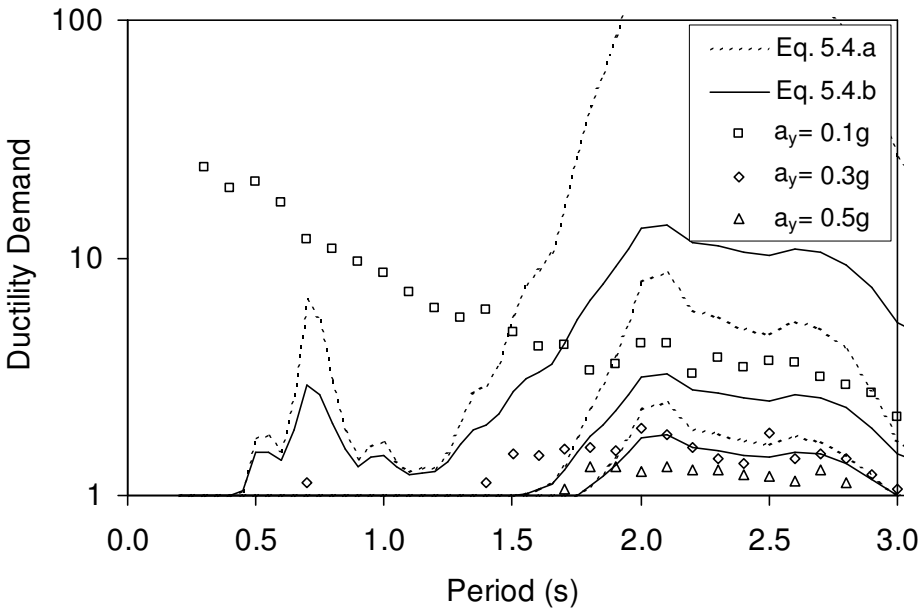

(a)

Figure 5.5. Comparison of calculated μ_{max} with Riddell et al. (2002) relationship: (a) east-west (b) north-south components.

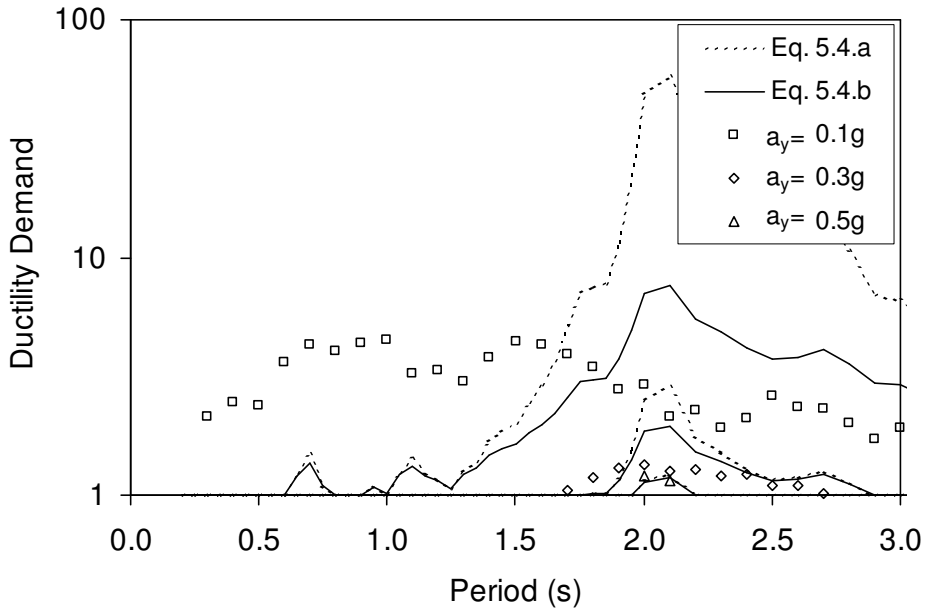

(b)

Figure 5.5 (continued).

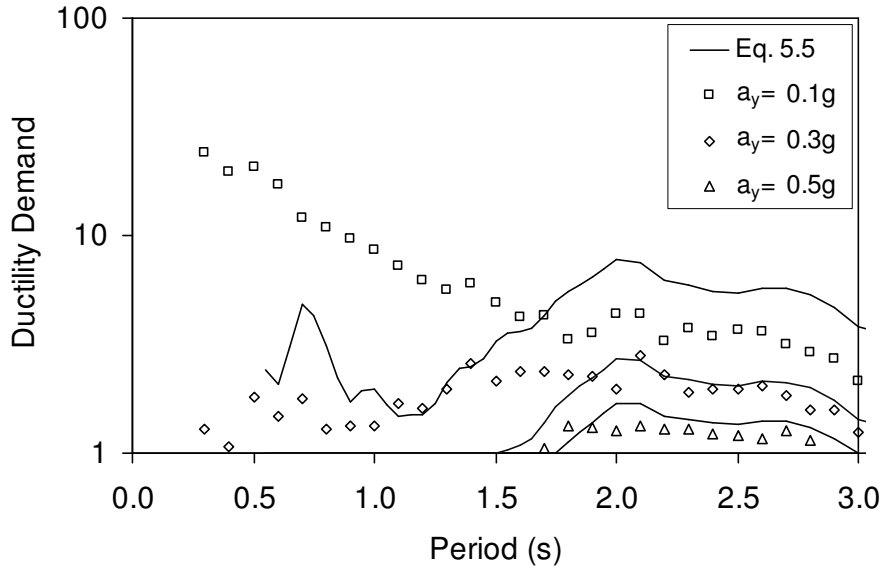

(a)

Figure 5.6. Comparison of calculated μ_{max} with Miranda (1993) relationship: (a) east-west (b) north-south components.

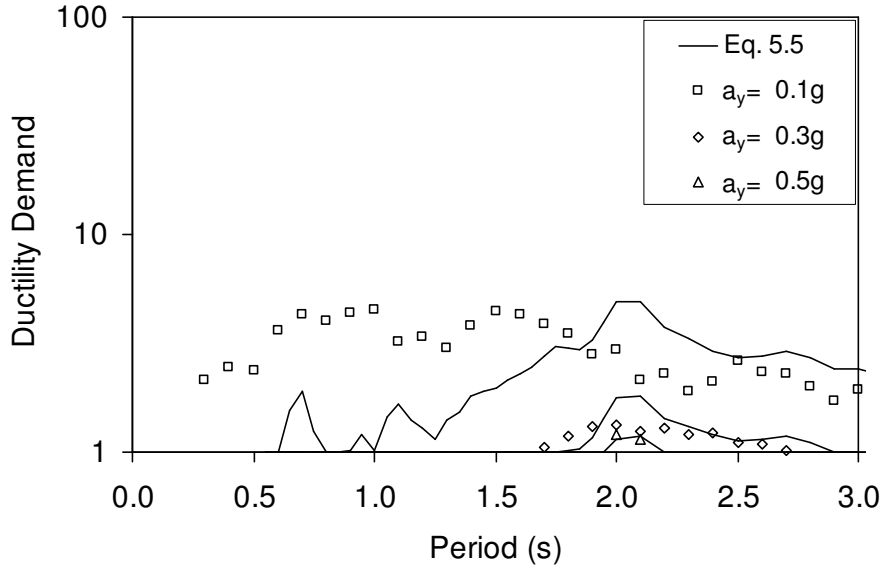

(b)

Figure 5.6 (continued).

The computed μ_{max} values are observed to be inconsistent with the approximate relationships, except for the NS component with Miranda (1993) relationship, which provides unconservative estimations for low a_y and period values. This may be explained by the extraordinary nature of the SCT records, due to strong site-amplification effects on the long-period component of the motion, resulting in insignificant amplitudes of motion in low-period ranges, but significantly high amplitudes of motion for high-period ranges. Development of a methodology for estimation of ductility demands for similar conditions are out of the scope of the study. On the other hand, to arrive practical conclusions, the issue is further investigated in Section 5.4. For further calculations on available Mexico City cases, computed μ_{max} values are directly utilized.

Above discussion on seismic demand is based on simple elastic-ideally plastic behavior, for which yield force is the same for both oscillation directions. In actual cases, however, this may not be valid, especially when a neighboring building does not allow the foundation to tilt in one particular direction. Also a significant irregularity in a soil profile may result in different yield force levels in different deformation directions. Accordingly, response of the elastic-ideally plastic system will be asymmetric, and calculated a_y values can be significantly different in

two oscillation directions. In that case, irrecoverable displacement demand tend to accumulate rather in the weaker direction. Possibly, however, the failure mode may alter in the stronger direction (i.e., to a mode governed by horizontal sliding of foundation without tilting). For demonstration purposes, additional analyses are performed by doubling the yield strength in one direction of the ideally elastic-perfectly plastic system, for the simulated motion. Calculated ductility demands for SCT records are compared with those obtained from symmetrical behavior in Figure 5.7. Significant increases are observed, which is important in investigation of available cases and practical design recommendations. As discussed in Section 1, in cases where elasto-plastic system practically yields only in one direction due to strong asymmetrical behavior, it is proposed to consider an analysis based on Newmark's sliding block analysis to calculate the irrecoverable displacement, since the duration characteristics of the input motion becomes important.

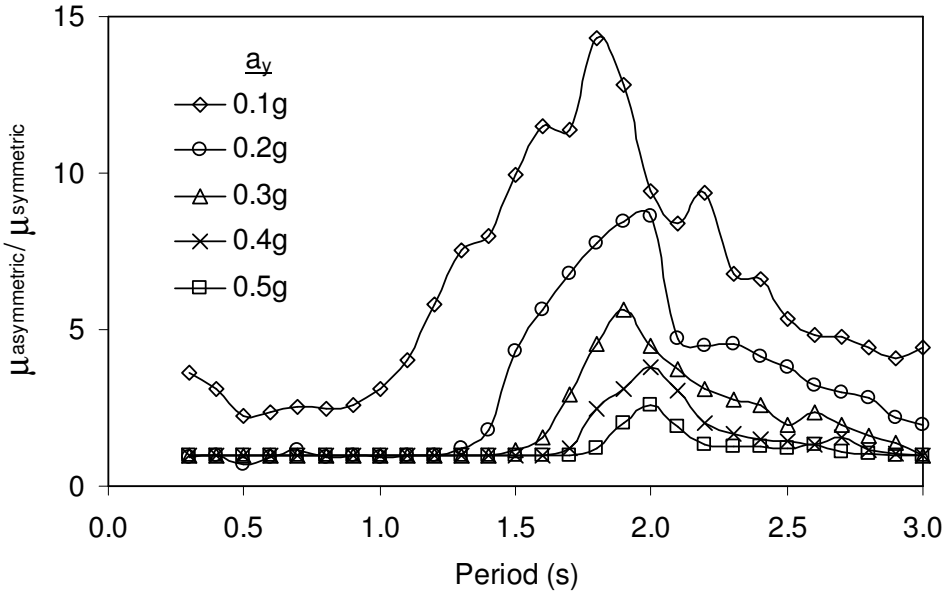

(a)

Figure 5.7. Comparison of ductility demand for the asymmetric system that the yield strength in one direction is doubled, with symmetrically behaving system: (a) EW component, (b) NS component of the SCT record.

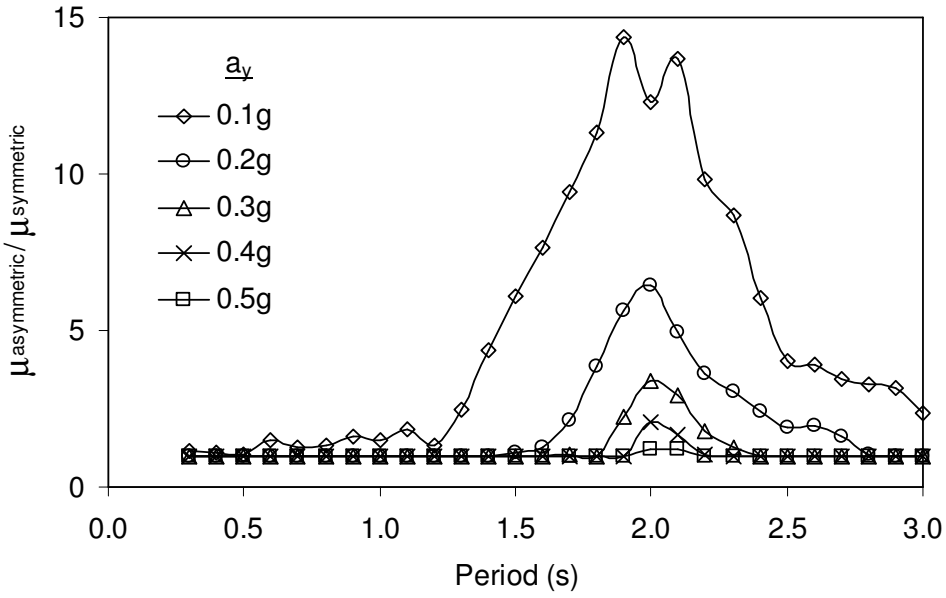

(b)

Figure 5.7 (continued).

Figures 5.7 a and b show that the ductility demands are very sensitive to any strength asymmetry in the system behavior, especially for period ranges close to the predominant site-period. However, the impact of asymmetrical behavior on ductility demand diminishes, as a_y increases. Hence, asymmetric systems with a_y values as low as 0.1g in the weaker direction will have significantly amplified ductility demands when compared to symmetric system response. On the other hand, for systems with a_y>0.3g, the amplification in the demand can be ignored, except for the cases that the period of the system is close to the predominant ground-motion period.

5.3.2. Available cases

Four cases presented by Mendoza and Auvinet (1988) are considered in this study. The cases involve two buidings with shallow mat foundations (cases Ia and Ib), and two with compensated foundations (cases II and III). The density of saturated silty clay of the Texcoco (Mexico City) silty clay is 1.2 t/m^3 as provided by Seed et al. (1988). The low value of density is due to extremely high natural water content of the soil. Considering very shallow water-table levels in the cases, the

buoyant unit weight of the soil is approximately 2 kN/m^3. It is assumed that, all case foundations have completed the consolidation process before the earthquake, and equation 4.47 is valid for calculation of M_y/VB ratio for the foundation.

Cases Ia and Ib are two buildings in a single block (Ic is the third building in the block). The block width is 16.75 m, and the total length of the block, which is equal to the sum of width of three buildings, is 40.3 m. Considering the generalized shape of the block, the weak direction is the east-west, where a street lies on the east. It is unclear whether there are similar-weight buildings on the west or not, from the provided scetch. It should be noted that, if these buildings were considered to stand alone, the weak direction would be the north-south direction, which is parallel to the width of each building.

Building Ia has foundation dimensions of 16.75 m and 14.10 m, with approximately rectangular mat foundation section. The building has six stories, with a height of 18.6 m. The net pressure (q_{net}) exerted on the soil by the foundation is 55 kPa. The soil embedment is 1.2 m, which can be ignored when compared to foundation dimensions, in calculations of bearing capacity. Hence, the static bearing capacity is calculated by the formula 4.28.b, utilizing N_γ=10 as discussed in Chapter 4. Hence, the drained static factor of safety is calculated as,

$$FS = \frac{0.5 \cdot 2 \cdot 16.75 \cdot 10}{55} = 3.0$$

Larger dimension (i.e. 16.75 m) is selected as the width, considering the block-behavior of the three buildings. Hence, the M_y/VB ratio is calculated by the equation 4.47 as 0.098. Tilting of the building is reported as 5.2% eastwards (i.e., towards the street site), and a pre-earthquake tilting is reported to be evident, due to a shallow pumping well installed near the corner of building, which lowered the water-table level to 2.5 m locally.

Building Ib has somewhat similar properties with the Ia: the building has foundation dimensions of 16.75 m and 12.90 m, with rectangular mat foundation section. The building has eight stories (Paolucci and Pecker, 1997), with building height in the order of 25 m. The pressure that is exerted on the soil by the foundation is 99 kPa. Considering 1.5 m foundation embedment, the net foundation pressure is estimated as 81 kPa. Similarly, the factor of safety against bearing

capacity failure is 2.1, which results in M_y/VB ratio of 0.066. The reported tilting of the building is 6.3% eastwards.

Case II has a compensated mat foundation with dimensions of 11.60 m width and 54.50 m length. Weak direction is the north-south direction. Total height from the foundation levels is 16.3 m. Embedment is 3.0 m, and ground water table is located at 1.60 m. The net pressure exerted on the foundation is 25 kPa. The building exhibited excessive tilting at the northwest corner, where heavy water tanks on the roof exerted approximately 30 kPa of additional pressure on foundation. The measured tilt at this corner is 2.9%. Hence, existing static load eccentricity and inclination can have a significant contribution on the building performance. Utilizing the total net pressure of 55 kPa, the factor of safety is calculated as 2.1, which results in M_y/VB ratio of 0.066.

Case III consist of an apartment building with foundation width 25.0 m and length 30.1 m. The height of the building is not provided. However, since the net pressure exerted on the compensated foundation is reported as 33 kPa, the building is assumed to have a similar height with Case II. The building has tilted significantly towards the west and south directions, with ratios of magnitude in the order of 2:1. Hence, the maximum tilting is towards the southwest corner, with a maximum differential displacement of 0.93 m with respect to northeast corner. It is reported that only 0.53 m of 0.93 m occurred during the earthquake: the remaining 0.4 m is due to water pumping at south-east corner before the earthquake. Hence, considering the total differential settlement 0.6 m towards the east (i.e., weak) direction, the tilting performance of the building can be estimated as approximately 1.4%. Tilting in the stronger direction is approximated as 0.6% and the static bearing capacity is estimated as 7.6, with a M_y/VB ratio of 0.18.

Based on the information provided, the effective heights ($\bar{h}$) of the buildings are estimated as two-thirds of the total height. Irrecoverable displacement demands compatible with the observed tilting are tabulated in Table 5.2. Utilizing ultimate M_y/VB ratios, calculated pseudo-static yield acceleration levels for these cases are also presented.

Table 5.2. Final calculation parameters for the Mexico City cases.

Case	h_n (m)	$\bar{h}$ (m)	B(m)	$\bar{h}/B$	M_y/VB	a_y(g)	θ_{ir} (%)*	u_{ir}(m) **
Ia	18.6	12.4	16.75	0.74	0.098	0.13	5.2(E)	0.64
Ib	25.	17.	16.75	1.01	0.066	0.066	6.3(E)	1.1
II	16.3	10.9	11.60	0.94	0.066	0.070	2.9(N)	0.32
III	16.	11.	25.0	0.44	0.18	0.41	1.4(E)	0.15

* Observed value in the field, letter in parenthesis is the tilting direction.

** Irrecoverable displacement demand is consistent with θ_{ir}: $u_{ir} = \bar{h} \cdot \theta_{ir}$

5.3.3. Comparison of the predicted and measured tilts

The case data in Table 5.2 are compared with calculated irrecoverable displacement demands due to SCT records in Figure 5.8. Since the fundamental periods of the buildings are not precisely known, a wide range of periods varying between 0.8 and 2.8 seconds are presented. Considering the data in Figure 5.1, the most probable period range of interest is between 1.0 s to 2.0 s for case buildings. Within this range, the SSI elongates the period of the total SSI system approximately 0.2 to 0.3 seconds, which can be practically ignored considering the uncertainty in T_s.

The cases II and III are reasonably consistent with the seismic demand. However, cases Ia and Ib yields higher tilting values with respect to those estimated based on the seismic demand on elasto-plastic system. These cases have relatively low a_y values, in the order of 0.1g. As discussed via Figure 5.7, these pseudo-static yield acceleration levels are very sensitive to strength asymmetries. On the other hand, the uncertainties involved in geotechnical and structural information on cases, as well as the unknown positions of the neighboring buildings than can provide strong asymmetry in bearing strength in one direction and alter the seismic demand on building due to structure-structure interaction, prohibits further discussion on results. However, it is also important to notice that the buildings Ia and Ib are adjacent, and could have influenced by the same reason causing asymmetric response. However, water-pumping near the corner of the building Ia does not appear to be a possible reason, since it cannot explain the tilting performance of Ib, and the direction of the excessive tilting.

Further information on cases is required for clarification of the existence of asymmetrical behavior.

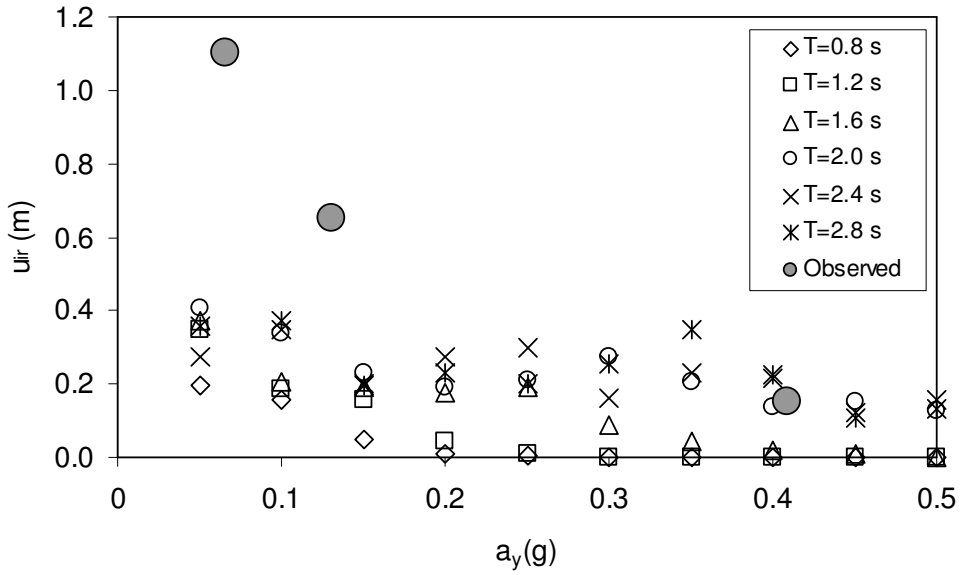

(a)

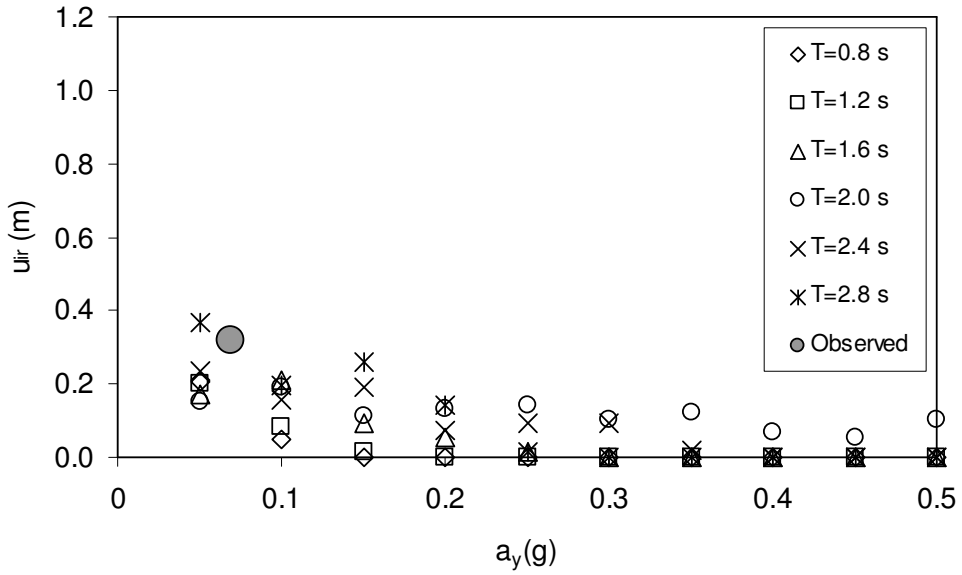

(b)

Figure 5.8. Comparison of Mexico City cases with the simplified methodology considering (a) EW component, and (b) NS component of SCT record.

The impact of site response, which dominates the ground response in Mexico City, is further investigated in Section 5.4. However, considering the inconsistency between simplified relationships used to estimate ductility demand and the calculated values based on SCT record, the seismic demand in Mexico City appears as a somewhat special case for seismic design. Restriction of the irrecoverable foundation rotation demands to relatively small values (e.g., at most 0.5˚ or 1%) result in relatively high a_y values, which in turn restrict the impact of strength asymmetry. However, such values of a_y would also mean nearly elastic response of the system. Hence, similar discussions are also made for the Adapazarı cases, where data with better quantity and quality is available.

5.4. Case Study: Adapazarı

Adapazarı constitutes another special case where excessive foundation displacements on silt-clay mixtures are observed. Due to the shallow ground water level in the city (at about 1.0 m below the ground surface), majority of the reinforced-concrete buildings have very shallow mat foundations, which are observed to behave rigidly as they displaced during 17 August earthquake. The mechanisms leading to excessive foundation displacements are still the subject of ongoing researches.

Low frequency enhancement and motion amplification effects of the deep alluvial basin was the obvious reason of excessive damage in the Adapazarı City. A detailed investigation of the site-effects on the ground response and consequent building damage were presented by Bakır et al. (2002). They concluded that, the predominant site period was over 1.5 s in Adapazarı, and could elongate further at sites with very soft shallow deposits.

The case data from Adapazarı is provided by Bray et al. (2001a, 2001b, 2004), Karaca (2001), and Yasuda et al. (2001). The cases documented by Bray et al. consists CPT and SPT tests nearby the case buildings with excessive settlements, and are referred to as “PEER cases” in this study. Additional cases from Cumhuriyet and Tığcılar districts, presented by Karaca, are referred to as “METU cases”. Both METU and PEER cases are re-investigated and new borings were drilled where deemed necessary, as part of the research aiming at investigation of the foundation displacements and undisturbed samples retrieved for triaxial tests. Locations of the borings, where undisturbed samples are

recovered, are presented in the Appendix A. Data provided by Yasuda et al. involves damage-survey results for foundations, such that average and maximum settlements, and angle of irrecoverable tilting of foundations are tabulated, along with the foundation width and number of stories of the buildings. Although the damage survey includes performance data of numerous foundations compared to PEER and METU cases, geotechnical information does not exist. Additional geotechnical information for shallow soft deposits in Adapazarı can also be found in the study by Sancio et al. (2002).

Although a detailed study on the range of fundamental periods of typical reinforced concrete structures in Adapazarı is not available, a study by Akkar et al. (2004), on the building stock encountered in Düzce, can provide useful information, assuming that the structural characteristics in the two cities are similar. Based on this data, which is plotted in Figure 5.9, 3 to 5-storey buildings, equation 3.77 is observed to provide a reasonable estimate of the structural period. However, significant scatter exists in the fundamental period for a given number of stories, which introduces further uncertainty in the calculations. As discussed in Chapter 3, the representative natural period of the soil-structure system is assumed to be 0.8 s for 4 to 6-story buildings in Adapazarı.

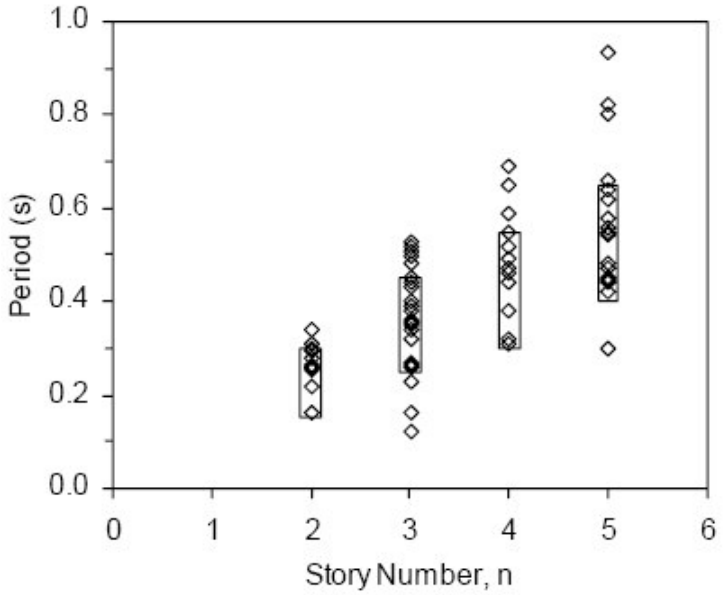

Figure 5.9. Range of fundamental periods for 37 buildings in Düzce (Akkar et al., 2004).

5.4.1. Seismic demand

During 17 August 1999 Kocaeli Earthquake, the only lateral component recorded at Sakarya (Adapazarı) station was EW, which is almost fault-parallel, along with the vertical component. The NS component was not recorded due to a malfunction. Accordingly, EW record is utilized for estimation of seismic demand in Adapazarı during 17 August 1999 earthquake. Unavailability of NS component consists a limitation in investigation of Adapazarı cases, and the actual demand may be underestimated to some extent

The second shortcoming is that, these records are taken at a stiff site, where conditions are not representative of the deep alluvium on which the majority of the city is situated. Hence, the records can not be directly utilized for the assessment of seismic demand for Adapazarı cases.

In order to simulate seismic demand realistically at deep alluvium sites in the city, one dimensional site response analysis is utilized. The site response analysis program Proshake, which implements the same equivalent linear procedure as SHAKE (Schnabel et al., 1972), is used for this purpose. Hence, nonlinear behavior of deposits is approximately considered by equivalent linearization.

The soil profile is based on the study by Bakır et al. (2002), in which the aftershock acceleration-histories simultaneously recorded at the stiff (i.e., same site with the instrument recording 17 August event) and alluvium sites are used to determine the transfer function. Utilizing smoothed transfer functions and deep borehole profiles, a consistent idealized profile is developed for site-response analyses. Calculated response spectra are observed to be consistent with the distribution of building damage on alluvium sites. Moreover, it is observed that, fundamental period for deep alluvium sites is around 1.5 s, and can approach to 2.0 s due to nonlinear behavior during strong seismic excitation. Soft and weak shallow soils can significantly alter the seismic demand similar to the Mexico City. For site response analysis, a 150 m deep profile is utilized, details of which are given in Table 5.3. Effect of soft shallow deposits on seismic demand is ignored, omitting the topmost layer surficial deposits. Acceleration histories of outcrop motion and calculated surface motion are plotted in Figure 5.10. Velocity-histories are plotted, in order to visualize the site effect on seismic demand (Figure 5.11). Acceleration and velocity spectra for both cases are compared in Figure 5.12.

Table 5.3. Mechanical properties of the soil profile utilized in site-response analyses.

Layer No.	*Material*	*Thickness (m)*	*Unit Weight (kN/m^3)*	*V_s (m/s)*	*Modulus Reduction and Damping Curve*
1	Clay	85.0	18	330	Ishibashi-Zhang (1993), PI=35
2	Gravel	15.0	18	730	Ishibashi-Zhang (1993), PI=0
3	Clay	50.0	18	410	Ishibashi-Zhang (1993), PI=35
4	Rock	(half-space)	24	1000	Schnabel et al. (1972), Rock curve

Depth of water table is 1.0 m.

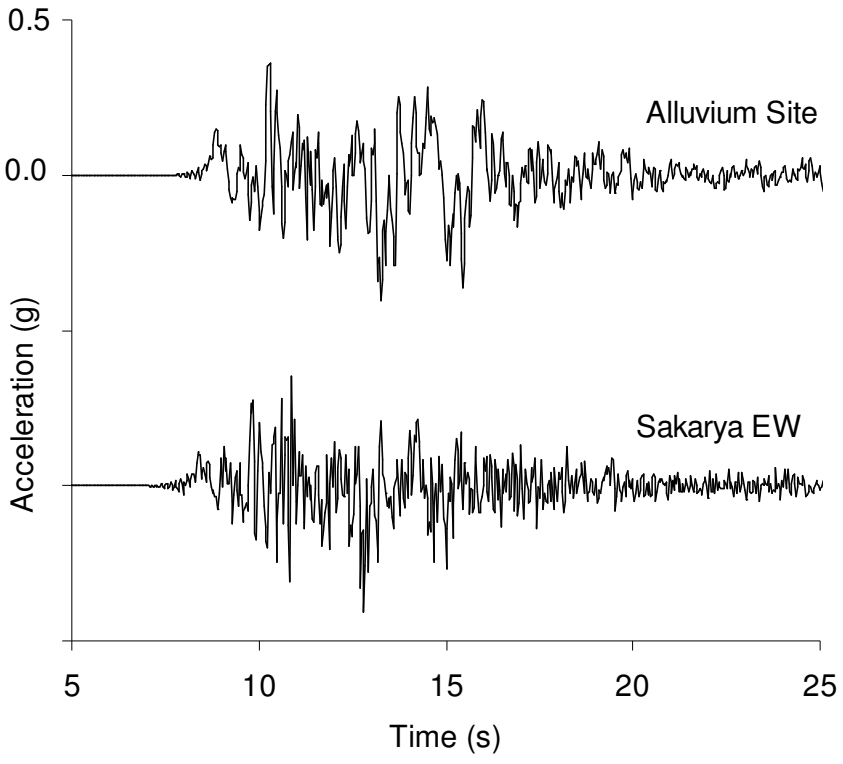

Figure 5.10. Acceleration-histories for outcrop motion (Adapazarı EW record), and the simulated motion for deep alluvium sites.

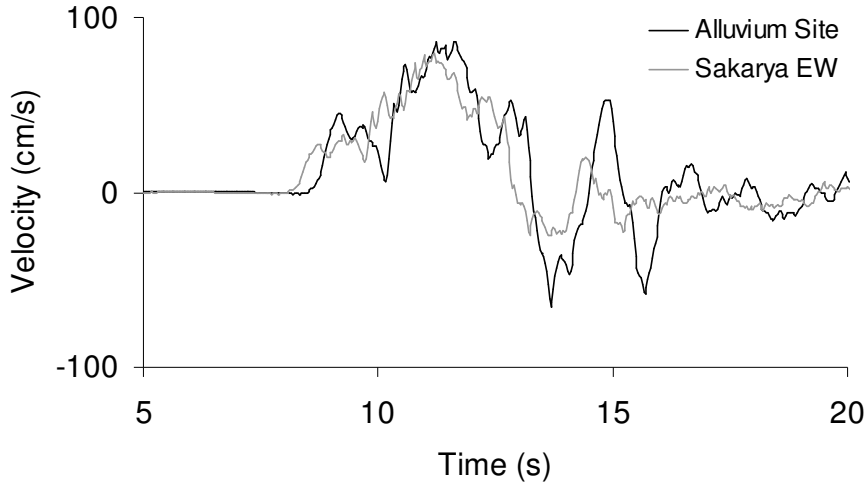

Figure 5.11. Comparison of velocity histories for outcropping (rock) motion and simulated surface (alluvium) motion.

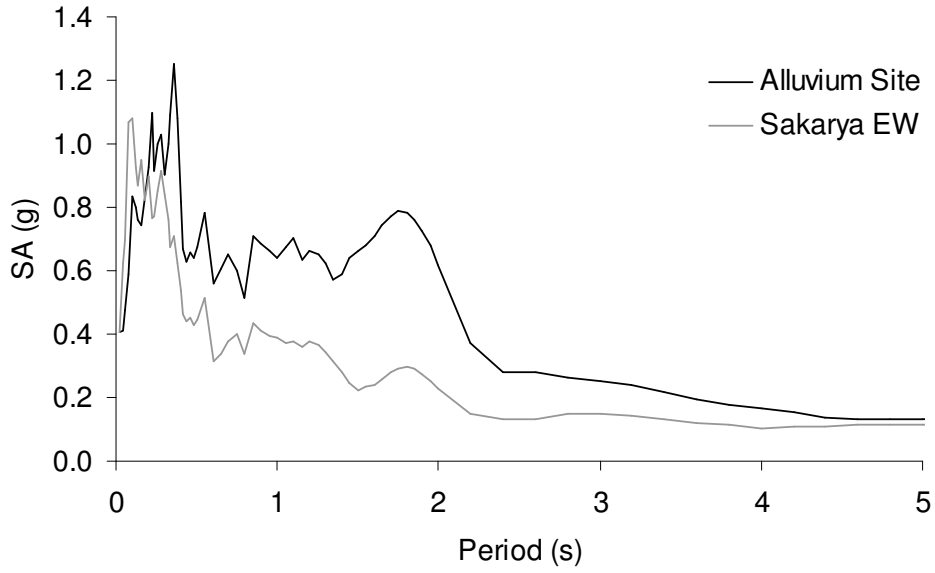

(a)

Figure 5.12. Comparisons of acceleration spectrum for outcrop and surface motions (5% damping).

Ductility demands for the generated motion are investigated for different R_y factors, and natural periods. Considering different yield acceleration values (a_y=0.1g, 0.3g, and 0.5g), ductility demands are calculated for different natural

periods, similar to the calculations for the Mexico City cases. The results are compared with the simple relationships for R_y-μ_{max} given in Section 5.2, utilizing calculated acceleration spectra for the motion. The comparisons for Newmark and Hall (1982), Riddel et al. (2002) and Miranda (1993) are presented in Figures 5.13 to 15. Calculated values are observed to agree with equations, for representative ranges of building periods. For the equations of Riddell et al. and Newmark and Hall, equations for the acceleration sensitive region (dashed lines in Figure 5.13 and 5.14) are valid for lower periods, and equations for the velocity-sensitive regions (continuous lines) are valid for the mid-period ranges in the plots.

Considering the Turkish Earthquake Code (Ministry of Public Works and Settlement, 1998), the City of Adapazarı is included in the zone of effective ground acceleration of 0.4g. In calculations of ductility demand, equation 5.3.b, which is consistent with the code, must be utilized. By the same methodology, ductility demands for different yield acceleration values (a_y) are calculated, based on code spectrum. For practical purposes, spectral values within acceleration-sensitive region are omitted, and spectral values within the velocity-sensitive region are extended towards lower period regions, considering the period ranges and R_y values of interest. Comparisons with those values obtained from simulated ground motion (alluvium site) are presented in Figure 5.16. It is observed that the ductility demands for simulated ground motion are compatible with the Z4 spectrum in the Turkish Earthquake Code.

In order to observe the sensitivity of inelastic response to strength asymmetry, increase in the ductility demand is investigated. For that purpose, the yield force level for the elasto-plastic system is doubled in one direction. Ductility demand of the asymmetric symmetric systems are compared in Figure 5.17. Although significant amplification in the demand for systems with a_y=0.1 and 0.2 is observed (i.e., in the order of 2 to 3) for the period range of interest, the amplification is insignificant for higher values of a_y. This is consistent with the conclusion that buildings with higher foundation aspect ratio will be more sensitive to the strength asymmetry, since a_y values are comparatively lower. On the other hand, sensitivity of the ductility demand to the strength asymmetry for the Adapazarı cases are considerably lower than for the case of SCT record in Mexico City.

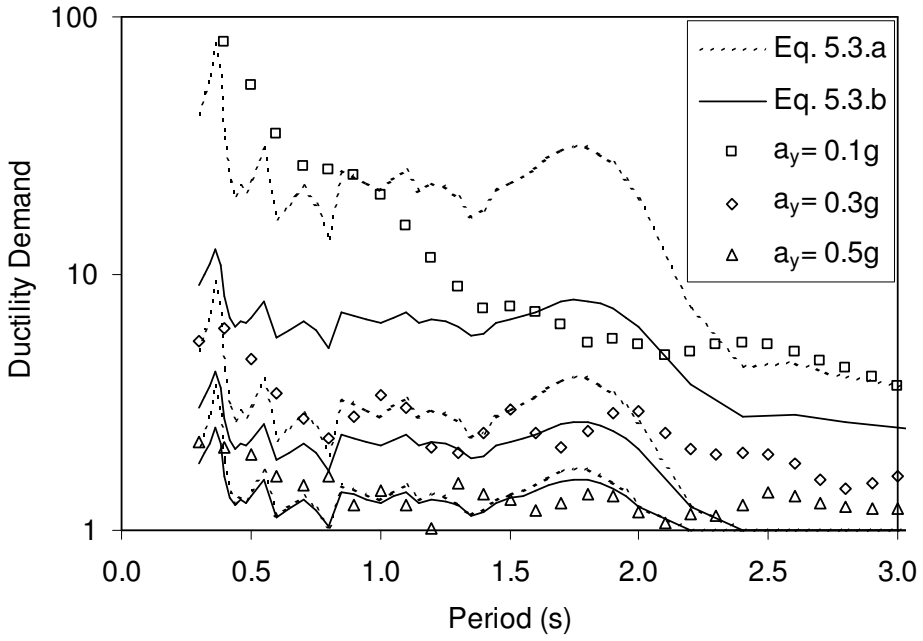

Figure 5.13. Comparison of calculated maximum μ with Newmark and Hall (1982) relationship.

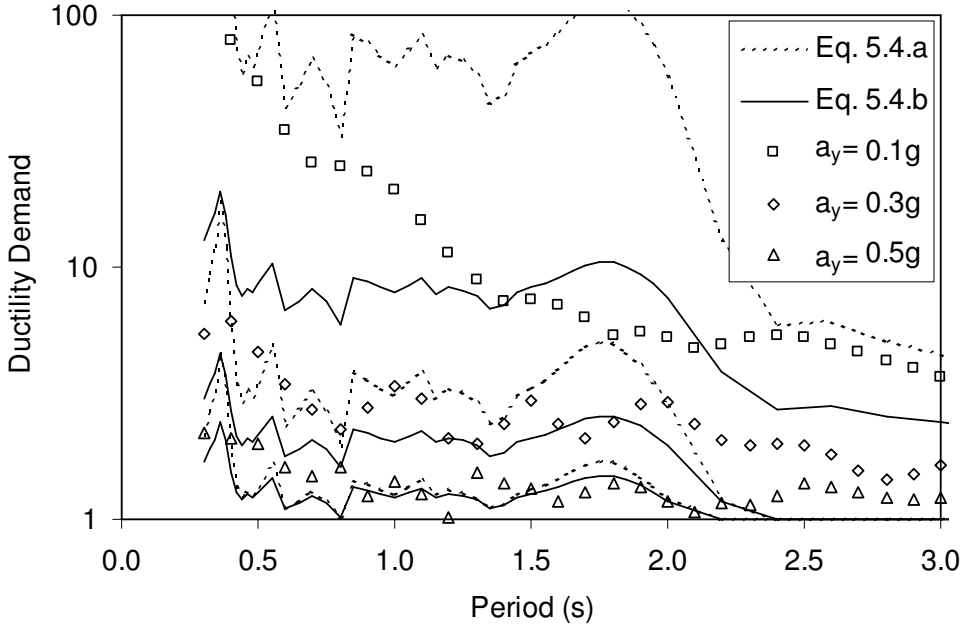

Figure 5.14. Comparison of calculated maximum μ with Riddel et al. (2002) relationship.

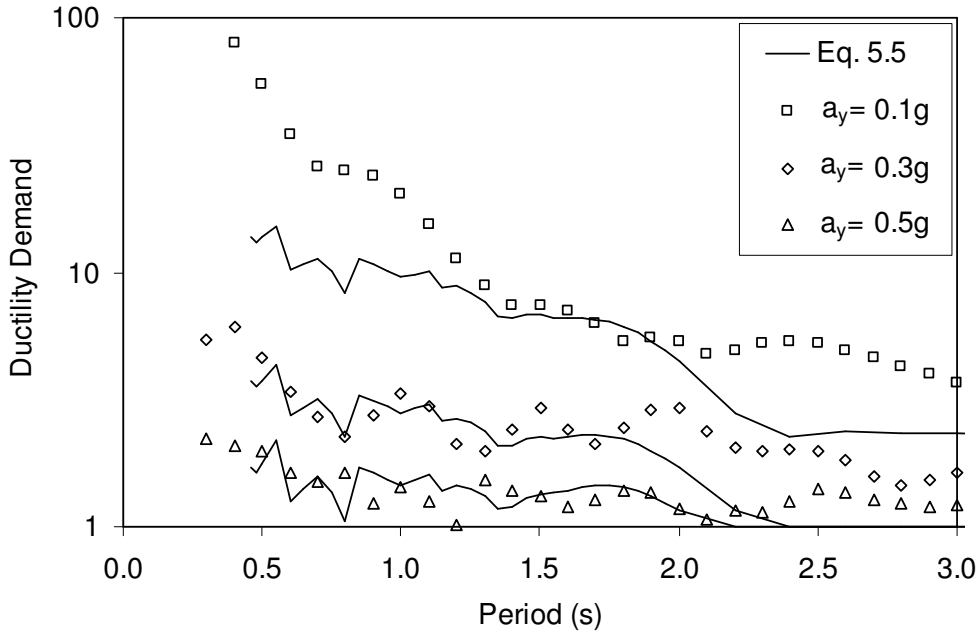

Figure 5.15. Comparison of calculated maximum μ with Miranda (1993) relationship.

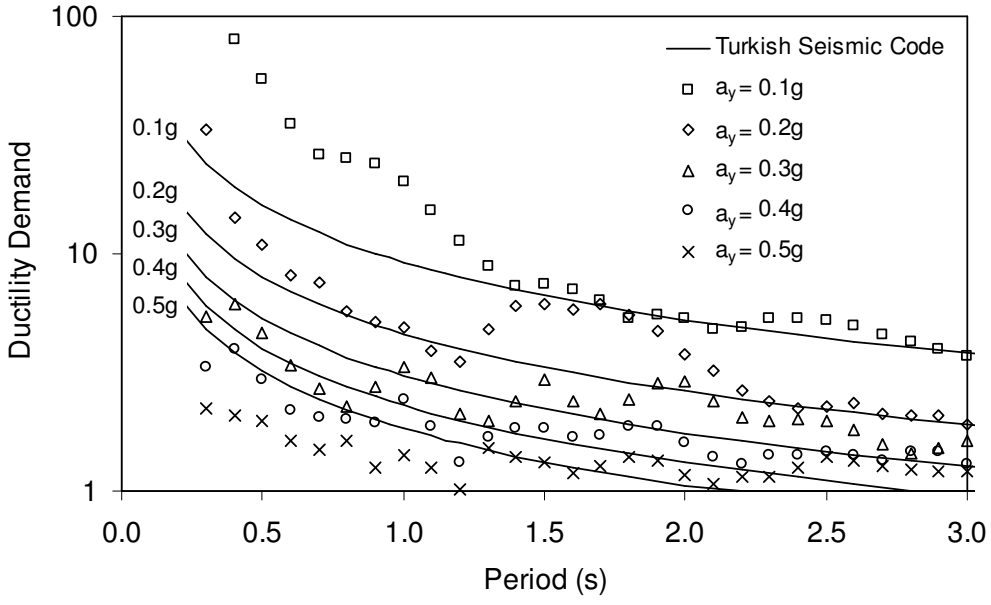

Figure 5.16. Comparison of ductility demand for the generated ground motion with the values corresponding to Turkish Code.

One important uncertainty in estimation of seismic demand on foundations is due to adjacent-construction style building stock in Adapazarı: Structure-structure interaction can result in significant deviations in the estimated seismic demand from the actual magnitudes.

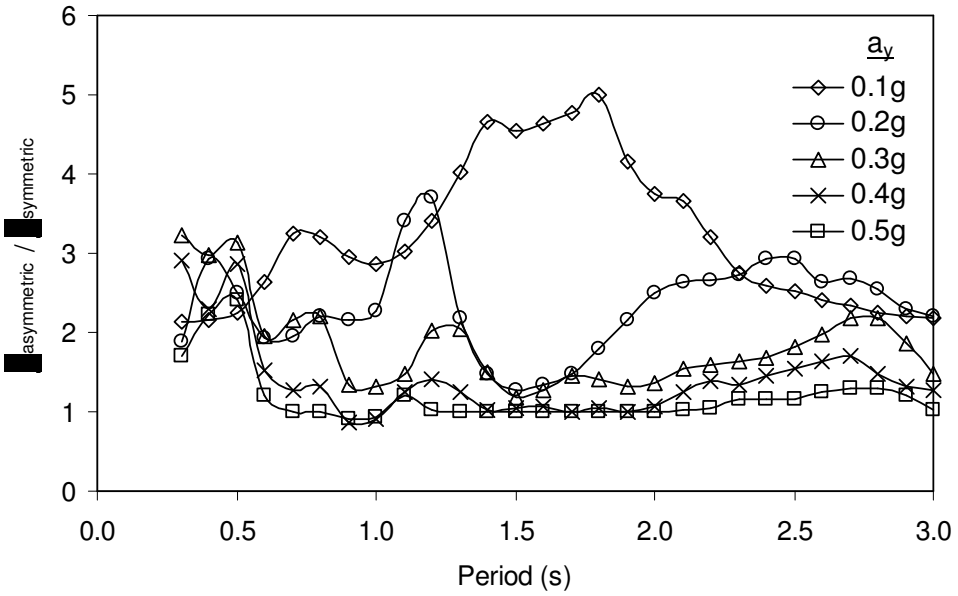

Figure 5.17. Comparison of ductility demand for the asymmetric system that the yield strength in one direction is doubled, with symmetrically behaving system, due to the simulated alluvium motion for Adapazarı.

Finally, utilizing equation 3.13, irrecoverable displacement demands (u_{ir}) for the alluvium site is calculated for periods T=0.6, 0.9, and 1.2 seconds, and plotted in Figure 5.18. It is observed that, for the generated acceleration-history for the soft site and the representative range of periods (i.e., about 0.8 s), the magnitude of u_{ir} is not significantly sensitive to the value of natural period of the system. However, uncertainties involved in cases regarding the natural period of the soil-structure interaction system ($\overline{T}$) and the actual seismic demand are inherent in this conclusion.

The equation for the representative curve obtained from a least-squares analysis fit on the data points in Figure 5.18 is,

$$u_{ir} = \frac{0.75}{1300^{a_y/g}} \qquad (5.6)$$

where, a_y is expressed in terms of g, and u_{ir} is in meters. Equation 5.6 is utilized in estimations of tilting for the case studies.

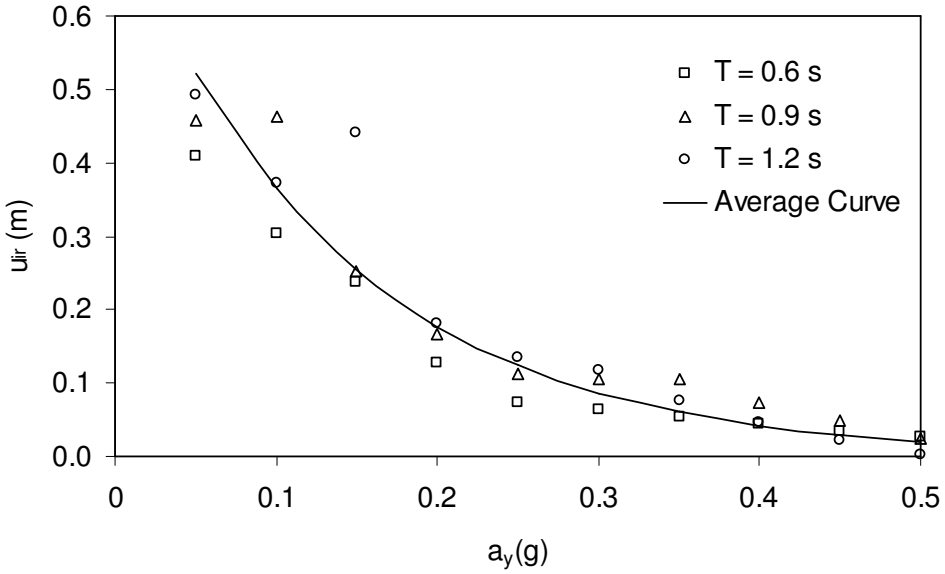

Figure 5.18. Plot of irrecoverable displacement demand (u_{ir}) for simulated alluvium motion, for different natural periods and a_y values.

5.4.2. Available cases

As presented in section 5.4, available cases are grouped into categories: a) PEER cases, b) METU cases, and the c) Yasuda et al. data. In this section some pertinent information for the cases are presented. Details of the data can be found in original studies.

5.4.2.1 The PEER cases

Cases A1 and A2 are located in the Cumhuriyet District. Case A1 is a 5-storey building, with a foundation width of 8.4 m. This building settled about 0.8 m on the average and tilted extremely, in the order of 5˚, towards the north-west corner during the earthquake, and was demolished after the earthquake. The PEER research group performed two separate borings, one near the north-west corner (SPT-A1), and one near the south-east corner (SPT-A2). Although the soil

profiles appear to be similar on both sides, consisting of silt-clay mixtures, the Torvane tests indicate lower shear-strength values in the borehole SPT-A1 (S_u=28,50,22,23,25,26 kPa) when compared to borehole SPT-A2 (S_u=18,48,53,35,31,37 kPa) between depths 2.0 and 6.0 m, implying a weaker profile on the northwest corner. Hence, asymmetric foundation response is expected. Case A2 is also a 5-story building with a foundation width of 12.9 m. This building settled uniformly (about 30 cm) without any observable tilting. The soil conditions beneath the foundation are similar to Case A1, possibly consisting a greater percentage of silt as revealed by the boring SPT-A3.

Case B1 is definitely a poor aspect-ratio building, with 5 stories and only 5.0 m of foundation width. This building toppled during the earthquake, and demolished afterwards (Figure 5.19). The shallow soil profile beneath the building is composed of sand-silt mixtures and silt-clay mixtures. The weak direction is the northeast. It is noticeable that, this building has a neighboring light-weight timber building on the northeast, and an adjacent similar-weight building on the opposite direction, implying a strong asymmetric behavior for the foundation system, and possible significant structure-structure interaction.

Figure 5.19. Case PEER-B1.

Site C is located in İstiklal district. Case C1 is demolished after the earthquake, possibly due to excessive structural damage, and there is no reliable information about its foundation displacements. On the other hand, C2 is a 5-story

building, with square-shaped foundation section: the foundation dimensions are 19.5 m width and 20.1 m length. This building has translated horizontally 57 cm towards west and 34 cm towards north, and settled significantly. Bray et al. (2001a) reports that the relative vertical movement between the pavement and the building is about 35 cm. When the site is revisited, it is observed that this difference could be due to bulging of the nearby soil around foundation, and actual average settlement is estimated about 10 cm. Case C3 is a similar structure without any significant sign of foundation displacements. Hence, only C2 is included in the analyses. The foundation soil conditions at this site are observed to be dominated with silt-clay mixtures as well.

Case E1 is observed to settle about 0.1 m on the average, tilted about 1˚ towards the east, and caused structural-damage on the adjacent 2-storey timber building. The building consisting the case is 5-story, and the L-shaped foundation has an average width of about 10.5 m in the weak direction. Silt-clay and sand-silt mixtures both exist in soil profile.

Case F1 is a 4-storey building with a rectangular foundation shape. The weak direction is the north-south, and the foundation width is 7.5 m. The building has settled about 0.3 m without noticeable tilting. However, existing 1-storey buildings adjacent to both sides on the weak direction may have limited the tilting during the earthquake. Both of these two buildings were demolished after the earthquake. Sand-silt and silt-clay mixtures again dominate the subsoil profile.

Site-G1 is a 4-story building with a rectangular foundation shape, and has a relatively low foundation aspect ratio when compared to cases G2 and G3. Since G1 has displayed no foundation settlement, this case is disregarded in the analyses. Cases G2 and G3 are two 5-story adjacent buildings, which tilted towards the free field, consistent by the weak foundation direction (Figure 5.20). Each building has average foundation width of about 8.0 m, and the weak direction is the southwest-northeast. Structure to structure interaction, and strong asymmetrical behavior of the foundation due to existence of a similar-weight building in one weak direction can be the reason for excessive tilting. Layers of silt-clay and silt-sand mixtures exists in the soil profile beneath the foundations. Only Case G2 is introduced in the analyses, since the results will be also representative for the case G3.

Figure 5.20. Cases PEER-G2 and -G3.

Finally, case H1 is a 4 story building, which settled about 10 cm, with barely noticeable tilting. Asymmetrical behavior is implied for the foundation system, due to existence of equal-weight buildings on both sides. The foundation has a width of 10.5 m, with the weak direction being NW-SE when considered as a stand-alone building. Silt-clay mixtures are observed to dominate the soil profile for this case.

5.4.2.2 The METU cases

Cases A1, A2, and A3 are located in Tığcılar District. Case A1 is a 5-story building with foundation dimensions of 8.9 m width and 24.6 m length. The weak direction is EW. The building is reported to tilt 1˚ to the north, and 1.5 to east. During the earthquake, two similar-weight adjacent buildings existed adjacent on the west. Case A2 is a 4-story building with foundation width of 7.0 m. The weak direction is the north-south direction, and the building tilted towards the free-field on the north. Existence of buildings on the south implies a strong asymmetric foundation behavior (Figure 5.21). Cases A3 and A4 are 4-story buildings standing adjacent to each other. The weak direction is the north-south direction when these buildings are considered separately. However, the buildings are observed to behave as a single block. Accordingly, the weak direction is considered to be the east-west direction. Therefore, the case A3 represents the behavior of the two buildings, which tilted about 1˚ to the east. The foundation width is assumed as 10.9 m for calculations. Besides the available boreholes, two additional borings

(i.e., GA-I and GA-II) were drilled in the field, near the corners of A1 and A3. The test locations and details are given in the Appendix A.

Figure 5.21. Case METU-A2.

Case B1 is located in Tığcılar District and close to Case A1. It is a 4-story building with foundation dimensions of 12 m width and 14 m length. The weak direction is the north-south direction. Although excessive settlement is reported for this building (~40 cm), no tilting observed. An additional boring (GB-I) is drilled nearby the building. The borehole location and the observed soil profile is given in the Appendix A. The boring data revealed that the saturated soft soils beneath the foundation is mainly composed of sand-silt mixtures with SPT blow counts of 4 to 5.

Case C1, which is a 4-story building with foundation width of 7.0 m, is disregarded since no plan view is provided for this case. This building is a case of excessive tilting (towards the street), and it is not clear if an adjacent building exists or not. Due to the considerably poor aspect ratio for the building this point is important. On the other hand, buildings with similar aspect ratios already exist in the data-base (e.g., Case METU-A2).

Cases D1, D2, D3 and D4 are located in the Cumhuriyet District. Case D1 has an irregular foundation section, which is approximated by a 11.0 m x 19.4 m rectangle in the study of Karaca. Although this 5-story building is reported to settle

about 80 cm during the earthquake, no detailed information is given regarding tilting. When the site was revisited, a new boring was opened near this building (GD-I as given in Appendix A), it was observed that the building had slightly tilted towards weak direction, about 1˚ to the west. Case D2 is a 3-story building, with no foundation settlement, and has a foundation width of 10.1 m. The weak direction is towards north, where the building constituting case D3 stands adjacent on the south. No tilting is observed for the building, but a horizontal translation (~8 cm) is observed in the (strong) west direction. Case D3 is a 4-story building with foundation dimensions 11 m and 18.1 m. The weak direction is east-west. This building is reported to settle 19 cm, with no foundation tilting. Case D4 is a 6-story building with foundation dimensions of 9.35 m width and 18.0 m length. However, it is observed that existence of a similar building adjacent to the north resulted in a system in which the foundations of the two buildings behaved as a single block. Also, building D3 may have prevented the foundation displacements in the south direction. This is consistent with the observation of very slight tilting of the block to the west, which is practically negligible: both buildings settled an equal amount (about 70 cm). Hence, the foundation width is accepted as 18.0 m (i.e., the width of the block) in calculations and the weak direction in east-west. A new borehole is opened nearby the Cases D3 and D4 (i.e., GD-II) at the location specified in the Appendix A. Being consistent with the logs provided in the study by Karaca, it is observed that soft silt-clay mixtures dominate the foundation soils.

Cases E1, to E5 are also located in the Cumhuriyet district. Additional three boreholes (i.e., GE-I, GE-II, and GE-III) are utilized in order to obtain undisturbed samples and re-investigation of the soil conditions. Similar to Site-D cases foundation soils are observed to be soft silt-clay mixtures. Case E1 is a 6-story building. The foundation dimensions are 18.0 m width and 29 m length. The building settled about 60 cm without any observable tilting. The weak direction is the NW-SE. Adjacent to this building, Case E2 stands, which is tilted extremely (more than 5˚) and demolished after the earthquake (Figure 5.22). The existence of heavy-block of case E1 adjacent on the north implies a strong asymmetry on the foundation behavior, and possible significant structure to structure interaction. Width of this building is estimated as 7.2 m. Cases 3, 4 and 5 displayed negligible foundation displacements and hence excluded from the analyses.

Figure 5.22. Case METU-E2 (Photo by Karaca, 2001).

Two additional cases are included to the Site-E cases presented in the study of Karaca, and referred to as E6 and E7. These cases are located on the south of the Site-E cases of Karaca, and their specific locations are given in the Appendix. Case E6 is a 5-story building with foundation dimensions of 17.2 m width and 21.0 m length. Case E7 is a 5-story building with foundation dimensions foundation dimensions 20.6 m in width and 21.6 m in length. Cases E6 and E7 settled about 40 and 20 cm respectively, without any noticeable foundation tilting. The boring GE-I revealed that the foundation subsoil conditions are similar to other Site-E cases and dominated by silt-clay mixtures.

Observed tilting versus foundation width for METU and PEER cases are plotted in Figure 5.23. The trend of decrease in irrecoverable tilting with increasing foundation width is clearly observable. In the plot, the rotations (y-axis) is limited with 5˚. Tilting of the foundations are truncated to nearest 0.5˚ interval, in order to further simplify the presentations. In practice, the estimations can only be approximate due to uncertainties discussed in Chapter 4.

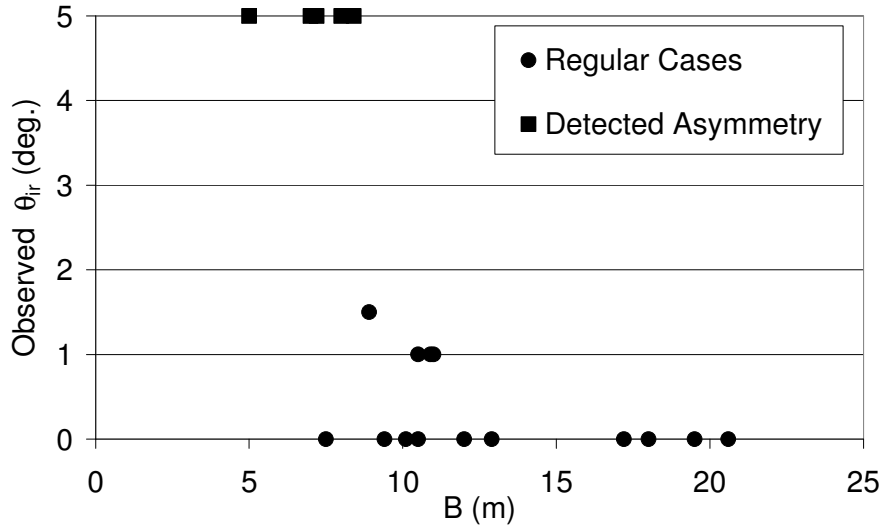

Figure 5.23. Plot of tilting versus foundation width of METU and PEER data utilized in this study.

5.4.2.3 Damage survey data presented by Yasuda et al. (2001)

In order to compare predictive capability of the methodology with the general observed trends in foundation displacements in Adapazarı, data provided by Yasuda et al. (2001) is also utilized. The data consisting observed foundation displacements of 68 building versus foundation width is plotted in Figure 5.24. Although case details, such as geotechnical information and location of neighboring buildings are not presented, plot of the data also supports the expectation that irrecoverable tilting of buildings would decrease as foundation width increases, for a given story-number. Infact, different reasons for excessive foundation displacements may be involved in these cases, such as sand-liquefaction, and bearing capacity failures. Also, the displacements may be due to interaction of adjacent structures, and mixed situations of bearing capacity failure involving soil-strength degradation.

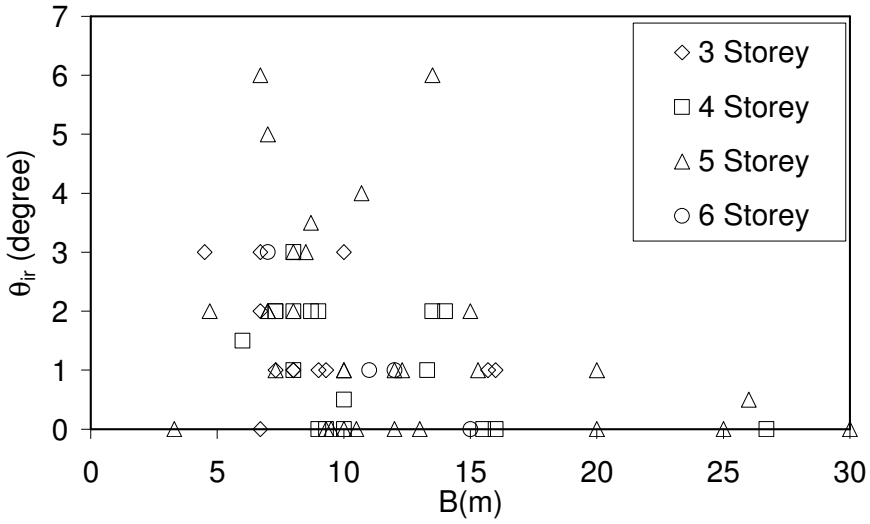

Figure 5.24. Foundation tilting versus width data for mat foundations in Adapazarı, by Yasuda et al. (2001).

5.4.3. Comparison of the procedure with the case data

In Adapazarı cases, the water table can practically be assumed to be at foundation level. Also, the foundation soils are assumed to have completed the consolidation process. Hence, the overturning moment capacity of a surficial mat foundation can be estimated utilizing equation 4.47. Substitution of equation 4.47 into 5.1 results in the relationship between the yield acceleration (a_y) and static factor of safety (FS) as,

$$\frac{a_y}{g} = \frac{B}{2\bar{h}} \cdot \frac{\log FS}{\log 266} \qquad (5.7)$$

Substituting equation 5.7 into 5.6, the relationship between irrecoverable relative displacements of the lumped mass and FS can be derived as,

$$u_{ir} = \frac{0.75}{1300^{\left(\frac{B}{2\bar{h}} \cdot \frac{\log FS}{\log 266}\right)}}$$

or, maximum irrecoverable tilting of the foundation in radians can be estimated introducing equation 5.2,

$$\theta_{ir} = \frac{0.75}{\bar{h} \cdot 1300^{\left(\frac{B}{2\bar{h}} \cdot \frac{\log FS}{\log 266}\right)}} \qquad (5.8.a)$$

or, in degrees,

$$\theta_{ir} = \frac{43}{\bar{h} \cdot 1300^{\left(\frac{B}{2\bar{h}} \cdot \frac{\log FS}{\log 266}\right)}} \qquad (5.8.b)$$

In order to utilize equation 5.8.b for practical investigations, typical equivalent heights ($\bar{h}$) for apartment buildings are required. For this purpose, building storey height (h_{st}) is assumed to be 3 m, except the entrance floor, which is assumed to be approximately 3.5 m high. Similarly, the storey masses (including that of foundation) are assumed to be constant, 1 ton/m^2 of distributed mass per storey. Total and equivalent heights for different numbers of total stress are given in Table 5.4. Equivalent heights can also be practically estimated also by calculating two-thirds of the total height of these buildings.

Hence, utilizing $\bar{h}$=9.5 m for a 5 storey building, irrecoverable foundation tilting demands are plotted in Figure 5.25, for different values of factor of safety. It is observed that, when the static factor of safety in the order of 3 to 5, it is not sufficient to prevent significant irrecoverable tilting of foundations of 5 storey buildings. As observed from Figure 5.25, a static factor of safety of 15 is required, corresponding to a foundation width of 15 m, in order to limit θ_{ir} to values less than 0.2°. Hence, foundations of most buildings on soft silt-clay mixtures in Adapazarı are expected to have experienced the ultimate load levels during Kocaeli earthquake.

Not only θ_{ir}, but also FS is dependent on h/B: FS will decrease as the building height increases, keeping the remaining parameters constant. In case the FS cannot be calculated precisely, the net bearing capacity for surficial foundation can be estimated roughly via equations 4.5 and 4.28.b or,

Table 5.4. Approximate total height for buildings and corresponding equivalent height ($\bar{h}$) for reduced model.

Number of Stories	Equivalent Height (m)	Total Height (m)
3	6.0	9.5
4	7.8	12.5
5	9.5	15.5
6	11.2	18.5
7	13.0	21.5

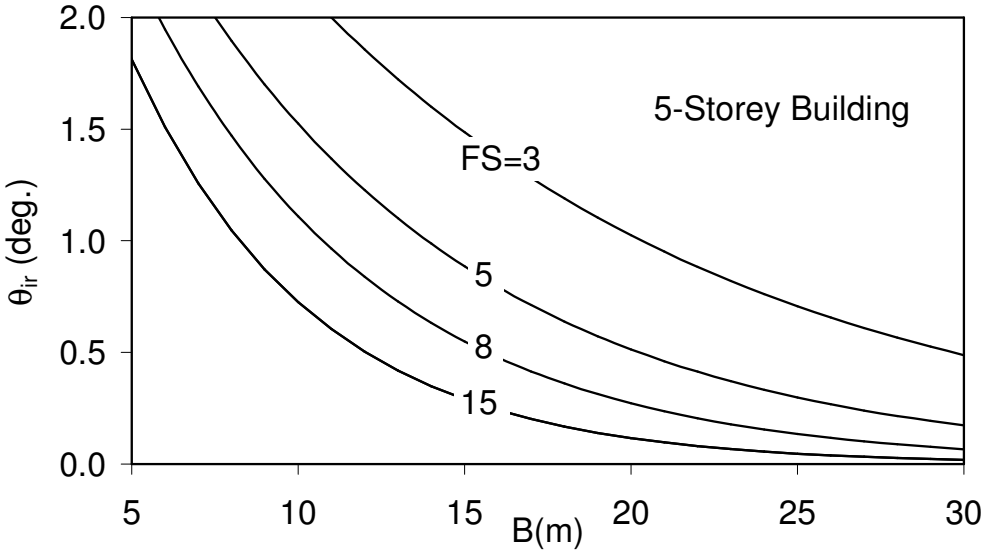

Figure 5.25. Plots of equation 5.8.b for different FS values.

$$FS = \frac{\frac{1}{2}\gamma_B B N_\gamma}{n \cdot 10^{kN/m^2}} \qquad (5.9)$$

where, γ_B is the buoyant unit weight of soil beneath foundation, and approximately is equal to 8 kN/m^3 in case of Adapazarı. Hence, stating B in meters, equation of factor of safety is simply,

$$FS = 0.4\,B\,\frac{N_\gamma}{n} \tag{5.10}$$

Hence, substituting equation 5.10 into equation 5.8.b, a direct relationship between building dimensions and irrecoverable tilting demand (in degrees) can be obtained:

$$\theta_{ir} = \frac{43}{\bar{h}\cdot 1300^{\left(\frac{B}{2\bar{h}}\cdot\frac{\log(0.4BN_\gamma)-\log(n)}{\log 266}\right)}} \tag{5.11}$$

Relationship between n and $\bar{h}$ is given in Table 5.4. Hence, the relationship between B, θ_{ir}, and N_γ is presented in Figure 5.26, for a 5-storey building.

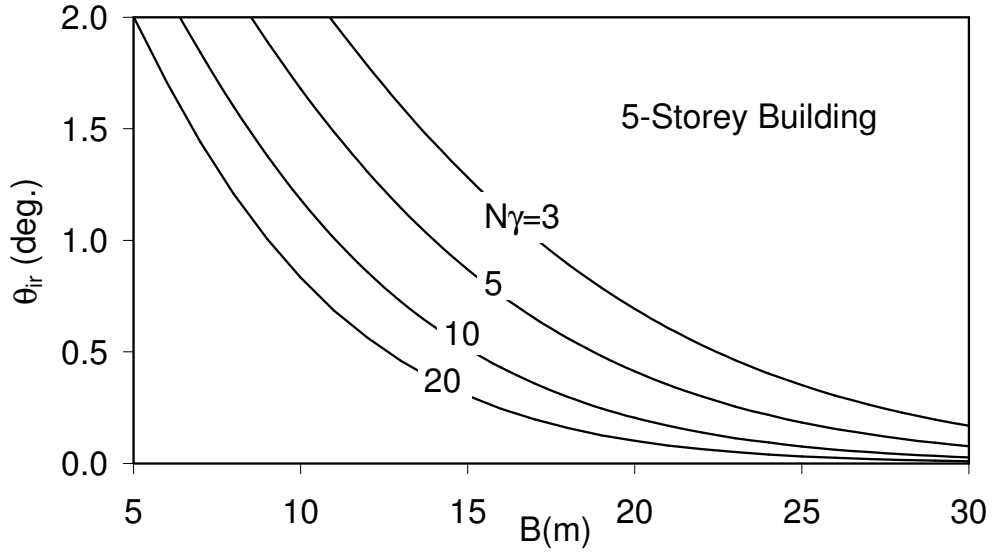

Figure 5.26. Sensitivity of irrecoverable foundation tilting to N_γ factor, for a 5-storey building.

For further practical applications, assumption of $N_\gamma \cong 10$ is selected as representative for foundations located on soft silt-clay mixtures, as discussed in Chapter 4. Hence, for n values between 3 and 6, the relationship between θ_{ir} and foundation width is plotted in Figure 5.27. Figure 5.27 is utilized in investigations of available Adapazarı cases with excessive foundation settlements. Although the correlation given in Figure 5.27 depends on a number of assumptions, the

observed trends are consistent with the general expectations, as well as with the site observations, indicating that irrecoverable tilting of foundations tend to increase with increasing storey number and decreasing foundation width.

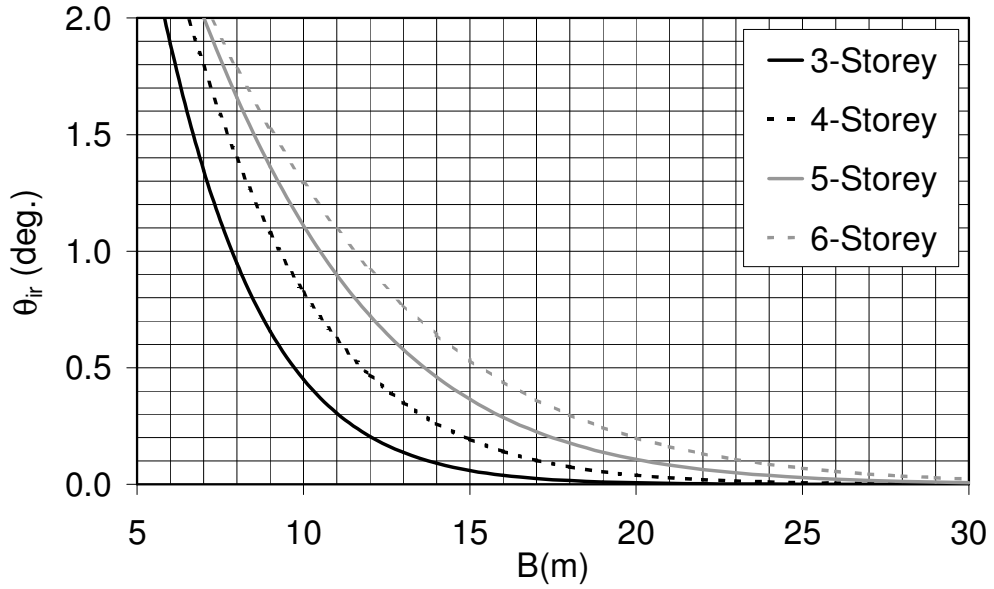

Figure 5.27. Relationship between number of stories, building (mat foundation) width, and irrecoverable tilting demand on foundation.

For verification purposes, the PEER and METU data are presented in Table 5.5. Reported values of tilting (truncated to the nearest multiplication of 0.5°) is compared with the estimated maximum irrecoverable tilting demands, which are determined by the plots in Figure 5.27, in the table.

Predicted and observed foundation performances are compared in Figure 5.28: The upper bound in observed values is selected to be 5 degrees. Hence, tilted buildings are to be located on 5 degree of observed tilting in y-axis. Four out of nineteen cases considered are observed to be effected strongly by the existence of adjacent similar-weight buildings, which do not conform with the general assumptions in this study. On the other hand, asymmetric behavior due to the soil profile irregularities is relatively more difficult to identify, which requires multiple investigation pits or drilling around a building. There exists only one such case (PEER - A1) detected in the considered data set. Observed and calculated values are tabulated in Table 5.5 in detail.

Table 5.5. Observed and predicted irrecoverable foundation tilting, for PEER and METU data based on Figure 5.27.

Case	n	B(m)	Average Settlement (m)	Observed Tilting (degree)	Predicted Tilting (degree)	Remark
A (PEER) - A1	5	8.4	0.8	~5	1.5	(a)
A (PEER) - A2	5	12.9	0.3	~0	0.6	
B (PEER) - B1	5	5.0	toppled	toppled	>2.0	(b)
C (PEER) - C2	5	19.5	0.1	~0	0.1	
E (PEER) - E1	5	~10.5	0.1	~1	1.0	(c)
F (PEER) - F1	4	7.5	0.3	~0	1.6	(d)
G (PEER) - G2	5	~8.0	toppled	toppled	1.7	(b),(c)
H (PEER) -H1	4	10.5	0.1	~0	0.7	
A (METU) - A1	5	8.9	0.4	~1.5	1.4	
A (METU) - A2	4	7.0	toppled	toppled	1.7	(b)
A (METU) - A3	4	10.9	0.4	~1	0.6	
B (METU) - B1	4	12.0	0.4	~0	0.5	
D (METU) - D1	5	11.0	0.8	~1	0.9	
D (METU) - D2	3	10.1	0.0	~0	0.4	
D (METU) - D3	6	9.4	0.7	~0	1.4	
E (METU) - E1	6	18.0	0.6	~0	0.3	
E (METU) - E2	6	7.2	high	high	2.0	(b)
E (METU) - E6	5	17.2	0.4	~0	0.2	
E (METU) - E7	4	20.6	0.2	~0	0.0	

(a) Strong asymmetric behavior of foundation is expected due to significant variation of shear strength of soils beneath the foundation.
(b) Strong asymmetric behavior of foundation is expected due to an equivalent-weight neighboring building.
(c) L-shaped foundation area: foundation width (B) is the average value for two different width values.
(d) One-storey buildings on each side may limit the tilting behavior significantly.

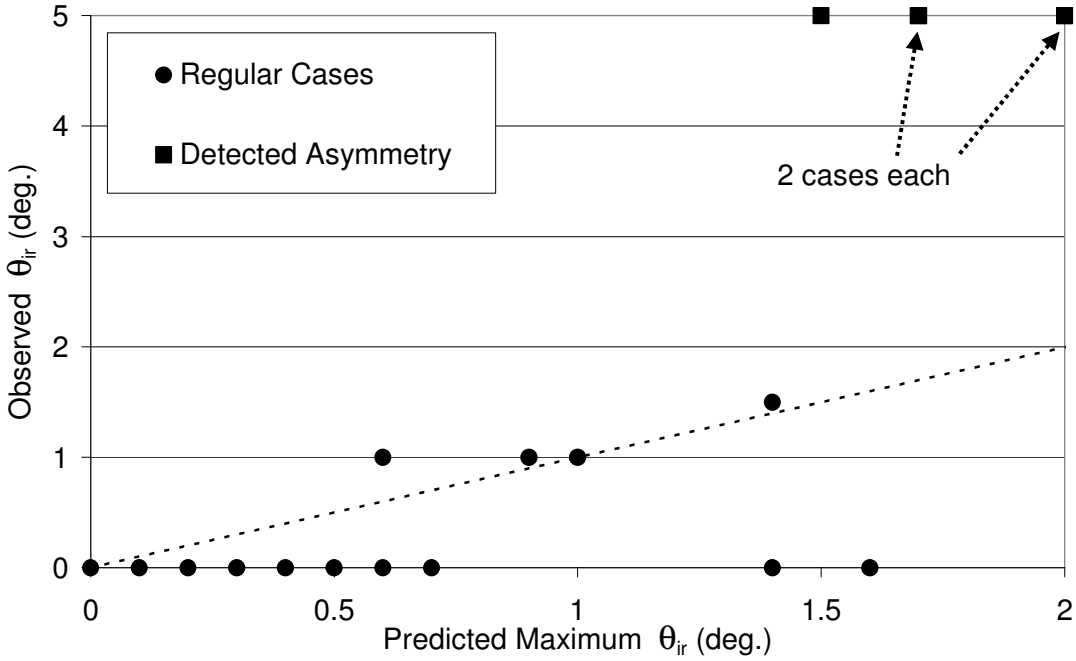

Figure 5.28. Comparison of estimated and measured tilts of available Adapazarı cases.

Response of toppled buildings are observed to be strongly effected by adjacent similar-weight buildings on one side, implying strong asymmetric behavior, and possible increase in driving forces due to structure to structure interaction. This condition is also observed in several cases of significantly tilted buildings, which are not included in this study due to the unavailability of geotechnical information. Hence, the buildings at block ends or those with adjacent buildings on one side have much greater potential for excessive tilting. In any case, considering the METU and PEER cases in Figure 5.28, poor foundation tilting performance is observed for cases that the calculated irrecoverable tilting values exceed 1.0º. Therefore, for utilization of the methodology described in this study for the design of shallow mats, it is possible to define an acceptable limit for tilting of foundations in calculations, so that excessive irrecoverable tilting can be prevented with the allowance of successive excursions of the ultimate load capacity of the shallow mats during severe seismic loading. In the case of adjacent building on one side, and unavailability of geotechnical data required to estimate the static bearing capacity of the foundation, this value would be decreased further.

In order to compare the predictive capability of the methodology with the general observed trends of foundation displacements in Adapazarı, data provided by Yasuda et al. (2001) is utilized. The data, which consists of 68 buildings with observed foundation displacements, is plotted in and compared with the curve for 5-storey buildings (Figure 5.27) in Figure 5.29. Although the curve for 5-storey buildings is observed to underestimate tilting in several cases, the trend is consistent in general with that of the data set. It is important to note that, no details regarding site or soil conditions for the cases are provided. Therefore, the data is likely to involve cases with strong asymmetric foundation response as discussed in the preceding. Also, soils with relatively low Φ´ values (i.e., considerably lower than 30˚) will yield lower values of N_γ values than 10, and hence lower static factors of safety than estimated in this study. Another reason for lower bearing capacity values is the possibly not completed consolidation of foundation soils. This is possible for those buildings before the earthquake.

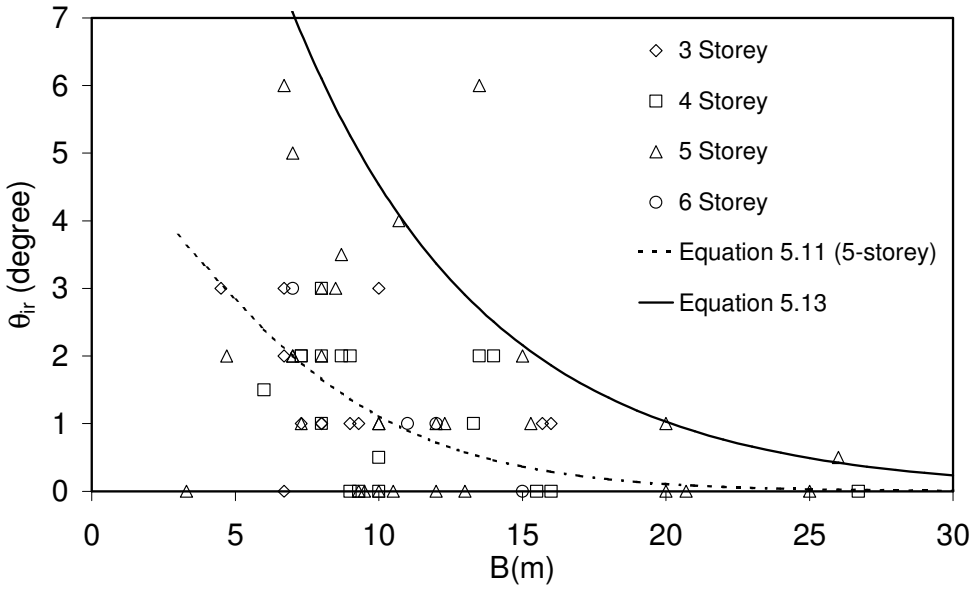

Figure 5.29. Comparison of predictive capability of calculation procedure with the data provided by Yasuda et al. (2001).

Equation 5.8, which forms the backbone of the methodology's for Adapazarı cases, is of the form,

$$\theta_{ir} = \frac{D_1}{(D_2)^B} \tag{5.12}$$

where, D_1 and D_2 are parameters dependent on seismic demand, static factor of safety, and building height. Choosing appropriate values to fit the most extreme cases, equation 5.12 is expressed as follows and plotted on Figure 5.29:

$$\theta_{ir} = \frac{20}{(1.16)^B} \tag{5.13}$$

This is equivalent to, for example, setting FS=3.0 and multiplying the u_{ir} with a factor of 4.4 for a typical 5-storey building ($\bar{h} = 9.5$m). The lower FS can be explained by the ongoing consolidation process beneath the building at the time of earthquake, which yields a lower N_γ value than 10. Another possibility that may yield to reduced FS is the pore-pressure build-up at sites consisting of sands and silty sands (i.e., liquefaction). The amplified u_{ir} value can be explained by the uncertainty in seismic demand at alluvium site, and uncertainty involved in estimation of natural periods of the SSI system, with possible strong potential for asymmetrical response. Another possible explanation for the increased values of u_{ir} as discussed by Miranda and Ruiz-Garcia (2002b), can be the strain-memory behavior of the cyclically tested soils, as stated in Chapter 2 may result in a similar behavior of the foundation, through a stiffness-degrading system. Hence, the displacement demands can be higher than those predicted by the idealized elasto-plastic system for soft sites.

Considering 5-storey buildings, which provide the upper-bound for Yasuda et al. data, in case these foundations are limited with 1.0˚ of rotation considering the generalized curve for 5-storey structures in Figure 5.27 (also plotted in Figure 5.29), no foundation width (B) lower than 10.5 m should be accepted. In this case, the 5-story buildings are expected to perform a limited irrecoverable tilting. When the data of Yasuda et al. is considered, there are only two outlier buildings: one with a width of B=10.7 m and a tilt of θ_{ir}=4˚, and other with B=13.5 m and θ_{ir}=6˚. Except these cases, the remaining buildings have foundation tilts in the order of 0˚ - 2˚, and majority of the buildings have tilts in the range of 0˚ - 1˚, which is consistent with the observed performance.

Hence, the driving mechanism for excessive foundation tilting discussed in this study is observed to be consistent with Adapazarı cases involving soft silt-clay mixtures. The methodology and relevant equations here are based on approximations, which can be further refined by future studies. These approximations can be associated to three main sources: approximations based on seismic demand, on load capacity of the system, and on pre-yield and post-yield deformation behaviors. Significant error involved in any approximation may result in deviation of calculated quantities from realistic estimations.

5.5. Impact of Site Response

As discussed in Chapter 1, the relatively high ground velocity and predominant ground period is the common observations for the Mexico-City and Adapazarı cases. Hence, large displacement demands for relatively long-period systems can be the result of site-response. Implementation of the site response in development of elastic and inelastic design spectra is out of the scope of this study. However, the significance of site-response on seismic demand over relatively low-bearing capacity foundations on soft soils is investigated.

The most significant observation on velocity-history of SCT record and the simulated Adapazarı motion on deep alluvium are the velocity pulses with periods consistent with the predominant ground period. Analysis results presented by Seed et al. (1988) for the Mexico City records showed that the predominant ground period, where PSV plot makes its peak, is consistent with the fundamental site period for a one-dimensional site response analyses. Bakır et al. (2002), also showed that the concentrated damage at deep alluvium sites in Adapazarı can be explained by amplification of the spectral values at periods near the site-period. In the velocity-history plots considered in the Mexico City and Adapazarı cases, velocity pulses with periods consistent with predominant site-periods and with amplitudes consistent with peak ground velocity are observable.

Hence, in order to visualize significance of the site-response on foundation performance, the records are compared with equivalent velocity pulses, with the hypothesis that site-response is responsible in development of velocity pulses, which in turn plays a significant role in inelastic displacement demand on low-strength systems. The analytical formulations presented by Makris and Roussos (2000) are used for the pulse expressions, which are originally developed to study

toppling of rigid blocks due to velocity pulses inherent in the near-field earthquake records. The C_n type velocity pulses are analytically expressed as,

$$\dot{u}_g(t) = \begin{cases} V_p \sin\left(\frac{2\pi}{T_p} t + \varphi\right) - V_p \sin(\varphi) & 0 \le t \le \left(n_p + \frac{1}{2} - \frac{\varphi}{\pi}\right) T_p \\ 0 & \left(n_p + \frac{1}{2} - \frac{\varphi}{\pi}\right) T_p < t \end{cases} \quad (5.14)$$

where, V_p is the amplitude, and T_p is the period of the velocity pulse, φ is the phase angle, n_p is the number of successive pulse cycles, and t is the time; first pulse initiates at t=0. The phase angle φ is dependent on n_p, and is equal to 0.21898 and 0.12873 rad for n_p=1 and n_p=2 respectively.

For the case of Adapazarı, a velocity pulse of type C_1 with amplitude 70 cm/s and period 1.8 s, which is compatible with the peak ground velocity and site period, is utilized. The pulse is compared with the velocity-history of generated motion in Figure 5.30.a. Velocity-spectrum with 5% damping ratio is plotted in Figure 5.30.b for comparison. In order to visualize the significance of this pulse for displacement demands on elasto-plastic SDOF systems, ductility demands due to generated motion is compared with those due to velocity pulse in Figure 5.31. Observed agreements confirm that, for low values of a_y (i.e., relatively low- strength systems) the velocity pulse, which is shaped by the site-response, practically plays a decisive role on the maximum inelastic response.

A similar analysis is performed for the SCT record of Mexico City. For the EW component of the motion, a C_2 type pulse with amplitude V_p=57 cm/s and period T_p=2.1 s, which are consistent with the peak ground velocity and site-period, is considered. The velocity pulse is compared with the actual pulse due to the SCT (EW) record in Figure 5.32, in terms of velocity-history and velocity-spectrum (SV) plots. Ductility demands for different a_y values are compared in Figure 5.33. Consistent results are also obtained for the NS component of the motion. Similar to the conclusions regarding Adapazarı motion, ductility demands due to the velocity pulse observed to be consistent with those due to actual record, especially for low-strength systems. The observation that the use of velocity pulse approach is successful in estimation of ductility demands when compared to use of simple R_y-μ_{max} relationships (Section 5.3.1) for low-strength systems, may have practical use

in site-response prediction. However, further studies are required to implement the site-response in practical seismic design.

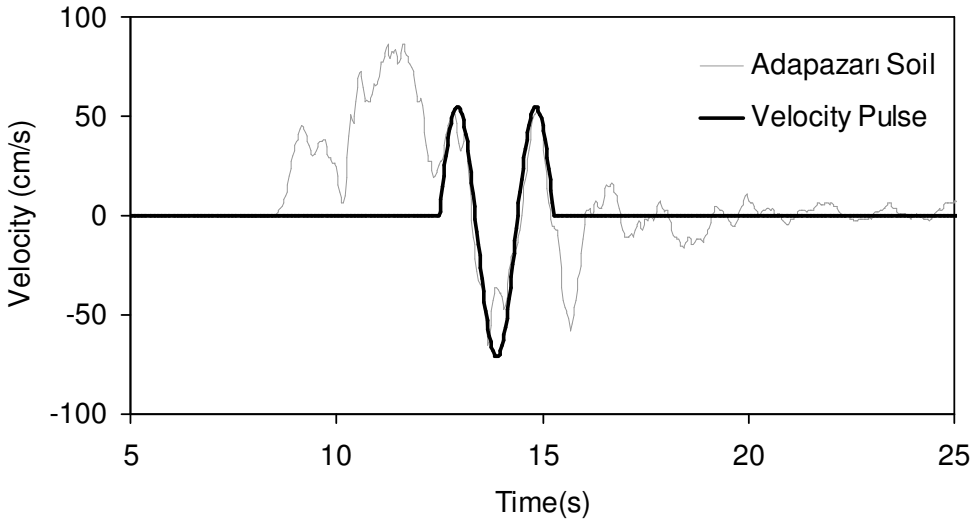

(a)

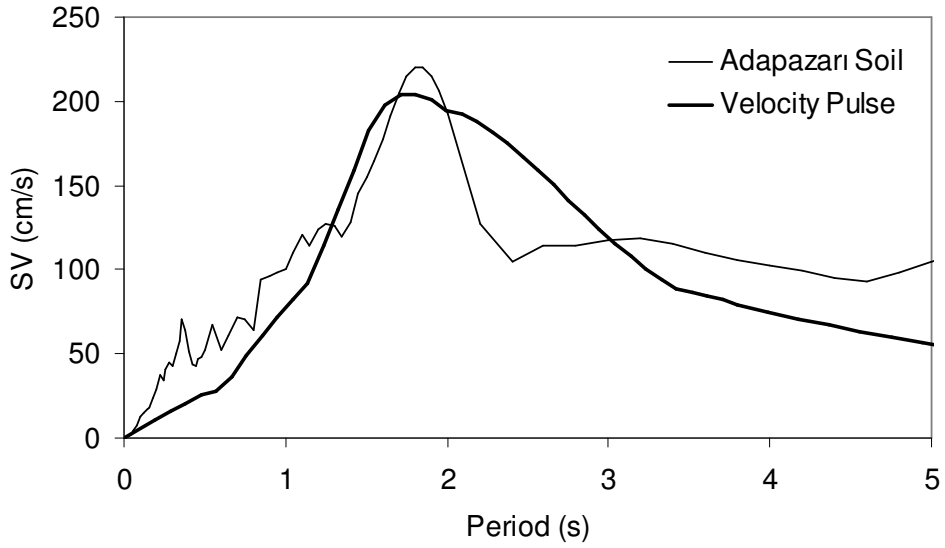

(b)

Figure 5.30. Comparison of the velocity pulse, having a peak velocity 70 cm/s and period 1.8 s, with generated ground motion: (a) velocity-history, (b) SV (5% damping).

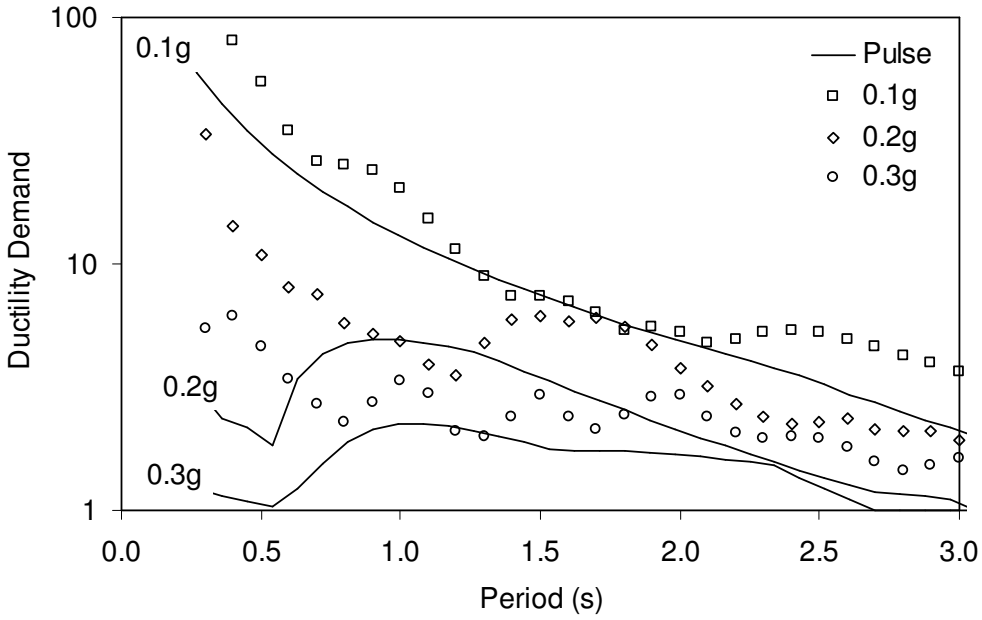

Figure 5.31. Comparison of ductility demands for generated alluvium motion and velocity pulse.

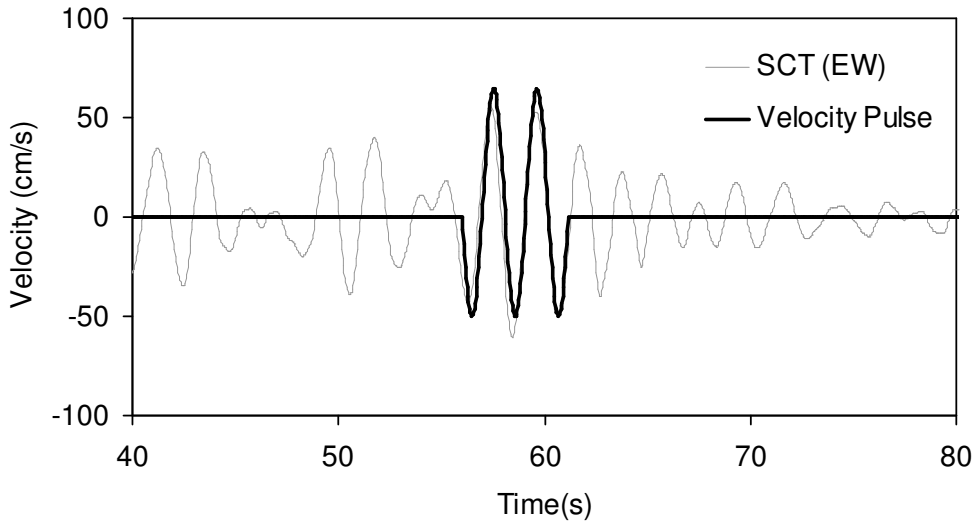

(a)

Figure 5.32. Comparison of the C_2 type velocity pulse, having a peak velocity of 57 cm/s and period 2.1 s, with EW component of SCT record: (a) velocity-history, (b) SV (5% damping).

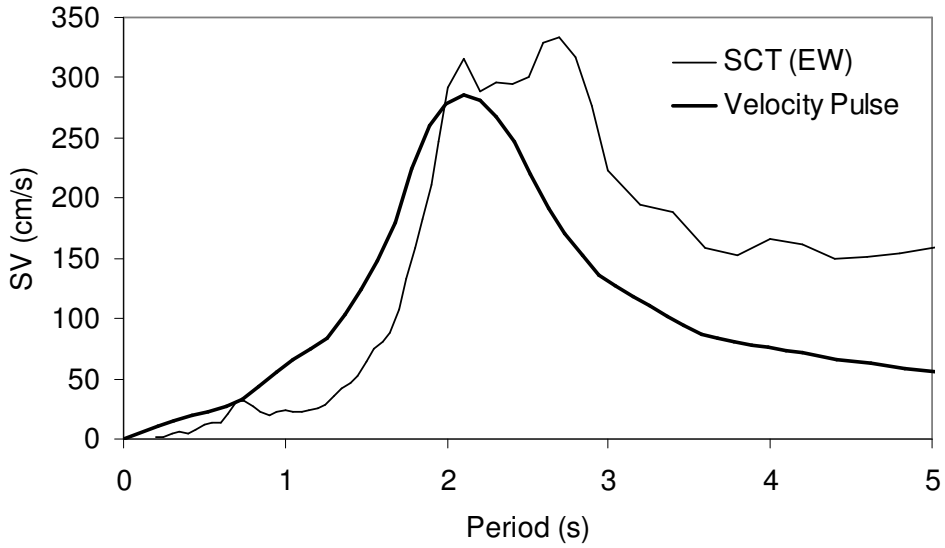

(b)

Figure 5.32 (continued).

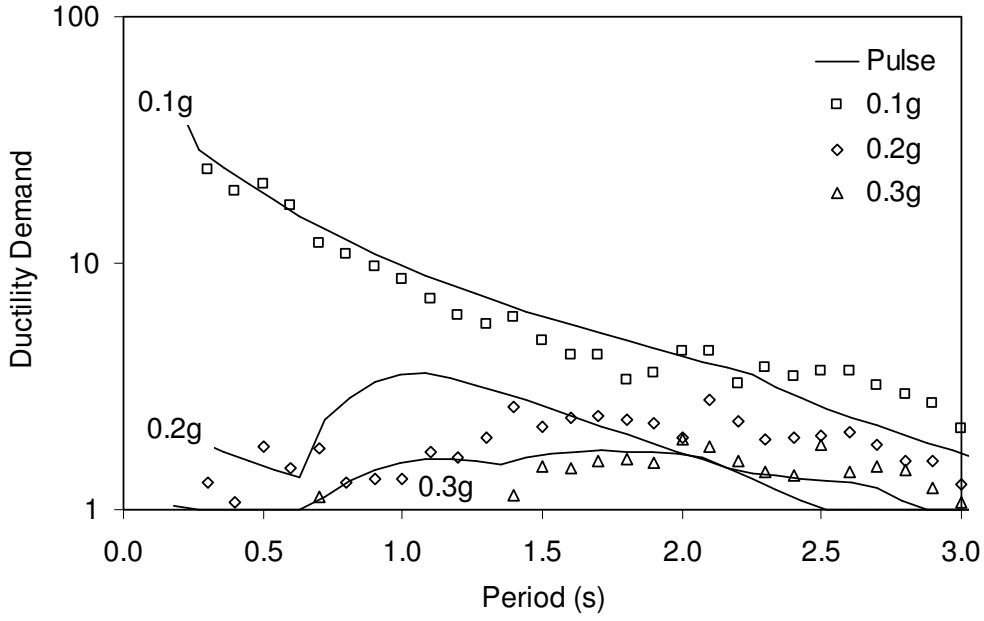

Figure 5.33. Comparison of ductility demands for SCT (EW) record and velocity pulse.

5.6. Conclusions

A simple methodology, based on the assumptions stated in Chapter 2 and 3 is developed for the shallow mat foundations resting on non-liquefiable soft deposits, such as silt and clay mixtures in Adapazarı and Mexico City. The methodology links the irrecoverable tilting demand on foundations to the design spectrum for the site, via the response of elastic-ideally plastic single-degree-of-freedom oscillator. Elastic mechanical property of the soil-structure system is represented by the natural period of the soil-structure-interaction system. The yield strength for the system is estimated by a pseudo-static analysis, based on finite-element method or on available analytical and empirical equations in literature. The inertial loads acting on the mass of foundation soil during seismic loading can be ignored for practical purposes.

As discussed in Chapter 4, one of the basic assumptions of the proposed calculation procedure is that, only load eccentricity acting on the foundation is considered, and all inelastic displacements are assumed to be due only to irrecoverable tilting of foundation. For the case of poor aspect ratio buildings (i.e., building is too high compared to foundation width), the load eccentricity will govern the ultimate load level on the foundation, and foundation tilting will govern the total irrecoverable displacements at the roof level. As the foundation width increases, the tilting mode deformations of the foundations will practically diminish. Hence, the calculation procedure is asymptotically correct in as h/B approaches to zero or goes to infinity. A detailed study, involving a more rigorous flow-rule for the foundation in order to calculate the true participations of irrecoverable tilting and horizontal translation as well as the settlement of the foundation, can be possible as an improvement of the calculation procedure.

Performance of the methodology is investigated utilizing foundation performance data from Adapazarı and Mexico City, where excessive tilting of shallow mat foundations on saturated soft silt-clay mixtures occurred widely. Although these foundations had static factors of safety more than 1.0 against bearing capacity failure (i.e., statically stable), the seismic loads induced successive excursions of ultimate load capacity of these foundations during seismic shaking. Despite significant potential uncertainties in the seismic demand and mechanical properties of these systems, the methodology provided consistent results with the observations. Following the methodology, it is possible to define a

foundation width to limit excessive tilting of foundations, utilizing the elastic design spectrum for the site, and mechanical properties of the soil and the structure. Based on the comparisons of the calculated irrecoverable tilting potential and the observed performance for the Adapazarı cases, the methodology provides satisfactory results for tilting angles up to about 1˚. For cases with higher calculated values of irrecoverable tilting potential, which involve foundations with considerably low a_y values, the actual tilting values significantly exceeds the calculated values, including the toppled buildings at worst. This is explained by the sensitivity of systems with comparatively low a_y values to asymmetrical behavior, most possibly due to existence of adjacent similar-weight structure. Hence, if possible, adjacent construction of buildings should be refrained, and sufficient free space should be left between their foundations, in order to provide symmetrical system behavior. Also, the geotechnical investigations should aim to capture the possible significant variations in strength in the shallow soil profile beneath the foundations, especially in the weak direction. Significance of asymmetrical behavior on overall inelastic response depends on the characteristics of the earthquake, such as the duration, and further study is required to refine the conclusions for practical applications. Although, the uncertainties (due to strong dependency of the surface motion on site characteristics) in the seismic demand and natural periods of case buildings in Mexico City prevent further practical discussions, accepting the SCT record as the representative seismic demand, only case III can be accepted with this criterion, which resulted in 0.8˚ (1.4%) of irrecoverable tilting of the foundation. Hence limitation of 1˚ for the Mexico City cases is also acceptable.

The methodology involves significant assumptions, which may lead to unconservative or conservative impact on the results. Hence, further studies are required to improve the methodology for application. Proposed further studies are presented in Chapter 6. It may be possible to extend the calculation procedure to cases other than shallow mats, and to foundation soils that display significant strength (and stiffness) degradation under seismic loading.

A final observation is that, excessive foundation displacements occurred on deep alluvium sites, where seismic loads are significantly amplified at periods around site periods. Hence, especially for the case of relatively low-strength systems, reliable estimations of seismic displacement demands for these sites play a crucial role in calculations. For the case of Adapazarı, simulated ground motion is

observed to be consistent with the demand prescribed in the Turkish Earthquake Code, and available R_y-μ_{max} relationships. Mexico City case is observed to be more problematic in this respect. However, it is also shown that, seismic inelastic displacement demands for these records can be simulated by a velocity pulse, with velocity amplitude in the order of PGV, and pulse period in the order of the fundamental site period. Further studies are required for refinement of these observations. However, considering the limitations of the study, it is recommended that site response studies for similar cases should be directed to development of a representative velocity pulse, which can be utilized besides the elastic design spectrum for the site.

CHAPTER 6

SUMMARY AND CONCLUSIONS

6.1. Summary

Cases with excessive displacements of mat foundations resting on saturated silt-clay mixtures were reported in Mexico City during 1985 Mexico Earthquake, and in Adapazarı during 1999 Kocaeli Earthquake. Soft surface deposits, shallow ground water table, mat foundations with limited embedment, and deep alluvial deposits with significant potential for site-amplification are the common features of these cases. Excessive tilting of foundations limited the post-earthquake serviceability of structures, in several instances, and this form displacements are particularly difficult to realign. Based on such field experience, a simple methodology to estimate irrecoverable tilting potential of shallow mat foundations on saturated soft fine deposits is developed in this study.

Seismic behavior of undisturbed samples, consisting of fine soils retrieved from relevant sites at Adapazarı, is investigated through triaxial tests via consolidated-undrained (CU) procedures. The soils that dominate shallow deposits are defined as either clayey silts or silty clays. These soils that cluster around A-line on the plasticity chart are referred to here as silt-clay mixtures. Considering the stress paths beneath the case foundations, the soils are anisotropically consolidated before the undrained test phase. Deformation behavior of Adapazarı silt-clay mixtures under seismic loads is investigated by undrained cyclic loading tests, in which the comparable load rates and amplitudes to seismic loading in Adapazarı are applied. Results of cyclic tests are also compared with the stress-strain plots of monotonic shear strength tests. The specimens are observed not to demonstrate any significant strength loss during cyclic loading, and can accumulate finite irrecoverable strains during successive excursions of the monotonic strength. However, irrecoverable strain accumulation per load cycle is

dependent on the viscous response of the specimen to rapid loading. Hence, omitting the viscous response to rapid loading, the behavior of foundation soils can be idealized as elastic-perfectly plastic, obeying Mohr-Coulomb yield criterion.

Hence, the behavior of structures resting on soft silt-clay mixtures is reduced to the response of a nonlinear SDOF oscillator, utilizing basic SSI formulations. Mechanical properties of the nonlinear soil-structure-interaction system can be represented by the natural period ($\overline{T}$), damping ratio (ζ), and yield acceleration (a_y) that should act on the mass of the SDOF oscillator. In order to calculate the overturning moment-history acting on the foundation, the total mass of the structure (ignoring that of foundation) is lumped at an equivalent height ($\overline{h}$) from the base of the structure. For simple apartment buildings that have practically constant storey-height the effective height is about two-thirds of the total height. For buildings with non-uniform storey-heights, simple equations to calculate the equivalent height are also derived. Estimation of a representative damping ratio is rather complicated, due to its dependence on frequency content of motion, soil stratification, and validity of simple correlations that are based on elastic halfspace assumption for the soil. Hence, it is proposed to utilize a small damping ratio (i.e., 5%) in the analyses, compatible with the damping ratio of the utilized elastic spectrum and inelastic displacement demand correlations.

The pseudo-static yield acceleration (a_y) that is required to initiate plastic flow of the foundation can be estimated utilizing available analytical formulae for simple cases. In more complicated cases involving significant soil stratification, or foundation shape irregularities, numerical approaches are useful in calculation of ultimate seismic load capacity of foundations. Hence, Plaxis, a finite-element package developed for geotechnical applications, is utilized in order to estimate seismic load capacity of shallow foundations. Considering that the available theoretical solutions in literature are based on rigid-plasticity assumption for the soil response, the material model is set to ideally elastic-perfectly plastic behavior. The elastic deformation modulus is set to a relatively high value to achieve a behavior similar to rigid-plasticity, so that available theoretical solutions in literature can be compared with the results, and that the foundation failure mode during plastic flow is restricted to general bearing capacity failure. For the case of purely cohesive soil, which behaves fully undrained, and the case of fully cohesionless soil, which

behaves fully drained, the numerical findings satisfactorily agree with the analytical approaches.

The ultimate overturning moment capacity of foundations are correlated to factor of safety against static bearing capacity failure of the foundation, and the aspect ratio (h/B) of the structure. On the other hand, the static bearing capacity can involve significant uncertainties in practical applications, which will in turn affect the ultimate seismic load capacity of foundations. Hence, reasonable estimations of static bearing capacity is essential to utilize these relationships reliably. The ultimate bearing capacity is very sensitive to variations in effective internal friction angle (Φ´). Also, dilatancy angle (Ψ) and roughness of foundation-soil interface are critical parameters which affects the ultimate bearing capacity of foundations significantly. Hence, based on observations from laboratory tests, and findings in literature, the value of bearing capacity factor N_γ is in the order of 10, which is representative for cases in Adapazarı and Mexico City, resting on normally-consolidated fine deposits without significant cohesion. The dilatancy angle is set to zero, which is consistent with test results, and any possible positive dilatancy angle will provide reserve strength for the yielding of the foundation-soil system.

However, the relationships provided for the fully undrained cohesive soils or fully drained cohesionless soils are not exactly representative for available cases. The shallow ground-water table in Adapazarı and Mexico City results in a consolidated-undrained behavior for the soils during seismic loading. That is, the soils beneath these buildings are expected to have completed most of their consolidation before the earthquake (i.e., practically zero excess pore-pressure beneath the foundations), and are forced to behave in undrained manner during rapid loading of the earthquake. Hence, utilizing the finite-elements approach, the stress paths for consolidated-undrained behavior is simulated for normally consolidated soils. It is shown that, not only the long-term static factor of safety (FS) against bearing capacity is lower for the case of shallow ground-water table, but also the seismic load capacity is lower for a given FS than the case with unsaturated soils. Hence, seismic bearing capacity failures are more likely to happen for cases with very shallow ground-water tables.

The relationship between the aspect ratio (h/B) and ultimate overturning moment capacity of the foundation is investigated utilizing different h/B ratios. It is shown that, for h/B>0.5 the load inclination (i.e., horizontal base shear acting on

foundation) can be practically omitted. For h/B ratios in the order of 0.5 or less, ignoring the base shear in calculations results in very significant overestimation of ultimate seismic load capacity of the foundation. In fact, the horizontal translation mode of displacement appear to be more significant for such cases. Hence, for development of a simple calculation procedure, the contribution of horizontal translation mode in total irrecoverable displacements is ignored, and the irrecoverable displacements at the structure's roof level is accepted to be due to the irrecoverable tilting of the foundation. On the other hand, in calculation of pseudo-static yield acceleration (a_y) for a foundation, only the gravitational load and its eccentricity are considered. Ignoring the impact of load inclination, a_y is overestimated for structures with low h/B ratio. It is assumed that, in calculation of irrecoverable tilting, the error due to omitting of partition of the translational mode of foundation displacements is compensated by the overestimation of yield acceleration. As a result, the irrecoverable tilting converges to zero as h/B ratio converges to zero.

Utilizing SCT records captured at alluvium sites in Mexico City during 1985 earthquake, and simulated acceleration-history for alluvium sites in Adapazarı during 1999 earthquake, the calculation procedure is validated by the available excessive foundation displacement cases in Mexico City and Adapazarı. The long-term bearing capacity of these foundations are estimated by setting N_γ=10 in bearing capacity calculations. It is observed that the calculation procedure provides consistent results with the observations, except for the systems with very low a_y values (i.e., very poor aspect ratios), since the inelastic displacement demands are very sensitive to behavior asymmetries for these systems.

Hence, in practical applications, it is proposed to limit the aspect ratio of the structures with mat foundations of insignificant embedment, such that the irrecoverable tilting demands calculated by the procedure given in the study do not exceed 1˚. Also, considering the impact of strength asymmetry over seismic behavior of foundations, it is proposed to avoid adjacent construction of buildings, and to provide keep sufficient free-space between foundations of neighboring structures. The calculations can be achieved utilizing either actual acceleration time-histories that are representatives of expected seismic demand, or utilizing elastic design spectrum and reliable R_y-μ_{max} relationships for SDOF systems.

Finally, the impact of deep alluvium, which is in common in both, the Adapazarı and Mexico City cases, on the inelastic displacement demands for the utilized acceleration-histories are further investigated. It is shown that, velocity pulses with periods compatible with the site-periods and amplitudes compatible with the PGV dominate the irrecoverable displacement demands on systems with low a_y values. Therefore, it is worthwhile to further investigate the irrecoverable foundation tilting demand on foundations of buildings with poor aspect ratios utilizing these velocity pulse-histories.

6.2. Conclusions

The conclusions reached, based on the experimental, analytical and numerical studies are dependent on the assumptions and limitations already stated in the study. Still, however, they provide a deeper insight to our understanding of seismic performance of shallow mat foundations resting on soft fine deposits, and can be utilized in development of seismic design criteria for prevention from excessive tilting of buildings during major earthquakes:

1) Considering seismic loading conditions, silt-clay mixtures with comparatively low shear strength are not liquefiable, considering the conventional definition of liquefaction. Instead, due to their low shear strength, strains can accumulate during severe seismic loading. However, the strain accumulation is counteracted by the viscous response of these materials. Hence, excessive foundation displacements for shallow mat foundations resting on soft silt-clay mixtures in Adapazarı can be explained by the seismic bearing capacity failure mechanism.

2) Irrecoverable strain potential of normally consolidated silt-clay mixtures during cyclic loading is shown to be correlated to rapid loading test results. A simple relationship is developed for irrecoverable strain rates between cyclic load tests and rapid loading tests. Based on the observations from cyclic tests in which the monotonic shear strength is not exceeded the relationship omits the irrecoverable displacements for stress levels below monotonic shear strength, and considers the strain accumulation for stress levels exceeding the shear strength.

3) During one-way loading tests (no shear stress reversals occur during testing), stiffness and shear strength during loading are observed to be practically unaffected by the strain-history. However, during two-way loading tests, the soil

specimens are observed to demonstrate a strain-memory behavior in both extension and compression directions. That is, for successive stress cycles, the specimen targets the previous maximum axial strain in the loading direction, and accumulates further irrecoverable strains over it. When the loading is reversed, the specimen targets the peak strain in the opposite loading direction. As the overall behavior, this implies a stiffness-degrading system for successive stress-reversals. Validation of such behavior for foundations requires further studies.

4) Viscous response of silt-clay mixtures of Adapazarı is observed to be dependent on the plasticity index and water content. For a given stress level above monotonic strength, the strain rate for irrecoverable strains is observed to increase with decreasing plasticity index and increasing water content. However, further tests are required to validate the observed relationships, since the Atterberg Limits of the specimens are observed to cluster very close to the A-line.

5) The effective angle of friction (Φ') of the silt-clay mixtures of Adapazarı are observed to be around 30°, assuming zero cohesion during the shear failure. No significant dilative behavior is observed during consolidated-undrained monotonic triaxial tests (i.e., $\Psi \cong 0°$). The Φ' values are comparable to the values reported for Mexico-City soils, but somewhat higher.

6) The behavior of foundation-soil system is idealized as ideally elastic-perfectly plastic with single-degree-of-freedom, to estimate the dynamic response including nonlinear soil-structure interaction effects. The linear system properties can be represented by the natural period, calculated using equation 3.24, and a frequency-dependent equivalent damping ratio. However, due to the difficulties involved in estimation of an equivalent damping ratio, it is proposed that a small damping ratio (i.e., 5%) can be utilized for practicality assuming that majority of the energy input to the system is dissipated by the hysteretic behavior of the inelastic system. Yield strength of the simplified soil-structure-interaction system can be estimated by pseudo-static approaches, in which the seismic forces are considered as static inertial forces. For calculations, the mass of the structure can be lumped at a height of about 2/3 of the total building height, which is referred to as the equivalent height. Considering the cases that involve structures with variable storey-heights, simple equations to estimate the equivalent height are also provided in the study.

8) A plastic flow rule is required to calculate the contributions of horizontal translation and rocking modes of foundation displacements in total plastic displacements at the level of equivalent height. However, considering the case of buildings with very poor aspect ratios (h/B), the horizontal translation mode of displacement is ignored, and total irrecoverable displacement is assumed to be only due to tilting mode of plastic deformations. Similarly, the horizontal seismic load capacity of the foundation is estimated, ignoring the load inclination and considering load eccentricity alone. The calculation procedure is representative for poor-aspect ratio buildings, and will converge to zero irrecoverable tilting for structures with very low aspect ratio. Hence, considering the Adapazarı observations, this assumption is asymptotically correct, and the error involved in calculations for intermediate aspect ratios can be investigated incorporating a flow rule for the foundation behavior in future studies.

9) Load-controlled finite-element analyses can be utilized in order to estimate the pseudo-static yield acceleration for foundations. For the case of shallow foundations, when horizontal seismic forces are considered, inertial forces acting on the soil body can be ignored, and the impact of seismic forces can be simulated considering inclined and eccentric loads acting at foundation level. Simple formulae exist in literature when drained (cohesionless) or undrained (cohesive) soil behavior is considered. However, these solutions are valid for rigid-plastic behavior and homogeneous, isotropic soil conditions, which may not be valid for every practical application. In case of significant deviations from these conditions, finite-element approaches presented in this study can provide a useful tool for load-capacity calculations. Validation of the numerical calculation procedure can be achieved utilizing the analytical formulae, provided that the stiffness of the soil in the model is sufficiently high to capture the rigid-plastic response, which is utilized in analytical solutions.

10) Eccentricity governs the ultimate seismic load capacity of the shallow mat foundation for buildings with aspect ratios (h/B) greater than 0.5. Hence, for these cases, the ultimate overturning moment capacity can be estimated ignoring the load inclination. Equations for calculation of ultimate overturning moment capacity of shallow foundations resting on homogeneous soils considering load eccentricity alone are given in the study. However, these equations will overestimate yield

acceleration and ultimate overturning moment capacity for buildings with relatively lower aspect ratios.

11) Regarding the examined cases in Adapazarı and Mexico City, the consolidation process beneath the foundations is assumed to be completed before the earthquake. If however the consolidation process is not practically complete, the static factor of safety against bearing capacity will be lower. Hence, the consolidated-undrained stress-path best represents the soil behavior beneath the foundations. For normally-consolidated soils, the pore-pressure increase during undrained loading is considered to be consistent with the elastic stress-path. It is observed that, for a given factor of safety against bearing capacity failure under static loads, the seismic load capacity of foundations are significantly lower for the case of undrained loading than that of drained loading. This is due to the fact that, considering the gravitational loads alone, the consolidated-undrained bearing capacity, which is relevant under seismic loading conditions, is lower than the case of fully drained loading.

12) Static factor of safety against bearing capacity failure (FS) can be utilized as a basic parameter to estimate the seismic load capacity of shallow foundations. For a given static factor of safety, the overturning moment capacity of shallow mat foundations is observed to be highest for the cohesive soil case, and lowest for the case of undrained saturated cohesionless soil. It is also concluded that, the FS values sufficiently large for static condition may not be adequate under seismic loading.

13) Determination of the static factor of safety, which is the basic parameter used to estimate the seismic load capacity of shallow foundations, involves significant uncertainties. For cohesionless soils the N_γ factor in bearing capacity calculations is very sensitive to variations in Φ'. Also, the N_γ factor depends on the roughness of the foundation-soil interface, and on the associativeness of the plastic soil behavior. Even the case of perfectly rough interface and associative flow rule, different values of N_γ have been reported in literature. In the case of inhomogeneous soil profiles, estimation of static bearing capacity can be further complicated. Hence, in estimations of seismic performance of shallow foundations, sufficient conservatism should be applied in determining the FS. Also, for future studies on the topic, it is advisable to normalize the results with the static factor of safety. In investigation of the cases from Adapazarı and Mexico City, N_γ factor is

presumed to be 10, considering the range of Φ′ for soft silt-clay mixtures, the prevailing nonassociative behavior (Ψ=0°), and the possibility of imperfect roughness of the foundation-soil interface.

14) A significant degree of uncertainty regarding the natural periods of the structures and the actual seismic demand in Mexico-City cases are involved. Similar uncertainties to a lesser degree exist also for the Adapazarı cases. However, assuming that the natural period of the linear SSI system ($\overline{T}$) is equal to 0.8 s, the calculation procedure is observed to be consistent with the observed tilting performances of the multistory reinforced concrete building structures. It is concluded that, in utilizing the presented methodology, the foundations should not be targeted to accumulate irrecoverable tilting greater than 1˚, which in fact introduces a limit on the aspect ratio of the building in turn. For higher levels of irrecoverable tilting, there exist cases with excessive foundation tilting, which include practically toppled buildings at worst.

15) Significant deviations from those estimated by the method for values of tilting greater than 1˚ is explained by the sensitivity of these cases to strength asymmetry in seismic foundation behavior. For cases with low a_y values, the inelastic displacement demand on elasto-plastic SDOF oscillator is observed to increase very significantly due to asymmetric yield strength in two oscillation directions. In order to limit the detrimental impact of strength asymmetry in foundation performance, it is advisable to refrain from adjacent building construction, and to leave sufficient free-space between building foundations. This precaution will not only prevent asymmetric foundation behavior, but also prevent deviation of the actual seismic demand from the estimations due to structure-structure interaction. It is also proposed to investigate the soil profiles at both sides of the width of mat foundations, in order to detect any significant potential of strength asymmetry. Further studies are required to clarify the impact of strength asymmetry on seismic performance of foundations.

16) Based on elastic response spectrum, simple relationships to estimate inelastic displacement demands for elasto-plastic systems are available. Reliable estimation of ductility demands for elasto-plastic systems is required for the application of proposed methodology. However, considering especially the case of SCT record, utilization of approximate relationships to estimate ductility demands can involve significant error on alluvium sites. This issue should be further

investigated, specifically for systems with low a_y levels. It is also observed that the inelastic response of such systems is governed by velocity pulses inherent in the records, which are introduced by the site response. The velocity pulses are observed to have amplitudes in the order of PGV and pulse periods in the order of the fundamental site-period. Hence, utilizing site-response analyses, similar representative velocity pulses can be developed for a given alluvium site for utilization of inelastic displacement demands for systems with low a_y values, such as foundations of poor aspect ratio buildings.

6.3. Recommendations for Future Research

The presented study is based on several assumptions and approximations, which can be improved through further research. These topics, which involve laboratory and analytical studies, are the following:

- The static factor of safety against bearing capacity failure should be calculated with reasonable accuracy for shallow foundations on silt-clay mixtures. Hence, this requires specific testing on undisturbed samples, the shear strength parameters should be studied in detail, developing correlations with index parameters (e.g., water content, clay fraction, etc.) and with in-situ tests (e.g., SPT, CPT, etc.). In case CU type triaxial tests are utilized for the purpose, the shear strength as well as pore-pressure parameters in both extension and compression type stress-paths should be measured. In the case of very loose or soft shallow deposits, for which undisturbed sampling is not possible, in-situ tests to measure shear strength (e.g., pressuremeter test, plate-loading test, vane test, etc.) can be utilized.
- The viscous response observed at increased rates of loading tends to limit the development of irrecoverable strains during transient loading. Also, the observed strain-memory behavior in successive stress-reversals results in a stiffness-degrading behavior. By conducting tests with irregular stress or strain-histories, these observations can be further verified and a simplified procedure to update the soil stiffness and strength depending on the magnitude and duration characteristics of the seismic loading.
- Utilizing the load-controlled model tests with saturated silt-clay mixtures, a plastic flow rule based on load eccentricity and inclination can be developed, for foundations resting on silt-clay mixtures. The flow rule can be coupled with

numerical analyses, in order to assess the participation of tilting and horizontal components of irrecoverable displacements. The results will be useful to improve the methodology developed in this study.

- The correlation between mechanical behavior of soils observed in triaxial tests, and actual foundation behavior depends more on judgment. It is important to investigate the relationship between triaxial test results and actual foundation behavior, in terms of stiffness degradation and visco-plastic behavior. Model tests can be utilized to develop such correlations as well as to verify the methodology developed in this study.
- The impact of soil stratification and foundation embedment can be clarified by similar pseudo-static numerical analyses similar to those presented in this study. The results can be useful in practical conclusions to estimate the ultimate seismic capacity of embedded foundations resting on inhomogeneous soils.
- The ultimate capacity of foundations resting on on normally-consolidated saturated soils under undrained loading conditions should be further investigated. More rigorous constitutive soil models, which simulate pore-pressure increase in undrained tests, can be implemented. However, accurate measurements of pore-pressures require low strain rates during the tests, so that the viscous deformation behavior during rapid loading is not considered in such studies.
- Conclusions regarding the ultimate load capacity of foundations are based on plane-strain analyses. Also, the available formulations in literature consider only in-plane seismic loading. However, inclusion of impact of out-of-plane inertial forces in analyses may result in significantly lower yield-accelerations. These issues can be clarified by three-dimensional analyses.
- In this study, it is assumed that the majority of input energy to the simplified soil-structure interaction system is dissipated by the hysteretic response of the elasto-plastic system. This, however, may be a significantly conservative assumption. A simplified methodology to estimate a more realistic damping ratio for nonlinear SSI system can be developed. Also, the impact of presumed value of V_s used for SSI calculations should be further investigated.

- The strength asymmetry is observed to increase irrecoverable displacement demands of foundations during seismic loading. Considering the foundations resting on highly-variable soil profiles, this issue should be further studied.
- As more geotechnical data becomes available, the cases presented in this study can be re-investigated, utilizing improvements over the calculation procedure. Also, the analyses in this study can be supplemented by more rigorous seismic demand calculations for the sites.

REFERENCES

Akkar S., Sucuoğlu H., Yakut A. (2004). "Displacement-based fragility Functions for low and mid-rise ordinary concrete buildings," submitted to *Earthquake Spectra* for publication.

Andersen K.H., Pool J.H., Brown S.F., and Rosenbrand W.F (1980).” Cyclic and static laboratory tests on Drammen clay”, *Journal of the Geotechnical Engineering Division*, A.S.C.E., Vol.106, No.5, pp.499-529.

Andersen K.H., Kleven A., and Heien D. (1988a). "Cyclic soil data for design of gravity structures,” *Journal of Geotechnical Engineering*, Vol.114, No.5, pp.517-539.

Andersen K.H., and Lauritzsen R. (1988b). "Bearing capacity for foundation with cyclic loads,” *Journal of Geotechnical Engineering*, Vol.114, No.5, pp.540-555.

Ansal A.M., and Erken A. (1989). “Undrained behavior of a normally consolidated clay under cyclic shear stresses,” *Journal of Geotechnical Engineering*, A.S.C.E., Vol.115, No.7, pp.968-983.

Ansal A., İyisan R., and Yıldırım H. (2001). "The cyclic behavior of soils and effects of geotechnical factors in microzonation," *Soil Dynamics and Earthquake Engineering*, Vol.21, pp.445-452.

Atkinson J.H. (2000). “Non-linear soil stiffness in routine design,” *Geotechnique*, Vol.50, Iss. 5, pp. 487-507.

Atkinson J. (1993). *An Introduction to the Mechanics of Soils and Foundations*, McGraw-Hill, London, 337 p.

Auvinet G., Pecker A., and Salençon J. (1996). "Seismic bearing capacity of shallow foundations in mexico city during the 1985 Michoacan earthquake,” *Eleventh World Conference on Earthquake Engineering*, Elsevier Science, Paper No.1966.

Bakır B.S., Sucuoğlu H., and Yilmaz T. (2002). "An overview of local site effects and the associated building damage during the 17 August 1999 İzmit earthquake,” *Bulletin of the Seismological Society of America,* Vol.92, No.1, pp.509-526.

Bakır B.S., Yılmaz M.T., Yakut A., and Gülkan P., (2004). “Re-examination of damage distribution in Adapazarı: geotechnical considerations,” in review for possible publication in *Engineering Structures*.

Bolton M.D., and Lau C.K. (1993). "Vertical bearing capacity factors for circular and strip footings on Mohr-Coulomb soil,” *Canadian Geotechnical Journal*, Vol.30, Iss.6, pp.1024-1033.

Bransby M.F. (2001). “Failure envelopes and plastic potentials for eccentrically loaded surface footings on undrained soil,” *International Journal for Numerical and Analytical Methods in Geomechanics*, Vol.25, pp.329-346.

Bray J.D., Sancio R.B., Youd L.F., Christensen C., Cetin O., Onalp A., Durgunoglu T., Stewart J.P.C., Seed R.B., Baturay M.B., Karadayilar T., and Oge C. (2001a). “Documenting incidents of ground failure resulting from the August 17, 1999 Kocaeli, Turkey Earthquake,” website: peer.*berkeley.edu/turkey/adapazari/phase1*, P.E.E.R., (last accessed date: August 2004).

Bray J.D., Sancio R.B., Durgunoglu H.T., Onalp A., Seed R.B., Stewart J.P., Youd T.L., Baturay M.B., Cetin K.O., Christensen C., Karadayilar T., and Emrem C. (2001b). "Ground Failure in Adapazarı, Turkey", *Lessons Learned From Strong Earthquakes,* Proceedings of the XVth ICSMGE Earthquake Geotechnical Engineering Satellite Conference, Ed: A.M. Ansal, Istanbul, pp.19-28.

Bray J.D., Sancio R.B., Durgunoglu T., Onalp A., Youd T.L., Stewart P., Seed R.B., Cetin O.K., Bol E., Baturay M.B., Christensen C., and Karadayılar T. (2004). "Subsurface characterization at ground failure sites in Adapazarı, Turkey," *Journal of Geotechnical and Geoenvironmental Engineering*, A.S.C.E., Vol. 130, No.7, pp.673-685.

Budhu M, and Al-Karni A. (1993). "Seismic bearing capacity of soils,” *Geotechnique*, Vol.43, No.1, pp.181-187.

Building Seismic Safety Council (2001). *NEHRP Recommended Provisions for Seismic Regulations for New Buildings and Other Structures*, *Part 1: Provision (FEMA 368),* Building Seismic Safety Council, Washington D.C.

Butterfield R., and Gottardi G. (1994). "A complete three-dimensional failure envelope for shallow footings on sand,” *Geotechnique*, Vol. 44, No.1, pp.181-184.

Chopra A.K. (1995). *Dynamics of Structures: Theory and Applications*, Prentice Hall, Upper Saddle River, New Jersey, 762 p.

Das B.M. (1999). *Principles of Foundation Engineering*, Brooks/Cole Publishing, California, 862 p.

Davis R.O, and Selvadurai A.P.S. (2002). *Plasticity and Geomechanics*, Cambridge University Press, Cambridge, U.K.

DeAlba, P., C.K. Chan, and H.B. Seed (1975). *Determination of soil liquefaction characteristics by large-scale laboratory tests*, Report EERC 75-14, E.E.R.C., University of California, Berkeley.

Dobry R., and Gazetas G. (1986). “Dynamic Response of Arbitrarily Shaped Foundations,” *Journal of Geotechnical Engineering*, A.S.C.E., Vol. 112, No. 2, pp. 109-135.

Dobry R., Gazetas G., and Stokoe K.H. (1986). “Dynamic Response of Arbitrarily Shaped Foundations,” *Journal of Geotechnical Engineering*, A.S.C.E., Vol. 112, No. 2, pp. 136-154.

Dormieux L., and Pecker A. (1995). "Seismic bearing capacity of foundation on cohesionless soil,” *Journal of Geotechnical Engineering*, A.S.C.E., Vol. 121, No.3, pp. 300-303.

Drescher A., and Detournay E. (1993). “Limit load in translational failure mechanisms for associative and non-associative materials,” *Geotechnique*, Vol.43, No.3, pp.443-456.

Dyvik R., Andersen K.H., Madshus C., and Amundsen T. (1989). "Model Tests of Gravity Platforms. I: Description,” *Journal of Geotechnical Engineering*, A.S.C.E., Vol. 115, No. 11, pp.1532-1549.

Erickson H.L., and Drescher A. (2002). “Bearing Capacity of Circular Footings,” *Journal of Geotechnical and Geoenvironmental Engineering*, A.S.C.E., Vol. 128, No.1, pp. 38-43.

Fishman K.L., Richards R.Jr., and Yao D. (2003). "Inclination Factors for Seismic Bearing Capacity,” *Journal of Geotechnical and Geoenvironmental Engineering*, A.S.C.E., Vol.129, No.9, pp.861-865.

Frydman S.,and Burd H. (1997). "Numerical sudies of bearing-capacity factor N_γ,” *Journal of Geotechnical and Geoenvironmental Engineering*, A.S.C.E., Vol.123, No.1, pp.20-29.

Gómez A., Ortega R., Guerrero JJ., Gonzáles E., Paniagua J.P., and Iglesias J. (1989). "The Mexico Earthquake of September 19, 1985- response and design spectra obtained from earthquake-damaged buildings,” *Earthquake Spectra*, Vol. 5, No. 1, pp.113-120.

Guo T., and Prakash S. (1999) “Liquefaction of Silts and Silt-Clay Mixtures,” *Journal of Geotechnical and Geoenvironmental Engineering*, Vol.125, No.8, pp.706-710.

Hansen B., and Christensen N.H. (1969). "Discussion of 'Theoretical bearing capacity of very shallow footings', by A. L. Larkins,” *Journal of Soil Mechanics and Foundation Division,* A.S.C.E., Vol.95, Iss.6, pp.1568-1572.

Hansen J.B. (1970). “A revised and extended formula for bearing capacity,” *Danish Geotechnical Institute Bulletin No.28*, Copenhagen.

Hausler E.A., and Sitar N. (2001). "Dynamic centrifuge testing on improved ground," in: *Fifteenth International Conference on Soil Mechanics and Geotechnical Engineering,* İstanbul, Turkey, *Session* 4.3, Recent Developments in Ground Improving, August 27-31.

Houlsby G.T., and Purzin A.M. (1999). "The bearing capacity of strip footing on clay under combined loading," *Proc. Roy. Soc*. No.455A, pp.893-916.

Hyde A.F.L., and Brown S.F. (1976). "The plastic deformation of a silty clay under creep and repeated loading," *Geotechnique*, Vol.26, No.1, pp.173-184.

Hyde A.F.L., and S.J. Ward (1985). "A pore pressure and stability model for a silty clay under repeated loading," *Geotechnique*, Vol.35, No.2, pp. 113-125.

Hynes-Griffin M.E., and Franklin A.G. (1984). "Rationalizing the seismic coefficient method", *Miscellaneous Paper GL-84-13*,U.S.A.C.E.W.E.S., Mississippi, 21 pp.

Hyodo M, Yamamoto Y, and Sugiyama M. (1994). "Undrained cyclic shear behavior of normally consolidated clay subjected to initial static shear stress," *Soils and Foundations*, Vol.34, No.4, pp.1-11.

Ingra T.S., and Baecher G.B. (1983). "Uncertainity in bearing capacity of sands," *Journal of the Geotechnical Engineering*, Vol.109, No.7, pp.899-914.

Ishihara K. (1993). "Liquefaction and flow failure during earthquakes," *Geotechnique*, Vol.43, Iss.3, pp.351-415

Ishihara K. (1996). *Soil Behavior in Earthquake Geotechnics*, Clarendon Press, Oxford, 350 p.

Lefebre G., LeBoueuf D. (1987). "Rate effects and cyclic loading of sensitive clays," *Journal of Geotechnical Engineering*, A.S.C.E., Vol.113, No.5, pp.476-489.

Jaky J. (1944). "The coefficient of earth pressure at rest," *Journal of the Society of Hungarian Architects and Engineers*, pp. 355-358.

Makdisi F.I., and Seed H.B. (1978). "Simplified procedure for estimating dam and embankment earthquake-induced deformations," *Journal of the Geotechnical Engineering Division*, A.S.C.E., Vol.104, No.GT7, pp.849-867.

Mendoza M.J., and Auvinet G. (1988)."The Mexico Earthquake of September 19, 1985- Behavior of Building Foundations in Mexico City," *Earthquake Spectra*, Vol.4, No.4, pp.835-853.

Newmark N. (1965). "Effects of earthquakes on dams and embankments," *Geotechnique,* Vol.15, No.2, pp. 139-160.

Karaca G. (2001). *An investigation into the large vertical displacements experienced by the structures in Adapazarı during 17 August 1999 Earthquake*, Ms.Thesis, M.E.T.U., 155 p.

Konrad J.M., and Wagg B.T. (1993). “Undrained cyclic loading of anisotropically consolidated clayey silts,” *Journal of Geotechnical Engineering*, A.S.C.E., Vol.119, No.5, pp.929-947.

Kumar J. and Mohan Rao V.B.K. (2002). "Seismic bearing capacity factors for spread foundations,” *Geotechnique*, Vo.32, No.2, pp.79-88.

Lambe T.W. (1967). "Stress path method", *Journal of the Soil Mechanics and Foundation Division*, A.S.C.E., Vol.93, No.SM6, pp.309-331
Lambe T.W., and Marr W.A. (1979). "Stress path method: second edition", *Journal of the Geotechnical Engineering Division*, A.S.C.E., Vol.105, No.GT6, pp.727-738.

Lefebvre G, Pfendler P. (1996). “Strain rate and preshear effects in cyclic resistance of soft clay,” *Journal of Geotechnical Engineering*, A.S.C.E., Vol.122, No.1, pp.21-26.

Liu L. and Dobry R. (1997). "Seismic response of shallow foundation on liquefiable sand,” *Journal of Geotechnical and Geoenvironmental Engineering*, A.S.C.E., Vol.123, No.6, pp.557-567.

Makdisi F.I., and Seed H.B. (1978). "Simplified procedure for estimating dam and embankment earthquake-induced deformations,” *Journal of the Geotechnical Engineering Division*, A.S.C.E., Vol.104, No.GT7, pp.849-867.

Makris N., and Roussos Y.S. (2000). "Rocking response of rigid block under near-source ground motions,” *Geotechnique*, Vol. 50, No. 3, pp. 243-262.

Matešić L, Vucetic M. (2003). “Strain-rate effect on soil secant modulus at small cyclic strains,” *Journal of Geotechnical and Geoenvironmental Engineering*, A.S.C.E., Vol.129, No.6, pp.536-549.

Matsui T., H. Ohara, and T. Ito (1980). “Cyclic stress-strain history history and shear characteristics of clay,” *Journal of the Geotechnical Engineering Division,* A.S.C.E., Vol. 86, No. GT10, 1101-1120.

Mendoza M.J., and Auvinet G. (1988)."The Mexico Earthquake of September 19, 1985- Behavior of Building Foundations in Mexico City,” *Earthquake Spectra*, Vol.4, No.4, pp.835-853.

Meyerhof G.G. (1963). “Some recent research on the bearing capacity of foundations,” *Canadian Geotechnical Journal*, Vol.1, No.1, pp.16-26.

Michalowski R.L. (1997). "An estimate of the influence of soil weight on bearing capacity using limit analysis,” *Soils and Foundations,* J.G.S., Vol.37, No.4, pp.57-64.

Ministry of Public Works and Settlement (1998). *Turkish Earthquake Code: Specifications for the Buildings to be Constructed in Disaster Areas*, Ankara, Turkey.

Miranda E. (1993). "Site-dependent strength-reduction factors,” *Journal of Structural Engineering*, A.S.C.E., Vol.119, No. 12, pp. 3503-3519.

Miranda E., and Ruiz-Garcia J. (2002a). "Evaluation of approximate methods to estimate maximum inelastic displacement demands," *Earthquake Engineering and Structural Dynamics,* Vol. 31, pp. 539-560.

Miranda E. and Ruiz-Garcia J. (2002b). "Influence of stiffness degradation on strength demands of structures built on soft soil sites," *Engineering Structures*, Vol. 24, pp. 1271-1281.

Mitchell R.J., and King R.D. (1977). "Cyclic loading of an Ottawa area Champlain Sea clay," *Canadian Geotechnical Journal*, Vol.14, pp.52-63.

Newmark N. (1965). "Effects of earthquakes on dams and embankments," *Geotechnique,* Vol.15, No.2, pp. 139-160.

Newmark N.M., and Hall W.J. (1982). *Earthquake Spectra and Design*, Earthquake Engineering Research Institute, Berkeley, California, pp. 29-37.

Ohara S., and H. Matsuda (1988). "Study on the settlement of saturated clay layer induced by cyclic shear," *Soils and Foundations*, Vol.28, No.3, 103-113.

Ortigao J.A.R. (1995). *Soil Mechanics in the Light of Critical State Theories: An Introduction*, A.A. Balkema, Rotterdam, Netherlands.

Paolucci R. (1997). "Simplified evaluation of earthquake-induced permanent displacements of shallow foundations," *Journal of Earthquake Engineering,* Vol.1 No.3, pp.563-579.

Paolucci R., and Pecker A. (1997a). "Seismic bearing capacity of shallow strip foundations on dry soils," *Soils and Foundations*, J.G.S., Vol.37, No.3, pp.95-105.

Paolucci R., and Pecker A. (1997b). "Soil inertia effects on the bearing capacity of rectangular foundations on cohesive soils," *Engineering Structures*, Vol.19, No.8, pp.637-643.

Parry R.H.G. (1995). *Mohr Circles, Stress Paths and Geotechnics*, E & FN Spon, London, 230 p.

Perlea VG. (2000). "Liquefaction of cohesive soils," in: Pak RYS, Yamamura J, editors. *Soil Dynamics and Liquefaction*, A.S.C.E. Special Publication No.107.

Perkins S.W., and Madson C.R. (2000). "Bearing capacity of shallow foundations on sand: a relative density approach," *Journal of Geotechnical and Geoenvironmental Engineering*, Vol.126, No.6, pp.521-530.

Pecker A. (1997). "Analytical formulae for the seismic bearing capacity of shallow strip foundations," in *Seismic Behavior of Ground and Geotechnical Structures,* ed: Seco e Pinto, Balkema, Rotterdam, pp.261-268.

Pecker A. (1998). "Capacity design principles for shallow foundations in seismic areas," in: *11th European Conference in Earthquake Engineering,* Key Lecture, Paris la Defense, pp.303-315.

Pekcan O. (2001). *Cyclic Behavior of Adapazarı Clayey Silts*, Ms.Thesis, M.E.T.U., 83 p.

Prandl, L. (1920). "Über die Härte plastischer Körper," *Nachr. Ges. Wiss. Göettingen, Math.-Phys. Kl.,* pp. 74-85.

Prevost J.H., Cuny B., and Scott R.F. (1981a). "Offshore gravity structures: centrifugal modeling," *Journal of the Geotechnical Engineering Division*, A.S.C.E., Vol.107, No.GT2, pp.125-141.

Prevost J.H., Cuny B., and Scott R.F. (1981b). "Offshore gravity structures: analysis," *Journal of the Geotechnical Engineering Division*, A.S.C.E., Vol.107, No.GT2, pp.143-165.

Procter D.C., Khaffaf J.H. (1984). "Cyclic triaxial tests on remoulded clays," *Journal of Geotechnical Engineering*, A.S.C.E. 1984; 110(10): 1431-1445.

Randolph M.F., and Puzrin A.M. (2003). "Upper bound limit anaysis of circular foundations on clay under general loading," *Geotechnique*, Vol.53, No.9, pp.785-796.

Richards R., and Elms D.G. (1979). "Seismic behavior of gravity retaining walls," *Journal of the Geotechnical Engineering*, A.S.C.E., Vol.105, No.GT4, pp.449-464.

Richards Jr.R., Elms D.G., and Budhu M. (1993). "Seismic bearing capacity and settlements of foundations," *Journal of Geotechnical Engineering*, A.S.C.E., Vol. 119, No.4, pp. 662-674.

Salençon J., and Pecker A. (1995). "Ultimate bearing capaciy of shallow foundations under inclined and eccentric loads. Part I: purely cohesive soil," European Journal of Mechanics A/Solids, Vol.14, No.2,pp.349-375

Sarma S.K. and Iossofelis (1990). "Seismic bearing capacity factors of shallow strip footings," *Geotechnique*, Vol.40, No.2, pp.265-273.

Sancio R.B., Bray J.D., Stewart J.P., Youd T.L., Durgunoğlu H.T., Önalp A., Seed R.B., Christensen C., Baturay B., and Karadayilar T. (2002). "Correlation between ground failure and soil conditions in Adapazarı, Turkey," *Soil Dynamics and Earthquake Engineering*, Vol.22, pp.1093-1102.

Seed H.B., Idriss I.M. (1982). *Ground Motions and Soil Liquefaction During Earthquakes,* EERI Monograph, Berkeley, CA; p.134.

Seed H.B., Lee K.L., Idriss I.M, and Makdisi R. (1973). *Analysis of the slides in the San Fernando dams during the earthquake of February 9, 1971*, Report No. EERC 73-2*,* Earthquake Engineering Research Center, University of California, Berkeley, 150 p.

Seed H.B., Romo M.P., Sun J.I., Jaime A., and Lysmer J. (1988). "The Mexico Earthquake of September 19, 1985- relationship between soil conditions and earthquake ground motions," *Earthquake Spectra*, Vol.4, No.4, pp.687-729.

Serff N., Seed H.B., Makdisi F.I., and Chang, C.-Y. (1976). *Earthquake-induced deformations of earth dams*, Report EERC 76-4, Earthquake Engineering Research Center, University of California, Berkeley, 140 p.

Siddiquee M.S., Tatsuoka F., Tanaka T., Tani K., Yoshida K., and Morimoto T. (2001). "Model tests and FEM simulation of some factors affecting the bearing capacity of a footing on sand," *Soils and Foundations*, J.G.S., Vol.41, No.2, pp.53-76.

Siefffert J.G., and Bay-Gress Ch. (2000). "Comparison of European bearing capacity calculatıon methods for shallow foundations," *Proc. Instn. Civ. Engrs. Geotech. Engrg.,* No.143, pp.65-74.

Skempton A.W (1954). "The pore pressure coefficients A and B," *Geotechnique*, Vol. 4, No. 4, pp.143-147.

Soubra A.H. (1999). "Upper-Bound Solutions for Bearing Capacity of Foundations," *Journal of the Geotechnical and Geoenvironmental Engineering,* A.S.C.E., Vol.125, No.1,pp.59-68.

Soubra A.H. (2000). "Closure: Upper-bound solutions for bearing capacity of foundations," *Journal of Geotechnical and Geoenvironmental Engineering*, A.S.C.E., Vol.126, Iss.9, pp.856-857.

Stewart J.P., Fenves G.L., and Seed R.B. (1999a). "Seismic soil-structure interaction in buildings. I: Analytical methods," *Journal of Geotechnical and Geoenvironmental Engineering*, A.S.C.E., Vol. 125, No. 1, pp. 26-37.

Stewart J.P., Seed R.B., and Fenves G.L. (1999b). "Seismic soil-structure interaction in buildings. II: Emprical findings," *Journal of Geotechnical and Geoenvironmental Engineering*, A.S.C.E., Vol. 125, No. 1, pp. 38-48.

Taiebat H.A., and Carter J.P. (2000). "Numerical studies of the bearing capacity of shallow foundations on cohesive soil subjected to combined loading," *Geotechnique*, Vol.50, No.4, pp.409-418.

Taiebat H.A., and Carter J.P. (2002). "Bearing capacity of circular foundations on undrained clay subjected to eccentric loads," *Geotechnique*, Vol.52, No.1, pp.61-64.

Terzaghi K. (1943). *Theoretical Soil Mechanics*, Wiley, New York.

Tokimatsu K., and H.B. Seed (1987). "Simplified procedures for the evaluation of settlements in sands due to earthquake shaking," *Journal of Geotechnical Engineering*, A.S.C.E., Vol. 113, No.8, 861-.

Ukritchon B, Whittle A.J., and Klangvijit C. (2003). "Calculations of bearing capacity factor Ng using numerical limit analyses," *Journal of Geotechnical and Geoenvironmental Engineering*, A.S.C.E., Vol.129, No.1, pp.468-474.

Vaid Y.P., Campanella R.G. (1973). "Time-dependent behavior of undisturbed clay," *Journal of the Geotechnical Division*, A.S.C.E., Vol.103, No.7, pp.693-709.

Vesic, A.S. (1973). "Analysis of ultimate loads of shallow foundations", *J.Soil. Mech. Found. Div.,* A.S.C.E., Vol. 99, No.SM1, pp.45-73.

Vucetic M. (1990). “Normalized behavior of clay under irregular cyclic loading,” *Canadian Geotechnical Journal*, Vol.27, 29-46.

Whitman R.V., and Lambe P.C. (1982). "Liquefaction: consequences for a structure,” in: *Proceedings of the Soil Dynamics and Earthquake Engineering Conference*, Southampton University, Vol.2, pp.941-949.

Wolf J.P. (1994). *Foundation Vibration Analysis Using Simple Physical Models*, Prentice-Hall, Englewood Cliffs, New Jersey, 423 p.

Wolf J.P. (1985). *Dynamic Soil-Structure* Interaction, Prentice-Hall, Englewood Cliffs, New Jersey, 466 p.

Wolf J.P. (1988). *Soil-Structure-Interaction Analysis in Time Domain*, Prentice-Hall, Englewood Cliffs, New Jersey, 446 p.

Yasuda S., Isisawa T., and Kazami K.(2001). "Liquefaction-induced settlements of buildings and damages in coastal areas during the Kocaeli and other earthquakes,” *Lessons Learned From Strong Earthquakes,* Proceedings of the XVth ICSMGE Earthquake Geotechnical Engineering Satellite Conference, Ed: A.M. Ansal, Istanbul, pp.33-42.

Yasuhara K. Murakami S. Toyota N. Hyde A.F.L. (2001). "Settlements in fine-grained soils under cyclic loading,” *Soils and Foundations*, J.G.S., Vol.41, No.6, pp.25-36.

Yin J.H., Wang Y.J., and Selvadurai A.P.S. (2001). “Influence of nonassociativity on the bearing capacity of a strip footing,” *Journal of Geotechnical and Geoenvironmental Engineering*, A.S.C.E., Vol.127,No.11,pp.985-989.

Yoshimi Y., and Tokimatsu K. (1977). "Settlement of Buildings on Saturated sand during earthquakes", *Soils and Foundations*, J.S.S.M.F.E., Vol.17, No.1, pp. 23-38.

Zadroga B. (1994). "Bearing capacity of shallow foundations on noncohesive soils,” *Journal of Geotechnical Engineering,* Vol.120, No.11, pp.1991-2008.

Zeevaert L. (1991). "Seismosoil dynamics of foundations in Mexico City Earthquake, September 19, 1985,” *Journal of Geotechnical Engineering,* Vol. 117, No. 3, pp.376-427.

Zeng X., and Steedman R.S. (1998). "Bearing capacity failure of shallow foundations in earthquakes,” *Geotechnique, Vol.48*, No.2, pp.235-256.

Zhou J., and Gong X. (2001). “Strain Degradation of Saturated Clay under Cyclic Loading Condition,” *Canadian Geotechnical Journal*, Vol.38, 208-212.

Riddel R., Garcia J.E., and Garces E. (2002). "Inelastic deformation response of SDOF systems subjected to earthquakes," *Earthquake Engineering and Structural Dynamics*, Vol. 31, pp. 515-538.

Zeevaert L. (1991). "Seismosoil dynamics of foundations in Mexico City Earthquake, 1985," *Journal of Geotechnical Engineering*, Vol. 117, No. 3, pp. 376-427.

APPENDIX A

BOREHOLE LOCATIONS

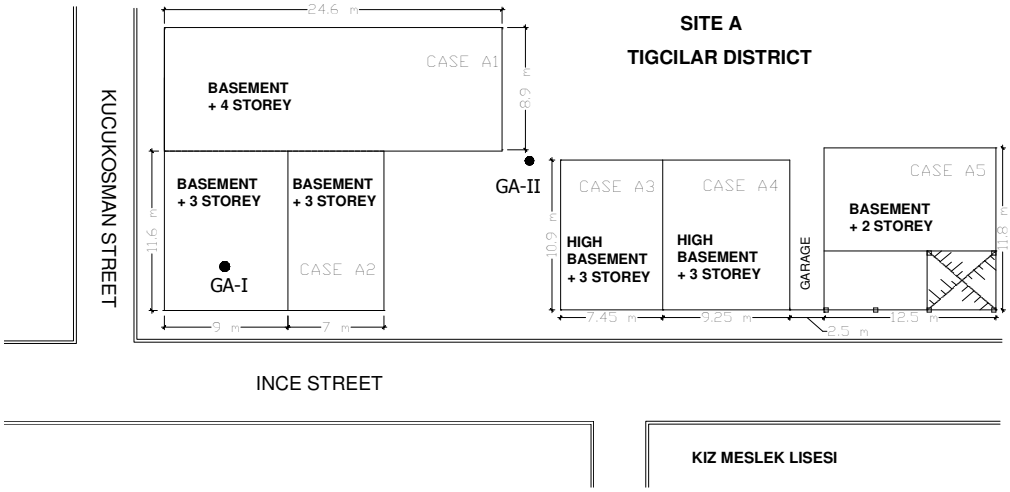

Figure A.1. Plan view of Site A (Karaca, 2001)

Table A.1. Borehole GA-I (N40°46′33″ E30°24′17″) details.

(a)

Depth (m)	Layer
0.0 – 1.0	Artificial fill
1.0 – 2.2	Dark gray sandy silt
2.2 – 6.0	Brown silt
6.0 – 7.5	Dark gray sand

Table A.1 (continued).

(b)

Depth (m)	Test ID
1.60	SPT#1: 1-2-3, 32 cm sample recovered (gray silt)
2.50	SPT#2: 2-1-3, 45 cm sample recovered (dark brown sandy silt)
3.35	SPT#3: 1-2-2, 45 cm sample recovered (0-35 brown silt, 35-45 gray clay)
5.00	UD#4
6.50	SPT#4: 2-4-7, no sample recovered
7.00	SPT#5: 4-3-4, (0-31 cm black sand)

Table A.2. Borehole GA-II (N40°46′31″ E30°24′17″) details.

(a)

Depth (m)	Layer
0.0 – 1.0	Artificial fill
1.0 – 3.4	Brown silt
3.4 – 4.8	Brown silty clay
4.8 – 7.0	Sandy silt / silty sand

(b)

Depth (m)	Test ID
1.50	SPT#1: 3-4-4, 35 cm sample recovered (brown silt)
3.00	UD#2: top 20 cm is lost (loose silt), only bottom 20 cm is recovered
4.00	UD#3
5.50	SPT#4: 1-2-2, no sample recovered

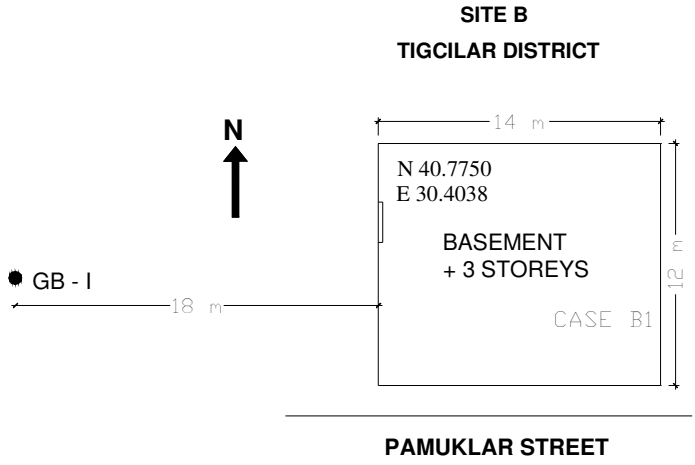

Figure A.2. Plan view of Site B (Karaca, 2001)

Table A.3. Borehole GB – I (N40°46′30″ E30°24′13″) details.

(a)

Depth (m)	Layer
0.0 – 0.5	Artificial fill
0.5 – 5.0	Brown silt
5.0 – 5.8	Brown silty clay

(b)

Depth (m)	Test ID
1.50	SPT#1: 1-2-2, no sample recovered
2.50	SPT#2: 2-2-3, 45 cm sample recovered (0-25 sandy silt, 25-45 clay)
3.50	SPT#3: 1-2-3, 36 cm sample recovered (brown clayey silt)
4.50	SPT#4: 2-2-3, 38 cm sample recovered
5.50	UD#5: only 30 cm sample recovered, stiff layer at 5.80 m

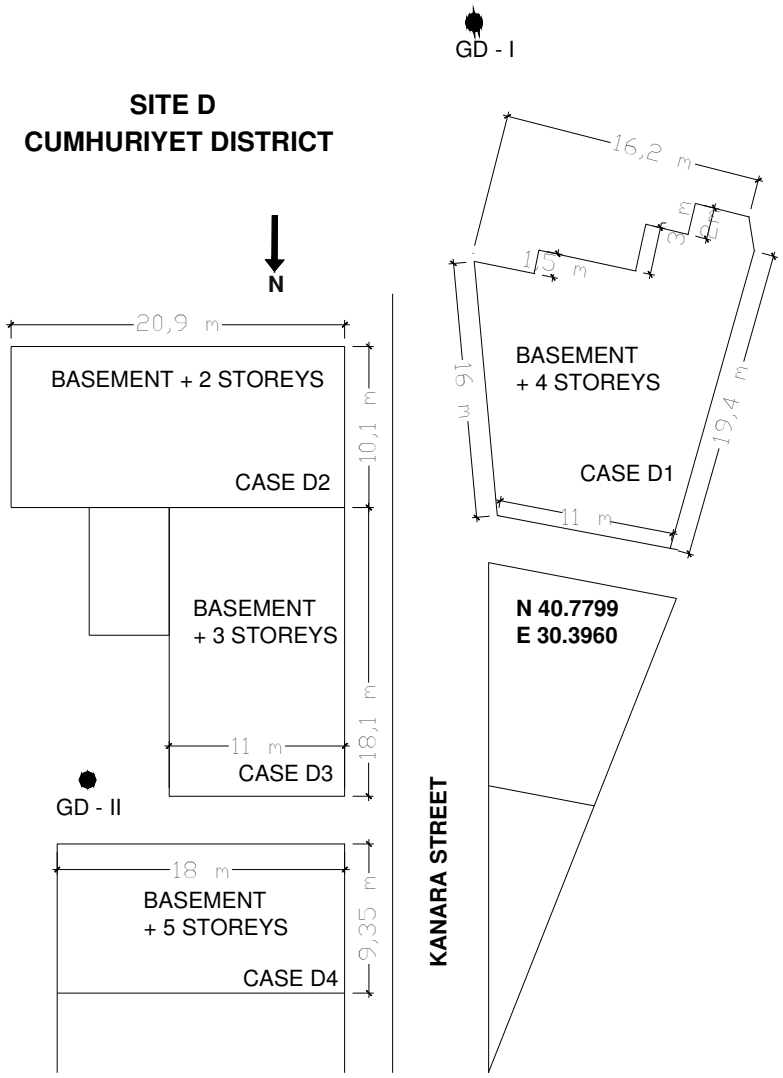

Figure A.3. Plan view of Site D (Karaca, 2001)

Table A.4. Borehole GD– I (N40°46′48″ E30°23′45″) details.

(a)

Depth (m)	Layer
0.0 – 1.5	Artificial fill
1.5 – 5.5	Plastic clay, plasticity is decreasing by depth
5.5 – 7.8	Dark green silty clay
7.8 – 10.5	Clay
10.5 – 11.0	Sand

Table A.4 (continued).

(b)

Depth (m)	Test ID
2.00	UD#1
4.50	UD#2
6.00	UD#3
10.50	SPT#1: 9-21-28, 44 cm sample recovered

Table A.5. Borehole GD– II (N40°46′47″ E30°23′45″) details.

(a)

Depth (m)	Layer
0.0 – 7.0	Plastic Clay

(b)

Depth (m)	Test ID
2.00	UD#1
5.00	UD#2

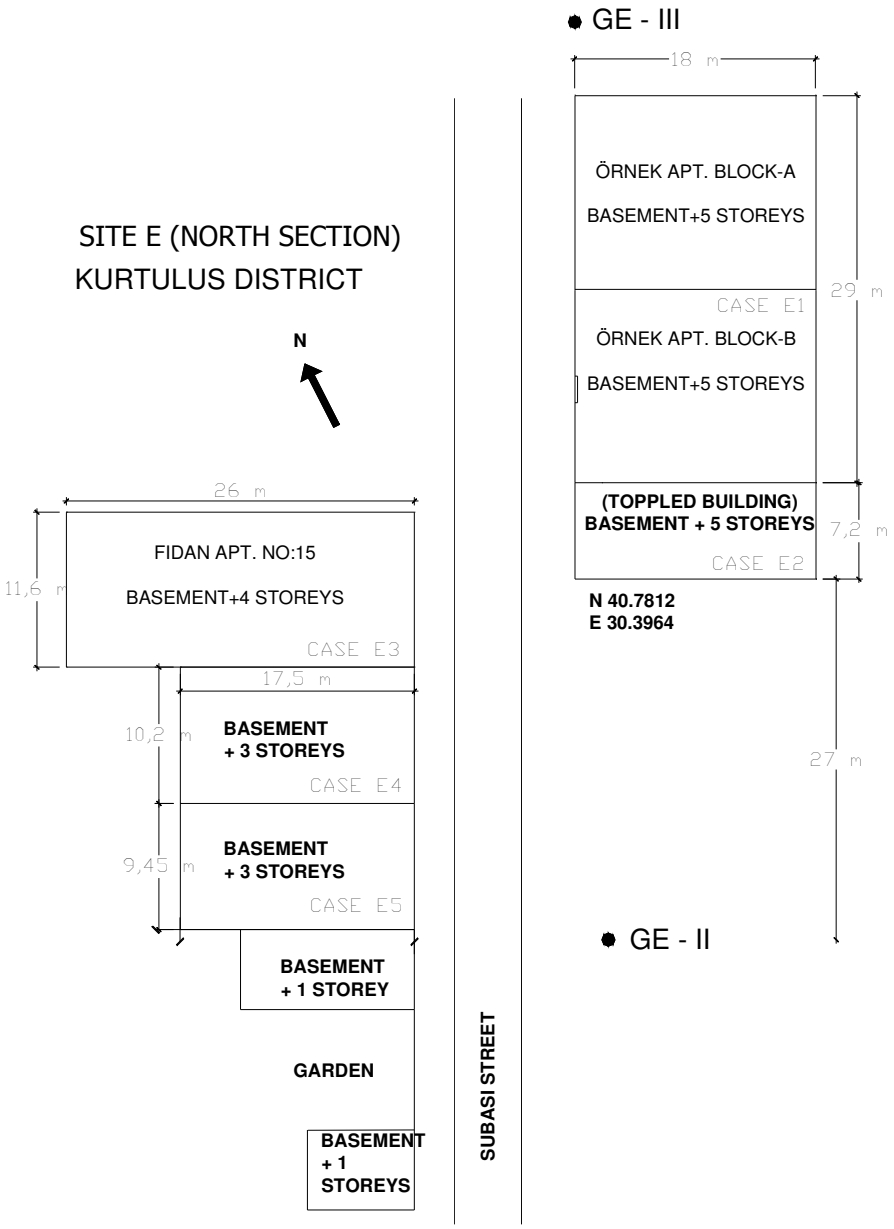

(a)

Figure A.4. Plan view of Site E (Karaca, 2001)

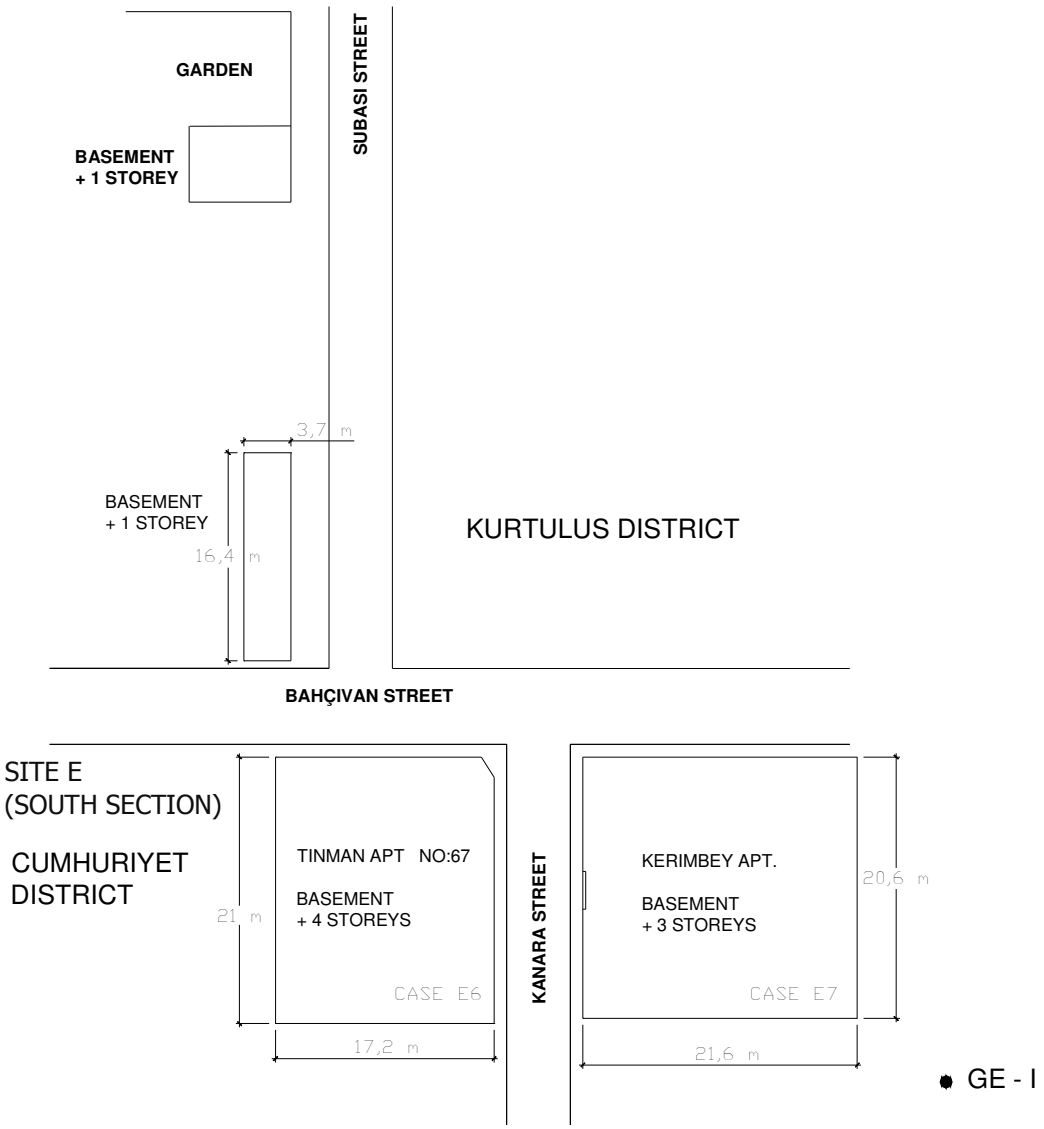

(b)

Figure A.4 (continued).

Table A.6. Borehole GE – I (N40°46′49″ E30°23′48″) details.

(a)

Depth (m)	Layer
0.0 – 1.5	Artificial fill
1.5 – 2.6	Organic, highly plastic dark green clay
2.6 – 7.5	Light brown plastic clay
7.5 – 10.0	Green silty clay

Table A.6 (continued).

(b)

Depth (m)	Test ID
2.20	UD#1
4.00	UD#2
6.25	UD#3

Table A.7. Borehole GE – II (N40°46′52″ E30°23′47″) details.

(a)

Depth (m)	Layer
0.0 – 1.7	Artificial fill
1.7 – 7.0	Light brown clay

(b)

Depth (m)	Test ID
2.30	UD#1
4.50	UD#2

Table A.7. Borehole GE – III (N40°46′54″ E30°23′47″) details.

(a)

Depth (m)	Layer
0.0 – 1.7	Artificial fill
1.7 – 4.0	Dark green organic clay
4.0 – 7.5	Brown clay

(b)

Depth (m)	Test ID
3.05	UD#1
5.00	UD#2
7.00	UD#3

APPENDIX B

TRIAXIAL TEST PLOTS

Monotonic Shear Strength Test Results

Table.B.1. Sample properties

Test Data									
Test No:	1	2	3	4	5	6	7	8	9
Initial height of the specimen (mm)	71	71	71	71	71	71	71	71	71
Initial diameter of the specimen (mm)	36	36	36	36	36	36	36	36	36
Initial mass of the specimen (g)	136	130	134	120	128	125	131	131	128
Bulk density (g/ml)	1.88	1.80	1.85	1.66	1.77	1.73	1.81	1.82	1.77
Mositure content (%) (before testing)	35	40	38	36	40	46	37	32	39
Mositure content (%) (after testing)	31	34	?	?	47	43	?	?	?
Cell pressure (kPa)	60	70	80	80	60	40	80	100	50
Proving ring constant Cp (kg/div.)	0.097	0.097	0.097	0.097	0.097	0.97	0.97	0.97	0.97
Consolidation stresses (kPa)									
σ_3	60	70	80	80	60	40	80	100	50
σ_1	90	100	120	120	140	140	200	200	170
Sample information									
Borehole No.	GE-1	GE-1	GE-1	GE-2	GE-2	GD-2	GD-2	GA-3	GD-2
Sample No.	1	2	3	1	1	1	1	3	1
Depth (m)	2.2	4.0	6.3	2.4	2.4	2.0	2.0	4.0	2.0
Atterberg Limits									
LL	39	50	37	36	49	43	43	32	34
PL	25	25	24	28	27	24	24	25	24
PI	14	25	13	8	22	19	19	7	10

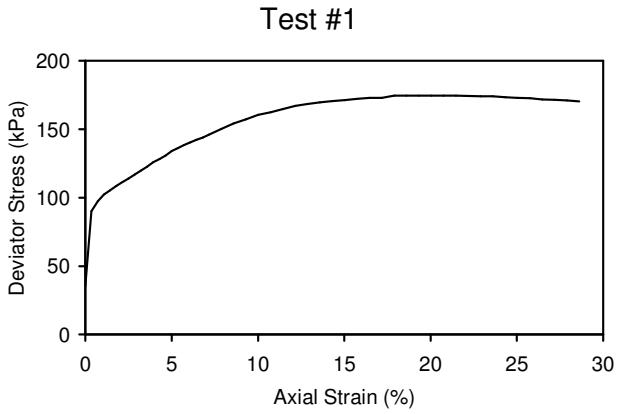

(a)

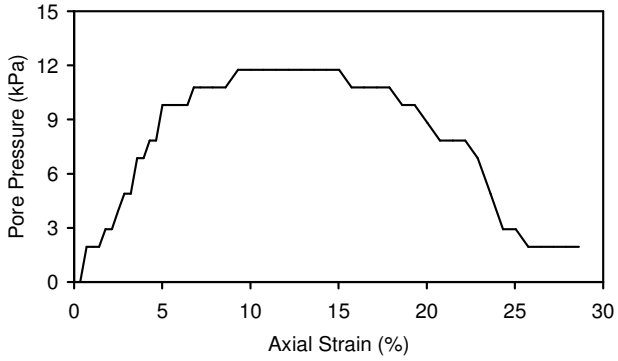

(b)

Figure B.1. Monotonic Loading Test #1.

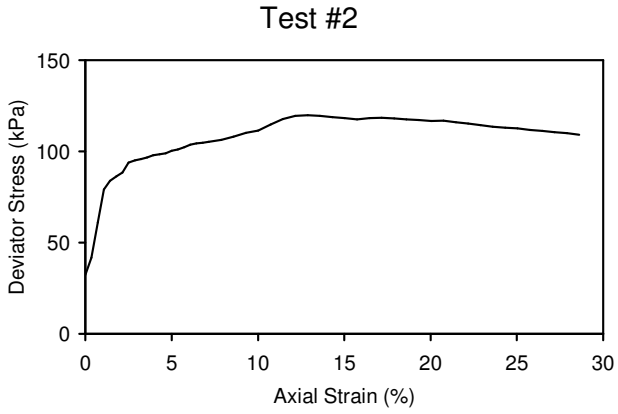

(a)

Figure B.2. Monotonic Loading Test #2.

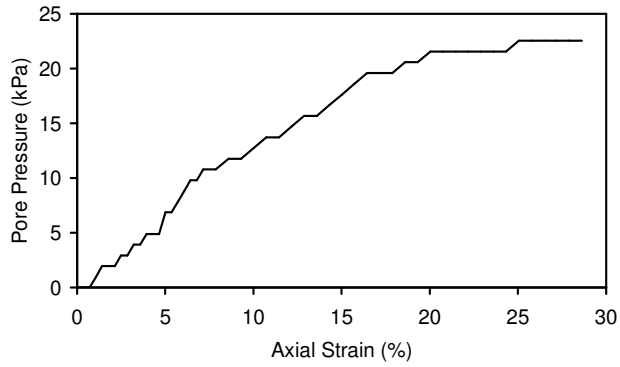

(b)

Figure B.2 (continued).

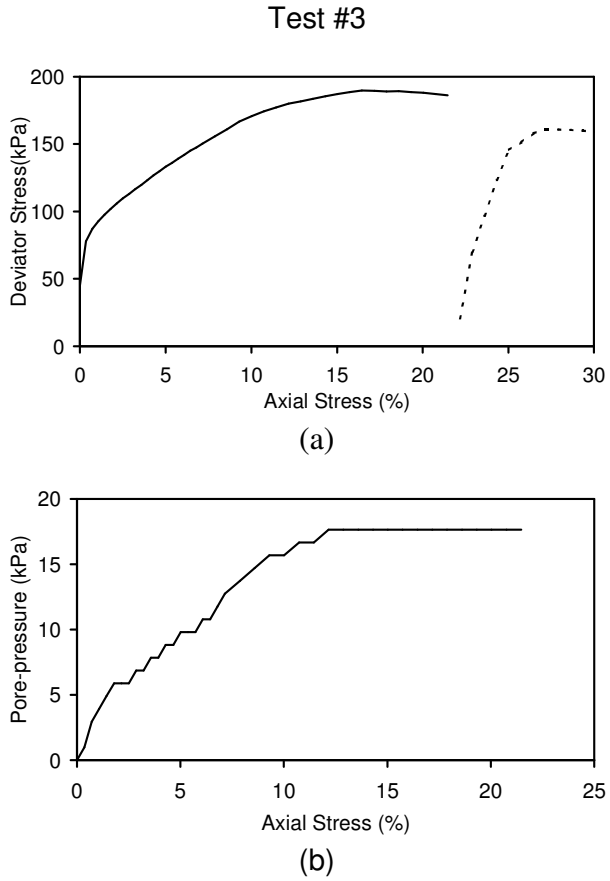

(a)

(b)

Figure B.3. Monotonic Loading Test #3.

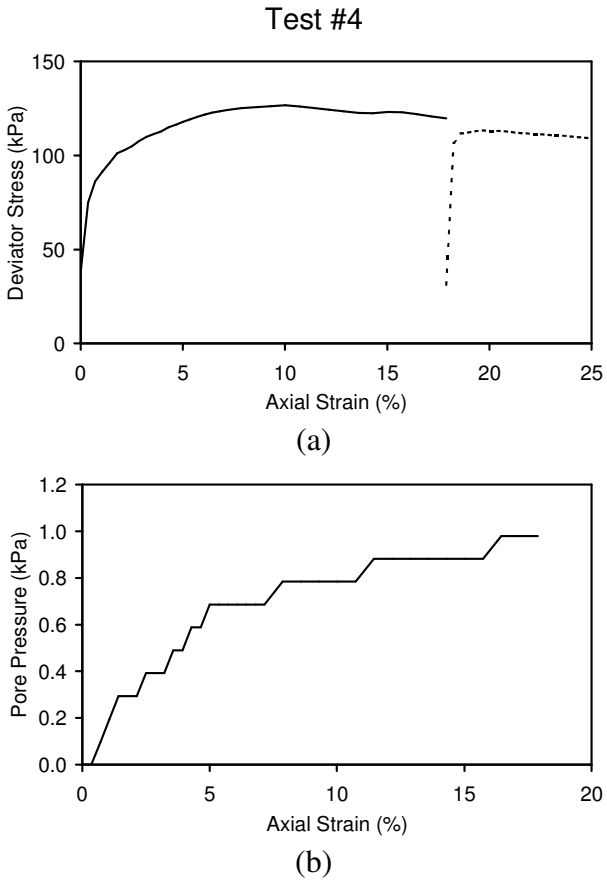

Figure B.4. Monotonic Loading Test #4.

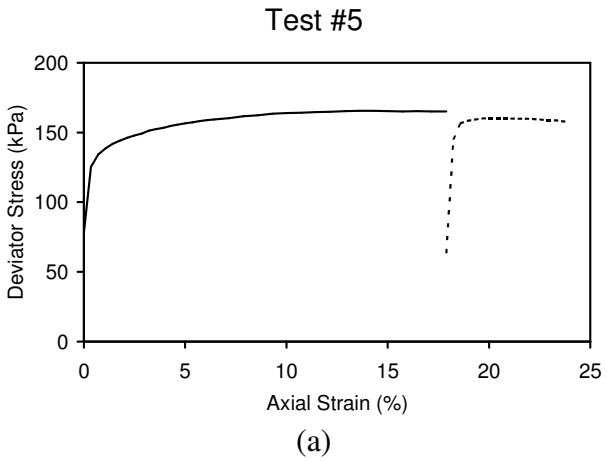

Figure B.5. Monotonic Loading Test #5.

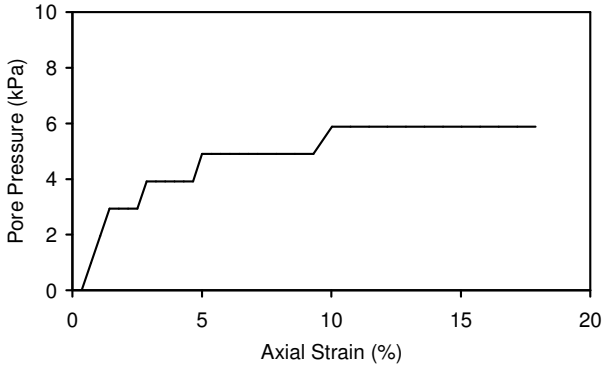

(b)

Figure B.5 (continued).

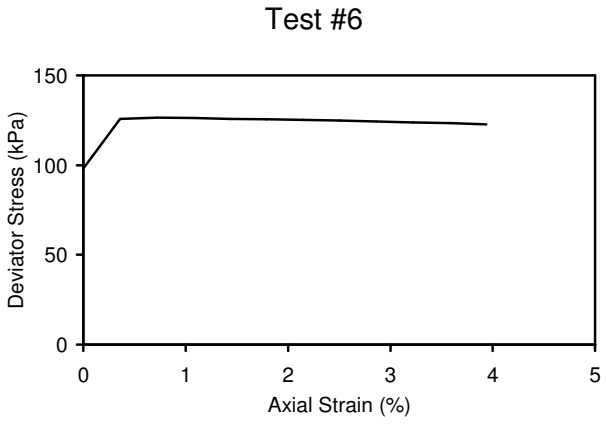

(a)

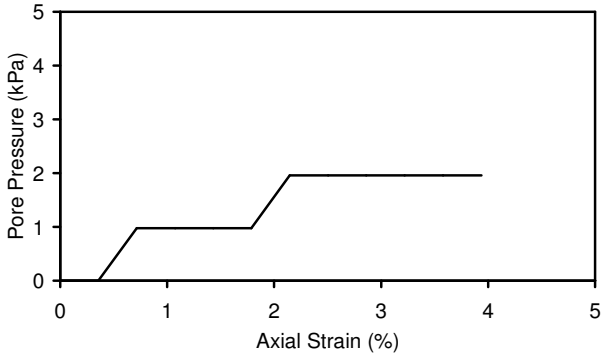

(b)

Figure B.6. Monotonic Loading Test #6.

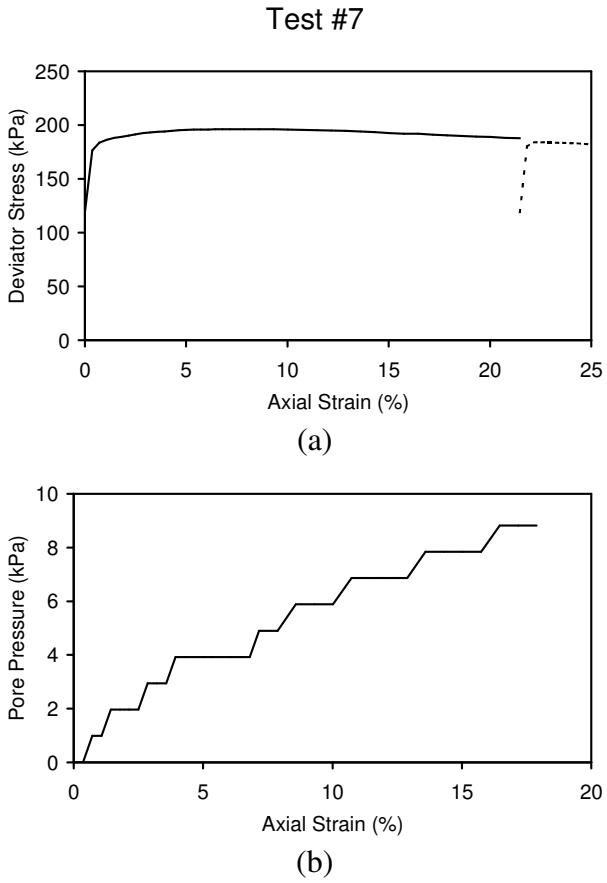

Figure B.7. Monotonic Loading Test #7.

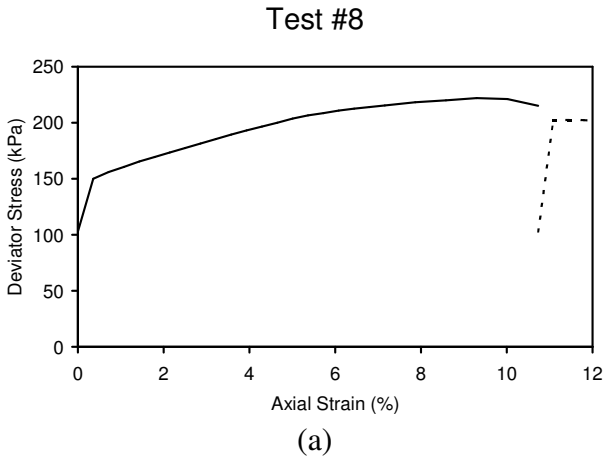

Figure B.8. Monotonic Loading Test #8.

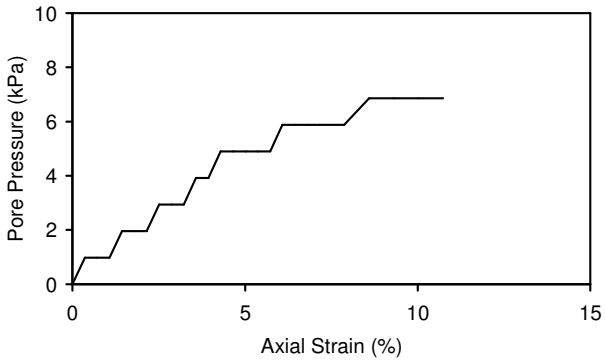

(b)

Figure B.8 (continued).

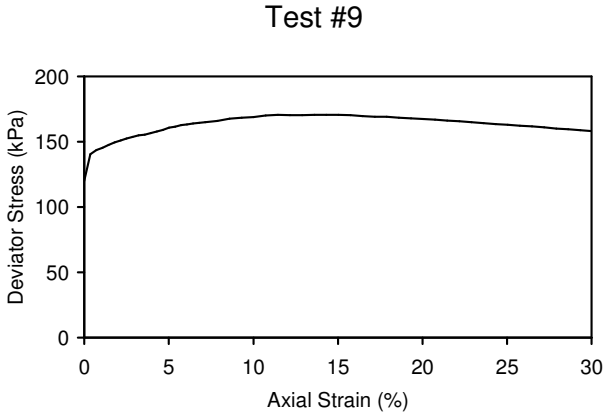

(a)

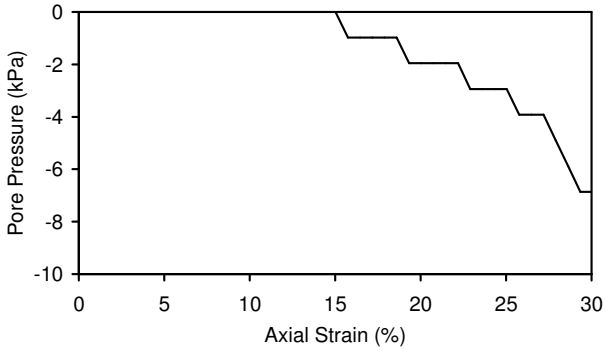

(b)

Figure B.9. Monotonic Loading Test #9.

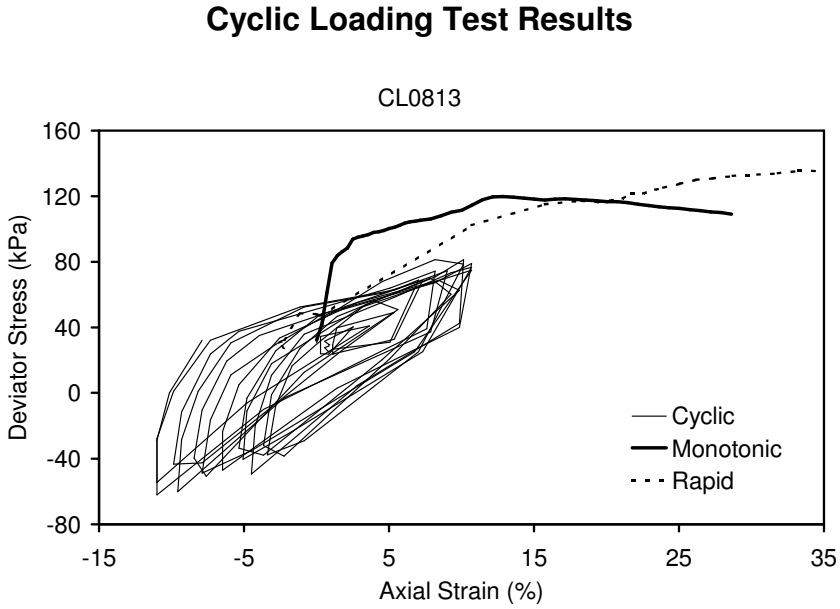

Figure B.10. Cyclic Loading Test CL0813.

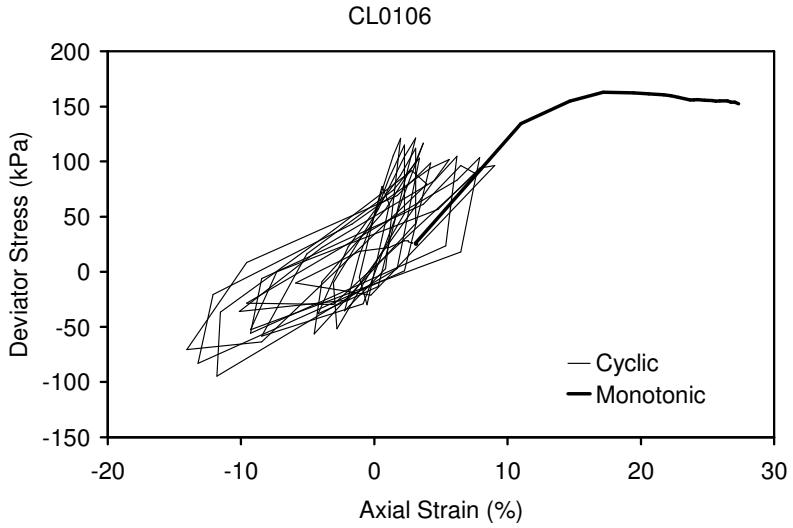

Figure B.11. Cyclic Loading Test CL0106.

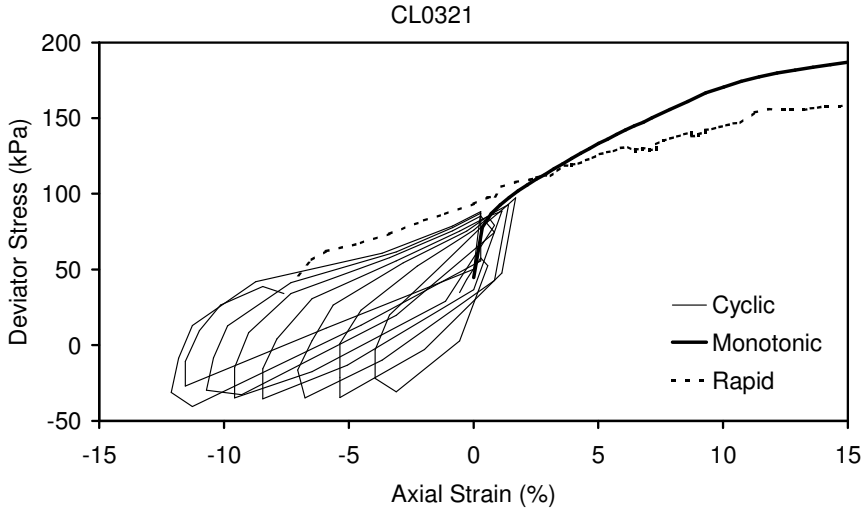

Figure B.12. Cyclic Loading Test CL0321.

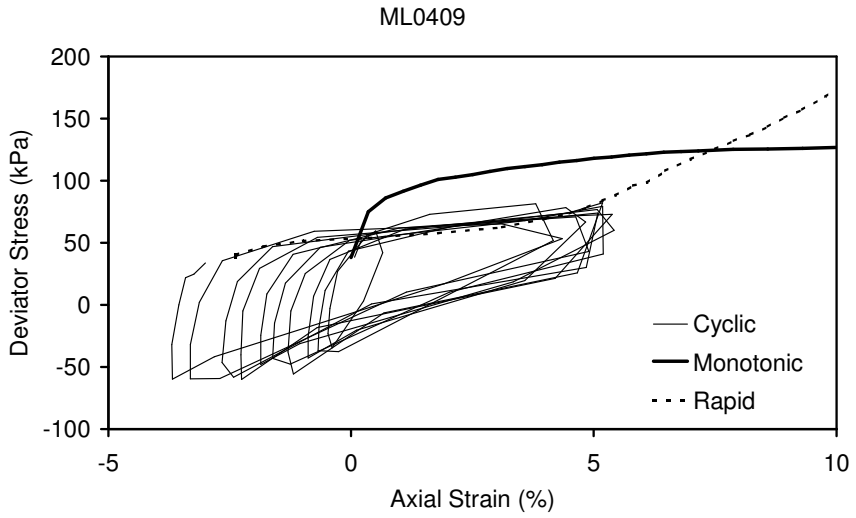

Figure B.13. Cyclic Loading Test CL0409.

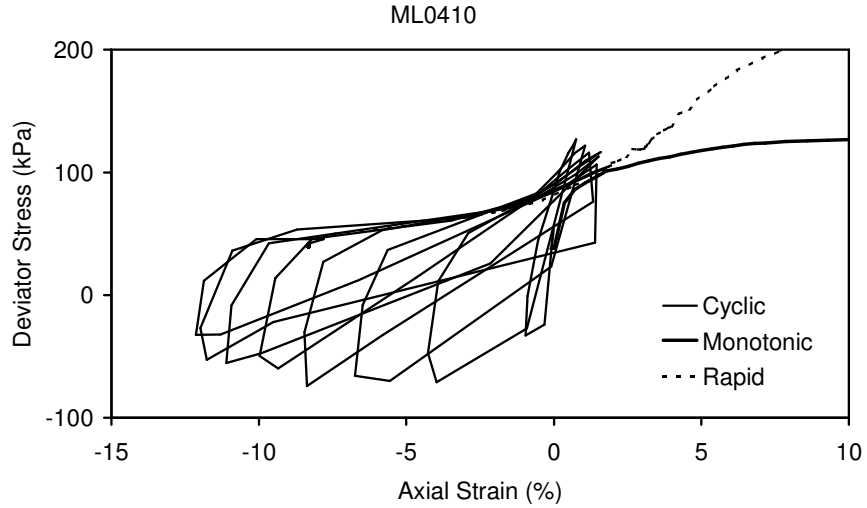

Figure B.14. Cyclic Loading Test ML0410.

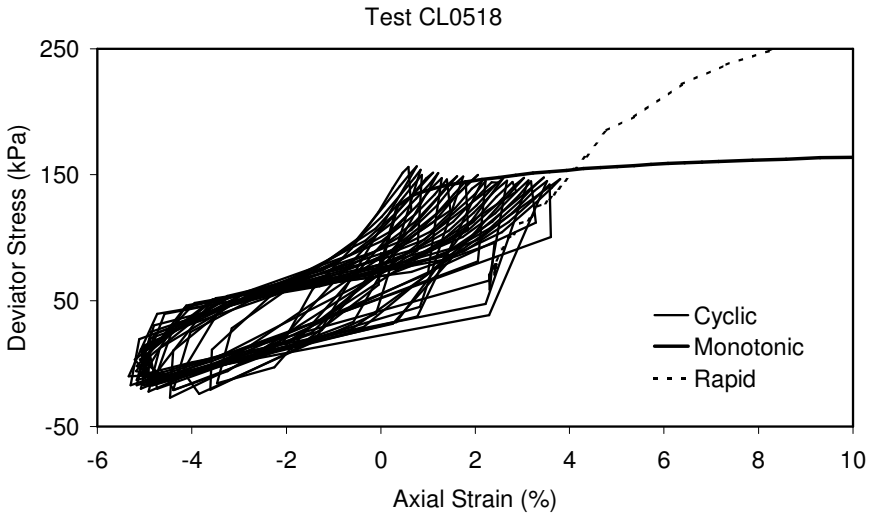

Figure B.15. Cyclic Loading Test CL0518.

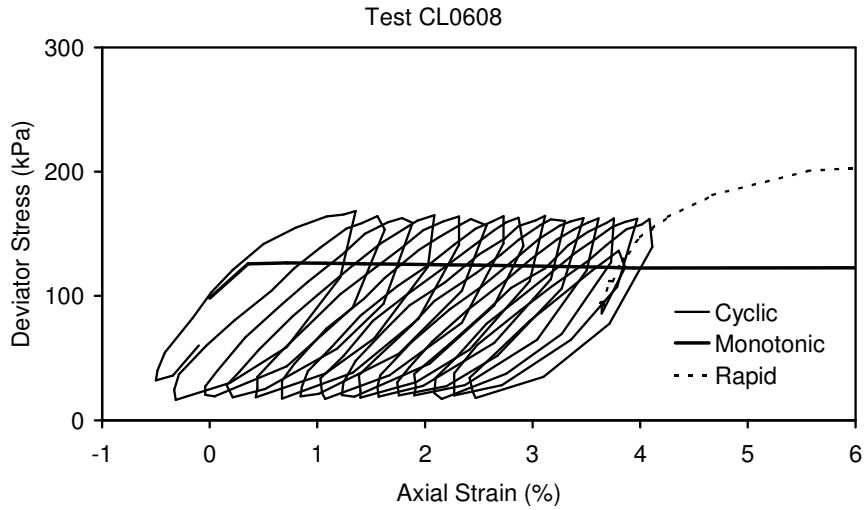

Figure B.16. Cyclic Loading Test CL0608.

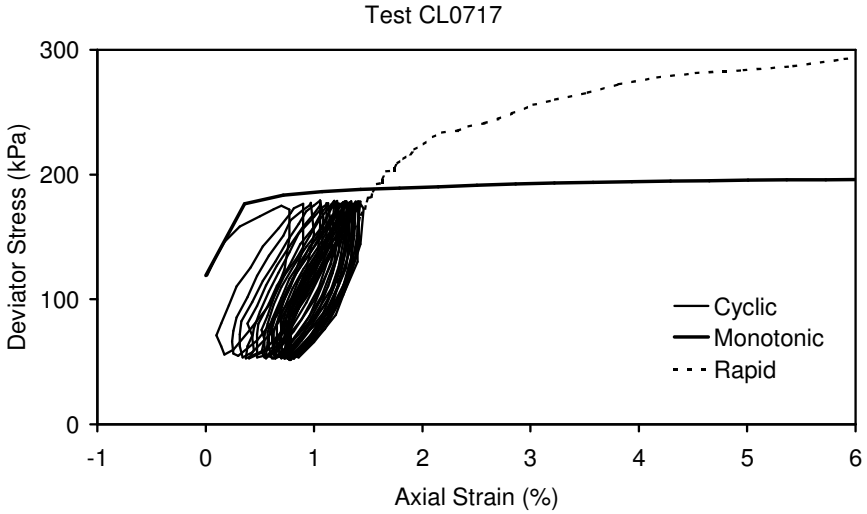

Figure B.17. Cyclic Loading Test CL0717.

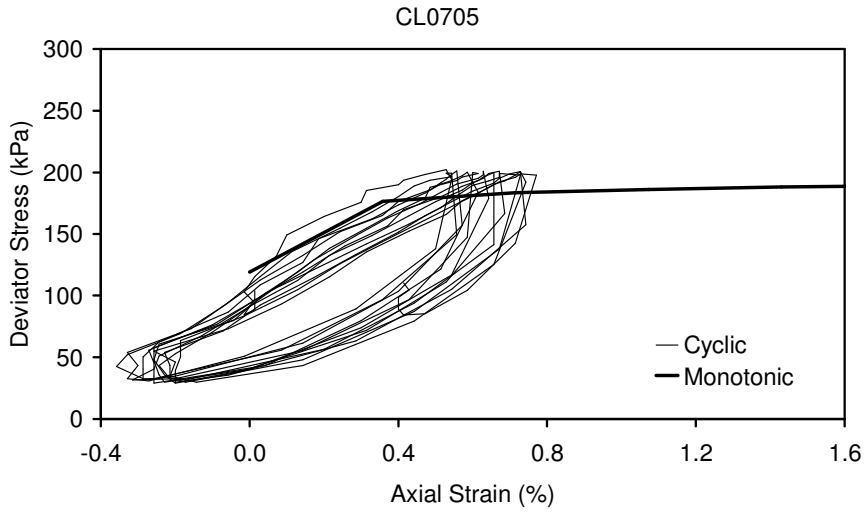

Figure B.18. Cyclic Loading Test CL0705.

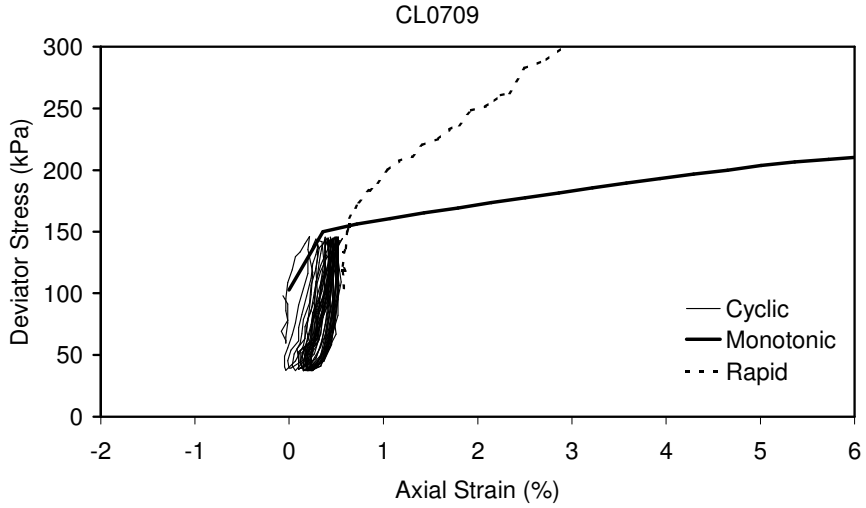

Figure B.19. Cyclic Loading Test CL0709.

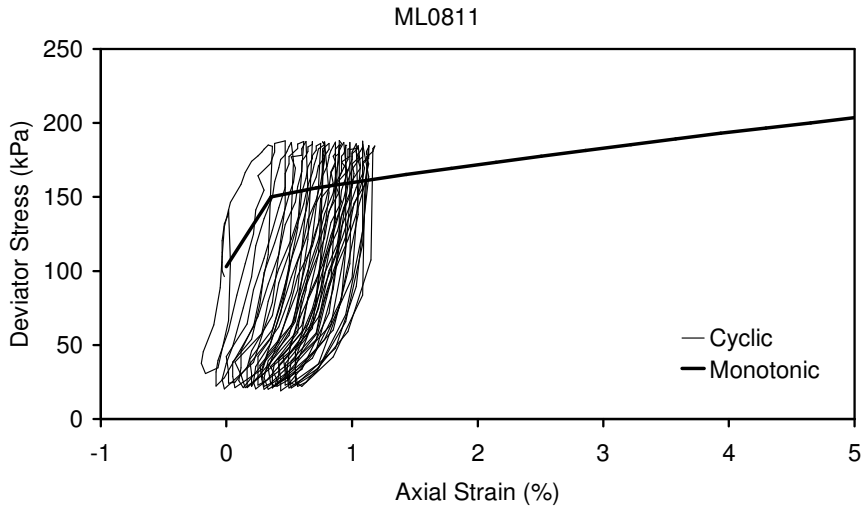

Figure B.20. Cyclic Loading Test ML0811.

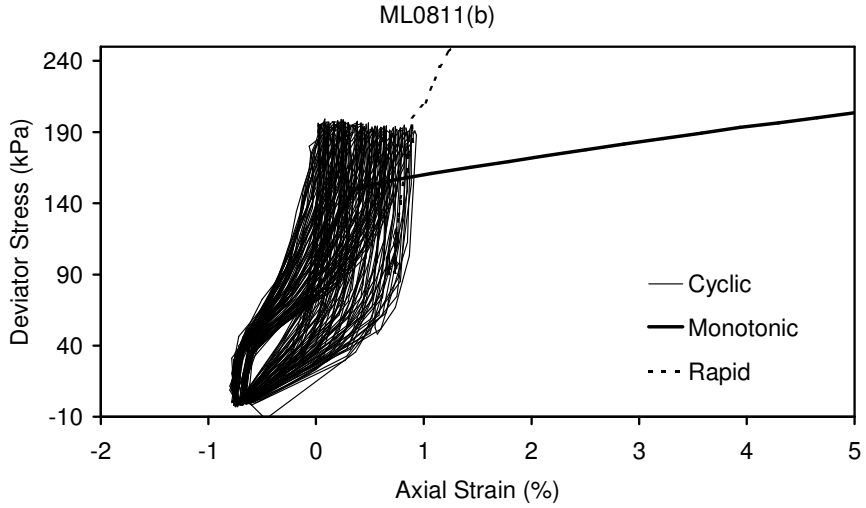

Figure B.21 Cyclic Loading Test ML0811(b).

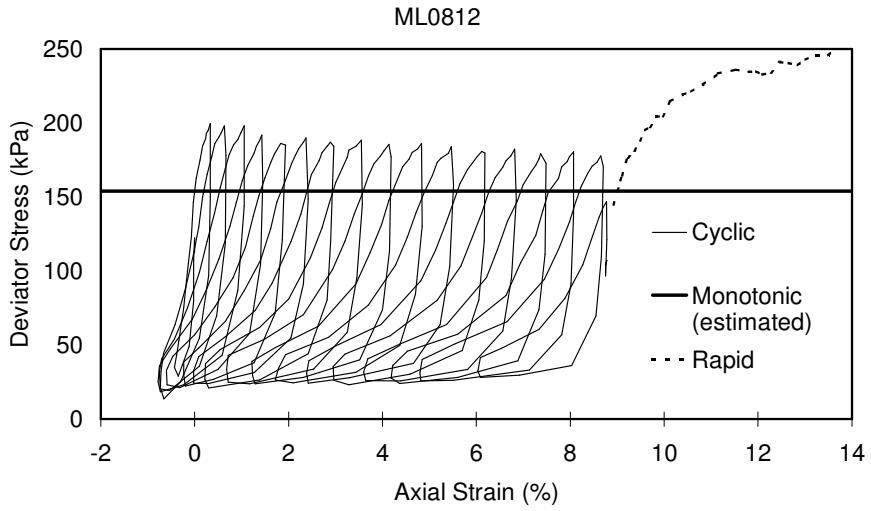

Figure B.22. Cyclic Loading Test ML0812.

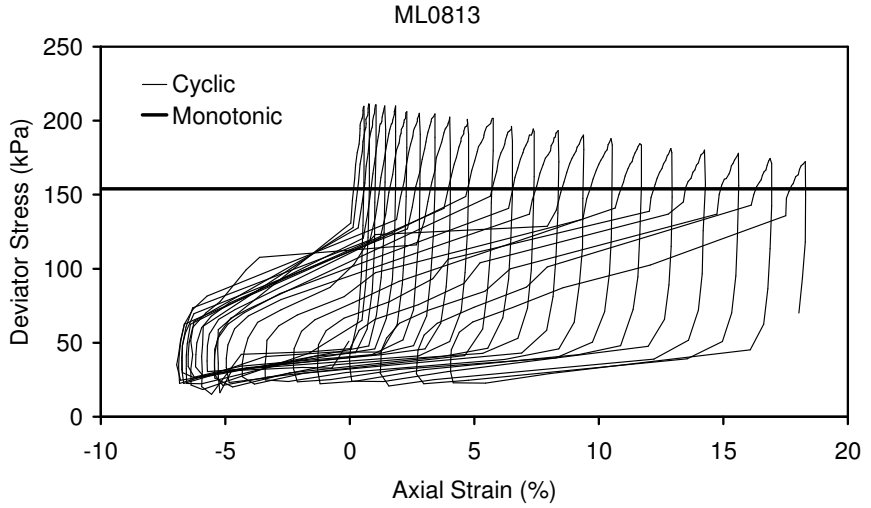

Figure B.23. Cyclic Loading Test ML0813.

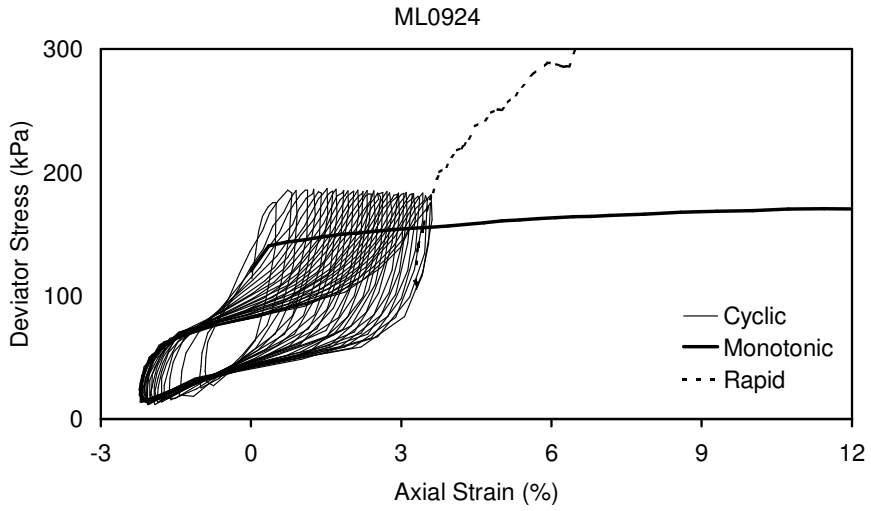

Figure B.23. Cyclic Loading Test ML0924.

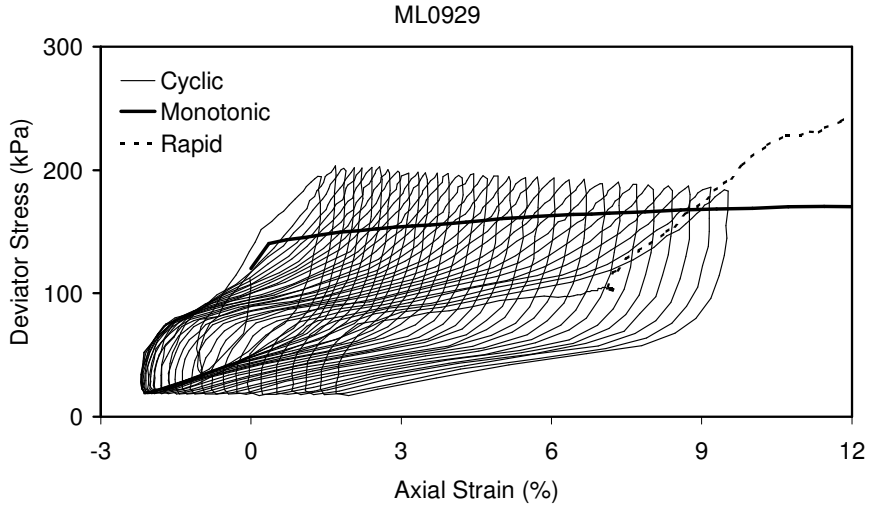

Figure B.24. Cyclic Loading Test ML0929.

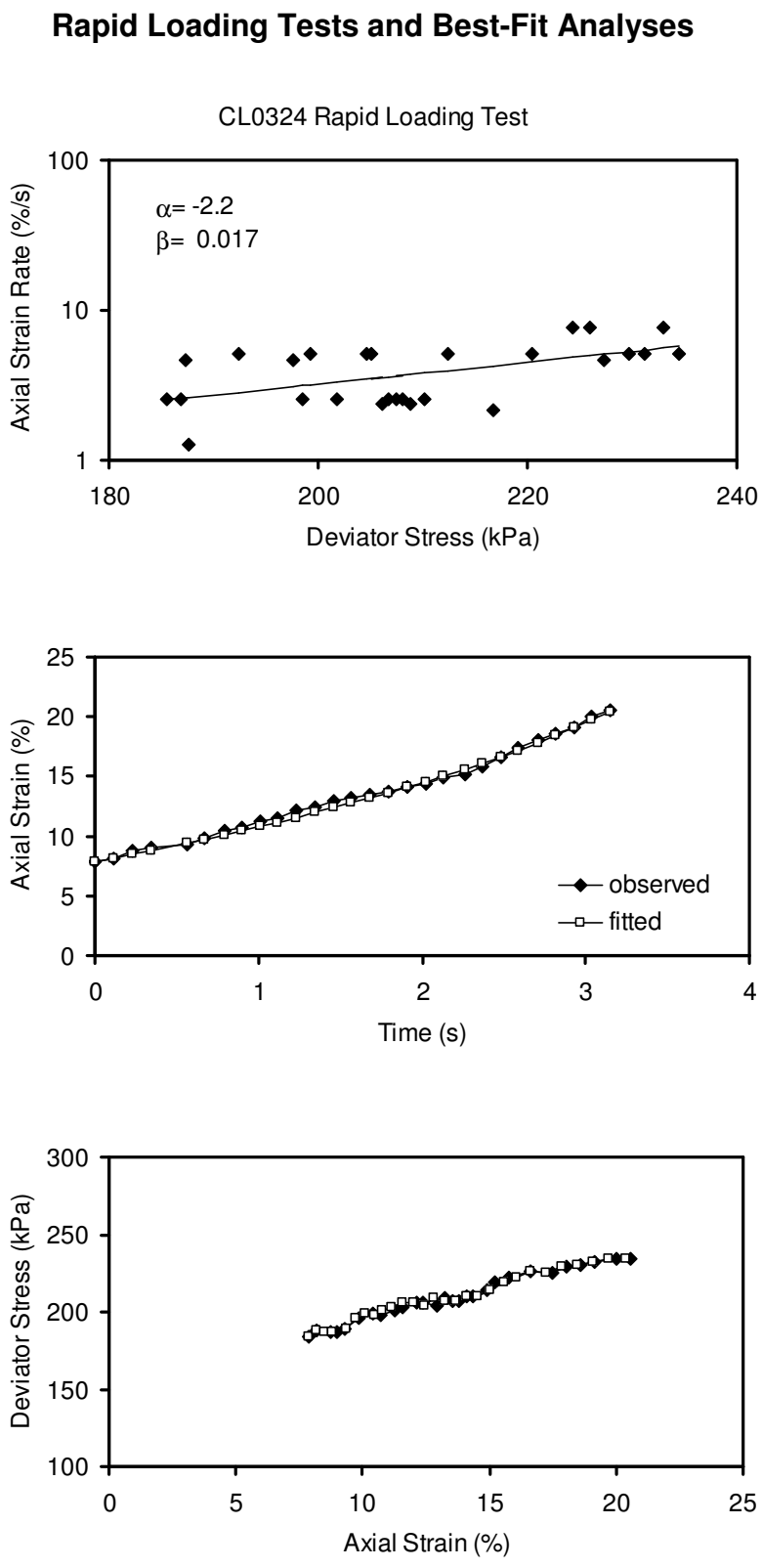

Figure B.25. Rapid loading test results and least squares fit for CL0324.

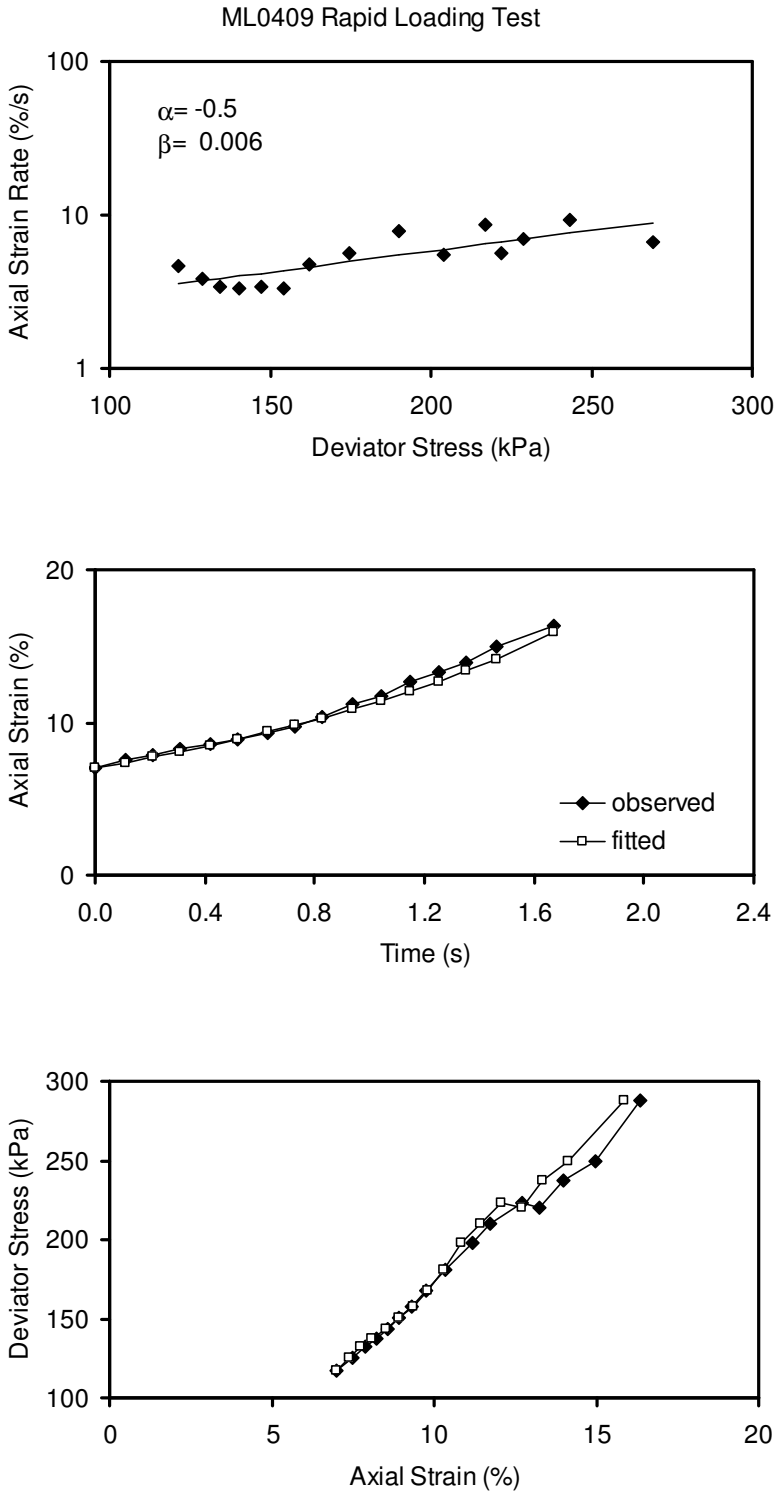

7

Figure B.26. Rapid loading test results and least squares fit for ML0409.

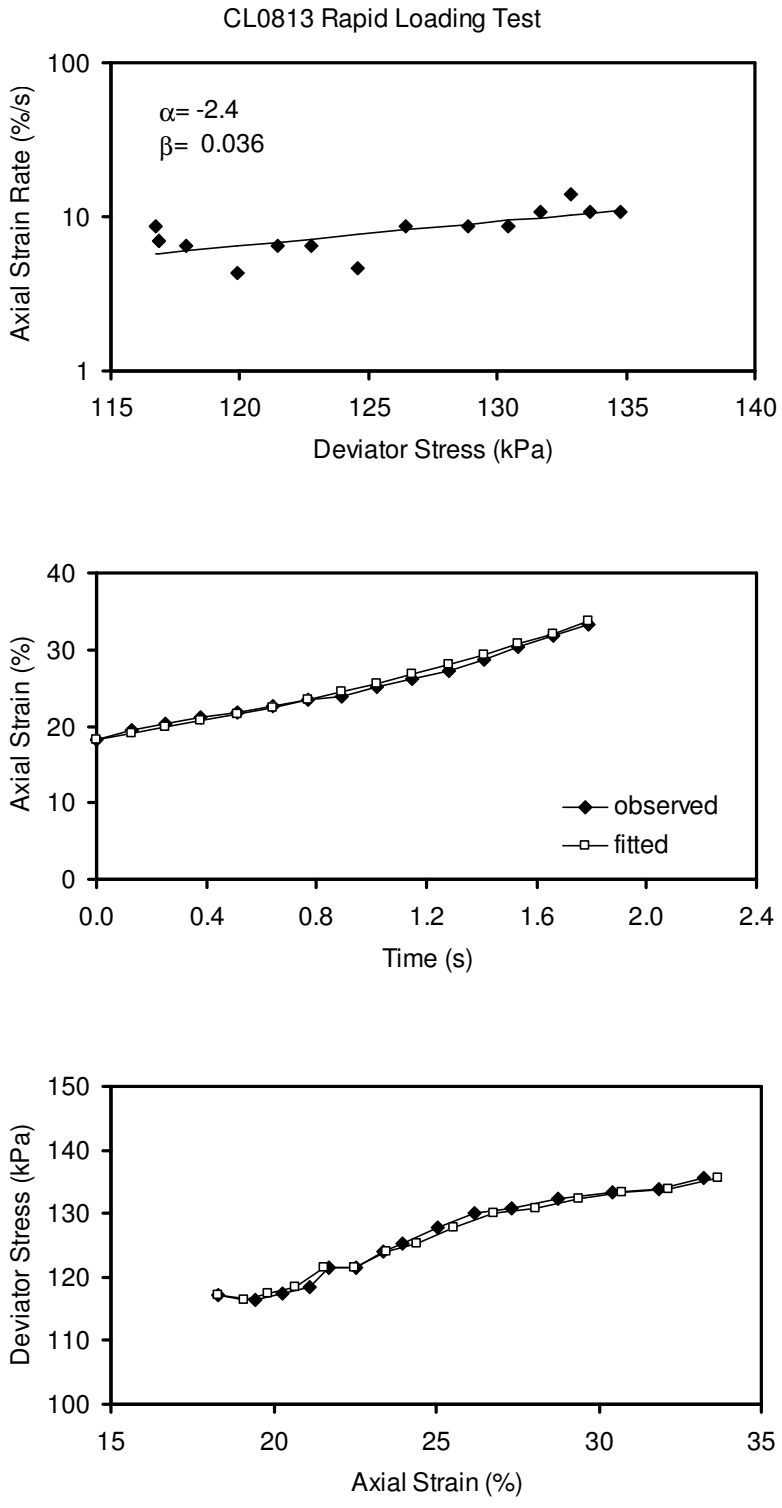

Figure B.27. Rapid loading test results and least squares fit for CL0813.

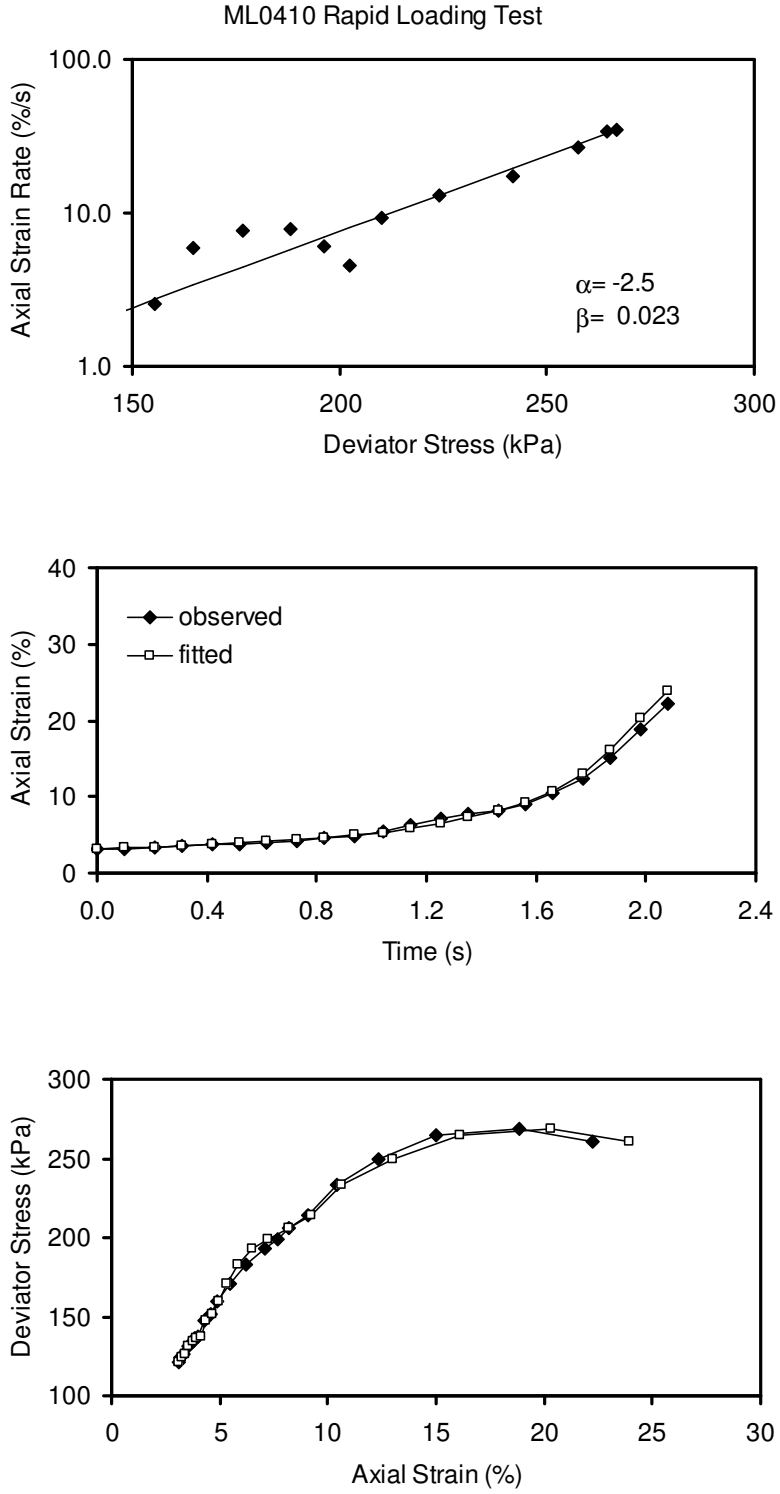

Figure B.28. Rapid loading test results and least squares fit for ML0410.

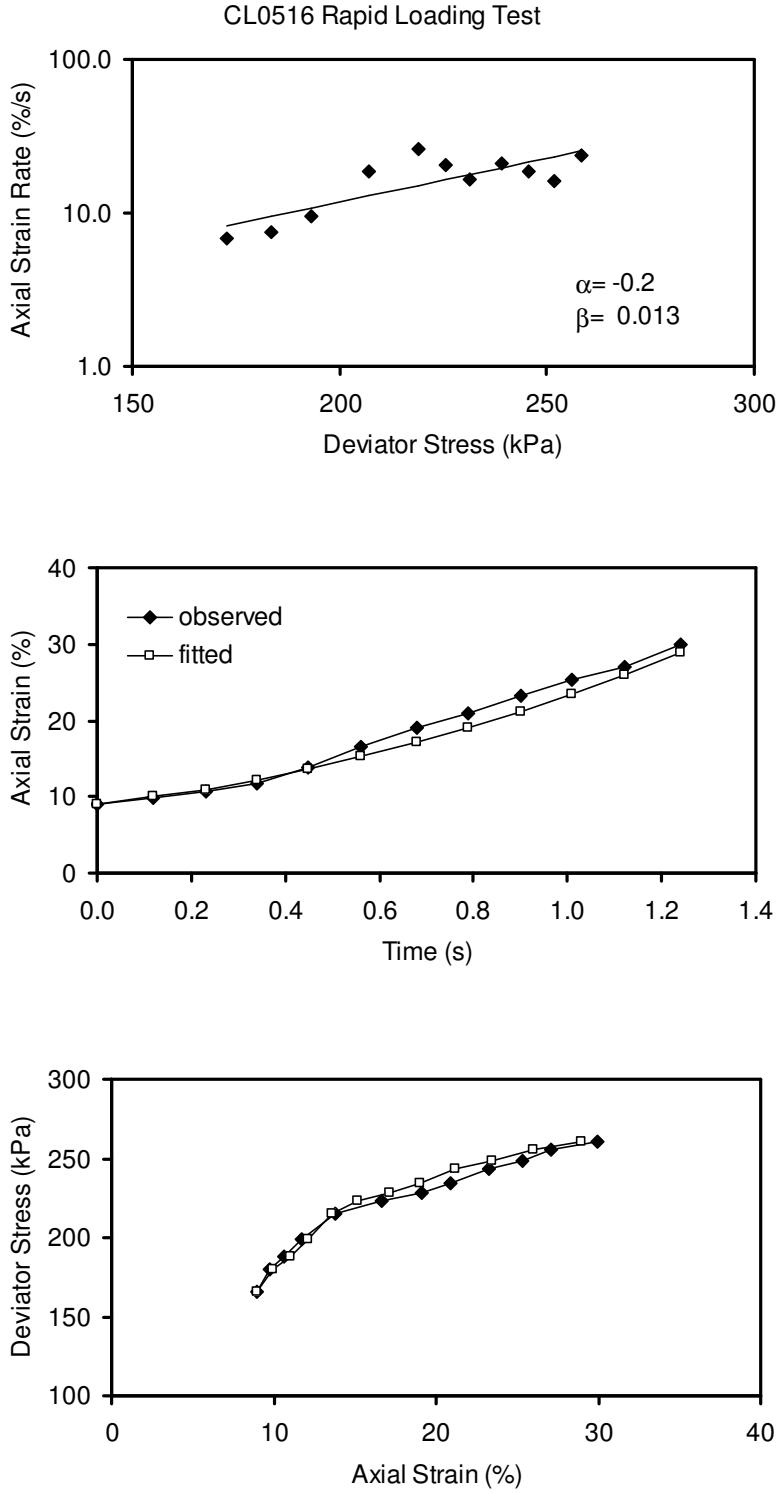

Figure B.29. Rapid loading test results and least squares fit for CL0516.

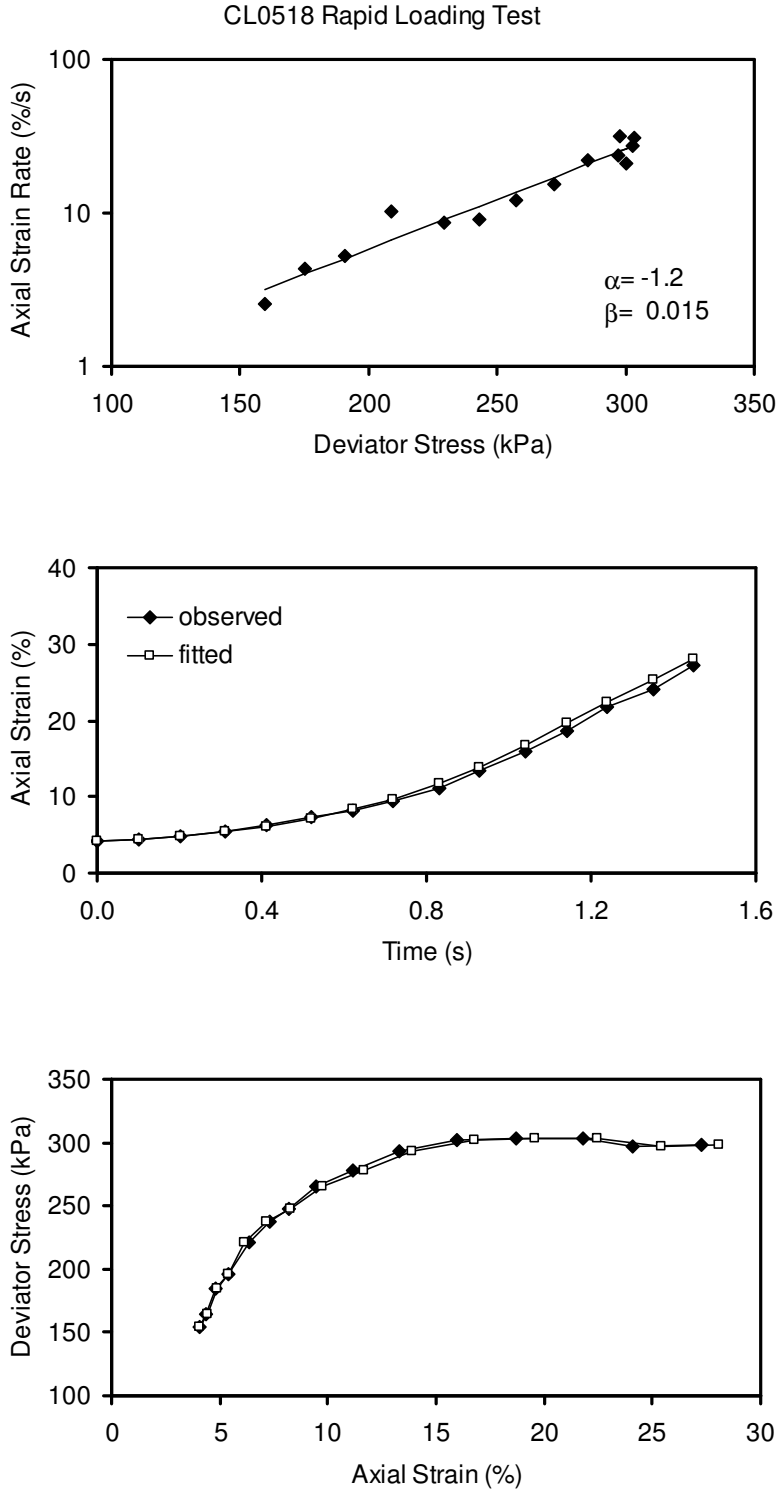

Figure B.30. Rapid loading test results and least squares fit for CL0518.

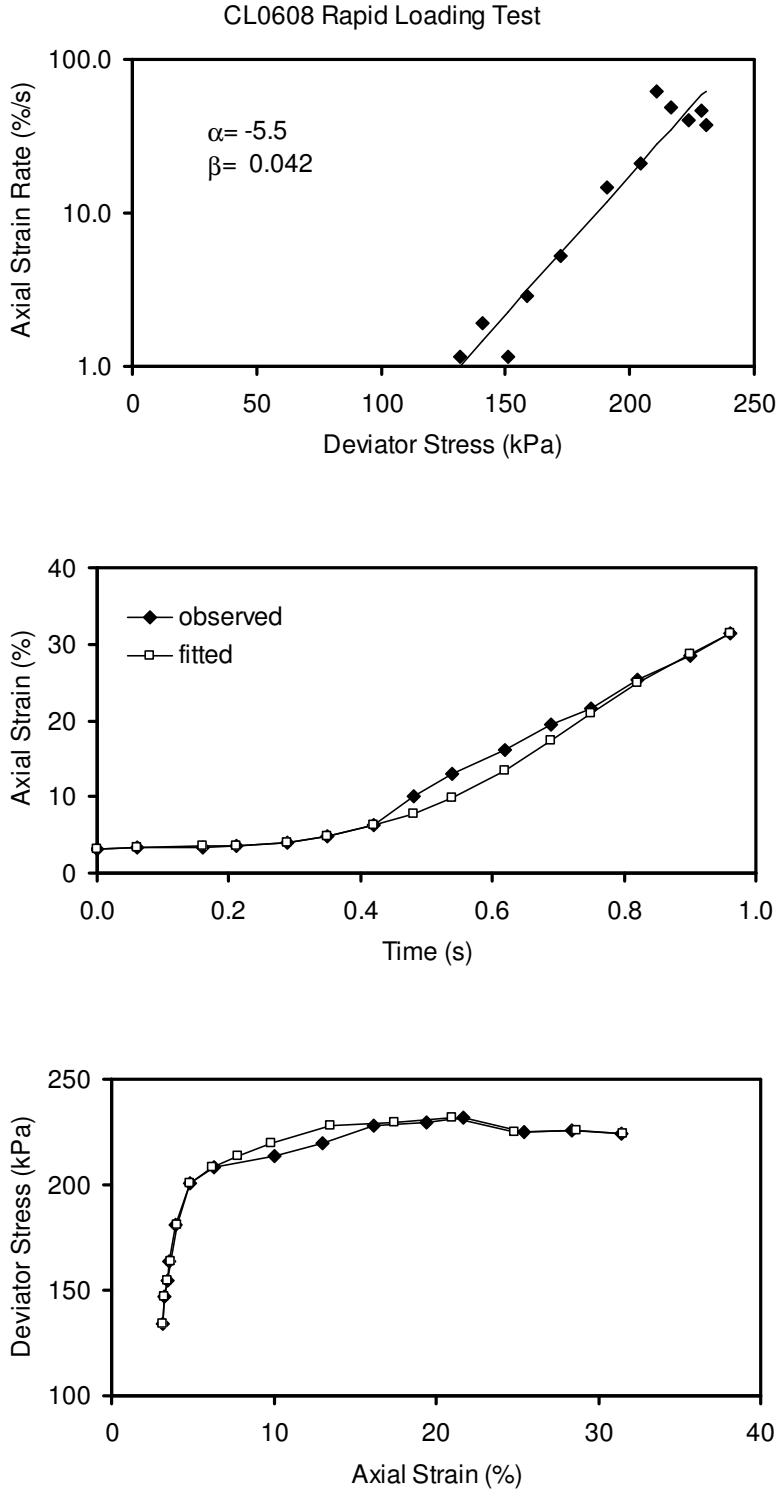

Figure B.31. Rapid loading test results and least squares fit for CL0608.

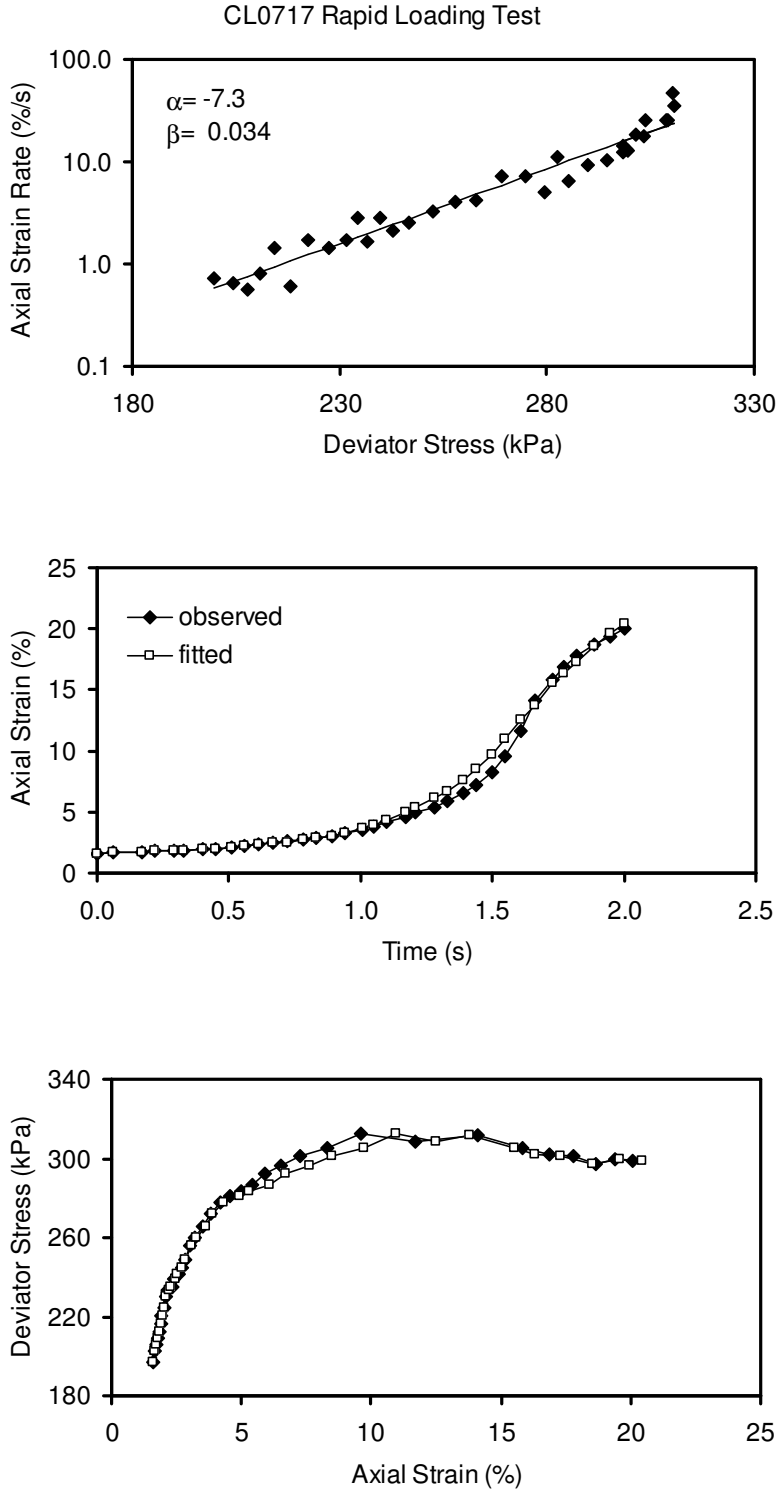

Figure B.32. Rapid loading test results and least squares fit for CL0717.

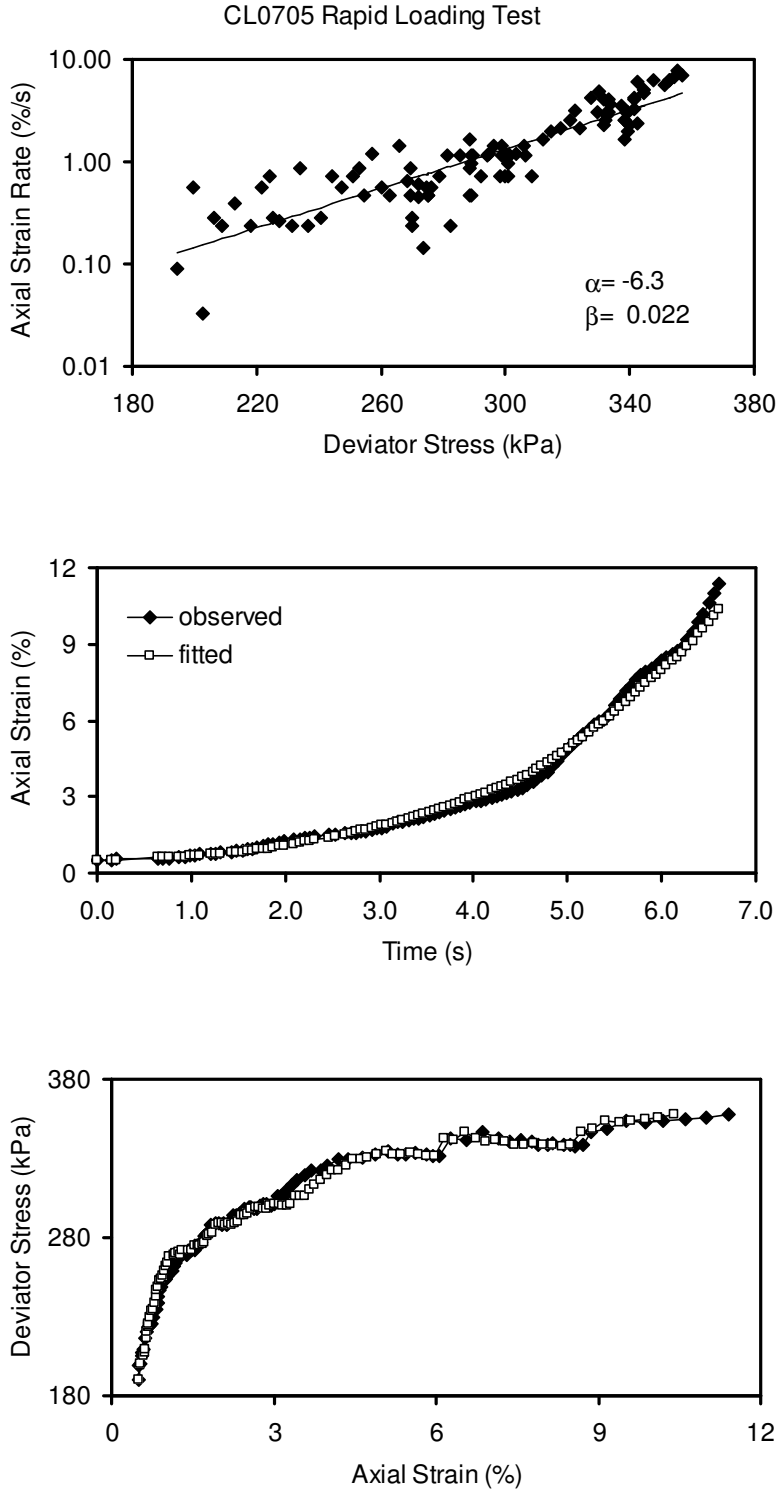

Figure B.33. Rapid loading test results and least squares fit for CL0705.

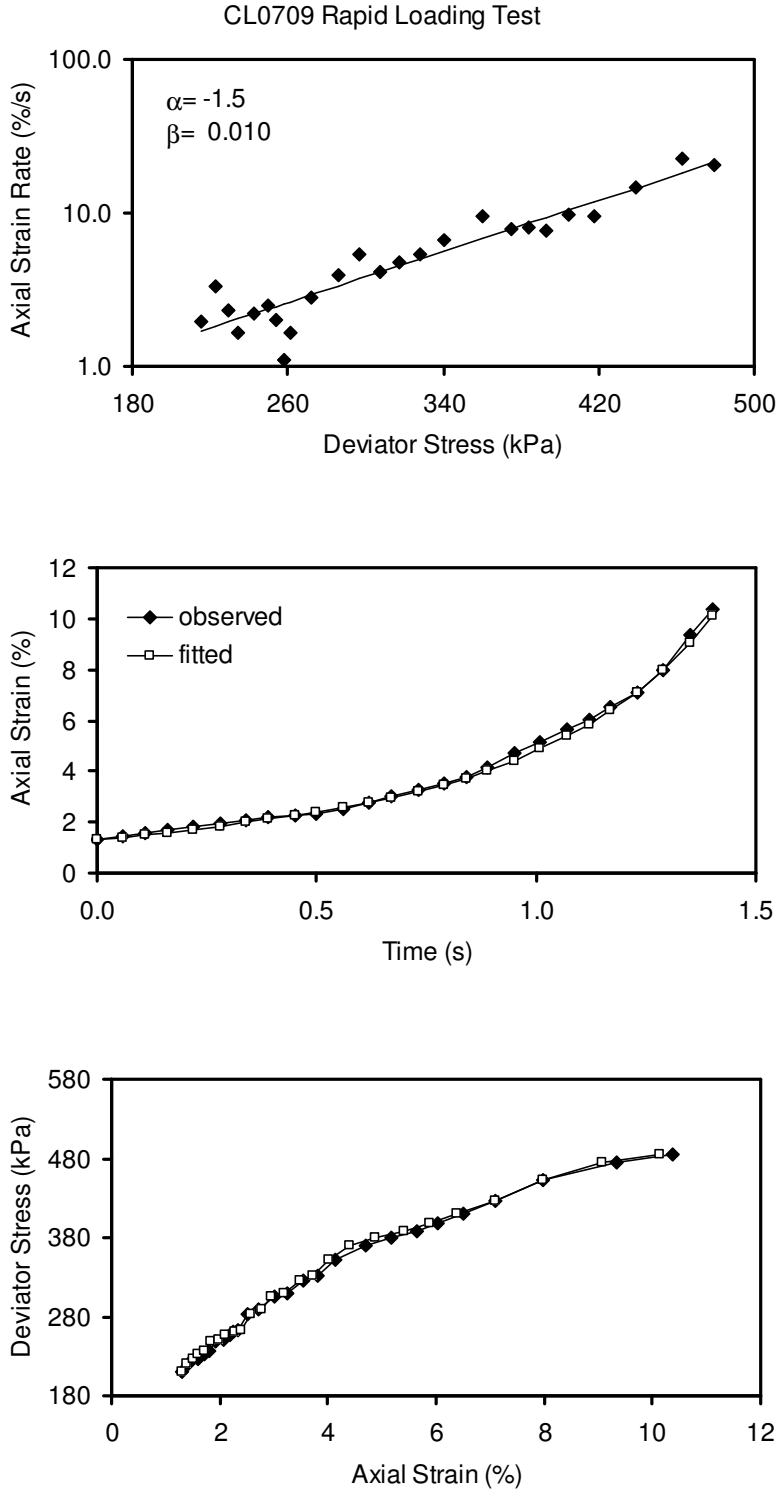

Figure B.34. Rapid loading test results and least squares fit CL0709.

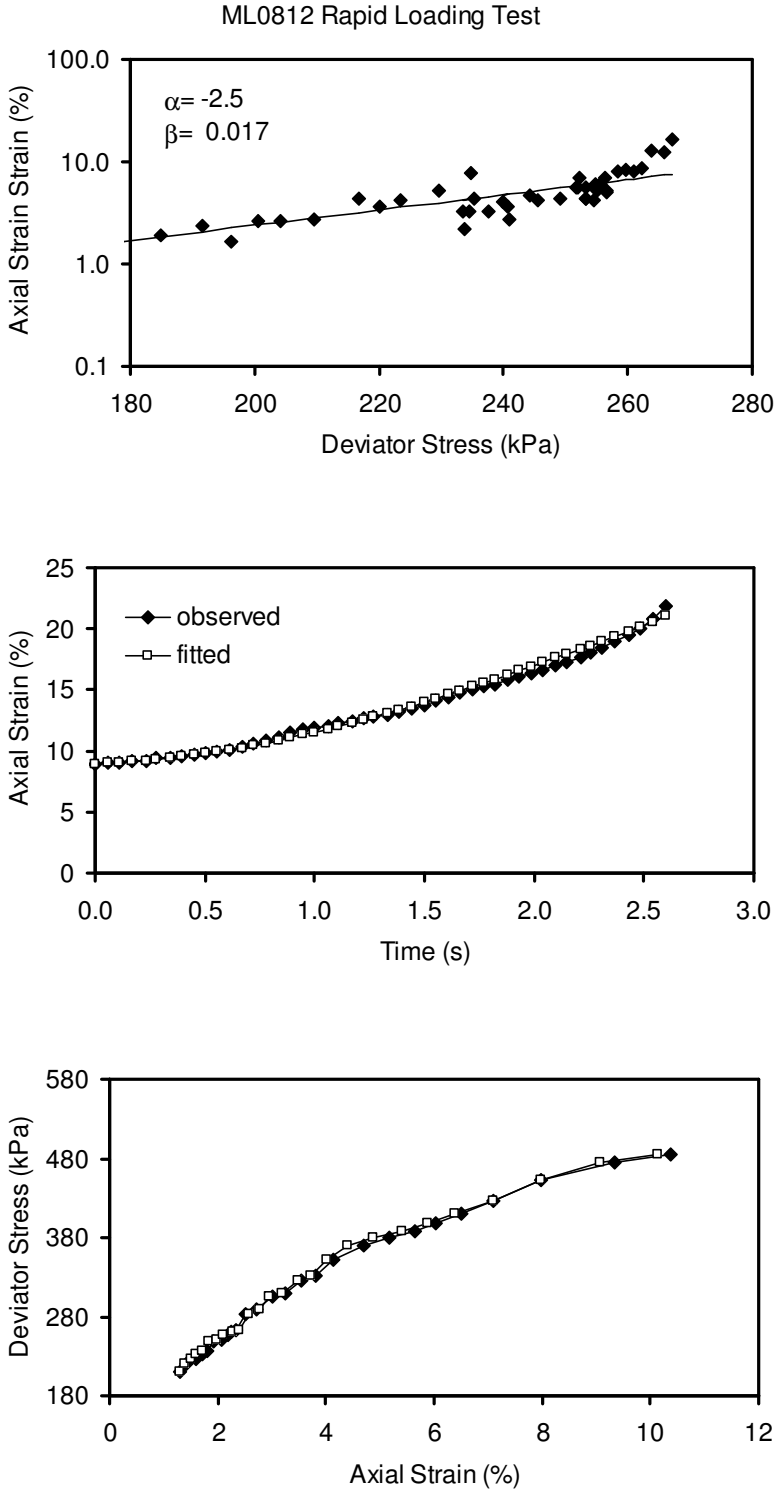

Figure B.35. Rapid loading test results and least squares fit for ML0812.

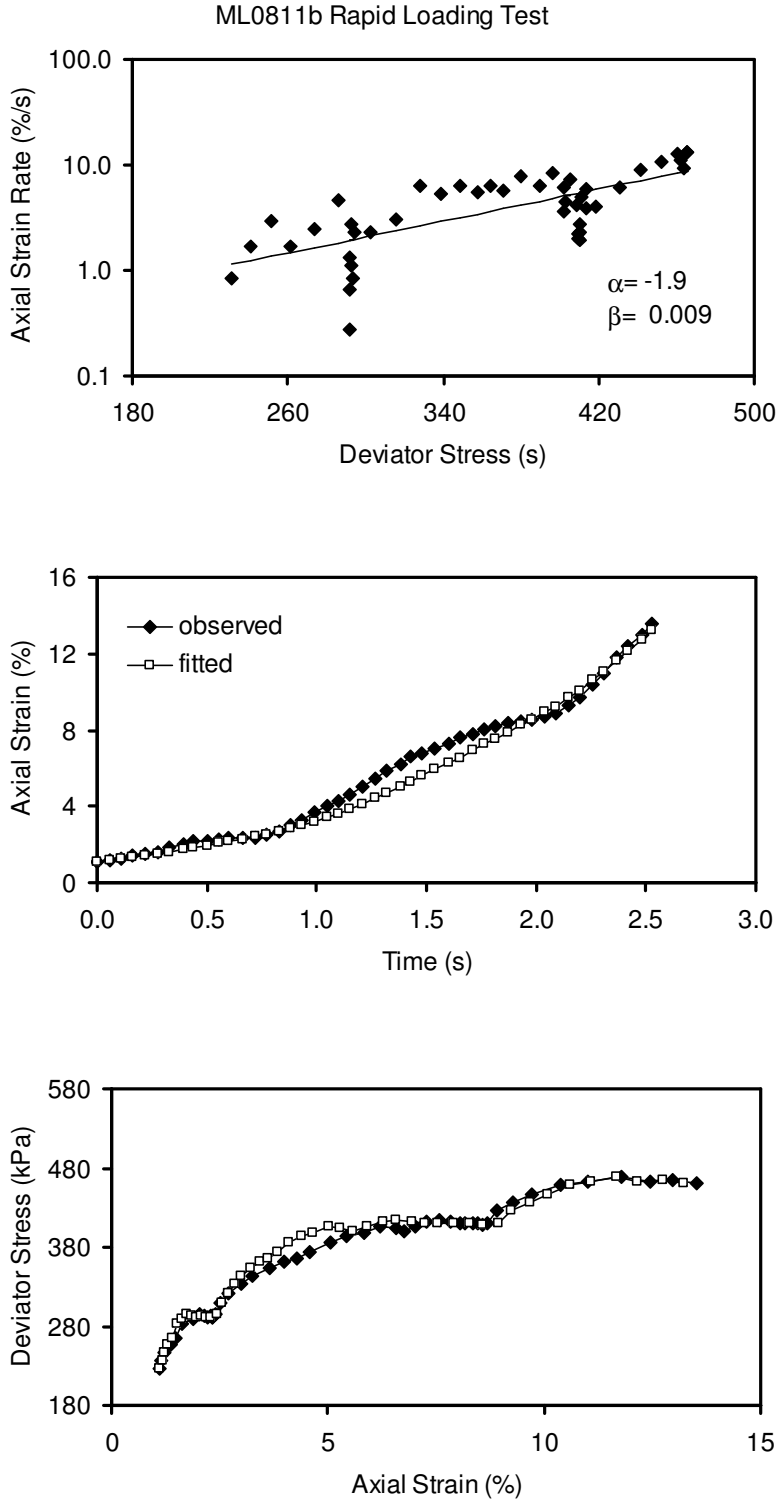

Figure B.36. Rapid loading test results and least squares fit for ML0811b.

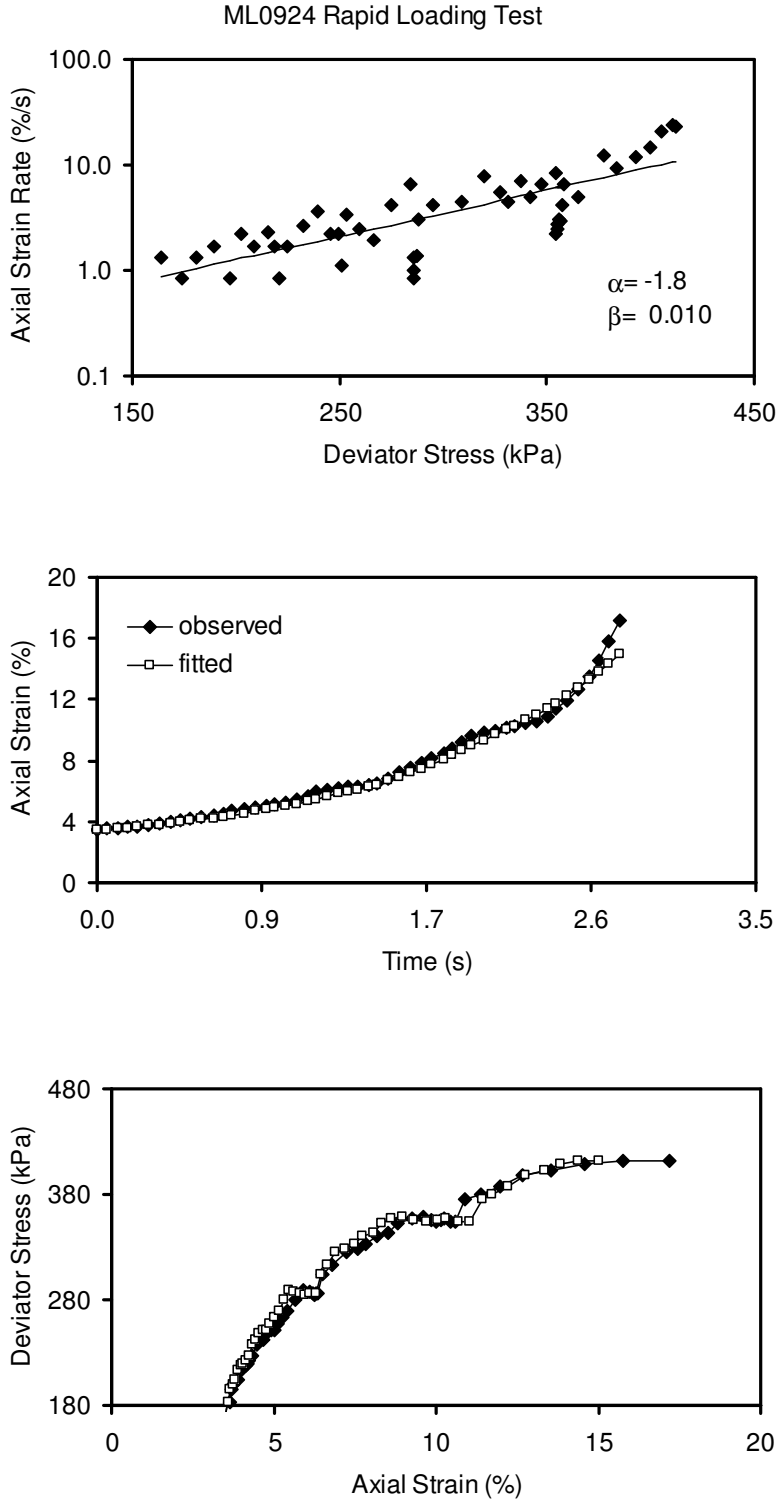

Figure B.37. Rapid loading test results and least squares fit for ML0924.

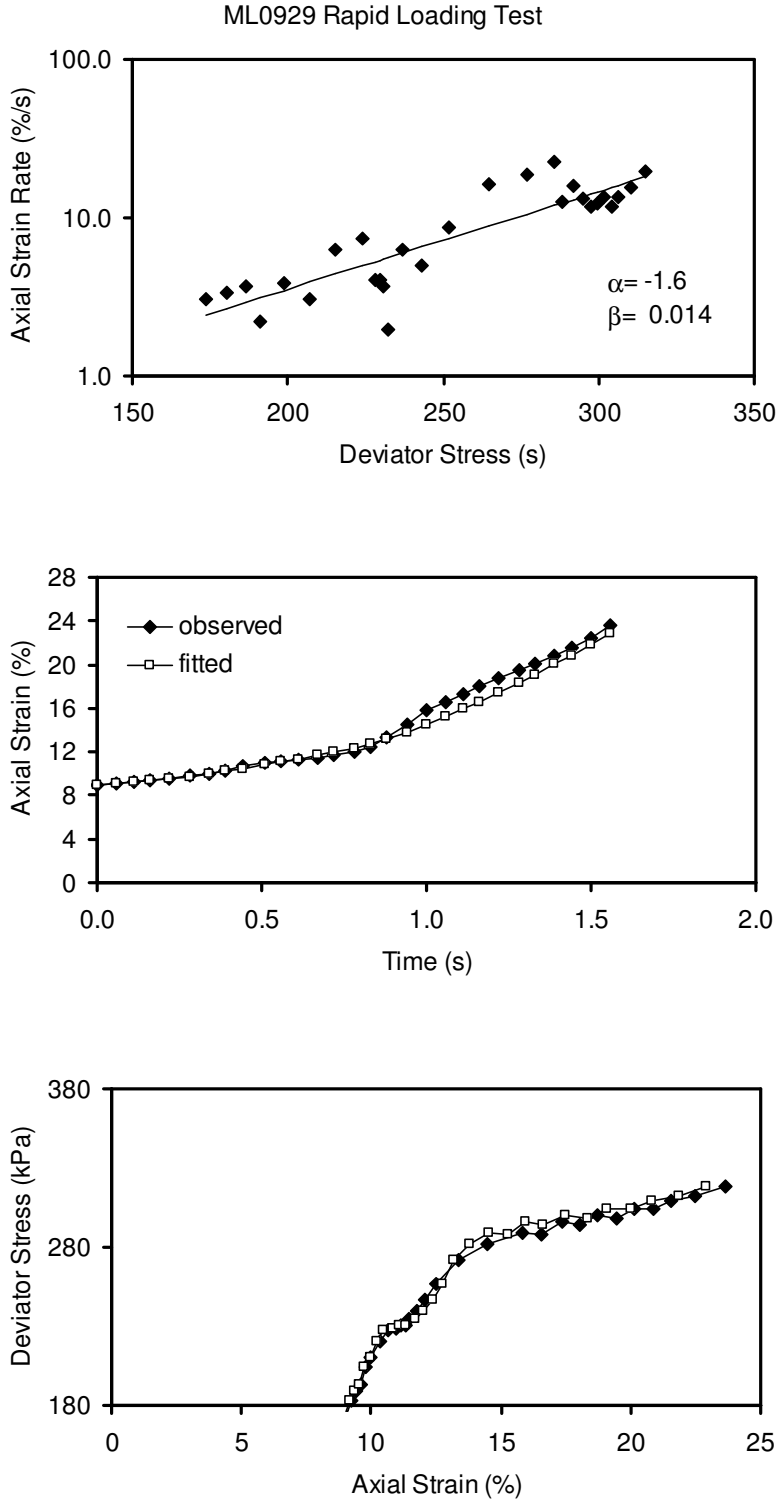

Figure B.38. Rapid loading test results and least squares fit for ML0929.

VITA

Mustafa Tolga Yılmaz was born in İzmir in 1975. He received his B.S. degree in Civil Engineering from the Middle East Technical University in 1997. Since 1998 he has been working as a research assistant in the Geotechnical Engineering Division of the same department. His main areas of interest are site response and seismic performance of shallow foundations.